Springer Theses
Recognizing Outstanding Ph.D. Research

Johannes Knolle

Dynamics of a Quantum Spin Liquid

Springer

Springer Theses

Recognizing Outstanding Ph.D. Research

More information about this series at http://www.springer.com/series/8790

Aims and Scope

The series "Springer Theses" brings together a selection of the very best Ph.D. theses from around the world and across the physical sciences. Nominated and endorsed by two recognized specialists, each published volume has been selected for its scientific excellence and the high impact of its contents for the pertinent field of research. For greater accessibility to non-specialists, the published versions include an extended introduction, as well as a foreword by the student's supervisor explaining the special relevance of the work for the field. As a whole, the series will provide a valuable resource both for newcomers to the research fields described, and for other scientists seeking detailed background information on special questions. Finally, it provides an accredited documentation of the valuable contributions made by today's younger generation of scientists.

Theses are accepted into the series by invited nomination only and must fulfill all of the following criteria

- They must be written in good English.
- The topic should fall within the confines of Chemistry, Physics, Earth Sciences, Engineering and related interdisciplinary fields such as Materials, Nanoscience, Chemical Engineering, Complex Systems and Biophysics.
- The work reported in the thesis must represent a significant scientific advance.
- If the thesis includes previously published material, permission to reproduce this must be gained from the respective copyright holder.
- They must have been examined and passed during the 12 months prior to nomination.
- Each thesis should include a foreword by the supervisor outlining the significance of its content.
- The theses should have a clearly defined structure including an introduction accessible to scientists not expert in that particular field.

Johannes Knolle

Dynamics of a Quantum Spin Liquid

Doctoral Thesis accepted by the Max Planck Institute
for the Physics of Complex Systems, Dresden, Germany

Springer

Johannes Knolle
Cavendish Laboratory
University of Cambridge
Cambridge, UK

ISSN 2190-5053 ISSN 2190-5061 (electronic)
Springer Theses
ISBN 978-3-319-23951-4 ISBN 978-3-319-23953-8 (eBook)
DOI 10.1007/978-3-319-23953-8

Library of Congress Control Number: 2015951196

Springer Cham Heidelberg New York Dordrecht London

Printed on acid-free paper

Springer International Publishing AG Switzerland is part of Springer Science+Business Media (www.springer.com)

Supervisor's Foreword

The insight that there exist physical systems outside our familiar framework of local order and disorder is not new—Wegner's groundbreaking work on gauge theories dates back to the 1970s, and Klitzing's experimental discovery of the quantum Hall effect stems from the 1980s. However, the ubiquity, complexity and richness of topological phenomena were not recognised until much later, with topological condensed matter physics now being arguably one of the most active branches of the field. A key challenge is the elusiveness of the experimental signatures involved, which is a direct consequence of the missing local order.

For insulating spin systems, where charge transport is not available as a diagnostic, this lack of distinctive fingerprints is particularly pressing, all the more so as developments over the last 15 years have provided numerous theoretical models of topological spin liquids in search of a materials realisation. Connecting theory with promising experiments is also limited by the lack of availability of exact approaches or controlled approximations for strongly interacting quantum systems in more than one spatial dimension.

The work in Johannes Knolle's thesis stands out in its successful exact evaluation of the dynamical structure factor of a fractionalised quantum spin liquid. This quantity, which can be directly probed in neutron scattering experiments, provides direct evidence, both qualitatively and quantitatively, for the fractionalisation of the electron into Majorana fermions and topological flux degrees of freedom.

Thus, it provides precisely the kind of information that has been lacking so far for the identification of salient experimental signatures of topologically ordered spin systems. As a consequence, experimental interest in these results has been immediate. Beyond this, the work is also of interest from a methodological point of view in many-body physics, because the calculation of the dynamical correlation function can be mapped exactly to that of a local quantum quench. This instance of an exactly soluble non-equilibrium problem is of interest in the a priori unrelated context of time-dependent coherent Hamiltonian evolution of quantum systems.

Overall, I hope that the material contained in this thesis will be of use not only to students interested in background and details of the theoretical developments underpinning this work, but also to researchers—theorists and experimentalists

alike—looking for a comprehensive, self-contained and clear exposition of the physics of quantum spin liquids in general, and the dynamical signatures of fractionalisation in particular.

Dresden, Germany
23 March 2015

Roderich Moessner

Preface

What is the nature of matter? This question has been fascinating ever since Democritus conjectured that all substances are made of indivisible atoms. One of the frontiers of modern physics represents the search for unconventional quantum phases. In contrast to fundamental constituents probed at enormous energy scales in particle physics, new phenomena can alternatively appear at low energies in condensed matter physics upon cooling. There, complex behavior arises from the interaction of a large number of particles, which are themselves simple. A familiar example is that of a bar magnet, whose countless electrons align their spins below a critical temperature and whose excitations are spinwaves. All spins point on average in a particular direction, which gives rise to a magnetization. A cornerstone of modern physics is Landau theory, which classifies phases of matter by their broken local symmetries with order parameters, e.g. the magnetization. However, in the focus of current research are topologically ordered phases falling outside of this canonical classification. They defy a description via local order parameters and present striking new phenomena, because new phases come with new excitations. Most prominent is the fractionalization of electrons into unusual particles: Majorana fermions (Kitaev 2006), Laughlin quasiparticles (Laughlin 1983), or magnetic monopoles (Castelnovo et al. 2008). However, their experimental detection is fundamentally complicated by the lack of local order. The objective of this thesis is to contribute to answering a key question: How can a topologically ordered phase be diagnosed in experiments?

Frustrated magnetic materials, in which not all interactions can be satisfied simultaneously, hold the promise of realizing topological quantum phases. In contrast to ordered magnets, frustration can lead to so-called quantum spin liquids (QSL), which remain disordered down to the lowest temperatures. These cooperative quantum phases of interacting spin systems do not break any local symmetry but exhibit topological order. Although various experimental instances of candidate QSLs are known, their identification remains challenging. The main result of this work is the discovery of discernible features of fractionalization, a hallmark of these elusive states of matter, in dynamical response functions, which are experimentally accessible.

This thesis presents an exact theoretical study of dynamical correlation functions in different phases of a two-dimensional quantum spin liquid. By calculating the dynamical spin structure factor and the Raman scattering cross section, I show that there are salient signatures—qualitative and quantitative—of the Majorana fermions and gauge fluxes emerging as effective degrees of freedom in the exactly solvable Kitaev honeycomb lattice model. The model is a representative of a class of spin liquids with Majorana fermions coupled to Z_2 gauge fields. The qualitative features of the response functions should therefore be characteristic for this broad class of topological states.

I begin the thesis with an introduction to frustrated magnetism and QSLs, with a focus on dynamical correlations probed in experiments. Next, I provide an introduction to the Kitaev model and discuss the exact solution, the QSL properties, and a promising proposal for a realization in late transition metal oxides.

The core of the thesis comprises my theoretical analysis of the dynamical spin correlation function via a mapping to a local quantum quench. I identify connections to two condensed matter paradigms: The venerable X-ray edge problem and the Anderson orthogonality catastrophe. I derive two complementary exact solutions of the resulting non-equilibrium problem. The first is based on the evaluation of Pfaffians, a generalization of determinants. The second borrows concepts from the theory of singular integral equations, which allows to obtain results in the thermodynamic limit.

In the "Results" chapter, I discuss the calculated spin structure factor in different gapped and gapless phases of the Kitaev model. Clear signatures of the emergent fractionalized particles will be visible as fingerprints betraying the presence of QSLs in future inelastic neutron scattering or electron spin resonance experiments. These include counterintuitive manifestations of quantum number fractionalization, such as a neutron scattering response with a gap even in the presence of gapless excitations, and a sharp component in the response despite the fractionalization of electron spin.

The next chapter deals with an extended Kitaev model incorporating an additional three spin interaction breaking time reversal symmetry. This exhibits a QSL phase harboring non-Abelian excitations, whose experimental detection is a central goal of current condensed matter physics. The mapping of the spin correlation function to a local quantum quench remains intact. I identify clear signatures of Majorana bound states in the structure factor, which distinguish between Abelian and non-Abelian phases. The incorporation of bond disorder, which is potentially present in real materials, reveals that the distinction is surprisingly robust.

The final chapter investigates an alternative experimental probe. I compute the inelastic Raman scattering response in the Kitaev model, which is related to a higher order dynamical spin correlation function. The addition of a small Heisenberg coupling breaks the integrability of the original model, and leads to an additional important contribution to the response, which can in turn be calculated as a modified quantum quench of Majorana fermions. Similar to the structure factor, salient features of the fractionalized quasiparticles are manifest in the response.

I close with a summary of my findings and an outlook. In general, exact results for correlation functions are specific to one dimensional systems, e.g. based on the exact Bethe-Ansatz solution (Bethe 1931). For the first time, my thesis provides this information in complete detail for a quantum spin liquid in more than one dimension. Since dynamical response functions have the advantage of probing the full excitation spectrum, this dissertation shows that they provide a valuable tool for diagnosing QSLs in candidate materials.

Cambridge, UK Johannes Knolle

References

H. Bethe, Zur Theorie der Metalle. German. Zeitschrift für Physik **71**(3–4), 205–226 (1931)
C. Castelnovo, R. Moessner, S.L. Sondhi, Magnetic monopoles in spin ice. Nature **451**(7174), 42–45 (2008)
A. Kitaev, Anyons in an exactly solved model and beyond. Ann. Phys. **321**(1), 2–111 (2006)
R.B. Laughlin, Anomalous quantum hall effect: an incompressible quantum fluid with fractionally charged excitations. Phys. Rev. Lett. **50**(18), 1395–1398 (1983)

Acknowledgements

Science is a collective enterprise. Thus, my thesis would not have been possible without the help of others.

First of all, I would like to thank my advisor Roderich Moessner for his invaluable guidance. He has shaped most of my understanding of condensed matter physics. The open intellectual atmosphere he created in his group allowed me to pursue different projects of interest during my PhD. He was always available even for discussing technical details, and his precise questions together with his physical intuition have often refocused my efforts in the right direction. He continues to be a role model of what it means to be a scientist.

During my time in Dresden, I have profited from two other close collaborations. In the beginning, Ilya Eremin introduced me to the craft of many-body theory. I am especially grateful that he taught me to value connecting theoretical ideas with actual experimental data. Ever since, I enjoy working with him on unconventional superconductivity.

As this thesis is about my work on quantum spin liquids, I would like to thank Dima Kovrizhin for a great collaboration. With his help, I have learned about Pfaffians and singular integral equations. But most importantly, he taught me never to be scared of new methods.

In the course of my PhD, I have benefited from the interaction with great scientists. I would like to express my gratitude to Andrey Chubukov, Natalia Perkins, and Rafael Fernandes for their great hospitality in Madison and Minneapolis, and for all the collaborations on iron-based superconductors. I would like to thank John Chalker for immensely helpful conversations during our collaboration on the Kitaev model and for sharing his ideas on frustrated magnetism. Furthermore, I give many thanks to Matthias Vojta, Carsten Timm, and Maria Daghofer for numerous insightful discussions during my time in Dresden. Last but not least, I enjoyed working with Jörg Schmalian, Peter Hirschfeld, Gia-Wei Chern, Alireza Akbari, Wenya Wang, Saurabh Maiti, Felix Ahn, Bernd Büchner, and Sergey Borisenko. I thank Nick Shannon for his hospitality in Okinawa.

I would like to acknowledge support from the *Studienstiftung des deutschen Volkes*, the *International Max Planck Research School for Dynamical Processes*

in Atoms, Molecules and Solids, and the *DFG Research Training Program GRK 1621*.

During my PhD, I enjoyed the atmosphere and the amazing organization of the *Max Planck Institute for the Physics of Complex Systems*, Dresden. I am glad that I could share in harmony an office with Matthias Merkel. He did not only have answers to all my software questions, but I remember countless discussions about physics and life. I also thank all members of the *Condensed Matter Group* for years of great coffee breaks, lunches, journal clubs, seminars, and physics discussions. I would like to mention Masud Haque, Ludovic Jaubert, Frank Pollmann, Andreas Laeuchli, Emil Bergholtz, Peter Fulde, Janik Kailasvuori, Masafumi Udagawa, Wladimir Tschischik, Arnab Das, Paul McClarty, Aroon O'Brien, Pedro Ribeiro, Ioannis Rousochatzakis, Luis Seabra, Adolfo Grushin, Jonas Kjaell, Abdollah Langari, Jens Bardarson, Vincenzo Alba, Andrey Antipov, Daniel Charrier, James LeBlanc, and many others.

I thank Vojtech Kaiser, Subhro Bhattacharjee, Johannes Motruk, Olga Petrova, and especially Mykola Maksymenko, Adam Smith and Franziska Knolle for proofreading parts of the thesis.

Finally, I would like to give thanks to my whole family and friends for encouragement during the last years whenever needed. In particular, I can always count on the invaluable support of my parents. Most importantly, Louise and Julian bring meaning and joy to my life. Above all, my love Franziska shares my dreams and happiness.

Contents

Chapter 1
Introduction

1.1 Motivation

What is the nature of matter? How can one thing change into another? Can human intervention bring about new forms of matter? Prior to modern science, speculations around these questions were already central to Greek natural philosophy and later to medieval Alchemy (Principe 2013). It is thought to be Thales of Miletus in the sixth century BC who introduced the idea that all substances are only different modifications of a single one. A century later, Democritus conjectured that everything is made of indivisible atoms. He proposed that the combination of a huge number of itself simple basic entities gives rise to the plethora of forms of matter we encounter. Following these traditions Alchemists of the Middle Ages experimented with the combination of simple substances to create new ones, e.g. their quest to master the transmutation of ordinary sulfur and mercury into gold. While this attempt was unsuccessful, their systematic experimental inquiry of the corpuscular nature of matter lay the foundations for modern chemistry (Newman 2006) and in the process they created valuable new materials, e.g. porcelain was rediscovered by J.F. Böttger in 1708 (Hildyard 1999).

Understanding phases of matter and creating new ones remains one of the great challenges of modern physics with central ideas of its prehistory reappearing. In condensed matter physics, it is well established that complex behavior arises from the interaction of a large number of itself simple particles. For example, the interaction of point-like electrons in a solid can lead to a seemingly endless variety of phenomena: magnetism, metallicity, superconductivity, etc. A fascinating aspect of this field is the way in which new phases are discovered and how they are understood. On the one hand, nature can be surprising, such that experimentalists stumble over new findings similar to Böttger. The discovery of *superconductivity* in 1911 by Heike Kamerlingh Onnes was totally unexpected and it took almost half a century until BCS theory (Bardeen et al. 1957) gave a satisfactory explanation in terms of a macroscopic quantum wave function, see discussion in Cooper and

J. Knolle, *Dynamics of a Quantum Spin Liquid*, Springer Theses,
DOI 10.1007/978-3-319-23953-8_1

Feldman (2011). On the other hand, there are much rarer instances in which theories predict new phases and the main challenge afterwards is the construction of necessary experimental conditions. For example, *Bose Einstein condensation*, a phase with a macroscopic number of indistinguishable particles in the same quantum state, was first discussed in the 1920s (Einstein 1924), but it took 70 years before its weakly interacting version was experimentally realized in a gas of cold atoms (Davis et al. 1995).

This thesis is devoted to the study of QSL, another elusive quantum state of matter predicted more than 40 years ago to appear in certain magnetic materials (Anderson 1973), but still not conclusively verified experimentally. The main objective of this thesis is the calculation of dynamical correlation functions in order to find salient signatures for diagnosing these sought-after phases in experiments and to gain a deeper understanding of *topological order* (Wen and Niu 1990), which is characterized as a phase without a local order parameter but with a particular ground state degeneracy. For a proper understanding of the latter, it is instructive to first introduce our modern canonical understanding of phases of matter and their transitions based on local symmetry.

Depending on thermodynamic quantities, such as temperature or pressure, systems can change their internal structure abruptly, so that new phases appear, e.g. the crystallization of H_2O molecules when water freezes to ice. Another example is a standard bar magnet made from a ferromagnetic material. In the simplest description, its basic degrees of freedom are tiny elementary bar magnets, or spins S_i, on lattice sites i which can either point up or down. A ferromagnetic interaction between nearest neighbor spins prefers them to point in the same direction, but at high temperatures all elementary spins fluctuate wildly. Hence, the average magnetization is zero, $M = \langle S_i \rangle = 0$. This paramagnetic phase and the form of the interaction do not distinguish between up and down direction, which is called a *symmetry*. However, at low temperatures the interaction forces spin to align and a particular direction is picked out, $|M| > 0$, such that all spins either point up or down on average—the symmetry is broken.

A cornerstone of modern physics and at the heart of our understanding of phases and their transitions is *Landau theory*. It is based on the idea of a local order parameter quantifying a symmetry breaking, e.g. the magnetization M of the bar magnet. Landau conjectured that close to the transition the thermodynamic potential, the free energy, can be expanded as a Taylor series in the order parameter and the temperature (Cardy 1996)

$$\Delta F(M,T) = \frac{1}{2} b(T) M^2 + \frac{1}{4} c(T) M^4 + \cdots \tag{1.1}$$

which completely neglects fluctuations around the average value M. The value of M minimizing $\Delta F(M,T)$ at a given T is the one realized in the system. Now, depending on the temperature behavior of the coefficients, this simple function can describe various different phase transitions. A common situation is given by $b(T) = b_0(T - T_c)$ and $c = c_0 > 0$ such that the minimum of $F(M,T)$ is found at

$M = 0$ or $M = \pm\sqrt{b/c}$ for $T > T_c$ or $T < T_c$. In this case the magnetization vanishes continuously at the phase transition $M \propto |T - T_c|^\beta$ with the *critical exponent* $\beta = \frac{1}{2}$. This type is known as a second order phase transition. Similarly, one can obtain, for example, first order transitions at which the magnetization jumps, for introductions see Cardy (1996), Goldenfeld (1992), and Chaikin and Lubensky (2000). Phases at lower temperatures have in general a lower symmetry than the Landau function or the microscopic Hamiltonian of the system, which is known as *spontaneous symmetry breaking*. In the above example the ferromagnetic spins in the ordered low temperature phase point in a particular direction, M is either $+\sqrt{b/c}$ or $-\sqrt{b/c}$, but $\Delta F(M, T)$ is insensitive to the sign.

The power of Landau theory stems from the idea that the construction of $\Delta F(M, T)$ in terms of order parameters is only dictated by the symmetry group of the Hamiltonian describing the problem—microscopic details are irrelevant. Although Landau theory is phenomenological, its universal predictions can be tested by experiments. Close to continuous transitions, it is expected that thermodynamic observable exhibit a power law behavior, e.g. $M \propto |T - T_c|^\beta$, and the critical exponents belong to different *universality classes*. The unifying element is that completely different microscopic models can have the same exponents belonging to the same universality class. For the above example, Landau theory gives the *mean-field* exponent $\beta = \frac{1}{2}$ for the ferromagnetic transition which is a good approximation in high dimensions. In low dimensions close to the critical point T_c, fluctuations in general alter this exponent. However, despite its limitations, Landau theory is also the starting point for incorporating fluctuations, e.g. via gradient terms, which leads to the Ginzburg–Landau theory, and later on to the description of critical phenomena via the renormalization group (Wilson 1971).

Landau theory and its extensions are so successful in describing phases and transitions between them, that it is easy to believe that they describe all there is. A first hint of phase transitions without local order parameters was given by Wegners dual formulation of certain Ising models in terms of lattice gauge theories. They exhibit non-analyticities in thermodynamic quantities and correlation functions as a function of temperature, which signal a phase transition, but without the appearance of a local order parameter (Wegner 1971). Overall, nature has turned out to be much richer as can be anticipated. In general, physics is driven by experiments challenging our always incomplete understanding. The discovery of the fractional quantum hall effect (FQHE) (Tsui et al. 1982) in a two dimensional electron gas, for which the Hall resistance $\rho_{xy} = \frac{h}{e^2}\frac{1}{\nu}$ is exactly quantized with rational prefactors ν, confirmed that there exist exotic phases beyond the Landau paradigm. The observation of distinct incompressible phases which cannot be distinguished on the basis of local symmetry paved the way towards the development of new concepts. The idea of *topological order* appeared (Wen and Niu 1990; Wen 2004) which allowed to understand totally unexpected phenomena such as *fractionalization*, e.g. the point like electron seemingly breaking apart (Laughlin 1983), see also Rajaraman (2001).

In the last three decades our theoretical understanding of topological phases beyond the Landau paradigm has advanced considerably and revolutionary applications have been proposed in the context of topological quantum computation

(Kitaev 2003; Nayak et al. 2008). However, beyond the FQHE the detection of these elusive states of matter has proven to be very challenging. A promising route is to search for topological order in collective quantum states of *frustrated* magnetic materials (Balents 2010). In particular, since Anderson's *resonating valence bond* (RVB) phase (Anderson 1973) was put forward to explain high temperature superconductivity in the cuprates (Anderson 1987), the search for the so-called QSL has gained momentum. This thesis is devoted to the study of such QSLs and how to detect them in experiments. By calculating dynamical correlation functions of an exactly solvable model with a QSL ground state, I show that clear signatures of fractionalization are visible in standard scattering experiments.

In the next section, I begin with an introduction into *frustrated magnetism* and *QSL* including a discussion of *topological order*. Afterwards, I discuss experimental signatures of frustrated magnets in current experiments of candidate materials. I close the chapter with recent results of inelastic neutron scattering (INS) experiments probing the full excitation spectrum of candidate QSL materials, which call for detailed theoretical investigations as provided by this thesis.

1.2 Frustrated Magnetism and Quantum Spin Liquids

Magnetic materials are ubiquitous in nature. The fact that iron ores attract other objects made of iron has been known for millennia. Already more than two thousand years ago the first application of magnetism was the Chinese invention of the compass needle (McElhinny 1984). Ever since, magnetic materials have found wide ranging applications ranging from electric guitars all the way to modern computers. A prominent example is the discovery of *giant magneto resistance* (Baibich et al. 1988), the big change in resistance depending on the direction of magnetization in thin film hetero-structures, which quickly lead to a tremendous increase in the performance of computer hard-disc drives.

In the development of modern physics, magnetic materials have provided a gratifying field in which simple models, which give rise to widely different phenomena, could be tested against experiments. For example, Onsagers exact solution of the two dimensional Ising model (Onsager 1944), which crudely describes ferromagnetic materials, proved a finite temperature phase transition and elucidates many of its thermodynamic signatures, for a nice discussion about the role of models in physics, see Peierls (1980). Afterwards, many ideas in the theory of critical phenomena such as scaling theory and the renormalization group were developed in the context of the Ising model (Kadanoff 1966; Wilson 1971); a thorough historical study can be found in Niss (2011).

In most magnetic materials fluctuations, which lead to a paramagnetic phase at high temperatures, become smaller by cooling such that systems develop some form of long range order below a critical temperature T_c. In the focus of current research are insulating materials with localized magnetic moments which show qualitatively different behavior because fluctuations remain large down to lowest

temperatures (Balents 2010). They are known as *frustrated magnets* because they contain competing interactions which cannot be fully satisfied. This thesis deals with the extreme quantum limit of a frustrated magnetic system in which the spins remain in a fluid-like state even at zero temperature because of large quantum fluctuations. In this chapter, I explain some of the key concepts of the field and define properties of long-sought QSLs. A more detailed account of the field including experimental aspects, materials physics, and theoretical developments can be found in the book Lacroix et al. (2011).

1.2.1 Frustrated Magnetism

I concentrate on effective spin descriptions such as the venerable Heisenberg model

$$\mathcal{H} = \sum_{ij} J_{ij} \mathbf{S}_i \cdot \mathbf{S}_j \tag{1.2}$$

in which spins on lattice sites $\mathbf{r}_i$ interact via exchange interactions. In a classical description, spins $\mathbf{S}_i$ are three component vectors. In a quantum mechanical description necessary at low temperatures (and small $|\mathbf{S}_i|$), they are spin operators defined by their spin algebra. The Heisenberg model describes insulating magnets for which the energy scale of charge fluctuations is much higher than any of the exchange couplings J_{ij} because of large Coulomb repulsion between localized electrons (Auerbach 1994). For a better understanding of frustrated magnetism, it is instructive to contrast its unusual behavior with the one of conventionally ordered magnets. Conventional systems order into a state with long range magnetic order below a critical temperature T_c. In a classical description of the ordered phase of the Heisenberg model the ground state is found by locating the minima of the Fourier transformation of the coupling constants

$$J(\mathbf{q}) = \sum_i J_{ij} e^{i\mathbf{q}(\mathbf{r_i}-\mathbf{r_j})} \tag{1.3}$$

and minimizing the energy by forming a spiral with pitch vector $\mathbf{q}$. The spin correlation function clearly shows long range magnetic order and behaves as

$$\langle \mathbf{S}_i \cdot \mathbf{S}_j \rangle \propto m^2 \cos\left[\mathbf{q} \cdot \left(\mathbf{r_i} - \mathbf{r_j}\right)\right]. \tag{1.4}$$

The transition from the paramagnetic high temperature state to this ordered state can be described by Landau theory. The order parameter, given by the magnetization $\mathbf{m_i} = \langle \mathbf{S}_i e^{\mathbf{q}\mathbf{r_i}} \rangle$, quantifies breaking of the $O(3)$ spin rotational symmetry and for $\mathbf{q} \neq 0$ also of translational symmetry. The low energy excitations of the ordered phase are long wavelength fluctuations of the order parameter. These spin waves are the Goldstone modes related to spontaneous breaking of the continuous

spin rotational symmetry by the ground state magnetic ordering (Chaikin and Lubensky 2000). In general, such a classical description carries over to conventional quantum magnets. Without quantum fluctuations in a classical system, $1 \ll S$, the magnetization is $m^2 = S^2$ at zero temperature, with $S = |\mathbf{S}_i|$ the total length of the spin. But normally the magnetization is reduced by quantum fluctuations, $m < S$, which can be calculated, e.g., by a $1/S$ spin wave expansion (Kittel 1963), see the introductory chapter of Chalker in Lacroix et al. (2011).

In contrast to this canonical behavior, frustrated magnets can evade magnetic ordering down to lowest temperatures. Frustration refers to the notion that competing interactions cannot be satisfied simultaneously. In the case of the Heisenberg model, it means that not all local energy costs of couplings J_{ij} can be minimized. In an intuitive picture, the large number of low energy configurations arising from the competition of frustrated interactions leads to abundant low energy fluctuations suppressing classical long range order, in extreme cases down to $m = 0$.

It is common to distinguish two prototypical types of frustration: First, geometric frustration on non-bipartite lattices with only nearest neighbor interactions. A simple example is the antiferromagnetic (AF) Heisenberg model on the triangular lattice, see Fig. 1.1 left panel (a), for which it is impossible to satisfy all three bonds on a given triangle. Second, competing longer range or anisotropic interactions can lead to frustration even on bipartite lattices. An extensively studied example is the $J_1 - J_2$ Heisenberg model on the simple square lattice

$$\mathcal{H}_{J_1-J_2} = J_1 \sum_{\langle i,j \rangle} \mathbf{S}_i \cdot \mathbf{S}_j + J_2 \sum_{\langle\langle i,j \rangle\rangle} \mathbf{S}_i \cdot \mathbf{S}_j \tag{1.5}$$

with nearest neighbor (N.N.) and next nearest neighbor (N.N.N.) pairs $\langle i,j \rangle$ and $\langle\langle i,j \rangle\rangle$, see Fig. 1.1 right panel (b). Its classical ground state is found by minimizing

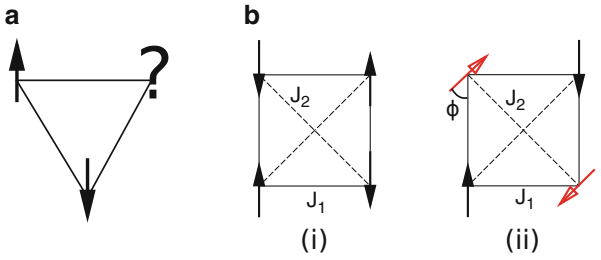

Fig. 1.1 Two prime examples of frustrated magnetic systems are shown. In the left panel (**a**), the third spin on a triangle is not able to minimize simultaneously the antiferromagnetic (AF) exchange energy with the two other spins. Left panel (**b**) depicts the $J_1 - J_2$ model with nearest neighbor (N.N.) and next nearest neighbor (N.N.N.) AF interactions on the square lattice. The classical ground state for $2J_1 > J_2$ in *(i)* is a standard N.N. Néel state. For $2J_1 < J_2$, *(ii)*, two interpenetrating N.N.N. Néel sublattices (*red* and *black*) with an arbitrary angle Φ in between N.N. spins minimize the classical ground state energy

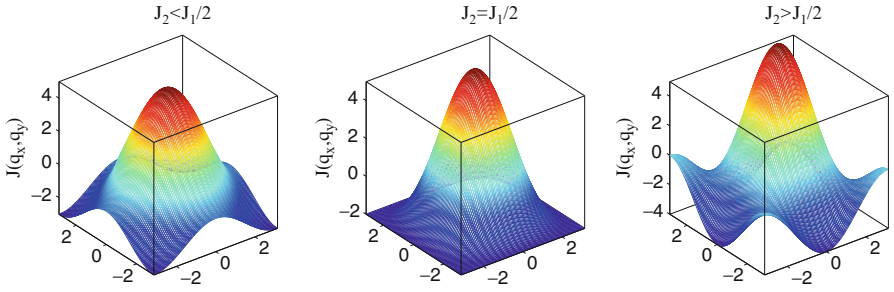

Fig. 1.2 The Fourier transform $J(\mathbf{q})$ of the exchange constants, Eq. (1.6), of the $J_1 - J_2$ model is shown. The pitch vector $\mathbf{q}$ of the classical spiral ground state is found by locating its minima. Depending on the N.N. and N.N.N. exchange constants three different regimes are found: *Left panel* $J_2 < J_1/2$, with minima at (π, π) which corresponds to the standard Néel ordering shown in Fig. 1.1b (i). *Right panel* $J_2 > J_1/2$, with minima at $(\pi, 0)$ and $(0, \pi)$ which leads to two interpenetrating Néel sublattices, see Fig. 1.1b (ii). The arbitrary angle Φ leads to a classical degeneracy of the ground states. Third, at the fully frustrated point $J_2 = J_1/2$ entire lines of momenta $q_x = (\pi, Q)$ or $q_y = (Q, \pi)$ for arbitrary Q minimize the energy and lead to a huge ground state degeneracy at the classical level, which opens the possibility for spin-disordered phases

$$J(\mathbf{q}) = 2J_1 \left(\cos q_x + \cos q_y\right) + 4J_2 \cos q_x \cos q_y \tag{1.6}$$

with respect to the spiral pitch vector $\mathbf{q}$. The behavior of $J(\mathbf{q})$ is shown in the first Brillouin zone for three different regimes in Fig. 1.2. For $J_2 < J_1/2$ the system shows simple AF order, Fig. 1.1b (i) because the minimum of the coupling constant $J(\mathbf{q})$ is found at $\mathbf{q} = (\pi, \pi)$, see Fig. 1.2 left panel.

But for $J_2 < J_1/2$ minima in Fig. 1.2 right panel are situated at momenta $\mathbf{q} = (\pi, 0)$ or $(0, \pi)$ which only fixes the N.N.N. AF orientation. The system decouples into two interpenetrating Néel sublattices with a free angle Φ between the N.N. spins as shown in Fig. 1.1b (ii). Incorporating quantum fluctuations via a $1/S$ expansion with Holstein–Primakoff bosons (Kittel 1963) shows that the ground state energy $E_{\text{g.s.}} = E_{\text{classical}} + O(1/S)$ is minimized for collinear states with $\Phi = 0, \pi$ (Shender 1982). In frustrated systems, classical ground state degeneracies do not arise because of symmetry but are accidental. Therefore, fluctuations vary for different ground states and can thus select states with largest entropy or lowest zero point energies. This phenomenon, very common for frustrated magnets, is known as *order by disorder*, whereby quantum or thermal fluctuations select a ground state out of a degenerate manifold (Villain et al. 1980).

The most interesting point of the $J_1 - J_2$ model is the fully frustrated situation $J_2 = J_1/2$ for which the classical energy is minimized for any state with $q_x = (\pi, Q)$ or $q_y = (Q, \pi)$ for arbitrary momenta Q, see Fig. 1.2 middle panel. Calculating the lowest order quantum corrections to the order parameter via Holstein–Primakoff bosons a_i

$$m = S - \frac{1}{V}\sum_i \langle a_i^\dagger a_j \rangle \tag{1.7}$$

one finds that the renormalization has an infrared divergence because the spin wave spectrum, $\omega_{\mathbf{q}} \propto |\sin q_x \sin q_y|$, has entire lines of zeros in the Brillouin zone (BZ) giving rise to arbitrarily large low energy fluctuations (Chandra and Doucot 1988). The fact that the magnetization m becomes negative signals the breakdown of the $1/S$ expansion even for $S \to \infty$.

More than two decades ago, it was conjectured that exotic spin-disordered, e.g. dimerized, states appear in a finite parameter region around the fully frustrated point $J_2 = J_1/2$ (Chubukov and Jolicoeur 1991). Unfortunately, the exact ground state of the model is not known to date and it is an ongoing debate whether it is a QSL or a valence bond crystal (VBC) (Reuther et al. 2011). Before explaining these two key concepts, I will introduce a simple extension of the $J_1 - J_2$ model for which the exact ground state is known. Thereby, I motivate the use of effective short range singlet dimer models which provide a natural setting for finding QSLs and VBCs, see the chapter of Lhuillier and Misguich in Lacroix et al. (2011).

By the addition of a four spin interaction

$$\begin{aligned}\mathcal{H}_{J_1-J_2-K} = \mathcal{H}_{J_1-J_2} + K \sum_{\{i,j,k,l\}} \big[&(\mathbf{S}_i \cdot \mathbf{S}_j)(\mathbf{S}_k \cdot \mathbf{S}_l) \\ &+ (\mathbf{S}_j \cdot \mathbf{S}_k)(\mathbf{S}_i \cdot \mathbf{S}_l) + (\mathbf{S}_i \cdot \mathbf{S}_k)(\mathbf{S}_j \cdot \mathbf{S}_l) \big]\end{aligned} \tag{1.8}$$

with $\{i, j, k, l\}$ around a plaquette in cyclic order, the extended $J_1 - J_2 - K$ model becomes exactly solvable at the fully frustrated point $J_2 = J_1/2$ and $K = J_1/8$ (Batista and Trugman 2004). It can be written as

$$\mathcal{H}_{J_1-J_2-K} = \frac{3J_1}{2}\sum_i \hat{P}_i \tag{1.9}$$

in terms of projectors $\hat{P}_i$, which projects the spin state on plaquette i onto total spin $S^i_{\text{tot}} = 2$ per plaquette. Any state with at least one singlet dimer per plaquette has $S^i_{\text{tot}} < 2$ and therefore minimizes the energy. There are two types of ground states: First, states which are product states of N.N. singlet dimers like the one in Fig. 1.3a. Note that there is an extensive number $2^{\sqrt{N}+1}$ (N total number of sites) of those states because it is possible to rotate all dimers along a diagonal by $\pi/2$ at no energy cost, as shown by the arrows. Second, states with interfaces between vertical and horizontal dimer configurations are also permissible ground states and necessarily contain defects at the intersection (not shown) (Batista and Trugman 2004).

What are low energy excitations above the dimerized ground state? After breaking a singlet dimer into a triplet state, both spin $1/2$ can move freely along the diagonal, see Fig. 1.3b. The two resulting excitations, called *spinons*, can be

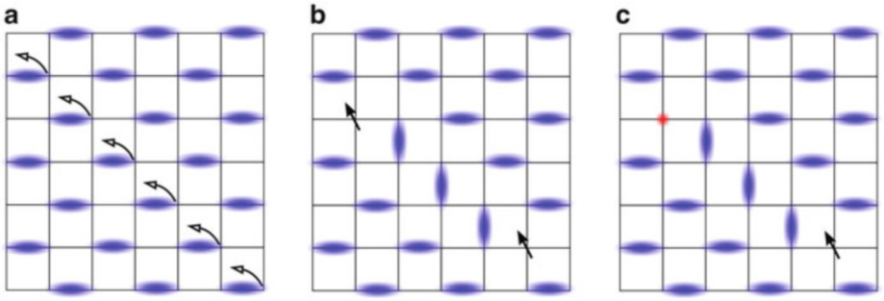

Fig. 1.3 Panel (**a**) shows one of the exact ground states of the extended $J_1 - J_2 - K$ model, Eq. (1.8). The *blue ellipses* denote singlet dimers. The *arrows* indicate that any diagonal array of dimers can be rotated by $\pi/2$, leading to another viable ground state. Panel (**b**) shows that two spinons of a broken dimer are free to move along the diagonal direction. The same is true for the holon and spinon, in which the hole of a removed electron breaks up, shown in panel (**c**)

separated arbitrarily far apart along the 1D diagonal chain without any energy cost. Therefore, they are a special fine-tuned example of *deconfined fractional excitations* in this singlet dimer setting of the $\mathcal{H}_{J_1-J_2-K}$ model. They are *fractional* because all local processes, e.g. breaking a dimer, are in terms of operators S_i^+, S_i^- which change the total spin of the system S_{tot} by ± 1, but each of the two spinons carries half of that quantum number and can be separated infinitely far apart. I explain the concept of *deconfinement* and *fractionalization* in more detail in the next section.

I want to end the discussion of the extended J_1-J_2-K model and its exact ground state with a schematic illustration of another important idea. Assume one electron with charge e and spin $1/2$ is removed from the system. This hole creates an empty site and a free spin $1/2$. Similar to the two spinons both entities can move freely along the diagonal, see Fig. 1.3c. The fact that the empty site, or *holon* without spin but with charge e, and the spinon, without charge but with spin $1/2$, can be separated is known as *spin-charge separation*.

1.2.2 Quantum Spin Liquids

Are the ground states of the extended $J_1 - J_2 - K$ model, which are product wave functions of regular singlet dimer coverings, true QSLs? The answer is *No*, despite the fact that these states fulfill a key feature, namely that spin correlations are short ranged. In such a short ranged singlet dimer state, they decay exponentially

$$\langle \mathbf{S}_i \cdot \mathbf{S}_j \rangle \propto e^{-\frac{|\mathbf{r}_i - \mathbf{r}_j|}{\xi}} \tag{1.10}$$

with some correlation length ξ. These states are not true QSL because they lack other defining features. They are not truly *liquid* in the sense that dimer–dimer correlation

functions have long range order. Although there is no generally accepted definition, I follow Misguich in Lacroix et al. (2011) and provide the following useful working definition of a *QSL*:

A QSL is a state without any spontaneous symmetry breaking at zero temperature, with decaying spin correlations, $\langle \mathbf{S}_i \cdot \mathbf{S}_j \rangle \to 0$ *for* $|\mathbf{r}_i - \mathbf{r}_j| \to \infty$*, and with fractional excitations.*

The inclusion of *fractional excitations* is crucial in the definition and entails a number of exotic properties of QSL, which are explained in the remainder of the section. Spins in a QSL are highly entangled due to coherent quantum fluctuations giving rise to *topological order* intimately connected to emergent *gauge fields* and *fractionalization* (Wen 1991, 2004).

In the following, I give a brief introduction into the physics of QSLs by introducing quantum dimer models (QDM). They can be thought of as effective models in the short range singlet dimer subspace with quantum fluctuations which resonate between different singlet dimer arrangements. QDM provide the simplest setting for the realization of QSL phases motivated by the RVB idea (Anderson 1973). Anderson observed that spin disordered wave functions are in principle possible ground states of frustrated two dimensional lattices (Anderson 1973). As an example he suggested as ground states

$$|\Phi_{\text{g.s.}}\rangle = \sum_c \Phi(c)|c\rangle \tag{1.11}$$

a coherent superposition of possible dimer coverings $|c\rangle$ on a lattice. The dimers are made up of (local) singlets $|ij\rangle = \frac{1}{\sqrt{2}}\left(|\uparrow_i\downarrow_j\rangle - |\downarrow_i\uparrow_j\rangle\right)$ which minimize the energy of the Heisenberg coupling between two spins $\langle ij|\mathbf{S}_i \cdot \mathbf{S}_j|ij\rangle = -\frac{3}{4}$. More recently this RVB physics (Anderson 1987) was extensively studied after the discovery of high temperature superconductivity in the cuprates (Bednorz and Muller 1986). Their parent materials were conjectured to be in a QSL phase which becomes superconducting when charge carriers are introduced by doping (Baskaran and Anderson 1988), for a review see Lee et al. (2006).

In connection to cuprates effective QDM were introduced, which model gapped short ranged RVB liquids with sites $\langle i, j\rangle$ restricted to N.N. (Rokhsar and Kivelson 1988). The original derivation was on the square lattice by restricting the Heisenberg Hamiltonian to the N.N. singlet dimer subspace (Rokhsar and Kivelson 1988). Unfortunately, it turns out that except for a special point the square lattice has a crystalline ground state arrangement of dimers similar to Fig. 1.3a and is not a true liquid.

The first example of a model with a short ranged RVB liquid phase is given by the QDM on the triangular lattice (Moessner and Sondhi 2001). I explain the main concepts of a QSL, including fractionalization and topological order, with this influential example. For additional details, the interested reader is referred to the pedagogical introduction in Moessner and Sondhi (2002). The Hamiltonian of the QDM on the triangular lattice is given by

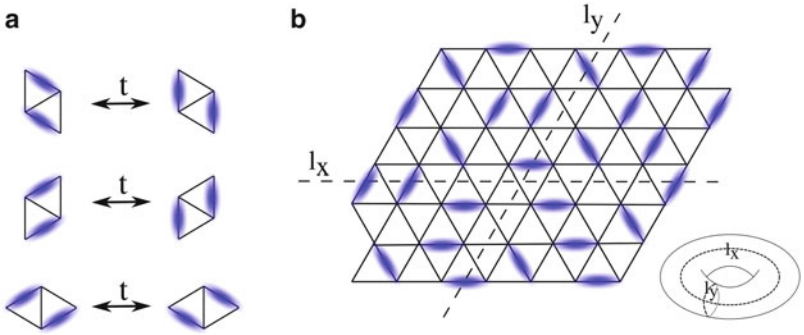

Fig. 1.4 Left panel (**a**) shows the three valence bond resonances of the quantum dimer model on the triangular lattice, Eq. (1.12). Panel (**b**) explains the partitioning of the QSL ground states into topological sectors by showing the two reference lines l_x, l_y (*dashed*) which wrap around the torus (*right bottom*) of the triangular lattice with periodic boundary conditions. The parities of the number of dimers crossing the reference lines are invariant under local transformations, e.g. the resonance moves of panel (a), thereby labeling the degenerate ground states

$$\mathcal{H}_{\text{QDM}} = \sum_{i=1}^{N_p} \left\{ -t \sum_{\alpha=1}^{3} \left(|\boxtimes\rangle\langle\boxtimes| + h.c. \right) + v \sum_{\alpha=1}^{3} \left(|\boxtimes\rangle\langle\boxtimes| + |\boxtimes\rangle\langle\boxtimes| \right) \right\} \tag{1.12}$$

with a sum i over all plaquettes N_p and α over the three different orientations shown in Fig. 1.4a. The first kinetic term describes a resonance between different dimer configurations and the second term introduces an energy penalty for flippable plaquettes. At the special Rokhsar–Kivelson (RK) point $v = t$ the ground state wave function is given by

$$|\Phi_{\text{g.s.}}^{\text{RK}}\rangle = \sum_{c}{}' |c\rangle \tag{1.13}$$

an equal amplitude superposition of all dimer coverings in a given *sector*, a term which is described below. This state does not have any local order, e.g. all spin and dimer correlation functions are short ranged. It was shown that this disordered phase persists for a finite parameter region $v/t < 1$ being a true QSL phase which harbors fractionalized excitations.

A simplified example of fractionalization was given at the end of the last section in which a triplet state can be separated into arbitrarily far apart spinons carrying spin $1/2$, see Fig. 1.3b. Note that for the extended $J_1 - J_2 - K$ model the picture is oversimplified since in such a regular dimer setting, or VBC, spinons are connected by a string of defects, which in general has a finite tension such that the two spinons cannot be separated far apart; they are *confined*. For the extended $J_1 - J_2 - K$ model

the string of rotated dimers does not cost energy only at the special fine-tuned and fully frustrated point. In addition, even there spinons can only move along the 1D diagonal directions and are otherwise confined.

In the triangular lattice QDM excitations are truly fractionalized via the same mechanism of breaking a dimer. However, now the two spinons from a broken singlet dimer can be separated without leaving a costly string or domain wall behind because of the disordered dimer background with exponentially decaying dimer correlations (Moessner and Sondhi 2001). It means that their separation to infinity costs only a finite amount of energy—a phenomenon known as *deconfinement*. In a similar fashion the model with a low density of holes exhibits spin-charge separation because holons and spinons are also deconfined.

In 1D systems spinons appear naturally as domain walls between ordered clusters (Tennant et al. 1995). Hence, the boundary of the string between two spinons is only given by the two endpoints of the wall, which only cost a finite amount of energy. In that sense fractionalization is much more natural in 1D. In a true QSL in 2D, it is the macroscopic superposition of a large number of dimer coverings from strong quantum fluctuations which makes the string between two separated spinons tensionless. More precisely, the difference in energy of a pair of N.N. spinons, $E(0)$, and the one of two separated spinons, $E(|\mathbf{r}|)$, is not divergent as the separation $|\mathbf{r}|$ goes to infinity, i.e. $\lim_{|\mathbf{r}|\to\infty} [E(|\mathbf{r}|) - E(0)] < \infty$. In essence, the string of rearranged dimers between two spinons only reshuffles dimer configurations which are already part of the ground state, hence it does not cost much energy (Balents 2010).

A final key concept for QSLs is *topological order* (Wen 1991), which was first introduced in the context of the FQHE (Wen and Niu 1990). Here, I will only give a brief account of the basic idea in connection with QSLs, for an extensive discussion see Wen (2004). A commonly accepted definition is the following:

In the absence of any symmetry breaking, topological order refers to a phase in which the number of degenerate ground states depends on the topology of the manifold, or its genus g, on which it is realized.

Again, as a pedagogical example of a topologically ordered phase, I will show that the ground state degeneracy of the triangular QDM depends on the genus of the underlying lattice. QDM are associated with hard constraints, namely that each site forms a dimer with one and only one of its N.N. sites. This has important consequences because locally changing a dimer configuration requires most of the time reordering of a number of other dimers. In fact, by only considering local plaquette flips, such as the kinetic term in the Hamiltonian, Eq. (1.12), one can show that there are loop operators which remain invariant. Therefore, one can separate the possible QSL ground states into different sectors which are not connected by any local plaquette flips but only by global flips.

In particular, consider the two reference lines l_x, l_y of the triangular lattice with periodic boundary conditions shown in Fig. 1.4b. A *sector* is defined by the two winding numbers $(W_x, W_y) = (-1^{n_x}, -1^{n_y})$ with n_x, n_y counting the number of dimers which intersect the lines l_x, l_y. Each sector gives rise to a ground state wave function, approximately Eq. (1.13). Hence, the ground state degeneracy for

the triangular lattice on the torus is 4. More generally, the ground state degeneracy is 2^{2g} for surfaces with genus g ($g = 0, 1$ for the sphere and the torus). The entirely new aspect of topological order is the fact that there is no local operator which can possibly detect the sector of the ground state. No local order parameter can account for the ground state degeneracy, and therefore, Landau theory is not applicable.

There is a close link between the presence of fractionalized excitations and topological order. This can be seen by observing that breaking a dimer into two spinons and moving one of them around the torus, e.g. around l_x, changes the corresponding winding number, W_x, and connects different topological sectors. This gives rise to an exponentially small energy splitting $\Delta E_0 \propto e^{-cL}$ of the ground states depending on the size of the system, L, and some constant c.

Finally, I want to mention the important concept of an *emergent gauge field description* of QSLs. The disordered ground state of the triangular lattice QDM is known as a Z_2 QSL because the effective theory describing interactions between its elementary excitations is a Z_2 gauge theory (Wen 1991). Other types of spin liquids give rise to other gauge theories, for details see the chapter by Misguich in Lacroix et al. (2011). In the current example, apart from gapped spinons the second elementary excitation of this short ranged RVB state is also gapped and called a *vison*. It can be approximated by a variational wave which is given by $|\Phi^{\mathrm{RK}}_{\mathrm{g.s.}}\rangle$ with additional Z_2 phase factors ± 1 for the dimer configurations entering the sum, see chapter of Moessner and Kaman in Lacroix et al. (2011). In the context of the Kitaev honeycomb lattice model (Chap. 2), a similar excitation and a connected gauge field description appears.

After having introduced the basic concepts, in the following I address a key question related to the realization of topologically ordered phases. How can a QSL be diagnosed in experiments?

1.3 Signatures and Dynamics of Unconventional Magnets

A good starting point for the identification of a QSL candidate material is to look for an unusual behavior in thermodynamic measurements, e.g. the magnetic susceptibility $\chi = \frac{\partial M}{\partial H}_{H\to 0}$, with H describing the external magnetic field. For standard ferromagnetic (FM) and antiferromagnetic materials a simple mean-field calculation, which is usually a good description away from the critical point $T_c \ll T$ where fluctuations are less important, gives $\chi \propto \frac{1}{T-\Theta_{\mathrm{CW}}}$ with a Curie–Weiss temperature $\Theta_{\mathrm{CW}} > 0$ for FM and $\Theta_{\mathrm{CW}} < 0$ for AF interactions between the spins. The standard behavior of the inverse susceptibility $1/\chi(T)$ for ordinary AF magnets is shown in Fig. 1.5a. Their actual ordering temperature is close to the Curie–Weiss temperature, $T_c \approx |\Theta_{\mathrm{CW}}|$. In frustrated magnets a large number of thermal and/or quantum fluctuations prevent ordering around $|\Theta_{\mathrm{CW}}|$, but unfortunately most compounds eventually do order at some $T_c \ll |\Theta_{\mathrm{CW}}|$, see Fig. 1.5b for a typical behavior. However, the observation of a large frustration parameter $f = \frac{|\Theta_{\mathrm{CW}}|}{T_c} > 100$

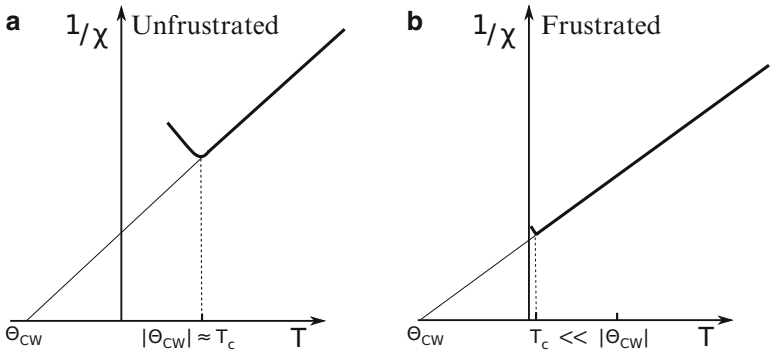

Fig. 1.5 The schematic evolution of the inverse magnetic susceptibility $1/\chi$ is shown as a function of temperature T. Left panel (**a**), in a standard unfrustrated AF magnet the magnetic ordering temperature T_c and the Curie–Weiss temperature $|\Theta_{\mathrm{CW}}|$ are similar. In a frustrated magnet, panel (**b**), order is strongly suppressed by fluctuations such that $T_c \ll |\Theta_{\mathrm{CW}}|$

is a good indication of a strongly frustrated material (Obradors et al. 1988; Ramirez 1994) providing a promising starting point for finding a QSL.

To narrow down the possibilities other thermodynamic measurements probing the low energy density of states are helpful. Even in unfrustrated low dimensional systems long range magnetic order is suppressed as a consequence of the Mermin-Wagner theorem (Chaikin and Lubensky 2000), which states that in strictly 1D and 2D isotropic systems long wavelength fluctuations prevent any ordering at finite temperatures. Even though real materials always display some kind of weak anisotropy and three dimensionality, thus, violating the assumptions of the theorem, fluctuations push the ordering to lower temperatures. However, frustrated systems do have a much higher density of low energy fluctuations as compared to unfrustrated ones, which can be observed as an unusually large specific heat at low temperatures, see, e.g., Ramirez et al. (1990). After such an observation, nuclear magnetic resonance (NMR) could be used to proof the absence of static moments, and thereafter thermal transport reveals mobility of the low energy excitations.

In the remainder, I want to concentrate on INS whose cross section in principle has access to the full dynamical spin structure factor (Lovesey 1984)

$$\frac{d^2\sigma}{d\Omega dE} \propto S^{ab}(\mathbf{q},\omega) \tag{1.14}$$

with $S^{ab}(\mathbf{q},\omega) = \frac{1}{N}\sum_{\mathbf{R}_i,\mathbf{R}_j} e^{-i\mathbf{q}(\mathbf{R}_i-\mathbf{R}_j)} \int_{-\infty}^{\infty} dt e^{i\omega t} \langle S^a(\mathbf{R}_i,t) S^b(\mathbf{R}_j,0)\rangle$, see chapter of Bramwell in Lacroix et al. (2011). Especially in single crystals it provides detailed information about dynamical spin correlations and the nature of the excitations. In general, dynamical response functions have the advantage that they provide access to the full excitation spectrum beyond the low energy properties probed, e.g., by thermodynamic measurements. In close comparison with theoretical predictions these experiments are able to diagnose the presence of QSL phases.

For a better understanding what unconventional INS signals look like, it is instructive to contrast them with the ones of standard magnets. First, I begin with experimental signatures of AF ordered materials, e.g. parent compounds of high temperature superconductors. Next, I go to more exotic behavior by showing a recent comparison of an INS experiment with an exact theoretical calculation for a spin chain compound which establishes the presence of fractional spinon excitations in 1D. Finally, I end with latest experimental results for higher dimensional QSL candidate materials which provide an excellent motivation for the objective of this thesis.

1.3.1 Spin Waves in High Temperature Superconductors

In systems with AFM order the single spin flip of a scattering neutron (a $S = 1$ excitation) directly probes coherent magnon excitations (also $S = 1$ excitations), which are the Goldstones modes of the symmetry broken state. In Fig. 1.6 two INS cross sections are shown for two parent high temperature superconductors. A key signature of long range order is the appearance of sharp dispersive modes with largest intensity at the AFM wave vector.

In the left panel (a), experimental data points of sharp excitations in energy and momentum are shown along a path in the BZ for the parent cuprate La_2CuO_4

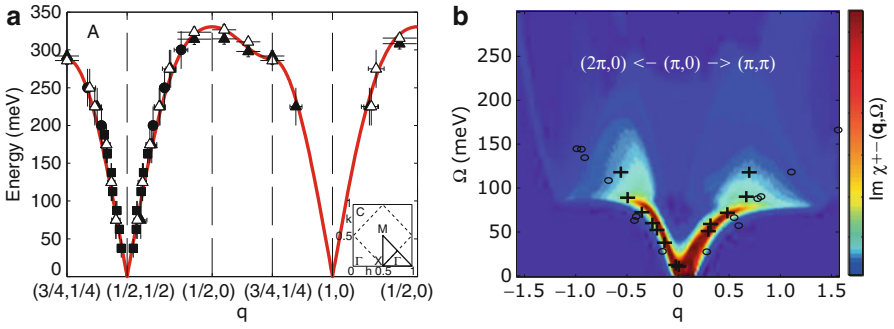

Fig. 1.6 The results of INS experiments are shown together with theoretical calculations for two different high T_c superconducting parent compounds with long range magnetic order. In the left panel (**a**), for the insulating parent cuprate La_2CuO_4 with an N.N. Néel state, a closed spin wave branch can be measured in the entire BZ (plotted along a path), adapted from Coldea et al. (2001). A linear spin wave theory calculation of a Heisenberg-like model (*red*) can account for the spectrum. In panel (**b**), an intensity plot of $S(\mathbf{q}, \omega)$ from a theoretical calculation of an itinerant model (with spin and charge d.o.f.) is plotted around the magnetic ordering wave vector $\mathbf{q} = (\pi, 0)$ for parent iron based superconductors (Knolle et al. 2010) with the INS data for $CaFe_2As_2$ (Diallo et al. 2009) (*crosses*) and (Zhao et al. 2009) (*circles*). Because of the metallic nature of the parent compounds coherent spin waves are quickly overdamped by particle-hole excitations away from the ordering wave vector

(Coldea et al. 2001). The magnetic state of the square lattice of copper atoms is a simple N.N. Néel state with an ordering wave vector $\mathbf{q} = (\pi, \pi)$ (which is (1/2,1/2) in the experimental notation). The INS signal of this insulating magnet consists of sharp dispersive spin wave branches inside the charge gap with a linear dispersion around the ordering wave vector $\mathbf{q} = (\pi, \pi)$ and around $\mathbf{q} = (0, 0)$. The red line is a theoretical calculation of a Heisenberg model based on a simple spin wave calculation via Holstein–Primakoff bosons, which captures the entire dispersing branch (Coldea et al. 2001). Note that in order to fit the dispersion away from the ordering vector, interactions beyond N.N. are necessary. Hence, non-universal high-energy features accessible in INS are used to refine the relevant Heisenberg model and to extract values of the exchange constants.

In the left panel (b), again sharp dispersive spin wave modes appear in the intensity plot of $S(\mathbf{q}, \omega)$ around the magnetic ordering wave vector $\mathbf{q} = (\pi, 0)$ for parent iron based superconductors (Knolle et al. 2010). The magnetic ground state of these layered materials with a square lattice of iron atoms consists of ferromagnetic iron chains aligned antiferromagnetically. Experimental data points are plotted on top of the theoretical calculation from two independent INS experiments (Diallo et al. 2009) (crosses) and (Zhao et al. 2009) (circles) for the parent compound $CaFe_2As_2$. For these materials coherent excitations are only seen around the ordering wave vector because the parent compounds are not insulating. Particle-hole excitations across the Fermi surface quickly overdamp the spin waves, which is captured in the theoretical calculation by taking into account the full spin and charge degrees of freedom of the electrons. In the case of parent compounds of iron based high temperature superconducting materials, a close comparison between theory and INS experiments has established the itinerant nature of the spin waves and has accounted for the difference in spin wave velocities in the two crystallographic directions.

1.3.2 Spinon Continuum in Spin Chains

In 1D Heisenberg systems strong quantum fluctuations prevent magnetic long range order down to zero temperature and the ground state has total $S_{\text{tot}} = 0$ (Auerbach 1994). For spin $1/2$ chains, the low energy excitations are spinons which appear as domain walls between ordered segments. In neutron scattering always even numbers of spinons are created because the induced spin flip of the neutron changes the total spin by $S = 1$ and spinons carry $S = 1/2$. Therefore a continuum of excitations is expected with sharp boundaries along the linearly dispersing onset (Tennant et al. 1995).

Figure 1.7 shows the INS results for the 1D spin chain compound $CuSO_4 \cdot 5D_2O$ (left going branch) together with an exact calculation (right going branch) of the corresponding Heisenberg model (Mourigal et al. 2013) based on the Bethe–Ansatz solution (Bethe 1931). These calculations, accounting for more than 99 % of the total spectral weight, confirm the presence of the spinon continuum. In addition, a

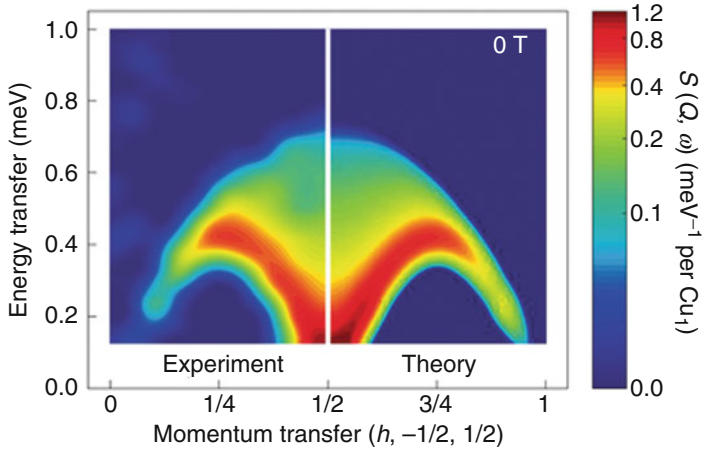

Fig. 1.7 The INS results (*left branch*) of for the Heisenberg spin chain compound $CuSO_4 \cdot 5D_2O$ are shown together with an exact calculation (*right branch*) based on the Bethe–Ansatz, adapted from Mourigal et al. (2013). The latter accounts for more than 99 % of the total weight, thereby confirming the presence of spinon excitations

close comparison with the experimental data reveals that two-spinon excitations only account for 71 % of the total weight and the rest arises from four- or higher-spinon excitations. Note that even in this 1D model with a long existing exact solution, the calculation of the structure factor only has become possible in recent years because the calculation of the necessary matrix elements is a highly demanding task (Caux 2009).

In general, high energy features are less universal than characteristic low energy properties. The latter are universal because they can be described by effective low energy field theories (Cardy 1996; Goldenfeld 1992), which are insensitive to microscopic details. For example, in the case of 1D spin chains similar to the one above, only the sharp linear onset of the spectrum together with the low energy continuum is universal. Nevertheless, the characteristic high energy behavior is extremely useful for determining the correct description and for confirming the presence of spinon excitations.

1.3.3 Neutron Scattering Results for Candidate Spin Liquids

Finally, I discuss recent INS results for a spin-disordered insulating magnet in more than one dimension. This is very rare because most frustrated magnetic materials eventually do show some kind of magnetic order at low enough temperatures albeit with a large frustration parameter f. For example, the honeycomb iridate Na_2IrO_3 was conjectured to be QSL described by the Kitaev model (Jackeli and Khaliullin

2009), see Sect. 2.3. However, susceptibility (Singh et al. 2012) and X-ray scattering experiments (Liu et al. 2011) have shown that the system develops 3D magnetic order below $T_c = 15\,\mathrm{K}$ with a frustration parameter of only $f \approx 10$. Subsequent INS experiments confirmed this picture and were used to distinguish between different candidate magnetic ground states which are close in energy because of frustration (Choi et al. 2012).

The spin 1/2 kagome-lattice antiferromagnet $ZnCu_3(OD)_6Cl_2$, which is known as *Herbertsmithite*, is one of the most promising candidate materials for the realization of a QSL. It does not show any signs of magnetic ordering down to $T = 50\,\mathrm{mK}$ (Mendels et al. 2007) but has a large Curie–Weiss temperature $|\Theta_{CW}| \approx 300\,\mathrm{K}$. The N.N. Heisenberg model on the kagome lattice is thought to be a good description of the low energy physics (Han et al. 2012). Indeed numerical computations indicate that its ground state is a gapped Z_2 spin liquid (Yan et al. 2011). Its properties are currently investigated (Depenbrock et al. 2012), but overall no conclusion even about the presence of a gap in the excitation spectrum has been reached (Iqbal et al. 2014).

Figure 1.8 shows the INS cross section for Herbertsmithite along a path in the BZ versus energy (left panel) and the energy integrated response over several BZs (right panel) (Han et al. 2012). The main feature to observe is the total absence of sharp modes or coherent excitations. The whole spectrum forms a continuum attributed to the presence of spinon excitations. Surprisingly, no spin gap is observed and the inferred structure factor cannot be explained by existing theories (Han et al. 2012). First phenomenological calculations point to a strong influence of vizon excitations on the structure factor of a Z_2 QSL in addition to spinon excitations (Punk et al. 2014).

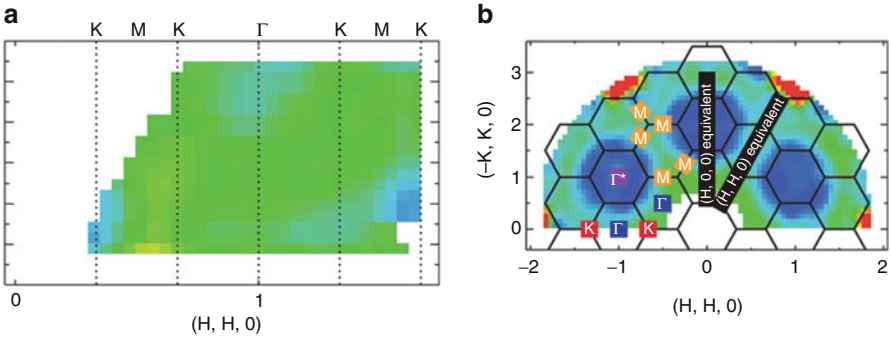

Fig. 1.8 The dynamic structure factor as measured by INS is shown for the kagome lattice antiferromagnet Herbertsmithite, which shows no sign of magnetic ordering down to $T = 50\,\mathrm{mK}$; figure adapted from Han et al. (2012). In the left panel (**a**), only a broad continuum is observed along a path through the BZ versus energy. In the right panel (**b**), features of the broad scattering are seen over the entire BZ integrated over a fixed energy range. The absence of sharp modes and boundaries is taken as strong evidence that the response arises from spinon excitations of a QSL

1.4 Thesis Outline

Clearly these experimental results call for detailed and controlled theoretical investigations. Due to the absence of reliable approximations beyond 1D, e.g. for the Heisenberg model on the kagome lattice, the task remains a big and open challenge. My thesis aims to provide such a complete analysis for a model in 2D. The availability of a full and exact calculation of a dynamical spin structure factor for an exactly solvable model can guide future experimental investigations and can serve as a benchmark for theoretical approximations.

The thesis is devoted to the Kitaev honeycomb lattice model and to a study of its dynamical correlation functions measurable in standard experiments. In Chap. 2, I introduce the Kitaev model. I explain in detail the exact solution in terms of Majorana fermions and discuss a possible experimental realization in Iridium based materials.

Chapter 3 is focused on the calculation of the dynamical spin correlations and the corresponding structure factor. It is shown that spin correlations are ultra short ranged and that the calculation takes the form of a quantum quench. In addition to an approximate treatment expanding in different number of particle states, I present two complementary exact solutions. The first one gives results for finite size systems and is based on the evaluation of Pfaffians. The second one allows to obtain results in the thermodynamic limit. It is based on the theory of singular integral equations exploiting connections to the so-called X-ray edge problem.

In Chap. 4, I show the results of my analysis in different gapped and gapless phases of the Kitaev model. The calculated structure factor has characteristic features which can be related to the emergent fractionalized excitations of the Kitaev QSL.

Having investigated the exact spin correlations in the original Kitaev model, Chap. 5 investigates those in an extended Kitaev model. The addition of a time reversal symmetry breaking three spin interaction leaves the exact solubility and the mapping of the spin correlations to a quantum quench intact, but leads to a new QSL phase with non-Abelian quasiparticles. I discuss the special role of flux excitations in this phase which locally bind Majorana fermions. I show that peculiar signatures of these bound states are manifest in the spin structure factor. I close the chapter with a brief investigation of exchange disorder and its influence on the structure factor.

In Chap. 6, I calculate the inelastic Raman scattering response of the Kitaev model with an additional small Heisenberg term which breaks the integrability. I show that signatures of fractionalization, a hallmark of a topologically ordered phase, are visible in the response. Even for very weak integrability breaking the change in the response is remarkable, revealing basic properties of the underlying phase by connecting otherwise orthogonal sectors. Hence, Raman scattering presents a valuable alternative experimental tool for diagnosing QSLs.

Finally in Chap. 7, I summarize the results and present my conclusions. Overall, this dissertation shows that dynamical response functions provide a valuable tool for diagnosing QSLs in candidate materials. I close the thesis with some open questions and with a discussion of promising directions for future research.

References

P. Anderson, Resonating valence bonds: a new kind of insulator? Mater. Res. Bull. **8**(2), 153–160 (1973)

P.W. Anderson, The resonating valence bond state in La2CuO4 and superconductivity. Science **235**(4793), 1196–1198 (1987)

A. Auerbach, *Interacting Electrons and Quantum Magnetism*. Graduate Texts in Contemporary Physics (Springer, New York, 1994)

M.N. Baibich, J.M. Broto, A. Fert, F.N. Van Dau, F. Petroff, P. Etienne, G. Creuzet, A. Friederich, J. Chazelas, Giant magnetoresistance of (001)Fe/(001)Cr magnetic superlattices. Phys. Rev. Lett. **61**(21), 2472–2475 (1988)

L. Balents, Spin liquids in frustrated magnets. Nature **464**(7286), 199–208 (2010)

J. Bardeen, L.N. Cooper, J.R. Schrieffer, Theory of superconductivity. Phys. Rev. **108**(5), 1175–1204 (1957)

G. Baskaran, P.W. Anderson, Gauge theory of high-temperature superconductors and strongly correlated Fermi systems. Phys. Rev. B **37**(1), 580–583 (1988)

C.D. Batista, S.A. Trugman, Exact ground states of a frustrated 2D magnet: deconfined fractional excitations at a first-order quantum phase transition. Phys. Rev. Lett. **93**(21), 217–202 (2004)

J. Bednorz, K. Muller, Possible high Tc superconductivity in the Ba-La-Cu-O system. Z. Phys. B Condens. Matter **64**(2), 189–193 (1986)

H. Bethe, Zur theorie der metalle (German). Z. Phys. **71**(3–4), 205–226 (1931)

J. Cardy, *Scaling and Renormalization in Statistical Physics*. Cambridge Lecture Notes in Physics (Cambridge University Press, Cambridge, 1996)

J.-S. Caux, Correlation functions of integrable models: a description of the ABACUS algorithm. J. Math. Phys. **50**(9), 095214 (2009)

P. Chaikin, T. Lubensky, *Principles of Condensed Matter Physics* (Cambridge University Press, Cambridge, 2000)

P. Chandra, B. Doucot, Possible spin-liquid state at large S for the frustrated square Heisenberg lattice. Phys. Rev. B **38**(13), 9335–9338 (1988)

S.K. Choi, R. Coldea, A.N. Kolmogorov, T. Lancaster, I.I. Mazin, S.J. Blundell, P.G. Radaelli, Y. Singh, P. Gegenwart, K.R. Choi, S.-W. Cheong, P.J. Baker, C. Stock, J. Taylor, Spin waves and revised crystal structure of honeycomb iridate Na2IrO3. Phys. Rev. Lett. **108**(12), 127204 (2012)

A.V. Chubukov, T. Jolicoeur, Dimer stability region in a frustrated quantum Heisenberg antiferromagnet. Phys. Rev. B **44**(21), 12050–12053 (1991)

R. Coldea, S.M. Hayden, G. Aeppli, T.G. Perring, C.D. Frost, T.E. Mason, S.-W. Cheong, Z. Fisk, Spin waves and electronic interactions in La2CuO4. Phys. Rev. Lett. **86**(23), 5377–5380 (2001)

L. Cooper, D. Feldman, *BCS: 50 Years* (World Scientific, Singapore, 2011)

K.B. Davis, M.O. Mewes, M.R. Andrews, N.J. van Druten, D.S. Durfee, D.M. Kurn, W. Ketterle, Bose-Einstein condensation in a gas of sodium atoms. Phys. Rev. Lett. **75**(22), 3969–3973 (1995)

S. Depenbrock, I.P. McCulloch, U. Schollwöck, Nature of the spin-liquid ground state of the S=1/2 Heisenberg model on the kagome lattice. Phys. Rev. Lett. **109**(6), 067201 (2012)

S.O. Diallo, V.P. Antropov, T.G. Perring, C. Broholm, J.J. Pulikkotil, N. Ni, S.L. Bud'ko, P.C. Canfield, A. Kreyssig, A.I. Goldman, R.J. McQueeney, Itinerant magnetic excitations in antiferromagnetic CaFe2As2. Phys. Rev. Lett. **102**(18), 187206 (2009)

A. Einstein, *Quantentheorie des einatomigen idealen Gases* (Verlag der Königlich-Preussischen Akademie der Wissenschaften, 1924), pp. 261–267. http://echo.mpiwg-berlin.mpg.de/ECHOdocuView?url=/permanent/echo/einstein/sitzungsberichte/PG8B073X/index.meta

N. Goldenfeld, *Lectures on Phase Transitions and the Renormalization Group* (Addison-Wesley, Advanced Book Program, Reading, 1992)

T.-H. Han, J.S. Helton, S. Chu, D.G. Nocera, J.A. Rodriguez-Rivera, C. Broholm, Y.S. Lee, Fractionalized excitations in the spin-liquid state of a kagome-lattice antiferromagnet. Nature **492**(7429), 406–410 (2012)

R. Hildyard, *European Ceramics*. V & A decorative Arts Series (University of Pennsylvania Press, Philadelphia, 1999)

Y. Iqbal, D. Poilblanc, F. Becca, Vanishing spin gap in a competing spin-liquid phase in the kagome Heisenberg antiferromagnet. Phys. Rev. B **89**(2), 020407 (2014)

G. Jackeli, G. Khaliullin, Mott insulators in the strong spin-orbit coupling limit: from Heisenberg to a quantum compass and Kitaev models. Phys. Rev. Lett. **102**(1), 017205 (2009)

L. Kadanoff, Scaling laws for Ising models near T_c. Physics **2**, 263–272 (1966)

A.Y. Kitaev, Fault-tolerant quantum computation by anyons. Ann. Phys. **303**(1), 2–30 (2003)

C. Kittel, *Quantum Theory of Solids* (Wiley, New York, 1963)

J. Knolle, I. Eremin, A.V. Chubukov, R. Moessner, Theory of itinerant magnetic excitations in the spin-density-wave phase of iron-based superconductors. Phys. Rev. B **81**(14), 140506 (2010)

C. Lacroix, P. Mendels, F. Mila, *Introduction to Frustrated Magnetism: Materials, Experiments, Theory*. Springer Series in Solid-State Sciences (Springer, Berlin, 2011)

R.B. Laughlin, Anomalous quantum hall effect: an incompressible quantum fluid with fractionally charged excitations. Phys. Rev. Lett. **50**(18), 1395–1398 (1983)

P.A. Lee, N. Nagaosa, X.-G. Wen, Doping a Mott insulator: physics of high-temperature superconductivity. Rev. Mod. Phys. **78**(1), 17–85 (2006)

X. Liu, T. Berlijn, W.-G. Yin, W. Ku, A. Tsvelik, Y.-J. Kim, H. Gretarsson, Y. Singh, P. Gegenwart, J.P. Hill, Long-range magnetic ordering in Na_2IrO_3. Phys. Rev. B **83**(22), 220403 (2011)

S. Lovesey, *Theory of Neutron Scattering from Condensed Matter*. International Series of Monographs on Physics 2 (Clarendon Press, Oxford, 1984)

M.W. McElhinny, *The Earth's Magnetic Field : Its History, Origin, and Planetary Perspective*. International Geophysics (Elsevier Science, Amsterdam, 1984)

P. Mendels, F. Bert, M.A. de Vries, A. Olariu, A. Harrison, F. Duc, J.C. Trombe, J.S. Lord, A. Amato, C. Baines, Quantum magnetism in the paratacamite family: towards an ideal Kagomé lattice. Phys. Rev. Lett. **98**(7), 077204 (2007)

R. Moessner, S.L. Sondhi, Resonating valence bond phase in the triangular lattice quantum dimer model. Phys. Rev. Lett. **86**(9), 1881–1884 (2001)

R. Moessner, S.L. Sondhi, Resonating valence bond liquid physics on the triangular lattice. Prog. Theor. Phys. Suppl. **145**, 37–42 (2002)

M. Mourigal, M. Enderle, A. Kloepperpieper, J.-S. Caux, A. Stunault, H.M. Ronnow, Fractional spinon excitations in the quantum Heisenberg antiferromagnetic chain. Nat. Phys. **9**(7), 435–441 (2013)

C. Nayak, S.H. Simon, A. Stern, M. Freedman, S. Das Sarma, Non-Abelian anyons and topological quantum computation. Rev. Mod. Phys. **80**(3), 1083–1159 (2008)

W.R. Newman, *Atoms and Alchemy: Chymistry and the Experimental Origins of the Scientific Revolution*. Morality and Society Series (University of Chicago Press, Chicago, 2006)

M. Niss, History of the Lenz-Ising model 1965-1971: the role of a simple model in understanding critical phenomena. Arch. Hist. Exact Sci. **65**(6), 625–658 (2011)

X. Obradors, A. Labarta, A. Isalgué, J. Tejada, J. Rodriguez, M. Pernet, Magnetic frustration and lattice dimensionality in $SrCr_8Ga_4O_19$. Solid State Commun. **65**(3), 189–192 (1988)

L. Onsager, Crystal statistics. I. A two-dimensional model with an order- disorder transition. Phys. Rev. **65**(3–4), 117–149 (1944)

R. Peierls, Model-making in physics. Contemp. Phys. **21**(1), 3–17 (1980)

L. Principe, *The Secrets of Alchemy*. Synthesis (University of Chicago Press, Chicago, 2013)

M. Punk, D. Chowdhury, S. Sachdev, Topological excitations and the dynamic structure factor of spin liquids on the kagome lattice. Nat. Phys. **10**(4), 289–293 (2014)

R. Rajaraman, Fractional charge. arXiv:cond-mat/0103366. Unpublished (2001)

A.P. Ramirez, Strongly geometrically frustrated magnets. Annu. Rev. Mater. Sci. **24**(1), 453–480 (1994)

A.P. Ramirez, G.P. Espinosa, A.S. Cooper, Strong frustration and dilution-enhanced order in a quasi-2D spin glass. Phys. Rev. Lett. **64**(17), 2070–2073 (1990)

J. Reuther, P. Wölfle, R. Darradi, W. Brenig, M. Arlego, J. Richter, Quantum phases of the planar antiferromagnetic J_1-J_2-J_3 Heisenberg model. Phys. Rev. B **83**(6), 064416 (2011)

D.S. Rokhsar, S.A. Kivelson, Superconductivity and the quantum hard-core dimer gas. Phys. Rev. Lett. **61**(20), 2376–2379 (1988)

E.F. Shender, Anti-ferromagnetic garnets with fluctuation-like interacting sub-lattices. Zh. Eksp. Teor. Fiz. **83**(1), 326–337 (1982)

Y. Singh, S. Manni, J. Reuther, T. Berlijn, R. Thomale, W. Ku, S. Trebst, P. Gegenwart, Relevance of the Heisenberg-Kitaev model for the honeycomb lattice iridates. Phys. Rev. Lett. **108**(12), 127203 (2012)

D.A. Tennant, R.A. Cowley, S.E. Nagler, A.M. Tsvelik, Measurement of the spin-excitation continuum in one-dimensional $KCuF_3$ using neutron scattering. Phys. Rev. B **52**(18), 13368–13380 (1995)

D.C. Tsui, H.L. Stormer, A.C. Gossard, Two-dimensional magnetotransport in the extreme quantum limit. Phys. Rev. Lett. **48**(22), 1559–1562 (1982)

J. Villain, R. Bidaux, J.-P. Carton, R. Conte, Order as an effect of disorder. J. Phys. France **41**(11), 1263–1272 (1980)

F.J. Wegner, Duality in generalized ising models and phase transitions without local order parameters. J. Math. Phys. **12**(10), 2259–2272 (1971)

X.G. Wen, Mean-field theory of spin-liquid states with finite energy gap and topological orders. Phys. Rev. B **44**(6), 2664–2672 (1991)

X.G. Wen, *Quantum Field Theory of Many-Body Systems: From the Origin of Sound to an Origin of Light and Electrons*. Oxford Graduate Texts (OUP, Oxford, 2004)

X.G. Wen, Q. Niu, Ground-state degeneracy of the fractional quantum Hall states in the presence of a random potential and on high-genus Riemann surfaces. Phys. Rev. B **41**(13), 9377–9396 (1990)

K.G. Wilson, Renormalization group and critical phenomena. I. Renormalization group and the kadanoff scaling picture. Phys. Rev. B **4**(9), 3174–3183 (1971)

S. Yan, D.A. Huse, S.R. White, Spin-liquid ground state of the S = 1/2 Kagome Heisenberg antiferromagnet. Science **332**(6034), 1173–1176 (2011)

J. Zhao, D.T. Adroja, D.-X. Yao, R. Bewley, S. Li, X.F. Wang, G. Wu, X.H. Chen, J. Hu, P. Dai, Spin waves and magnetic exchange interactions in CaFe2As2. Nat. Phys. **5**(8), 555–560 (2009)

Chapter 2
Kitaev's Honeycomb Lattice Model

In this chapter, I introduce Kitaev's honeycomb lattice model (Kitaev 2006) explaining in detail the exact solution in terms of Majorana fermions. The model is a rare example of an exactly solvable interacting quantum model in 2D. It is a representative of a whole class of spin liquids with Majorana fermions coupled to Z_2 gauge fields. As such, it has become the workhorse for model calculations of interacting and topologically ordered systems in 2D. Many aspects have been investigated, e.g., the effect of disorder (Willans et al. 2010, 2011; Lahtinen et al. 2014), the topological ground state degeneracy (Mandal et al. 2012), transitions between different topological phases (Feng et al. 2007; Shi et al. 2009), the fidelity susceptibility (Mukherjee et al. 2012), the defect production after a quench (Sengupta et al. 2008), and the entanglement entropy (Yao and Qi 2010).

One of the beautiful aspects of the model is its simple form:

$$\hat{H} = -J_x \sum_{\langle ij \rangle_x} \hat{\sigma}_i^x \hat{\sigma}_j^x - J_y \sum_{\langle ij \rangle_y} \hat{\sigma}_i^y \hat{\sigma}_j^y - J_z \sum_{\langle ij \rangle_z} \hat{\sigma}_i^z \hat{\sigma}_j^z. \tag{2.1}$$

It consists of spin $1/2$, represented by Pauli matrices $\hat{\sigma}_j^a$, on the vertices of the honeycomb lattice. They only interact via N.N. Ising exchange. The special ingredient crucial for the exact solubility are the directional dependent Ising interactions $\hat{\sigma}_i^a \hat{\sigma}_j^a$,which pick out different components, $a = x, y, z$, depending on the three inequivalent bond directions $\langle ij \rangle_a$ connecting the vertices, see Fig. 2.1 for an illustration. Because of its simple form several proposals exist for an experimental realization (Duan et al. 2003; Micheli et al. 2006; Jackeli and Khaliullin 2009; Chaloupka et al. 2010; Okamoto 2013). I will present one of them at the end of this chapter. Next, I outline the original exact solution in terms of Majorana fermions and static Z_2 fluxes (Kitaev 2006).

J. Knolle, *Dynamics of a Quantum Spin Liquid*, Springer Theses,
DOI 10.1007/978-3-319-23953-8_2

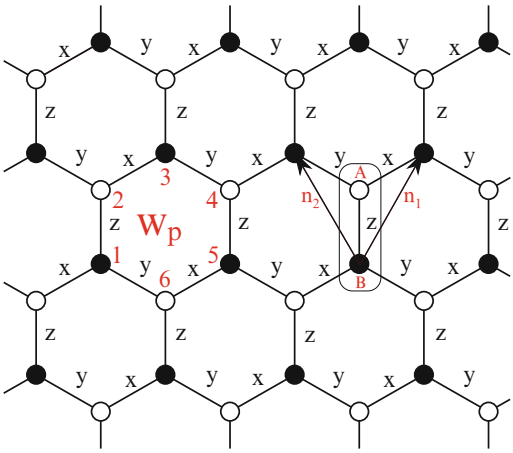

Fig. 2.1 The honeycomb lattice is shown with its three inequivalent bond directions x, y, z. The flux operator W_p, a product of spin operators around a plaquette, is highlighted in *red*. The elementary unit cell consists of two basis sites A and B (*open and full circles*) connected by lattice vectors $\mathbf{n}_1$ and $\mathbf{n}_2$

2.1 Exact Solution and Projection

The remarkable observation of Alexei Kitaev was that a large number of *constants of motion* exist for the model. In fact, for each plaquette p, there exists an operator

$$\hat{W}_p = \hat{\sigma}_1^x \hat{\sigma}_2^y \hat{\sigma}_3^z \hat{\sigma}_4^x \hat{\sigma}_5^y \hat{\sigma}_6^z, \tag{2.2}$$

which is the product of all spins along the six corners of the plaquette with their spin components corresponding to the outwards pointing bond direction, see Fig. 2.1 red. All different plaquette operators commute with each other, $\left[\hat{W}_p, \hat{W}_{p'}\right] = 0$. In addition, they also commute with the entire Hamiltonian $\left[\hat{W}_p, \hat{H}\right] = 0$, thus they are static. Due to the fact that $\hat{W}_p^2 = 1$ the eigenvalues are $\hat{w}_p = \pm 1$. In the following, these Z_2 operators are called *flux operators*. The choice of the name will be clear later on. For $\hat{w}_p = +1$ the plaquette p is *flux free*, for $\hat{w}_p = -1$, it is said that it *has a flux*. The full Hilbert space

$$\mathcal{L} = \bigoplus_{\{\hat{w}_1,\ldots,\hat{w}_N\}} \mathcal{L}_{\{\hat{w}_1,\ldots,\hat{w}_N\}} \tag{2.3}$$

can be separated into all different flux sectors $\mathcal{L}_{\{\hat{w}_p\}}$ for different sets of $\{\hat{w}_1, \ldots, \hat{w}_N\}$ on each plaquette. In a system with N unit cells with periodic boundary conditions, there are $2N$ sites for N different plaquettes. The full Hilbert

space has dimension 2^{2N}, but only 2^N different flux sectors exist. Hence, each sector has still an exponentially large size of 2^N and remains, in general, a challenging problem.

In the last decades different fractionalization techniques have been introduced to capture unconventional magnetic ordering phenomena, in particular for QSLs (Lacroix et al. 2011). Normally, these methods do not permit exact solutions but only provide useful mean-field decoupling schemes of the remaining quartic interaction terms. As such, most often they are uncontrolled approximations. Fortunately, in the case of the Kitaev model a fractionalization in terms of Majorana fermions turns out to be exact. As shown below, this can be traced back to the extensive number of conserved flux operators. In this thesis, I follow the original proposal of Kitaev, in which spins fractionalize into Majorana fermions. It is also possible to use different exact fractionalization techniques, e.g. Jordan–Wigner transformations (Feng et al. 2007; Chen and Nussinov 2008). The relation between the two different transformations is explained in Mandal et al. (2012).

Following Kitaev (2006), I introduce four Majorana fermions

$$c_i, b_i^x, b_i^y, b_i^z \text{ with } \{b_i^a, b_j^{a'}\} = 2\delta_{ij}\delta_{a,a'} \text{ and } \{c_i, c_j\} = 2\delta_{ij} \tag{2.4}$$

($a = x, y, z$) on every lattice site i. These are called *Majorana fermion* operators because similarly to standard complex fermions they anticommute for different indices, but in contrast, they are their own complex conjugate $c_i^\dagger = c_i$ such that their square is unity $c_i^2 = 1$. In fact, they can be thought of as either the real or imaginary part of a standard complex fermion. It is always possible to build a single complex fermion f_i out of two Majorana fermions. For explicit calculations of matrix elements, I always work in standard complex fermionic terms, because only then it is possible to construct a vacuum state which is annihilated by all destruction operators.

The spins are represented in terms of the Majorana fermions

$$\sigma_i^a = ic_i b_i^a, \text{ such that } \left\{\sigma_j^a, \sigma_j^b\right\} = 2\delta_{a,b} \text{ and } \left[\sigma_j^a, \sigma_k^b\right] = 0 \text{ for } j \neq k \tag{2.5}$$

reproduces the standard Pauli spin algebra. The Kitaev Hamiltonian in terms of Majorana fermions is written as

$$H = i \sum_{a,\langle ij\rangle_a} J_a \hat{u}_{\langle ij\rangle_a} c_i c_j \text{ with bond operators } \hat{u}_{\langle ij\rangle_a} \equiv i b_i^a b_j^a, \tag{2.6}$$

which is still quartic in fermion operators. Note, $\hat{u}_{\langle ij\rangle_a} = -\hat{u}_{\langle ji\rangle_a}$ and in the remainder I use the convention that $i \in A$ sublattice and $j \in B$ sublattice.

It turns out that the bond operators have again eigenvalues $u_{\langle ij\rangle_a} = \pm 1$. Hence, the problem can be reduced to a problem of free fermions. All bond operators commute with H and amongst each other such that the Hamiltonian can again be

block diagonalized in different sets of $\{u_{\langle ji\rangle_a}\}$, thereby reducing the Hamiltonian to a quadratic form in fermion operators. Rewriting the flux operators, Eq. (2.2), in terms of Majoranas leads to

$$W_p = u_{21}u_{23}u_{43}u_{45}u_{65}u_{61}. \tag{2.7}$$

The product of all link variables around a plaquette defines the flux sector. From this relation it becomes transparent why the static operators $\hat{W}_p$ are called *fluxes*: A particle moving around a plaquette p picks up a phase $w_p = \pm 1$ similar to an Aharonov–Bohm like flux of either π or 0.

What are the different Hilbert space dimensions? Again, for $2N$ spins the original spin Hamiltonian has dimension 2^{2N}. Expressing the Hamiltonian in terms of four Majoranas enlarges the Hilbert space dimension to 4^{2N}, because each Majorana itself has a nominal dimension of $\sqrt{2}$ which can be seen from the fact that two Majoranas combine into a single complex fermion with dimension 2. To get rid of the artificially enlarged Hilbert space dimensions a constraint needs to be introduced. From the spin algebra of spin 1/2 it follows that $\hat{D}_j = -i\hat{\sigma}_j^x\hat{\sigma}_j^y\hat{\sigma}_j^z = 1$. In terms of Majoranas this reduces to $D_j = b_j^x b_j^y b_j^z c_j$, which has Eigenvalues ± 1 because $D_j^2 = 1$. Note that the hat signals that I work in the original Hilbert space of spin variables, whereas, operators in terms of Majorana fermions in the artificially enlarged Hilbert space come without a hat. A state vector in the physical Hilbert space $|\Phi_{\text{phys}}\rangle$ needs to satisfy $D_j|\Phi_{\text{phys}}\rangle = |\Phi_{\text{phys}}\rangle$ and in general it is necessary to project all states in the enlarged Hilbert space

$$P|\Phi\rangle = \prod_j \frac{1 + D_j}{2}|\Phi\rangle = |\Phi_{\text{phys}}\rangle. \tag{2.8}$$

Observe that all operators D_j commute with H and with all spin operators σ_i^a written in terms of Majorana fermions. The artificially enlarged Hilbert space from the transformation of the spins to Majorana fermions is evident since several sets $\{u_{\langle ji\rangle_a}\}$ give the same flux sector $\{\hat{w}_p\}$. In fact, the transformation leads to an emergent Z_2 gauge theory. At each lattice site a variable $\theta_i = \pm 1$ can be introduced which transforms the Majorana fermions as $c_i \to \theta_i c_i$ and the link variables as $u_{ij} \to \theta_i u_{ij}\theta_j$. This gauge transformation does not change the flux sectors and leaves the energy spectrum within a given flux sector invariant. The $2N$ lattice sites give 2^{2N} different choices for the sets $\{\theta_1, \ldots, \theta_{2N}\}$, thus the 2^{4N} states of H are 2^{2N} fold degenerate.

In the following, I introduce complex fermions in order to clarify the projection onto physical states, Eq. (2.8), and I show that for certain operators $\hat{O}$ the projection is unnecessary because matrix elements $\langle\Phi|POP|\Phi\rangle$=$\langle\Phi|O|\Phi\rangle$ are independent of the projection. The four different Majorana fermions, Eq. (2.5), can be combined into two *complex* fermions, see Fig. 2.2 for an illustration. First, *bond fermions* (Baskaran et al. 2007; Yao et al. 2009)

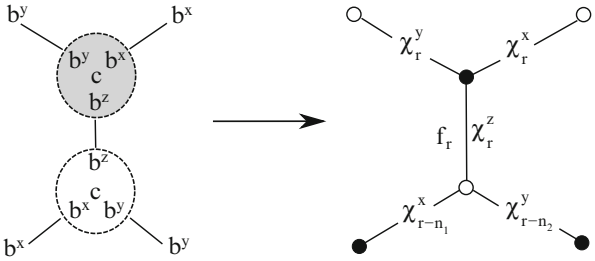

Fig. 2.2 The representation of spins in terms of four Majorana fermions is shown in the *left*. *White* and *grey circles* denote A and B sublattices. On the *right* the corresponding complex *bond fermion* construction is depicted schematically

$$\chi^{\dagger}_{\langle ij\rangle_a} = \frac{1}{2}(b^a_i - ib^a_j) \text{ and } \chi_{\langle ij\rangle_a} = \frac{1}{2}(b^a_i + ib^a_j) \text{ such that}$$
$$\hat{u}_{\langle ij\rangle_a} = 2\chi^{\dagger}_{\langle ij\rangle_a}\chi_{\langle ij\rangle_a} - 1 \tag{2.9}$$

with i on sublattice A and N.N. $\langle ij\rangle_a$ along the bond direction a. The link variables $\hat{u}_{ij}$ are simply related to the occupation number of bond fermions. Note, in a slightly different notation $\mathbf{r}$ is the unit cell coordinate with basis site A and B on the two sublattices, see Fig. 2.2, such that $\left(\chi^a_{\mathbf{r}}\right)^{\dagger} = \chi^{\dagger}_{\langle ij\rangle_a}$ and $\chi^a_{\mathbf{r}} = \chi_{\langle ij\rangle_a}$.

Second, I work with complex *matter fermions*

$$f_{\mathbf{r}} = \frac{1}{2}(c_{A\mathbf{r}} + ic_{B\mathbf{r}}) \text{ and } f^{\dagger}_{\mathbf{r}} = \frac{1}{2}(c_{A\mathbf{r}} - ic_{B\mathbf{r}}) \tag{2.10}$$

which obey the standard anti-commutation relations of fermions. Note, they are also gauge dependent.

The Hilbert space of H, Eq. (2.6), is now a direct product of bond (or gauge) degrees of freedom and matter fermions $|\Phi\rangle = |F\rangle \otimes |M\rangle$ (F for *flux* and M for *matter*). The occupation of $\chi^{\dagger}_{\langle ij\rangle_a}\chi_{\langle ij\rangle_a}|F\rangle = \frac{\hat{u}_{\langle ij\rangle_a}+1}{2}|F\rangle$ determines the flux sector. In a given flux sector with operators $\hat{u}_{\langle ji\rangle_a}$ replaced by their Eigenvalues $u_{\langle ji\rangle_a}$, Eigenstates of the corresponding Hamiltonian H are the matter Eigenstates $|M\rangle$. Note, in principle the notation should distinguish between the Hamiltonian $H_{\hat{u}}$ (dimension 2^{4N}) and H_u (dimension 2^N), similarly $|M\rangle$ should be $|M_\chi\rangle$. However, for simplicity I have omitted the extra labels. Moreover, I will mostly work in the ground states flux sector with all link variables set to $+1$.

Going back to the projection operator, Eq. (2.8), I rewrite the local operator D_i on the two sublattices in terms of complex fermions

$$\begin{aligned} D_{A\mathbf{r}} &= \left[\left(\chi^x_{\mathbf{r}}\right)^{\dagger} + \chi^x_{\mathbf{r}}\right]\left[\left(\chi^y_{\mathbf{r}}\right)^{\dagger} + \chi^y_{\mathbf{r}}\right]\left[\left(\chi^z_{\mathbf{r}}\right)^{\dagger} + \chi^z_{\mathbf{r}}\right]\left[f^{\dagger}_{\mathbf{r}} + f_{\mathbf{r}}\right] \\ D_{B\mathbf{r}} &= \left[\left(\chi^x_{\mathbf{r}-\mathbf{n_1}}\right)^{\dagger} - \chi^x_{\mathbf{r}-\mathbf{n_1}}\right]\left[\left(\chi^y_{\mathbf{r}-\mathbf{n_2}}\right)^{\dagger} - \chi^y_{\mathbf{r}-\mathbf{n_2}}\right]\left[\left(\chi^z_{\mathbf{r}}\right)^{\dagger} - \chi^z_{\mathbf{r}}\right]\left[f^{\dagger}_{\mathbf{r}} - f_{\mathbf{r}}\right] \end{aligned} \tag{2.11}$$

such that the projection operator becomes

$$P = \frac{1 + \sum_{\nu,\mathbf{r}} D_{\nu\mathbf{r}} + \sum_{\nu,\mathbf{r}<\nu',\mathbf{r}'} D_{\nu\mathbf{r}} D_{\nu'\mathbf{r}'} + \cdots \prod_{\nu,\mathbf{r}} D_{\nu\mathbf{r}}}{2^{2N}}. \tag{2.12}$$

Next, I define $D = \prod_j D_j$ and P', which is the sum of all operators in P that change the bond fermion number in a nonequivalent way. Finally, the projection operator, Eq. (2.8), can be factorized into Yao et al. (2009)

$$P = P' \frac{1 + D}{2} = \frac{P' \left[1 + (-1)^{N_\chi + N_f}\right]}{2} \tag{2.13}$$

with N_χ and N_f the total number of bond and matter fermions. The projection operator either annihilates states with odd total fermion number or puts even parity states into a superposition of all nonequivalent bond fermion numbers (Yao et al. 2009).

Finally, I can show that operators $\hat{O}$ which can be arbitrary products of spin operators but which do not change the bond fermion number can be calculated in unprojected states $|\Phi\rangle = |F\rangle \otimes |M\rangle$ (Yao et al. 2009; Baskaran et al. 2007). A concrete example is given by nearest neighbor spin-spin correlators.

$$\langle\Phi|POP|\Phi\rangle = \langle\Phi|OP|\Phi\rangle = \left\langle \Phi \left| O \frac{\left[1 + (-1)^{N_\chi + N_f}\right]}{2} \right| \Phi \right\rangle = \langle\Phi|O|\Phi\rangle. \tag{2.14}$$

In the equation I have used that P commutes with all spin operators and in P' all terms except the identity change the bond fermion number. The last equality is ensured by always working with even total number of fermions, which is always possible by simply changing the gauge in a given flux sector. In the remainder of the thesis I neglect the projection operator because it is unnecessary for the correct calculation of the specific correlation functions in the thermodynamic limit in which I am interested in; see Sect. 6 on Raman scattering in the Kitaev model for an exception, especially Eq. (6.25) .

2.1.1 Relation Between Hamiltonians and Bogoliubov Transformations

In a given flux sector for a particular set of link variables the Hamiltonian in terms of Majorana matter fermions takes the form

$$H = \frac{i}{2} \begin{pmatrix} c_A & c_B \end{pmatrix} \begin{pmatrix} F & M \\ -M^T & -D \end{pmatrix} \begin{pmatrix} c_A \\ c_B \end{pmatrix} \tag{2.15}$$

with the $N \times N$ matrix $M_{ij} = u_{\langle ij\rangle_a} J_a$. Here, c_A/c_B is the shorthand notation of the vector $c_{A\mathbf{r}}/c_{B\mathbf{r}}$ of length N. For the pure Kitaev model, Eq. (2.1), the $N \times N$ next nearest neighbor matrices F_{ij} and D_{ij} are identical zero, but in order to realize a non-Abelian phase they will appear in Chap. 5. For the flux free translationally invariant system $F = D$ even in the non-Abelian phase, but the symmetry between sublattices A and B can be broken explicitly by flux insertion. In fact, Eq. (2.15) is the most general form of a non-interacting Majorana Hamiltonian. In order to be hermitian matrices F and D need to be skew symmetric ($F^T = -F$ and $D^T = -D$) such that the whole Majorana matrix is skew symmetric (Kitaev 2006).

Following Eqs. (2.9) and (2.10), I introduce complex fermions $c_A = f^\dagger + f$ and $c_B = i(f^\dagger - f)$ to obtain

$$H = \frac{1}{2} \begin{pmatrix} f^\dagger & f \end{pmatrix} \begin{pmatrix} h & \Delta \\ \Delta^\dagger & -h^T \end{pmatrix} \begin{pmatrix} f \\ f^\dagger \end{pmatrix} \tag{2.16}$$

with

$$h = (M + M^T) + i(F - D) \tag{2.17}$$

$$\Delta = (M^T - M) + i(F + D). \tag{2.18}$$

The matter Hamiltonian in a given gauge is quadratic in fermions and of the Bogoliubov de-Gennes form, which can be solved exactly. Let T be the unitary transformation that diagonalizes the Hamiltonian (Blaizot and Ripka 1986) with $TT^\dagger = 1$ and

$$T \begin{pmatrix} h & \Delta \\ \Delta^\dagger & -h^T \end{pmatrix} T^\dagger = \begin{pmatrix} E & 0 \\ 0 & -E \end{pmatrix} \tag{2.19}$$

such that the diagonal form reduces to

$$H = \sum_{n>0} E_n a_n^\dagger a_n - \frac{1}{2} \sum_{n>0} E_n \tag{2.20}$$

with positive Eigenvalues E_n. For $N \times N$ sites of each sublattice, F, M, D, h, Δ are $N \times N$ matrices which gives N positive Eigenvalues E_n. Explicitly the Bogoliubov transformations are given by Blaizot and Ripka (1986)

$$\begin{aligned} f_i &= X_{ik}^T a_k + Y_{ik}^\dagger a_k^\dagger \\ f_j^\dagger &= Y_{jl}^T a_l + X_{jl}^\dagger a_l^\dagger \end{aligned} \tag{2.21}$$

with $N \times N$ matrices X,Y and an implicit summation over double indices. The ground state is defined by $a_i|0\rangle = 0$ and its energy is $E_{\text{g.s.}} = -\frac{1}{2}\sum_{n>0} E_n$. Recall that the final spectrum in a given flux sector is independent of a particular gauge.

To find the global minimum of the full Hamiltonian, Eq. (2.6), it is in principle necessary to compare all ground state energies $E_{\text{g.s.}}(\{\hat{w}_p\})$ of all possible flux sectors. Fortunately, it is known that in a translationally invariant system the ground state is flux free (Lieb 1994). I can put, e.g., all $u_{\langle ij\rangle_a} = +1 \overset{\wedge}{_{\langle ij\rangle}}$. This flux state is called $|F_0\rangle$ with the corresponding matter fermion ground state $|M_0\rangle$. Different flux sectors are separated by nonzero energy gaps such that at low enough temperatures it is reasonable to restrict calculations to the lowest flux sector (Kitaev 2006).

Since it will be important later on, I want to clarify how eigenstates of different flux sectors can be related to each other. Let b and a be the operators in which two different flux sectors are diagonal. For definiteness, I assume a system with extra fluxes (sublabel $_F$) and one without fluxes (sublabel $_0$). Each system is diagonalized by its own Bogoliubov transformation

$$\begin{pmatrix} X_0^* & Y_0^* \\ Y_0 & X_0 \end{pmatrix} \begin{pmatrix} f \\ f^\dagger \end{pmatrix} = \begin{pmatrix} a \\ a^\dagger \end{pmatrix} \quad \text{with the inverse} \quad \begin{pmatrix} X_0^T & Y_0^\dagger \\ Y_0^T & X_0^\dagger \end{pmatrix} \begin{pmatrix} a \\ a^\dagger \end{pmatrix} = \begin{pmatrix} f \\ f^\dagger \end{pmatrix}, \tag{2.22}$$

as well as,

$$\begin{pmatrix} X_F^* & Y_F^* \\ Y_F & X_F \end{pmatrix} \begin{pmatrix} f \\ f^\dagger \end{pmatrix} = \begin{pmatrix} b \\ b^\dagger \end{pmatrix} \quad \text{with the inverse} \quad \begin{pmatrix} X_F^T & Y_F^\dagger \\ Y_F^T & X_F^\dagger \end{pmatrix} \begin{pmatrix} b \\ b^\dagger \end{pmatrix} = \begin{pmatrix} f \\ f^\dagger \end{pmatrix}. \tag{2.23}$$

Via these transformations both systems can be related

$$\begin{pmatrix} \mathcal{X}^* & \mathcal{Y}^* \\ \mathcal{Y} & \mathcal{X} \end{pmatrix} \begin{pmatrix} a \\ a^\dagger \end{pmatrix} = \begin{pmatrix} b \\ b^\dagger \end{pmatrix} \tag{2.24}$$

with

$$\begin{pmatrix} \mathcal{X}^* & \mathcal{Y}^* \\ \mathcal{Y} & \mathcal{X} \end{pmatrix} = \begin{pmatrix} X_F^* X_0^T + Y_F^* Y_0^T & X_F^* Y_0^\dagger + Y_F^* X_0^\dagger \\ Y_F X_0^T + X_F Y_0^T & Y_F Y_0^\dagger + X_F X_0^\dagger \end{pmatrix}. \tag{2.25}$$

The ground state of the system with extra fluxes , $b|M_F\rangle = 0$, can be obtained from the ground state of the flux free system, $a|M_0\rangle = 0$, as (Blaizot and Ripka 1986)

$$|M_F\rangle = \det\left(\mathcal{X}^\dagger \mathcal{X}\right)^{\frac{1}{4}} e^{-\frac{1}{2}\mathcal{F}_{ij} a_i^\dagger a_j^\dagger} |M_0\rangle \quad \text{with} \quad \mathcal{F}_{ij} = \left[\mathcal{X}^{*-1}\right]_{il} \mathcal{Y}_{lj}^*. \tag{2.26}$$

From this expression I can read off the overlap of the two ground state wave functions:

$$\langle M_F | M_0 \rangle = \det\left(\mathcal{X}^\dagger \mathcal{X}\right)^{\frac{1}{4}}. \tag{2.27}$$

2.2 Ground State Flux Sector

In the flux free ground state sector, denoted by H_0, the system is translationally invariant, $M_{ij} = +\delta_{\langle ij\rangle_a} J_a$. It can be easily solved by Fourier transformation to momentum space, $f_{\mathbf{q}} = \frac{1}{\sqrt{N}} \sum_{\mathbf{r}} e^{i\mathbf{q}\mathbf{r}} f_{\mathbf{r}}$, such that

$$H_0 = \sum_{\mathbf{q}} \left(f_{\mathbf{q}}^\dagger \, f_{-\mathbf{q}} \right) \begin{pmatrix} \xi_{\mathbf{q}} & -\Delta_{\mathbf{q}} \\ -\Delta_{\mathbf{q}}^* & -\xi_{\mathbf{q}} \end{pmatrix} \begin{pmatrix} f_{\mathbf{q}} \\ f_{-\mathbf{q}}^\dagger \end{pmatrix}. \tag{2.28}$$

The Hamiltonian looks just like a superconductor with a momentum dependent gap $\Delta_{\mathbf{q}} = -i\mathrm{Im}S(\mathbf{q})$ and the *normal state* dispersion $\xi_{\mathbf{q}} = \mathrm{Re}S(\mathbf{q})$. The adjacency matrix is given by $S(\mathbf{q}) = \sum_{\mathbf{n_i}} J_{\alpha(\mathbf{n_i})} e^{i\mathbf{q}\mathbf{n_i}}$ with lattice vectors $\mathbf{n}_z = (0,0)$, $\mathbf{n}_1 = \mathbf{n}_x = \left(\frac{1}{2}, \frac{\sqrt{3}}{2}\right)$ and $\mathbf{n}_2 = \mathbf{n}_y = \left(-\frac{1}{2}, \frac{\sqrt{3}}{2}\right)$, see Fig. 2.1. Since the gap $\Delta_{\mathbf{q}}$ is purely imaginary a simplified Bogoliubov transformation solves the problem (Kitaev 2006)

$$\begin{pmatrix} f_{\mathbf{q}} \\ f_{-\mathbf{q}}^\dagger \end{pmatrix} = \begin{pmatrix} \cos\theta_{\mathbf{q}} & i\sin\theta_{\mathbf{q}} \\ i\sin\theta_{\mathbf{q}} & \cos\theta_{\mathbf{q}} \end{pmatrix} \begin{pmatrix} a_{\mathbf{q}} \\ a_{-\mathbf{q}}^\dagger \end{pmatrix} \tag{2.29}$$

with $\tan 2\theta_{\mathbf{q}} = -\frac{\mathrm{Im}(S)}{\mathrm{Re}(S)}$. Finally, the diagonalized Hamiltonian is given by

$$H_0 = \sum_{\mathbf{q}} |S(\mathbf{q})| (2a_{\mathbf{q}}^\dagger a_{\mathbf{q}} - 1). \tag{2.30}$$

The ground state is a state without fermions, $a_{\mathbf{q}}|M_0\rangle = 0$, and ground state energy $E_{\mathrm{g.s.}} = -\sum_{\mathbf{q}} |S(\mathbf{q})|$. The excitation spectrum $E(\mathbf{q}) = 2|S(\mathbf{q})|$ of fermionic matter excitations $a_{\mathbf{q}}^\dagger|M_0\rangle$ is gapless if $|J_z| < |J_x| + |J_y|$ (and permutations). At the isotropic point, $J_x = J_y = J_z$, the dispersion resembles that of graphene with fermions hopping on the honeycomb lattice, see Fig. 2.3. In this gapless B phase, there are two Dirac points at $\mathbf{Q} = \pm(\frac{2\pi}{3}, -\frac{2\pi}{3})$ (for $J_x = J_y = J_z$) with a linear energy spectrum $E(\mathbf{q}) \propto |\mathbf{q}|$ in their close vicinity, see Fig. 2.3. Once the exchange constants become anisotropic the Dirac points start to move in the Brillouin zone until they merge and annihilate, such that for $|J_z| > |J_x| + |J_y|$ (and permutations) the spectrum is gapped (called *A* phase). The phase diagram is summarized in Fig. 2.4 in a ternary plot with $J_x + J_y + J_z = 1$. Note that in the *B* phase the lowest excitations are matter fermions and flux excitations are gapped. Deep in the *A* phases the situation is reversed, such that the lowest possible excitations are fluxes because the gap of the Majorana spectrum quickly exceeds the flux gap. In fact, in the strong dimer limit $J_x = J_y \ll J_z$ the lowest flux gap, which is the difference in ground state energies with and without a flux pair, vanishes as $\Delta_F \propto \frac{J_x^4}{J_z^3}$ (Kitaev 2006).

After having presented the exact solution for the lowest flux sector, I want to clarify why the ground state of the Kitaev honeycomb model is called a *quantum spin liquid*. In general, the most prominent of the defining features of a QSL is that

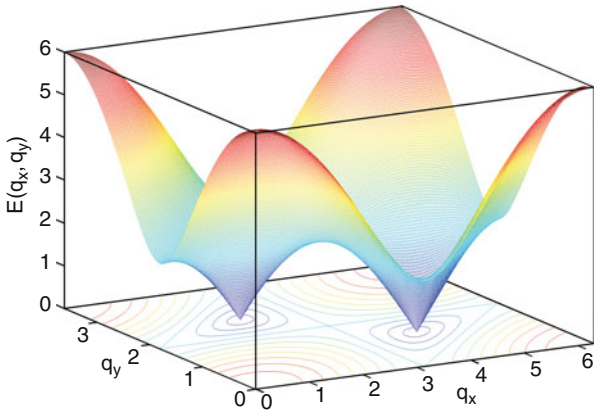

Fig. 2.3 The spectrum $E(\mathbf{q})$ of the matter fermions in the ground state flux sector is shown in the first Brillouin zone. The two Dirac cones lead to a linearly vanishing density of states at low energies

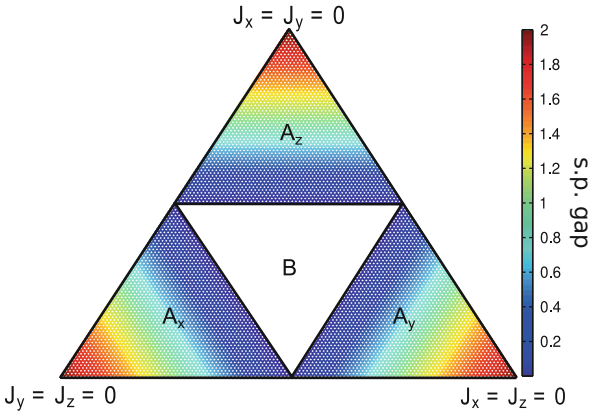

Fig. 2.4 The phase diagram of the Kitaev model is shown in a ternary plot with $J_x + J_y + J_z = 1$. The *central triangle* around the isotropic point $J_x = J_y = J_z$ is the gapless B phase with a gapless Dirac spectrum of the matter fermions. The *outer triangles* (A phases) have a gapped single particle spectrum. The *colorbar* represents the linearly increasing value of the fermionic single particle gap in the ground state flux sector

spin correlations are short ranged even at zero temperature. So far, this is not obvious for the Kitaev model. However, I will explicitly show in the next chapter that spin correlations are actually ultra short ranged. They are strictly zero beyond N.N. due to a selection rule from the flux sector. What is clear until this point is the fact that the fractionalization of spins into Majorana fermions and static fluxes is exact. As discussed in the introduction, fractionalization is another prominent feature of QSLs, similar to the appearance of the emergent gauge structure. All together, these features make the Kitaev model a prime example of a QSL. Moreover, because of its

exact solubility it has become the workhorse for model calculations of topologically ordered phases in 2D. The pure honeycomb model as described until now harbors gapless and gapped QSL phases, see Fig. 2.4, and its excitations can be shown to obey Abelian statistics (Kitaev 2006). In Chap. 5, I will show that the model can straightforwardly be extended to give rise to a gapped QSL with non-Abelian excitations (Kitaev 2006).

2.3 Experimental Realization

One of the appealing features of the Kitaev model is its simplicity, which brings its actual realization within experimental reach. There are two main directions for realizing the model. First, there are proposals built upon strongly correlated d-electron compounds with sizable spin orbit coupling, e.g. Iridates (Jackeli and Khaliullin 2009; Chaloupka et al. 2010; Okamoto 2013). Second, there exist ideas centered around quantum simulators in cold atomic systems in which laser fields can induce anisotropic effective spin exchange for ensembles of either fermionic atoms (Duan et al. 2003), or for polar molecules (Micheli et al. 2006). In the following, I concentrate on the first direction and explain the main idea of a possible realization in a solid state material.

In this context, Jackeli and Khaliullin (2009) put forward a promising proposal by deriving superexchange models for Mott–Hubbard systems with partially filled t_{2g} orbital levels and with strong spin orbit (SO) coupling. As an example they studied exchange interactions between Ir^{4+} ions in layered Iridate compounds A_2IrO_3 with A = Li,Na. In such transition metal compounds the effective interaction can be quite large giving rise to Mott insulating states (Imada et al. 1998). In general, the effective interaction is determined by the ratio of local on-site Coulomb repulsion and the bandwidth, which is fixed by the overlap between adjacent d-orbitals of the transition metal. In these compounds, the bandwidth can be small since it is usually determined by the indirect transfer through p orbitals of ligand atoms (here oxygen). As a consequence the effective interaction becomes large.

In layered A_2IrO_3 materials the relevant 3d orbital has total angular momentum $L = 2$, with a tenfold degeneracy (five for the orbital part $L_z = -2, -1, 0, 1, 2$ and another two for each spin). In a cubic crystal field surrounding the degeneracy is partially lifted into a higher energy e_g level (fourfold degenerate) and a lower t_{2g} level (sixfold degenerate). In Iridates the Ir ion has a d^5 configuration which can be viewed as a hole in this lower manifold. The t_{2g} manifold is spanned by the three orbitals with effective angular momentum $L = 1$, $|xy\rangle, |xz\rangle, |yz\rangle$. Strong spin-orbit coupling entangles the spin S and the effective orbital angular momentum L lifting the sixfold degeneracy into twofold (total $J = \frac{1}{2}$) and fourfold (total $J = \frac{3}{2}$) degenerate levels. The splitting between these levels is of order λ, which is the SO coupling constant. For late transition metal ions, e.g. Ir, it can be sizable up to $\lambda \approx 400\,\text{meV}$ making it the largest energy scale in the system (Schirmer et al. 1984).

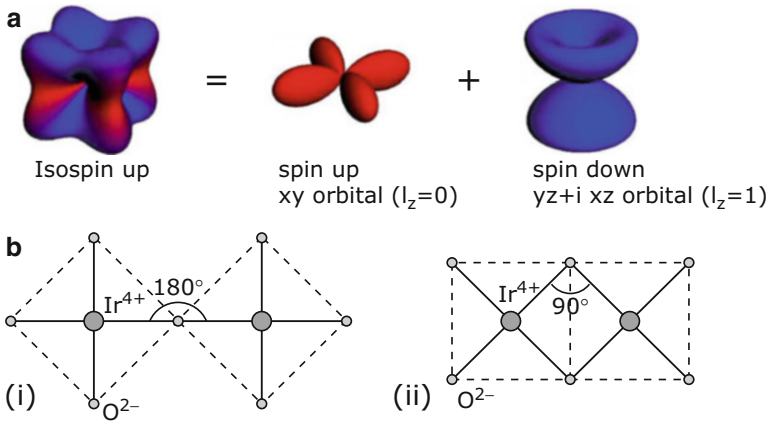

Fig. 2.5 The density profile of an isospin up state is shown in panel **(a)**, figure adapted from Jackeli and Khaliullin (2009). Because of crystal fields and strong spin orbit coupling the effective isospin state is a coherent superposition of spin and orbital components which leads to anisotropic exchange interactions depending on the surrounding bonding geometry. In panel **(b)**, two different bonding directions for the intermediate oxygens are displayed. The effective exchange interactions are mostly mediated through these ligand oxygens and the 90° bonding, *(ii)*, leads to highly anisotropic J_x, J_y, J_z coupling constants

The single hole resides in the Kramers doublet of the effective isospin $J = \frac{1}{2}$ and the wave functions are a coherent superposition of orbital and spin states. The spatially anisotropic $|xz\rangle$ and $|yz\rangle$ orbitals lead to peculiar isospin densities in real space. An example is shown in Fig. 2.5a.

The key observation of Jackeli and Khalliulin was that the exchange Hamiltonian for the effective isospin strongly depends on the bonding geometry. The main ingredient is the position of the ligand oxygen atom through which the dominant exchange process is mediated. Two different bonding angles with either 180° or 90° are shown in Fig. 2.5b (i) and (ii). For a pair of Ir-ions connected via two 90° bonds of intermediate Oxygens, Fig. 2.5b (ii), the exchange processes with parallel J_z and antiparallel J_z have *different* intermediate electronic configurations involving the $J = \frac{3}{2}$ part. It is this difference which gives the anisotropic J_x, J_y, J_z couplings along the bond.

In a cubic system with a periodic replacement of some of the magnetic ions by nonmagnetic ones, the [111] direction can form a honeycomb lattice with three inequivalent bonds, see Fig. 2.6. The transition metal Ir is shown in light blue and the ligand Oxygen as a small open circle (nonmagnetic ion in black). The three different Ir–Ir bonds (green, red, blue) are bridged by three inequivalent 90° bonds via the Oxygens which leads to highly anisotropic exchange interactions that exactly reproduce the Kitaev Hamiltonian (Jackeli and Khaliullin 2009).

In real materials, the instantiation of a pure Kitaev model is highly unlikely because of deviations from a perfect 90° bonding geometry. At best a Kitaev-Heisenberg model with a small Heisenberg contribution might be

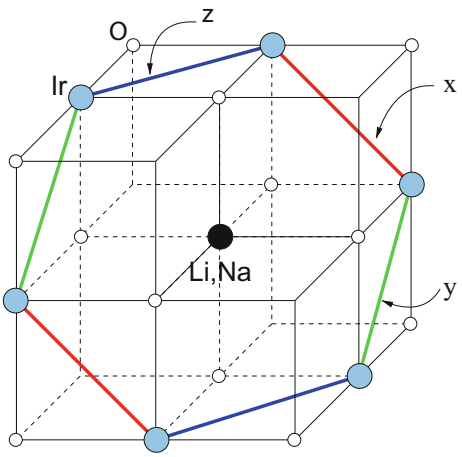

Fig. 2.6 A sketch of a layered iridate compound A_2IrO_3 (A = Li,Na) is shown, adapted from Jackeli and Khaliullin (2009). In a cubic system with periodic replacement of some of the magnetic ions (here Iridium in *light blue*) by nonmagnetic ones (here Li or Na in *black*), the [111] direction can form a honeycomb lattice with three inequivalent bonds. Iridium ions interact via super-exchange via the oxygen atoms (*white small circles*) such that the three different bond directions (*green*, *red*, *blue*) are proposed to realize the Kitaev Hamiltonian

realized (Mazin et al. 2013; Singh et al. 2012). However, several theoretical studies have shown that the Kitaev spin liquid regime is stable for a small but nonzero value of Heisenberg coupling (Chaloupka et al. 2010; Reuther et al. 2011). Spin correlations still decay exponentially, as long as the Heisenberg exchange is sufficiently weak compared to the Kitaev exchange couplings.

References

G. Baskaran, S. Mandal, R. Shankar, Exact results for spin dynamics and fractionalization in the Kitaev model. Phys. Rev. Lett. **98**(24), 247201 (2007)

J.-P. Blaizot, G. Ripka, *Quantum Theory of Finite Systems* (MIT Press, Cambridge, 1986)

J. Chaloupka, G. Jackeli, G. Khaliullin, Kitaev-Heisenberg model on a honeycomb lattice: possible exotic phases in iridium oxides. Phys. Rev. Lett. **105**(2), 027204 (2010)

H.-D. Chen, Z. Nussinov, Exact results of the Kitaev model on a hexagonal lattice: spin states, string and brane correlators, and anyonic excitations. J. Phys. A Math. Theor. **41**(7), 075001 (2008)

L.-M. Duan, E. Demler, M. Lukin, Controlling spin exchange interactions of ultracold atoms in optical lattices. Phys. Rev. Lett. **91**(9), 904021–904024 (2003)

X.-Y. Feng, G.-M. Zhang, T. Xiang, Topological characterization of quantum phase transitions in a spin-model. Phys. Rev. Lett. **98**(8), 087204 (2007)

M. Imada, A. Fujimori, Y. Tokura, Metal-insulator transitions. Rev. Mod. Phys. **70**(4), 1039–1263 (1998)

G. Jackeli, G. Khaliullin, Mott insulators in the strong spin-orbit coupling limit: from heisenberg to a quantum compass and Kitaev models. Phys. Rev. Lett. **102**(1), 017205 (2009)
A. Kitaev, Anyons in an exactly solved model and beyond. Ann. Phys. **321**(1), 2–111 (2006)
C. Lacroix, P. Mendels, F. Mila, *Introduction to Frustrated Magnetism: Materials, Experiments, Theory*. Springer Series in Solid-State Sciences (Springer, Berlin, 2011)
V. Lahtinen, A.W.W. Ludwig, S. Trebst, Perturbed vortex lattices and the stability of nucleated topological phases. Phys. Rev. B **89**(8), 085121 (2014)
E.H. Lieb, Flux phase of the half-filled band. Phys. Rev. Lett. **73**(16), 2158–2161 (1994)
S. Mandal, R. Shankar, G. Baskaran, RVB gauge theory and the topological degeneracy in the honeycomb Kitaev model. J. Phys. A Math. Theor. **45**(33), 335304 (2012)
I.I. Mazin, S. Manni, K. Foyevtsova, H.O. Jeschke, P. Gegenwart, R. Valentí, Origin of the insulating state in honeycomb iridates and rhodates. Phys. Rev. B **88**(3), 035115 (2013)
A. Micheli, G.K. Brennen, P. Zoller, A toolbox for lattice-spin models with polar molecules. Nat. Phys. **2**(5), 341–347 (2006)
V. Mukherjee, A. Dutta, D. Sen, Quantum fidelity for one-dimensional Dirac fermions and two-dimensional Kitaev model in the thermodynamic limit. Phys. Rev. B **85**(2), 024301 (2012)
S. Okamoto, Doped Mott insulators in (111) bilayers of perovskite transition- metal oxides with a strong spin-orbit coupling. Phys. Rev. Lett. **110**(6), 066403 (2013)
J. Reuther, R. Thomale, S. Trebst, Finite-temperature phase diagram of the Heisenberg-Kitaev model. Phys. Rev. B **84**(10), 100406 (2011)
O.F. Schirmer, A. Forster, H. Hesse, M. Wohlecke, S. Kapphan, Paramagnetic resonance and near-infrared optical absorption of $SrTiO_3$:Ir^{4+}. J. Phys. C Solid State Phys. **17**(7), 1321 (1984)
K. Sengupta, D. Sen, S. Mondal, Exact results for quench dynamics and defect production in a two-dimensional model. Phys. Rev. Lett. **100**(7), 077204 (2008)
X.-F. Shi, Y. Yu, J.Q. You, F. Nori, Topological quantum phase transition in the extended Kitaev spin model. Phys. Rev. B **79**(13), 134431 (2009)
Y. Singh, S. Manni, J. Reuther, T. Berlijn, R. Thomale, W. Ku, S. Trebst, P. Gegenwart, Relevance of the Heisenberg-Kitaev model for the honeycomb lattice iridates. Phys. Rev. Lett. **108**(12), 127203 (2012)
A. Willans, J. Chalker, R. Moessner, Disorder in a quantum spin liquid: flux binding and local moment formation. Phys. Rev. Lett. **104**(23), 237203 (2010)
A. Willans, J. Chalker, R. Moessner, Site dilution in the Kitaev honeycomb model. Phys. Rev. B: Condens. Matter Mater. Phys. **84**(11), 115146 (2011)
H. Yao, X.-L. Qi, Entanglement entropy and entanglement spectrum of the Kitaev model. Phys. Rev. Lett. **105**(8), 080501 (2010)
H. Yao, S.-C. Zhang, S.A. Kivelson, Algebraic spin liquid in an exactly solvable spin model. Phys. Rev. Lett. **102**(21), 217202 (2009)

Chapter 3
Dynamic Spin Correlations: Mapping to a Quantum Quench

The main objective of the thesis is to calculate the exact dynamic spin correlation function of the Kitaev QSL. As discussed in the introduction, the possibility to obtain exact results for interacting and nontrivial quantum systems is usually restricted to 1D systems, but the solubility of the Kitaev model extends this possibility to 2D. Many aspects of the Kitaev model were studied since its publication, but surprisingly no results for the full time dependence of correlation functions existed. However, a word of caution is necessary! Similar to the situation of the Bethe-Ansatz in 1D, obtaining exact spectra can be much easier than calculating exact correlation functions (Caux 2009). In fact the full spectrum of the Heisenberg chain is known since the thirties of the last century (Bethe 1931) but the full time (or frequency) dependence of the spin correlation function was just recently obtained and remains a challenging numerical task (Caux 2009; Mourigal et al. 2013). It turns out that the situation is similar in the case of the Kitaev model, for which I calculate the spin correlation function numerically exactly. I discuss at the end of this chapter what I precisely mean by *numerically exact* results.

In the following I calculate the dynamical structure factor which can be directly measured in INS and ESR experiments (Lovesey 1984)

$$S(\mathbf{q},\omega) = \frac{1}{N}\sum_{\mathbf{R}_i,\mathbf{R}_j}\sum_{a,b} e^{-i\mathbf{q}(\mathbf{R}_i-\mathbf{R}_j)}\int_{-\infty}^{\infty} dt e^{i\omega t} S_{ij}^{ab}(t) \tag{3.1}$$

with the standard spin correlation function

$$S_{ij}^{ab}(t) = \langle 0|\hat{\sigma}_i^a(t)\hat{\sigma}_j^b(0)|0\rangle. \tag{3.2}$$

Here i and j are lattice sites at positions $\mathbf{R}_i$ and $\mathbf{R}_j$. I concentrate on the zero temperature response such that $|0\rangle = |F_0\rangle|M_0\rangle$ is the ground state of the Kitaev model.

J. Knolle, *Dynamics of a Quantum Spin Liquid*, Springer Theses,
DOI 10.1007/978-3-319-23953-8_3

The structure of the chapter is as follows. First, I rederive a mapping of the spin correlation function to a local quantum quench which is the starting point for the exact calculations. I show that static and dynamic spin correlations are ultra short ranged due to a selection rule from the static flux sector. Next, I calculate sum rules which relate equal time correlations to the full dynamical response. A first step towards a full solution can be taken by studying the Lehmann representation. I show how to evaluate contributions from few particle processes. Afterwards, I calculate the exact correlation functions for finite size systems via many-body path integrals which leads to an expression in terms of Pfaffians. Next, in order to obtain the structure factor in the thermodynamic limit, I exploit connections of the local quantum quench to the venerable X-ray edge problem. I show how to reduce the problem to the one of finding a solution to a singular integral equation (SIE). The latter is solved via a beautiful mathematical method of Muskhelishvili.

3.1 Exact Mapping and Selection Rules

A first and important step for studying the dynamic spin correlation function was done in Baskaran et al. (2007), who showed that only on-site and N.N. correlations are non-zero. In addition, they derived an expression for the time dependence of the spin correlation function, but they did not attempt to evaluate it. In this section, I follow their main idea and I rederive the exact mapping to a local quantum quench before proceeding with an exact evaluation.

3.1.1 Mapping to a Quench

The ground state of the Kitaev model is flux free and I use a particular gauge with all Eigenvalues $u_{\langle ij\rangle_a} = +1$. From Eq. (2.9) follows that the corresponding occupation of the bond fermions is $\chi^\dagger_{\langle ij\rangle_a}\chi_{\langle ij\rangle_a}|F_0\rangle = 1|F_0\rangle$, hence $\chi^\dagger_{\langle ij\rangle_a}|F_0\rangle = 0$. With the help of these bond fermions, Eq. (2.9), I express all spin operators, Eq. (2.5), as

$$\begin{aligned}\sigma^a_i &= ic_i(\chi_{\langle ij\rangle_a} + \chi^\dagger_{\langle ij\rangle_a}) \text{ with } i \in \text{sublattice } A\\ \sigma^a_j &= c_j(\chi_{\langle ij\rangle_a} - \chi^\dagger_{\langle ij\rangle_a}) \text{ with } j \in \text{sublattice } B,\end{aligned} \tag{3.3}$$

such that the spin correlation function between spins on A and B sublattices can be written as $S^{ab}_{ij}(t) = \langle M_0|\langle F_0|ic_i(t)\chi^\dagger_{\langle ij'\rangle_a}(t)c_j(0)\chi_{\langle i'j\rangle_b}(0)|F_0\rangle|M_0\rangle$. Note that i' and j' are fixed by the spin components a and b which define the corresponding bond direction. With the time dependence in Heisenberg representation, $O(t) = e^{iHt}Oe^{-iHt}$, I obtain

$$S_{ij}^{ab}(t) = \langle M_0|\langle F_0|ie^{iHt}c_i(0)\chi^{\dagger}_{\langle ij'\rangle_a}(0)e^{-iHt}c_j(0)\hat{\chi}_{\langle i'j\rangle_b}(0)|F_0\rangle|M_0\rangle \tag{3.4}$$

with the full Kitaev Hamiltonian in terms of matter and gauge d.o.f. $H = H_{\hat{u}}$. To derive an expression which only depends on the matter degrees of freedom c_i, I commute the bond operators $\chi^{\dagger}$ to the right to let them act on the ground state of the gauge sector $|F_0\rangle$. I use the identity (von Delft and Schoeller 1998)

$$Be^{A'} = e^{A'-D}B \text{ if } \left[A', B\right] = DB \text{ and } [D, B] = 0 \tag{3.5}$$

which is similar to the well-known Baker–Haussdorff formula. Since the Hamiltonian is diagonal in the bond fermion numbers, the commutator $\left[\chi^{\dagger}_a\chi_a, \chi^{\dagger}_{a'}\right] = \chi^{\dagger}_{a'}\delta_{a,a'}$ gives the first non-trivial result

$$\chi^{\dagger}_{\langle ij\rangle_a}e^{-iH_0t} = e^{-it\left(H_0+V_{\langle ij\rangle_a}\right)}\chi^{\dagger}_{\langle ij\rangle_a} \text{ with } V_{\langle ij\rangle_a} = -2J_aic_ic_j. \tag{3.6}$$

Here, I have already used the fact that I study correlations in the ground state sector, such that $H_0 = H_{u=+1}$ refers to the homogeneous Majorana hopping Hamiltonian with all Eigenvalues $u_{\langle ij\rangle_a} = +1$. The new Hamiltonian $H_{\langle ij\rangle_a} = H_0 + V_{\langle ij\rangle_a}$ has locally flipped the sign of the hopping along the bond $\langle ij\rangle_a$ which is equivalent to adding two extra fluxes on the two plaquettes on each side of the bond. In more general terms (Baskaran et al. 2007) commuting $\chi^{\dagger}_{\langle ij\rangle_a}$ past $e^{iH_{\{u\}}}$ in a particular gauge field configuration of a given flux sector, changes the gauge field locally by changing the number of $\chi_{\langle ij\rangle_a}$ fermions. The configuration of local Z_2 fluxes on the two plaquettes neighboring the bond $\langle ij\rangle_a$ is reversed.

In the final step, I eliminate the bond degrees of freedom. In the ground state $\langle F_0|\hat{\chi}^{\dagger}_{\langle ij'\rangle_a}\hat{\chi}_{\langle i'j\rangle_b}|F_0\rangle = \delta_{i,i'}\delta_{j,j'} \equiv \delta_{a,b}\delta_{\langle ij\rangle,a}$. Thus, the first main result is an expression of the dynamic spin correlation function only in terms of matter fermions (Baskaran et al. 2007):

$$S_{ij}^{ab}(t) = -i\langle M_0|e^{iH_0t}c_ie^{-it(H_0+V_{\langle ij\rangle_a})}c_j|M_0\rangle\delta_{a,b}\delta_{\langle ij\rangle,a} \tag{3.7}$$

with $V_{\langle ij\rangle_a} = -2iJ_ac_ic_j$ and $i \in A, j \in B$.

I want to discuss important features of this equation: First, note that spin correlations are ultra-short ranged; the symbol $\delta_{\langle ij\rangle,a}$ encodes that all correlations beyond nearest neighbors $\langle ij\rangle$ are strictly zero. In addition, the component a along the bond $\langle ij\rangle_a$ dictates which specific component of the correlator $S_{ij}^{ab}\delta_{a,b}$ is non-zero. This unusual behavior can be traced back to the static nature of the fluxes and arises due to selection rules of the flux sector (Baskaran et al. 2007). All spin operators are products of a Majorana fermion operator and a bond operator, which changes the occupation number of gauge fermions χ, see Eq. (3.3). Such a change is equivalent to altering the occupation of fluxes on the left and right plaquette neighboring the bond. Hence, spin operators can symbolically be written as

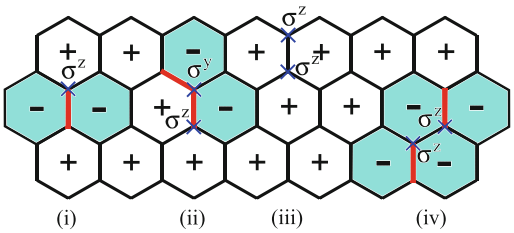

Fig. 3.1 The action of various spin operators on the flux free ground state is shown schematically. A spin operator σ_i^a flips the sign of the link variable $u_{\langle ij\rangle_a}$ (with j defined by the bond direction a) which changes the number of fluxes neighboring the bond $\langle ij\rangle_a$, see *(i)*. A two spin operator is only nonzero if it conserves the number of fluxes. Therefore, $\langle \sigma_i^a \sigma_j^b\rangle \neq 0$ only for $a = b$ along the corresponding bond direction $\langle ij\rangle_a$ such that *(ii)* and *(iv)* vanish but not *(iii)*

$$\sigma_i^a \rightarrow ic_i \hat{\Pi}^{\text{left}}_{\langle ij\rangle,a} \hat{\Pi}^{\text{right}}_{\langle ij\rangle,a} \tag{3.8}$$

with operators $\hat{\Pi}^{\text{left/right}}_{\langle ij\rangle,a}$ flipping the corresponding fluxes (Baskaran et al. 2007). When calculating dynamical correlations $S_{ij}^{ab}(t) = \langle 0|\hat{\sigma}_i^a(t)\hat{\sigma}_j^b(0)|0\rangle$ in the ground state (or any other Eigenstate) the first spin operator adds two fluxes neighboring the b bond starting at site j. Since fluxes are static the bond fermion number is conserved under time evolution. Therefore, the second spin operator has to remove the same fluxes. In general, the second spin adds two fluxes neighboring the a bond starting at site i. However, to get a nonzero correlation it can only act on the very same site j or on the N.N. site along bond b because different flux sectors are orthogonal. These intuitive selection rules are illustrated in Fig. 3.1.

Second, observe the special time dependence in Eq. (3.7). Although this expression had been derived in Baskaran et al. (2007) no attempt to calculate the full dynamics was made. Calculating the spin correlation function reduces to a quadratic Majorana fermion problem because both H_0 and $H_{\langle ij\rangle_a} = H_0 + V_{\langle ij\rangle_a}$ are quadratic, but it still remains a challenging task since it is now a non-equilibrium problem. In fact, Eq. (3.7) is an exact mapping of the spin correlation function to a local *quantum quench*. A Majorana fermion c_j added to the ground state $|M_0\rangle$ of H_0 is evolved forward in time with a different Hamiltonian $H_{\langle ij\rangle_a}$. Since $e^{-itH_{\langle ij\rangle_a}}|M_0\rangle$ creates extra particles and shakes up the Fermi sea, it was conjectured (Baskaran et al. 2007) that the non-equilibrium problem is equivalent to a classic X-ray edge problem (Nozieres and DeDominicis 1969), in which the sudden switching on of a local potential impurity in a Fermi liquid leads to a singular frequency behavior of the X-ray response. As discussed in depth in Sect. 3.4, the physics turns out to be different, as no singular frequency or time behavior arises. The underlying reason is that H_0 has a linearly vanishing density of states as a function of energy because of the Dirac spectrum. Furthermore, $H_{\langle ij\rangle_a}$ only conserves parity but not particle number in terms of matter fermions $f_{\mathbf{r}}$, Eq. (2.10).

The ground state flux sector of the Kitaev model is translationally invariant and spin correlations are very short ranged. Therefore, only few real space components are necessary for the calculation of the structure factor, Eq. (3.1). Only four real

space correlators, two site diagonal $S^{zz}_{A0A0/B0B0}$ and two nearest neighbor $S^{zz}_{A0B0/B0A0}$, need to be calculated. Here and in the following, I put the unit cell coordinate $\mathbf{r} = 0$ and obtain

$$S^{zz}_{A0B0}(t) = -i\langle M_0|e^{iH_0t}c_{A0}e^{-it(H_0+V_z)}c_{B0}|M_0\rangle \tag{3.9}$$

$$S^{zz}_{A0A0}(t) = \langle M_0|e^{iH_0t}c_{A0}e^{-it(H_0+V_z)}c_{A0}|M_0\rangle \tag{3.10}$$

$$S^{zz}_{B0B0}(t) = \langle M_0|e^{iH_0t}c_{B0}e^{-it(H_0+V_z)}c_{B0}|M_0\rangle \tag{3.11}$$

$$S^{zz}_{B0A0}(t) = i\langle M_0|e^{iH_0t}c_{B0}e^{-it(H_0+V_z)}c_{A0}|M_0\rangle \tag{3.12}$$

$$\text{with } V_z = -2iJ_z c_{A0}c_{B0}. \tag{3.13}$$

The other correlators S^{xx} or S^{yy} can be obtained by interchanging $J_x \to J_z \to J_y \to J_x$ or $J_y \to J_z \to J_x \to J_y$. In the remainder of this chapter, I present derivations for the first N.N. component, $S^{zz}_{A0B0}(t)$, since all others are very similar. For completeness, I list the final result for all of them.

3.1.2 Sum Rules and Static Correlations

A good check for a calculation of the dynamical correlation functions is given by the sum rules

$$\begin{aligned} S^{zz}_{A0A0/B0}(0) &= \int_{-\infty}^{+\infty} dt\delta(t)S^{zz}_{A0A0/B0}(t) \\ &= \frac{1}{2\pi}\int_{-\infty}^{+\infty} d\omega \int_{-\infty}^{+\infty} dt e^{i\omega t}S^{zz}_{A0A0/B0}(t) \\ &= \frac{1}{2\pi}\int_{-\infty}^{+\infty} d\omega S^{zz}_{A0A0/B0}(\omega), \end{aligned} \tag{3.14}$$

which connect the equal time correlation functions to the full frequency behavior of the dynamical response. I checked that my calculations fulfill the sum rules by calculating $S^{zz}_{A0B0}(t=0) = -i\langle M_0|c_{A0}c_{B0}|M_0\rangle$, the equal time correlator given by

$$S^{zz}_{A0B0}(t=0) = \frac{1}{N}\sum_{\mathbf{q}} \cos\left(2\theta_{\mathbf{q}}\right) \tag{3.15}$$

with the Bogoliubov angle derived in Sect. 2.2. At the isotropic point I obtain $S^{zz}_{A0B0}(t=0, J_x = J_y = J_z = 1) = 0.5248657$ in the thermodynamic limit $N \to \infty$. In Fig. 3.2 the equal time correlation function is shown in the full phase diagram. The isolated Ising dimer limit $S^{zz}_{A0B0}(t=0, J_x = J_y = 0, J_z = 1) = 1$ is quickly approached as $J_x, J_y \ll J_z$.

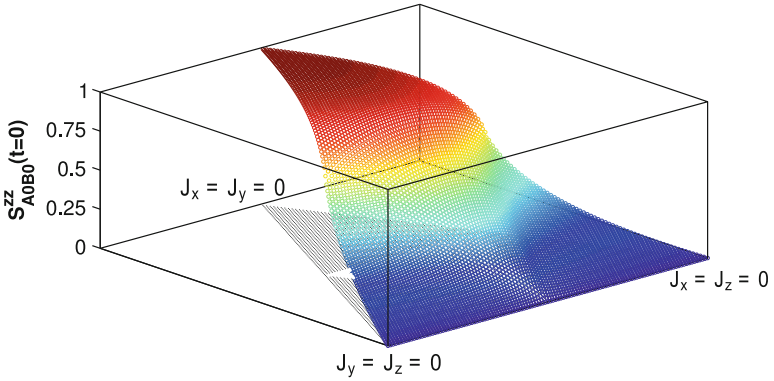

Fig. 3.2 The behavior of the N.N. equal time correlation function $S^{zz}_{A0B0}(t = 0)$ is shown in the phase diagram parameterized by $J_x + J_y + J_z = 1$

3.2 Few-Particle Response and Dynamical Phase Diagram

For a first insight into the full dynamical response $S^{zz}_{ij}(t)$, it is instructive to study the Lehmann representation by inserting the identity $\mathbf{1} = \sum_{\tilde{\lambda}} |\tilde{\lambda}\rangle\langle\tilde{\lambda}|$ into Eq. (3.9).

$$S^{zz}_{A0B0}(t) = -i \sum_{\tilde{\lambda}} e^{it(E_0 - E^F_{\tilde{\lambda}})} \langle M_0|c_{A0}|\tilde{\lambda}\rangle\langle\tilde{\lambda}|c_{B0}|M_0\rangle \tag{3.16}$$

which gives in frequency space

$$S^{zz}_{A0B0}(\omega) = -2\pi i \sum_{\tilde{\lambda}} \langle M_0|c_{A0}|\tilde{\lambda}\rangle\langle\tilde{\lambda}|c_{B0}|M_0\rangle \delta\left[\omega - \left(E^F_{\tilde{\lambda}} - E_0\right)\right]. \tag{3.17}$$

Here, $|\tilde{\lambda}\rangle$ is the basis of many-body Eigenstates of the Hamiltonian $H_z = (H_0 + V_z)$ with the corresponding many-body Eigenenergies $E^F_{\tilde{\lambda}}$; E_0 is the ground state energy of H_0. Central aspects of the dynamical response already become transparent from Eq. (3.17).

First, in both gapped and gapless phases, the response vanishes below the two-flux gap $\Delta = E^F_0 - E_0$, which is the difference between the ground state energies in a system with and without an extra flux pair. At the isotropic point $\Delta \simeq 0.26J$ (Kitaev 2006). It is remarkable that in an INS experiment the response of a gapless QSL shows an excitation gap which is directly related to the emergent gauge field.

Second, above the gap Δ, the response reflects the physics of the matter sector. An important consequence of the fact that H_0 and H_z conserve matter fermion parity is that the non-zero contributions to Eq. (3.17) come only from excited states $|\tilde{\lambda}\rangle$ with parity opposite to the ground state $|M_0\rangle$. As a result, two distinctively different alternatives arise: either (I) the ground states of H_0 and H_z have the same parity,

in which case the states $|\tilde{\lambda}\rangle$ must contain an odd number of excitations, or (II) the ground states have opposite parity and $|\tilde{\lambda}\rangle$ contains an even number of excitations, a condition that is also fulfilled by the ground state of H_z.

From Eq. (3.16) I can calculate the contribution from different number of particle states by studying the contributions from zero excitations $|M_F\rangle$, single particle excitations $|\lambda\rangle = b_\lambda^\dagger |M_F\rangle$ with energy E_λ^F, two particle excitations $|\lambda, \lambda'\rangle = b_\lambda^\dagger b_{\lambda'}^\dagger |M_F\rangle$ with energy $E_{\lambda,\lambda'}^F = E_\lambda^F + E_{\lambda'}^F$, etc. Note the missing tilde for the single particle states and energies.

$$
\begin{aligned}
S^{zz}_{A0B0,(0)}(\omega) &= -2\pi i \langle M_0|c_{A0}|M_F\rangle\langle M_F|c_{B0}|M_0\rangle \delta\left[\omega - \left(E_0^F - E_0\right)\right] \qquad (3.18)\\
S^{zz}_{A0B0,(1)}(\omega) &= -2\pi i \sum_\lambda \langle M_0|c_{A0}b_\lambda^\dagger|M_F\rangle\langle M_F|b_\lambda c_{B0}|M_0\rangle \delta\left[\omega - \left(E_\lambda^F - E_0\right)\right]\\
S^{zz}_{A0B0,(2)}(\omega) &= -2\pi i \sum_{\lambda,\lambda'} \langle M_0|c_{A0}b_\lambda^\dagger b_{\lambda'}^\dagger|M_F\rangle\langle M_F|b_{\lambda'} b_\lambda c_{B0}|M_0\rangle \delta\\
&\qquad \left[\omega - \left(E_\lambda^F + E_{\lambda'}^F - E_0\right)\right]\\
&\text{etc.}
\end{aligned}
$$

3.2.1 Zero-Particle Contribution: δ-Function at the Flux Gap

For case (II) the sector with zero excitations is an important special case, distinct from the sectors with two, four, or more excitations because it contains only a single state: The ground state of H_z. Its contribution to $S^{zz}_{A0B0}(\omega)$ is sharp in frequency, whereas the contributions from sectors with non-zero excitation numbers are broad.

The calculation of the δ-function for case (II) faces a technical problem. In principle, in Sect. 2.1.1, the relation between different flux sectors was established. In particular, whether or not both ground states have the same parity can be calculated by finding the non-zero parameter region of the overlap $|\langle M_F|M_0\rangle|^2 = \sqrt{\det\left(\mathcal{X}^\dagger\mathcal{X}\right)}$, with $|M_F\rangle$ being the ground state of H_z.

The ground state of the two flux sector can be obtained from Eq. (2.26), $|M_F\rangle = \det\left(\mathcal{X}^\dagger\mathcal{X}\right)^{\frac{1}{4}} e^{-\frac{1}{2}\mathcal{F}_{ij}a_i^\dagger a_j^\dagger}|M_0\rangle$, but this way $|M_F\rangle$ always has the same parity as $|M_0\rangle$, because fermions are created in pairs. One way to cure problem is to take advantage of the gauge structure. The Kitaev model conserves parity of the total number of fermions $N = N_f + N_\chi$, a sum of bond N_χ and matter fermions N_f, see the projection operator Eq. (2.13). A simple gauge transformation can change the parity of bond and matter sectors while keeping the total parity intact. Since Majorana fermions are their own adjoints $c_{A0}c_{A0} = 1$, a modified form of the Lehmann representation is obtained by inserting the new identity operator $\mathbf{1} = c_{A0}\sum_{\tilde{\lambda}}|\tilde{\lambda}\rangle\langle\tilde{\lambda}|c_{A0}$ into Eq. (3.9)

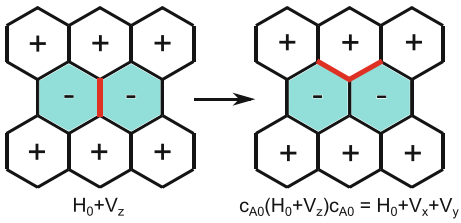

Fig. 3.3 An illustration of the gauge transformation $c_{A0}(H_0 + V_z)c_{A0} = (H_0 + V_x + V_y)$ is shown. Instead of a single flipped bond variable $u_{A0B0} = -1$, illustrated by the *red bond in the left panel*, the two other inverted link variables in *red* (*right panel*) define the same flux sector. This gauge transformation changes the parity of the corresponding ground states while the overall parity of $N_\chi + N_f$ is conserved. It is used to calculate the even number of particle contribution of the Lehmann representation, Eq. (3.19). Note that the spectrum E_n^F of (H_0+V_z) and $(H_0+V_x+V_y)$ is identical

$$S^{zz}_{A0B0}(t) = -i\sum_{\tilde{\lambda}} \langle M_0|e^{iH_0t}c_{A0}e^{-i(H_0+V_z)t}c_{A0}|\tilde{\lambda}\rangle\langle\tilde{\lambda}|c_{A0}c_{B0}|M_0\rangle \tag{3.19}$$

$$= -i\sum_{\tilde{\lambda}} \langle M_0|e^{iH_0t}e^{-i(H_0+V_x+V_y)t}|\tilde{\lambda}\rangle\langle\tilde{\lambda}|c_{A0}c_{B0}|M_0\rangle. \tag{3.20}$$

I have used the fact that

$$c_{A0}e^{-i(H_0+V_z)t}c_{A0} = e^{-ic_{A0}(H_0+V_z)c_{A0}t} \text{ with } c_{A0}(H_0 + V_z)c_{A0} = (H_0 + V_x + V_y) \tag{3.21}$$

and $V_x = -2iJ_xc_{A0}c_{B0+\mathbf{n_1}}$, $V_x = -2iJ_yc_{A0}c_{B0+\mathbf{n_2}}$ is just a gauge transformation within the same flux sector. All signs of the hoppings along the three bonds sharing site $A0$ are reversed, see Fig. 3.3 for an illustration. Now many-body states $|\tilde{\lambda}\rangle$ are taken to be Eigenstates of $(H_0 + V_x + V_y)$. Note the energies $E^F_{\tilde{\lambda}}$ are unchanged but the parity of the new ground state, called $|M_F^{x,y}\rangle$ is opposite to the parity of the ground state $|M_F\rangle$ of (H_0+V_z). Hence, in case (II) when the overlap $|\langle M_F|M_0\rangle|^2 = 0$ is zero due to different parities, the overlap $|\langle M_F^{x,y}|M_0\rangle|^2 = \sqrt{\det\left([\mathcal{X}^{x,y}]^\dagger\,\mathcal{X}^{x,y}\right)}$ is non-zero. In the remainder, I omit the label^{x,y} if clear from the context.

Again, for the δ-function contribution I restrict the sum $\sum_{\tilde{\lambda}}$ to zero excitations, namely to only the ground state:

$$S^{zz}_{A0B0,(0)}(t) = -ie^{it(E_0-E_0^F)}\langle M_0|M_F^{x,y}\rangle\langle M_F^{x,y}|c_{A0}c_{B0}|M_0\rangle. \tag{3.22}$$

I show the explicit calculation of the matrix element $\langle M_F^{x,y}|c_{A0}c_{B0}|M_0\rangle$ and of all site diagonal and N.N. contributions in Appendix D. The main idea behind the calculation of all multi-particle contributions is to express $|M_F^{x,y}\rangle$ in terms of $|M_0\rangle$, and to rewrite all operators $c_{A0/B0}$, b_λ in terms of operators $a_\mathbf{q}$, which diagonalize the

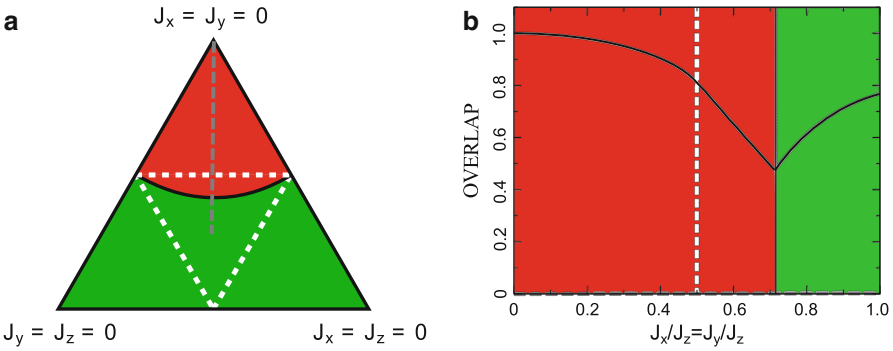

Fig. 3.4 The ground state and dynamical phase diagrams of the model is shown in panel (**a**), parameterized by $J_x + J_y + J_z = 1$. The phase with gapless fermionic excitations fills the *central triangle*, while gapped phases occupy the three *outer triangles*. The dynamical response $S^{zz}(\mathbf{q}, \omega)$ includes a δ-function from zero particle excitations in the red region of panel (**a**), but not in the *green* region. The weight of the δ-function is proportional to the ground state overlap $|\langle M_F^{x,y}|M_0\rangle|^2$, Eq. (3.23). Its evolution is shown in panel (**b**) along the *gray dashed line* $J_x/J_z = J_y/J_z$ highlighted in panel (**a**). At $J_x/J_z = J_y/J_z \approx 0.71$ this overlap drops to zero since the parity of the ground state changes, but the overlap $|\langle M_F|M_0\rangle|^2$ of the gauge equivalent Hamiltonian $H_0 + V_z$ becomes nonzero in the *green* region

flux free sector and annihilate its ground state $a_{\mathbf{q}}|M_0\rangle = 0$, see Sects. 2.2 and 2.1.1. The zero-particle contribution to the structure factor gives a δ-function in frequency, here for $\mathbf{q} = 0$

$$S^{zz}_{(0)}(\mathbf{q} = \mathbf{0}, \omega) = 8\pi \sqrt{[\mathcal{X}^{x,y}]^\dagger \mathcal{X}^{x,y}}\, \delta\left(\omega - \left[E_0^F - E_0\right]\right) \times \left\{ \frac{1}{N} \sum_{\mathbf{k}} \cos^2 \theta_{\mathbf{k}} + \frac{1}{N} \sum_{\mathbf{k},\mathbf{q}} \cos\theta_{\mathbf{k}} \mathrm{Im}\left[\mathcal{F}_{\mathbf{k},\mathbf{q}}\right] \sin\theta_{\mathbf{q}} \right\} \quad (3.23)$$

with the Bogoliubov angles $\theta_{\mathbf{k}}$, Eq. (2.29), and the $\mathcal{F}$ matrix relating the flux free and two flux sector, Eq. (2.26).

In Fig. 3.4 I show the dynamical phase diagram. The dynamical response $S^{zz}(\mathbf{q}, \omega)$ includes a δ-function contribution sharp in ω in the red region of panel (a), but not in the green region. In the red region only even number of particle processes contribute, in the green region only odd numbers. The weight of the δ-function is proportional to the ground state overlap $\sqrt{[\mathcal{X}^{x,y}]^\dagger \mathcal{X}^{x,y}}$, Eq. (3.23), whose evolution along the gray dashed line $J_x/J_z = J_y/J_z$ is shown in panel (b). At $J_x/J_z = J_y/J_z \approx 0.71$ the overlap drops to zero since the parity of the ground state changes. At this point the overlap $|\langle M_F|M_0\rangle|^2$ becomes nonzero.

3.2.2 Single- and Two-Particle Contributions

In case (I), both ground states of the two flux sectors have the same parity, see the green region in Fig. 3.4. The first contribution arises due to single particle excitations

$$S^{zz}_{A0B0,(1)}(t) = -i \sum_{\lambda} e^{it(E_0 - E^F_\lambda)} \langle M_0 | c_{A0} b^\dagger_\lambda | M_F \rangle \langle M_F | b_\lambda c_{B0} | M_0 \rangle. \tag{3.24}$$

The derivation of the matrix elements, $\langle M_0 | c_{A0/B0} b^\dagger_\lambda | M_F \rangle$, is shown in Appendix D. The final result is

$$\begin{aligned} S^{zz}_{(1)}(\mathbf{q} = \mathbf{0}, \omega) = \; & 8\pi \sqrt{\mathcal{X}^\dagger \mathcal{X}} \sum_{\lambda} \delta\left(\omega - \left[E^F_\lambda - E_0\right]\right) \\ & \times \frac{1}{N} \sum_{\mathbf{k},\mathbf{q}} \cos\theta_{\mathbf{k}} \left[\mathcal{X}^{-1}\right]_{\mathbf{k},\lambda} \left[\mathcal{X}^{-1}\right]^\dagger_{\lambda,\mathbf{q}} \cos\theta_{\mathbf{q}}. \end{aligned} \tag{3.25}$$

For case (II) in order to fulfill the parity constraint, the next contribution beyond the δ-function, Eq. (3.23), arises from doubly excited states.

$$S^{zz}_{A0B0,(2)}(t) = -i \sum_{\lambda,\lambda'} \langle M_0 | e^{iH_0 t} e^{-iH_{x,y} t} b^\dagger_\lambda b^\dagger_{\lambda'} | M^{x,y}_F \rangle \langle M^{x,y}_F | b_{\lambda'} b_\lambda c_{A0} c_{B0} | M_0 \rangle \tag{3.26}$$

The final two-particle contribution to the structure factor is

$$\begin{aligned} S^{zz}_{(2)}(\mathbf{q} = \mathbf{0}, \omega) = \; & 8\pi \sqrt{\left[\mathcal{X}^{x,y}\right]^\dagger \mathcal{X}^{x,y}} \sum_{\lambda,\lambda'} \delta\left(\omega - \left[E^F_\lambda + E^F_{\lambda'} - E_0\right]\right) \\ & \times \left\{ |G^2_{\lambda,\lambda'}|^2 + \frac{1}{2} \mathrm{Re}\left[i G^4_{\lambda,\lambda'} \left[G^2_{\lambda,\lambda'}\right]^* \right] \right\} \end{aligned} \tag{3.27}$$

with matrix elements $G^2_{\lambda,\lambda'}$ and $G^4_{\lambda,\lambda'}$ again given in Appendix D. In Chap. 4 showing the results, I compare the different contributions of zero-, single-, and two-particle excitations to the full response. For the 1D Heisenberg chain 70 % of the total weight of the structure factor are due to single particle excitations (Han et al. 2012). In contrast, it turns out that for the Kitaev model at the isotropic point ($J_x = J_y = J_z$) already 98 % of the total weight are captured by single particle excitations, compare to Fig. 4.4.

3.3 Exact Pfaffian Approach

Up to this point, I have explained how to calculate the spin correlations up to two-particle processes. However, the objective is to calculate the exact correlation function which in principle amounts to summing all multi-particle processes $|\lambda' \dots \lambda\rangle = b^\dagger_{\lambda'} \dots b^\dagger_\lambda |M_0^F\rangle$ in the Lehmann representation, Eq. (3.16). Instead, I go a different route and derive an exact expression in terms of Pfaffians via many-particle path integrals, see Appendix A for details. Pfaffians are generalizations of determinants for antisymmetric matrices. Their definition and some of their properties are given in Appendix A.1. In this *Pfaffian approach* the correlation function can be evaluated exactly for finite size systems.

I begin by rewriting Eq. (3.9) and all other site diagonal and N.N. real time correlators in terms of Bogoliubov particles $a_\mathbf{q}$ that diagonalize the flux free system, see Sect. 2.1.1 in particular Eq. (2.22),

$$S^{zz}_{A0B0}(t) = e^{itE_0} \sum_{q,l} \left[X_{q0} + Y_{q0}\right] \mathcal{M}_{q,l} \left[X^\dagger_{0l} - Y^\dagger_{0l}\right] \tag{3.28}$$

$$S^{zz}_{A0A0}(t) = e^{itE_0} \sum_{q,l} \left[X_{q0} + Y_{q0}\right] \mathcal{M}_{q,l} \left[X^\dagger_{0l} + Y^\dagger_{0l}\right] \tag{3.29}$$

$$S^{zz}_{B0B0}(t) = e^{itE_0} \sum_{q,l} \left[X_{q0} - Y_{q0}\right] \mathcal{M}_{q,l} \left[X^\dagger_{0l} - Y^\dagger_{0l}\right] \tag{3.30}$$

$$S^{zz}_{B0A0}(t) = e^{itE_0} \sum_{q,l} \left[X_{q0} - Y_{q0}\right] \mathcal{M}_{q,l} \left[X^\dagger_{0l} + Y^\dagger_{0l}\right]. \tag{3.31}$$

The main difficulty is to find an exact expression for the matrix element

$$\mathcal{M}_{q,l}(t) = \langle M_0 | a_q e^{-it(H_0+V_z)} a^\dagger_l | M_0 \rangle. \tag{3.32}$$

A sketch of the derivation is as follows: I construct a generating functional via a fermion coherent state path integral for the exponential of the Hamiltonian with a Bogoliubov de-Gennes form (with anomalous terms $a^\dagger a^\dagger$ + h.c.). The matrix elements are computed as derivatives with respect to the appropriate sources. With the help of the Bogoliubov transformation, which relates the two flux sectors, Eq. (2.24), it is possible to evaluate the Matsubara sums which I encounter in the path integral formulation. Finally, the Gaussian integrals over antisymmetric matrices lead to Pfaffians (Zinn-Justin 2002). A detailed derivation is given in Appendix A and I only state the final result for a finite size system with N unit cells.

As discussed in Sect. 2.1.1, the a operators (which diagonalize H_0) and the b operators (which diagonalize $H_0 + V_z$) are related via Eq. (2.24) as $a_i = \mathcal{X}^T_{ik} b_k + \mathcal{Y}^\dagger_{ik} b^\dagger_k$. I define the antisymmetric matrix

$$\hat{S}^{-1}_{i,j} = \begin{bmatrix} -\mathcal{B}_{i,j} & \mathcal{A}_{i,j} \\ -\mathcal{A}^T_{i,j} & -\mathcal{C}_{i,j} \end{bmatrix} \tag{3.33}$$

with

$$\begin{aligned} \mathcal{A}_{i,j} &= \mathcal{X}^T_{ik}\mathcal{X}^\dagger_{jk} n^-(E^F_k) + \mathcal{Y}^\dagger_{ik}\mathcal{Y}^T_{jk} n^+(E^F_k) \\ \mathcal{B}_{i,j} &= \mathcal{X}^T_{ik}\mathcal{Y}^\dagger_{jk} n^-(E^F_k) + \mathcal{Y}^\dagger_{ik}\mathcal{X}^T_{jk} n^+(E^F_k) \\ \mathcal{C}_{i,j} &= \mathcal{Y}^T_{ik}\mathcal{X}^\dagger_{jk} n^-(E^F_k) + \mathcal{X}^\dagger_{ik}\mathcal{Y}^T_{jk} n^+(E^F_k) \end{aligned} \tag{3.34}$$

and $n^{\mp}(E^F_k) = 1/\left(1 + e^{\pm itE^F_k}\right)$ the standard Fermi function with the inverse temperature replaced by $\beta = \pm it$ and the single particle energies E^F_k of the two flux sector (summation over double indices). In addition, I need the $2N \times 2N$ diagonal matrix $\hat{B}$ given by $\hat{B} = \text{diag}\left[1 + e^{-itE^F_1}, \ldots, 1 + e^{-itE^F_N}, 1, \ldots, 1\right]$, as well as, $\hat{S}^{-1}_{[2N-l,q]}$ which is the $(2N-2) \times (2N-2)$ matrix derived from $\hat{S}^{-1}$ with lines $(2N-l)$ and q, as well as, columns $(2N-l)$ and q removed.

In the final expression, products of $\det\left(\hat{B}\right)$ with Pfaffians of $\hat{S}^{-1}_{[2N-l,q]}$ appear. While the former can become very large the latter is very small which creates large numerical errors. To circumvent the problem, I take advantage of the property $\text{Pf}(BAB^T) = \det(B)\text{Pf}(A)$ for an arbitrary matrix B. However, the dimension of $\hat{S}^{-1}_{[2N-l,q]}$ is $(2N-2) \times (2N-2)$ while $\hat{B}$ is $2N \times 2N$. With the expansion formula for Pfaffians, Eq. (A.5), I can cure this mismatch. The matrix $\hat{S}^{-1}_{\{2N-l,q\}}$ has size $2N \times 2N$ with 0's on rows and columns $(2N-l)$, q and matrix elements $\hat{S}^{-1}_{q,2N-l} = -1$ and $\hat{S}^{-1}_{2N-l,q} = +1$ such that $\text{Pf}\left(\hat{S}^{-1}_{[2N-l,q]}\right) = \text{Pf}\left(\hat{S}^{-1}_{\{2N-l,q\}}\right)$. Finally, I combine everything to derive the final result

$$M_{q,l}(t) = e^{-itE^F_0}(-1)^{\frac{N(N-1)}{2}} \left\{\text{Pf}\left(\hat{B}\hat{S}^{-1}_{\{2N-l,q\}}\hat{B}^T\right) - \delta_{q,l} \cdot \text{Pf}\left(\hat{B}\hat{S}^{-1}\hat{B}^T\right)\right\} \tag{3.35}$$

which is evaluated numerically. Here, $E^F_0 = -\frac{1}{2}\sum_{n>0} E^F_n$ is the ground state energy of the two flux sector.

This form of the matrix element enables an exact calculation of the correlation function up to arbitrarily long times. However, it is restricted to a small number of lattice sites because the size of the matrices grows exponentially. Due to the extra fluxes the system is not translationally invariant. When working in real space instead of reciprocal space the matrices are sparse which leads to a better numerical performance. I can evaluate systems up to 600 lattice sites which still show strong finite size effects in the gapless phase of the Kitaev model, especially in form of revivals due to periodic boundary conditions.

3.4 Exact X-Ray Edge Approach

Calculating the correlation function exactly in the thermodynamic limit ($N \to \infty$) requires a different method because the Pfaffian approach is limited to small system sizes. In this section, I express the spin correlation function, Eq. (3.7), in terms of bond fermions $f_{\mathbf{r}}$, Eq. (2.10). This results in expressions formally equivalent to the venerable X-ray edge problem, which is introduced in detail below. I work in interaction representation (Abrikosov et al. 2012) and I obtain for the nearest neighbor correlator

$$S^{zz}_{A0B0}(t) = \langle \mathbb{T}[f_0(t) + f_0^\dagger(t)][f_0^\dagger(0) - f_0(0)]S(t,0)\rangle \tag{3.36}$$

with the time evolution governed by the bare Hamiltonian $f_{\mathbf{r}}(t) = e^{iH_0 t} f_{\mathbf{r}} e^{-iH_0 t}$. The S-matrix is given by

$$S(t,0) = e^{iH_0 t} e^{-it(H_0+V_z)} = \mathbb{T} e^{-i\int_0^t dt' V_z(t')} \tag{3.37}$$

with the standard time ordering operator $\mathbb{T}$. The average is the usual $\langle \ldots \rangle = \langle M_0 | \ldots | M_0 \rangle$.

The main simplification and the reason why a mapping to an X-ray edge problem is possible can be traced back to the particularly simple form of the *impurity* $V_z = -2iJ_z c_{A0} c_{B0}$ in terms of complex matter fermions

$$V_z(t) = -4J_z \left(f_0^\dagger(t) f_0(t) - \frac{1}{2} \right). \tag{3.38}$$

In fact, $V_z(t)$ is only a simple local but time dependent on-site potential of the form $f_0^\dagger(t) f_0(t)$. In the remainder of the section, I disregard the constant phase $e^{-i2J_z t}$ from V_z and restore it only in the end.

The ground state $|M_0\rangle$ is the vacuum for operators $a_{\mathbf{q}}$, which are superpositions of creation and annihilation operators $f_{\mathbf{q}}$, see Eq. (2.29). Therefore, normal $G_0(t,t') = -i\langle \mathbb{T} f(t) f^\dagger(t')\rangle$ and anomalous $F_0(t,t') = -i\langle \mathbb{T} f(t) f(t')\rangle$ bare Greens functions (GF) of the bond fermions are expected, because both f and $f^\dagger$ acting on the ground state is nonzero. Whereas in the previous Pfaffian calculation in terms of operators $a_{\mathbf{q}}$ the anomalous terms appeared in V_z and the ground state was simple, it seems that in terms of matter fermions a simple V_z is exchanged for a complicated ground state with off-diagonal contributions. Fortunately, this is not the case because the anomalous bare GF is zero due to the sublattice symmetry of the Kitaev model, see Appendix B.1. Moreover, due to the fact that V_z is proportional to the number operator $f_0^\dagger f_0$, the full anomalous GF is zero as well: $F_0(t,t') = 0$ leads to $\langle f_0(t) \mathbb{T} e^{-i\int_0^t dt' V_z(t')} f_0(0)\rangle = 0$, similar to the hermitian conjugates.

Modifications of the original Kitaev model can destroy this simplification (Tikhonov and Feigelman 2010). In such a case the approach in terms of Pfaffians is still applicable, but the present treatment in terms of an X-ray edge problem

would not be possible. Moreover, a non-zero magnetic field adds site off-diagonal anomalous terms to the expression of the correlation function (Tikhonov et al. 2011) which further complicates the problem.

For the pure Kitaev model the correlation function, Eq. (3.36), is reduced to the seemingly simple looking equation

$$S^{zz}_{A0B0}(t) = i\,[G(t,0) + G(0,t)] \tag{3.39}$$

(for the site diagonal $S^{zz}_{A0A0}(t) = S^{zz}_{B0B0}(t) = i\,[G(t,0) - G(0,t)]$) with the full positive time GF

$$G(t,0) = -i\langle \mathbb{T} f(t) f^{\dagger}(0) e^{-i\int_0^t dt_1 V_z(t_1)} \rangle \tag{3.40}$$

and the full negative time GF

$$G(0,t) = -i\langle \mathbb{T} f(0) f^{\dagger}(t) e^{-i\int_0^t dt_1 V_z(t_1)} \rangle. \tag{3.41}$$

Note that the time ordered exponential is exactly the same in both cases, thus, $G(0,t)$ is not a standard GF for negative time arguments. The expressions for the full GF are precisely of the form of a Fermi-edge, or X-ray edge, problem (Nozieres and DeDominicis 1969; Gogolin et al. 1998).

3.4.1 X-Ray Edge Problem

The X-ray edge is a classic condensed matter problem (Mahan 1967; Nozieres and DeDominicis 1969; Ohtaka and Tanabe 1990; Gogolin et al. 1998). It is a foundation for our understanding of local quantum quenches and, in addition, it provides a rare example of a non-trivial exactly solvable many-body problem. The X-ray edge becomes manifest in singular photo-absorption spectra of simple metals close to the energy of the Fermi level ϵ_F, which is counted from the bottom of the band. An X-ray beam pointed at a piece of metal can excite an electron from a localized core level at energy ϵ_c to the conduction band. Afterwards, an electron from the Fermi sea recombines with the core hole and a photon is emitted, see Fig. 3.5. A first simple guess that the absorption, and emission, rate $I(\omega)$ beyond the absorption threshold $\omega_{\rm th} = \epsilon_{\rm F} - \epsilon_c$ is proportional to the density of states $N(\omega)$

$$I(\omega) \propto N(\omega)\theta\,(\omega - \omega_{\rm th}) \tag{3.42}$$

turns out to be wrong. The reason is the sudden creation of a localized potential due to the static core hole that is left behind. The problem is actually a true non-equilibrium problem of a local quantum quench, see Fig. 3.5 for an illustration:

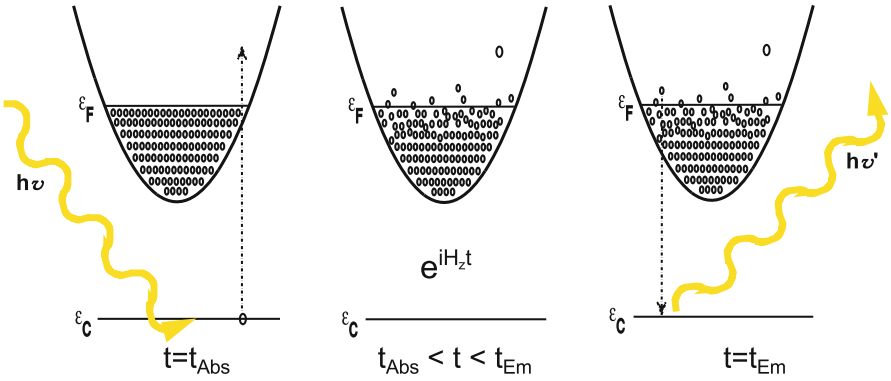

Fig. 3.5 A schematic picture of the classic X-ray edge problem. An X-ray photon excites a localized electron from a core level at ϵ_c to the conduction band above the Fermi energy ϵ_F. It leaves behind a local potential from the core hole that shakes up the Fermi sea. Eventually an electron recombines with the core hole and a photon is emitted

- At $t = t_{\mathrm{Abs}}$ a local on-site potential from the static core hole is switched on and an additional electron is added to the formerly unperturbed Fermi sea.
- The Fermi sea is perturbed and it propagates forward in time with the extra potential.
- At $t = t_{\mathrm{Em}}$ the local potential is sharply switched off. The additional electron in the Fermi sea is removed by recombining with the core hole.

Two processes strongly change the naive guess for $I(\omega)$, Eq. (3.42): First, conduction electrons scatter of the local potential which modifies the local density of states. Second, the sudden switching of the potential creates an infinite number of low-energy electron-hole pairs such that the initial many-body wave function of the unperturbed Fermi sea $|\Psi_0\rangle$ is orthogonal to the final state $|\Psi_F\rangle$ of the perturbed Fermi sea with the extra potential. This is the famous *orthogonality catastrophe* (Anderson 1967). It states that despite the fact that the single particle wave functions with and without the local potential differ only slightly by a phase shift, the overlap of the entire many-body Slater determinants goes to zero in the thermodynamic limit for arbitrary weak potential strength.

$$|\langle\Psi_0|\Psi_F\rangle| \propto \left(\frac{1}{N}\right)^{\beta} \xrightarrow[N\to\infty]{} 0. \tag{3.43}$$

The X-ray edge can be thought of as a dynamical version of the *orthogonality catastrophe* with the emission being changed to the singular form

$$I(\omega) \propto \left(\frac{1}{\omega - \omega_{\mathrm{th}}}\right)^{\alpha} \theta\,(\omega - \omega_{\mathrm{th}}) \tag{3.44}$$

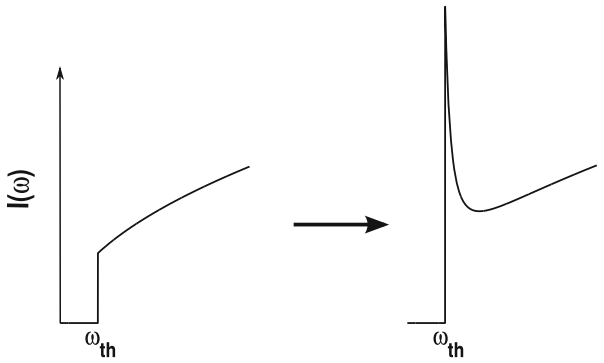

Fig. 3.6 The qualitative change of the X-ray absorption rate $I(\omega)$ is shown once the dynamical nature of the core hole potential is taken into account. Instead of simply being proportional to the density of states of the conduction band, $I(\omega)$ becomes a power-law divergent function at the sharp threshold $\omega_{\rm th} = \epsilon_{\rm F} - \epsilon_c$

which is illustrated in Fig. 3.6. The power law exponents α and β are actually related and can be calculated exactly in terms of phase shifts for the case of a Fermi liquid (Gogolin et al. 1998).

3.4.2 Singular Integral Equations

The famous exact solution of the X-ray edge problem (Nozieres and DeDominicis 1969) proceeds via a mapping to a Riemann–Hilbert problem, which is known in the mathematical literature in the context of complex valued differential equations (Muskhelishvili 1953). However, for the present purpose of calculating exact spin correlations in the Kitaev model several problems appear. The exact solution treats only long time asymptotics, but I am explicitly interested in the full dynamical behavior. In addition, the form of present bare GF is not of the simple asymptotic Fermi liquid form, $G_0 \propto 1/t$, which spoils the exact mapping to a Riemann–Hilbert problem, and hence, forbids an exact analytical solution. In the following, I rely on a related method introduced in the theory of SIEs which in the end allows an exact numerical solution.

To proceed, I split the problem into a product of connected and disconnected contributions $G(t,0) = G_c(t,0)L(t,0)$ (Abrikosov et al. 2012) (analogous for $G(0,t)$).

$$G(t,0) = -i \underbrace{\frac{\langle \mathbb{T} f(t) f^\dagger(0) e^{-i\int_0^t dt_1 V(t_1)}\rangle}{\langle \mathbb{T} e^{-i\int_0^t dt_1 V(t_1)}\rangle}}_{\text{connected diagrams } G_c} \underbrace{\langle \mathbb{T} e^{-i\int_0^t dt_1 V(t_1)}\rangle}_{\text{disconnected diagrams } L} . \tag{3.45}$$

As derived in Appendix B.2 the connected GF can be calculated from the Dyson equation

$$G_c(t,0) = G_0(t,0) - 4J_z \int_0^t dt_1 G_0(t,t_1) G_c(t_1,0), \tag{3.46}$$

which has the form of a Fredholm integral equation of the second kind (Press et al. 2007). It is singular due to the finite integration boundaries. The second contribution to the full GF from the disconnected parts can be fully determined from the connected GF with the help of the linked cluster theorem

$$\begin{aligned} L(t,0) &= \langle \mathbb{T} e^{-i\int_0^t dt_1 V(t_1)} \rangle \\ &= \exp\left[\sum_{i=1}^{\infty} (-) \frac{(4J_z)^i}{i} \int_0^t dt_1 \cdots \int_0^t dt_i G_0(t_1,t_2) G_0(t_2,t_3) \cdots G_0(t_i,t_1) \right], \end{aligned} \tag{3.47}$$

see Appendix B.2.1 for details.

The first and obvious trial for finding a solution is a numerical discretization of the Dyson equation, Eq. (3.46), in real time. The fact that $G_0(t_j,t_i) = G_0(t_j - t_i)$ with t_j and t_i in the interval $[0,t]$ is a Toeplitz matrix, where each descending diagonal in the matrix is constant, lends itself to exploit asymptotic forms of large Toeplitz matrix series (Gutman et al. 2011). After having implemented these asymptotic forms numerically, I discovered that unfortunately the whole numerical procedure in real time is hampered by a finite jump of the bare GF $G_0(t)$ at $t = 0$. Such a discontinuity leads to bad convergence properties of the discretized Eigenvalue problem (Press et al. 2007). Overall, via this real time discretization it is possible to calculate the full dynamical correlation function in the thermodynamic limit for time intervals up to $t = 20$ in the gapless phase. This is still too short for a reasonable resolution in frequency space.

A different approach is to Fourier transform the Dyson equation to frequency space. It has the obvious advantage of having finite integrals due to finite bandwidth of the single particle density of state $N(\omega)$. I obtain a new integral equation in which the singularity from the finite integration range in Eq. (3.46) is transformed to a $1/\omega$ singularity in the integrand, see Eq. (B.22) in Appendix B.3.

For the exact solution, I adapt a formalism first introduced in Grebennikov et al. (1977) for the X-ray edge problem. The mathematical foundation is explained in the influential book by Muskhelishvili (1953). It is based on the simple and beautiful idea to reduce a SIE to a non-SIE with the same solutions. The central point is best sketched by writing the Dyson equation in frequency space in operator form. The task is to find the function G_c via the SIE

$$f = \hat{K}_2 G_c \tag{3.48}$$

with the singular integral operator $\hat{K}_2$ and the inhomogeneity f. By acting on the SIE with a specially constructed integral operator $\hat{K}_1$ it is possible to construct a new integral equation

$$\hat{K}_1 f = \hat{K}_1 \hat{K}_2 G_c \tag{3.49}$$

which is non-singular and has the same solutions. Finding such an operator $\hat{K}_1$ is in general a hopeless enterprise, but for the special case of a Cauchy type singularity, namely $1/\omega$, a general recipe for constructing the appropriate $\hat{K}_1$ exists (Muskhelishvili 1953). Despite the simple basic idea the mathematical details are quite cumbersome so that they are relegated to Appendix B.3.

In the end, I have derived a numerically well-converging non-SIE. I find that with 8001 frequency steps for the bandwidth, the errors are not visible on the scale of the figures, see Chap. 4 with the results.

3.4.3 Adiabatic Approximation

A simple approximation taking into account scattering on the local potential but completely neglecting the dynamical switching is an adiabatic approximation of the local impurity potential V_z. I assume that the flux pair is switched on adiabatically from $t = [-\infty, \infty]$ such that the S-matrix $S(t,0) = \mathbb{T}e^{-i\int_0^t dt' V_z(t')}$ is replaced by $S(\infty,-\infty) = \mathbb{T}e^{-i\int_{-\infty}^{\infty} dt' V_z(t')}$ (Abrikosov et al. 2012). The full GF, Eq. (3.40), is replaced by

$$G(t,0) \xrightarrow{\text{adiabatic}} G^{\text{ad}}(t,0) = -i\langle \mathbb{T} f(t) f^\dagger(0) e^{-i\int_{-\infty}^{\infty} dt_1 V_z(t_1)} \rangle \tag{3.50}$$

such that the Dyson equation, Eq. (3.46), is non-singular

$$G_c^{\text{ad}}(t,0) = G_0(t,0) - 4J_z \int_{-\infty}^{\infty} dt_1 G_0(t,t_1) G_c^{\text{ad}}(t_1,0) \tag{3.51}$$

and can be solved by Fourier transformation $G_0(t,0) = \frac{1}{2\pi}\int_{-\infty}^{\infty} d\omega G_0(\omega) e^{i\omega t}$, which gives

$$G_c^{\text{ad}}(\omega) = \frac{G_0(\omega)}{1 + 4J_z G_0(\omega)}. \tag{3.52}$$

For the X-ray edge in a Fermi liquid such an approximation is very poor since it cannot account for the edge singularities. However, the Kitaev model differs from a simple Fermi liquid. It has a Dirac spectrum which gives a linearly vanishing density of states for $\omega \to 0$, see Fig. 3.7 blue curve $N(\omega) = \text{Im}G_c^A(\omega)$. For this reason, there is no Anderson orthogonality catastrophe, which is well known from Graphene at

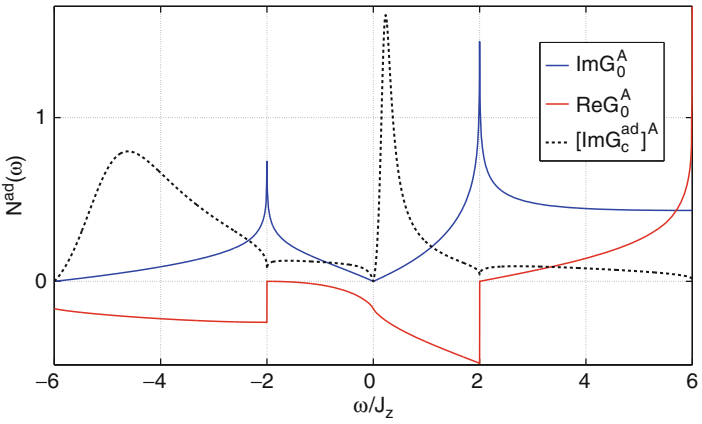

Fig. 3.7 The imaginary (*solid blue*) and real (*solid red*) part of the bare Greens function is shown for the isotropic point $J_x = J_y = J_z = 1$ together with the local density of states in the adiabatic approximation $N^{\mathrm{ad}}(\omega) = \mathrm{Im}\left[G_c^{\mathrm{ad}}\right]^A(\omega)$ (*black dashed*). Note the peak from the van Hove singularity at $\omega = 2J_z$ in the single particle density of states $N(\omega) = \mathrm{Im}G_c^A(\omega)$ leads to a dip in the adiabatic approximation, see Eq. (3.53)

zero doping (Hentschel and Guinea 2007; Yang and Lee 2007; Röder et al. 2011). From finite size scaling I obtain the $N \to \infty$ overlap $|\langle M_0|M_F\rangle| = 0.76929$, see also Fig. 2.27. I will show in the results Chap. 4 that no singular behavior is observed even in the full dynamical problem. In fact, several qualitative features of the exact structure factor can be understood by relating it to the adiabatic approximation. The local density of states $N^{\mathrm{ad}}(\omega) = \mathrm{Im}\left[G_c^{\mathrm{ad}}\right]^A(\omega)$ is calculated from the standard advanced GF (Abrikosov et al. 2012) denoted by the label^A

$$\mathrm{Im}\left[G_c^{\mathrm{ad}}\right]^A(\omega) = \frac{\mathrm{Im}G_0^A(\omega)}{\left[1 + 4J_z\mathrm{Re}G_0^A(\omega)\right]^2 + \left[\mathrm{Im}G_0^A(\omega)\right]^2}. \tag{3.53}$$

The adiabatic DOS $N^{\mathrm{ad}}(\omega)$ is shown for the isotropic point $J_x = J_y = J_z = 1$ together with the bare DOS $N(\omega) = \mathrm{Im}G_0^A(\omega)$ (blue) and $\mathrm{Re}G_0^A(\omega)$ (red) in Fig. 3.7. For a comparison of the exact response with the adiabatic approximation of the structure factor, see Fig. 4.3. Note that the peak of the van Hove singularity from the saddle points in the dispersion (Castro Neto et al. 2009) at $\omega = 2J_z$ leads to a dip in $N^{\mathrm{ad}}(\omega)$, which is easily understood from Eq. (3.53) since $N^{\mathrm{ad}}(\omega) \to \frac{1}{\mathrm{Im}G_0^A(\omega)}$ for $\omega \to 2J_z$. The broad peak in $N^{\mathrm{ad}}(\omega)$ is determined by the resonance condition that $\left[1 + 4J_z\mathrm{Re}G_0^A(\omega)\right]^2$ is minimal.

In a similar fashion, I revisit the Lehmann representation, Eq. (3.16), in the adiabatic approximation. I rewrite the N.N. correlation function, Eq. (3.9), as

$$\begin{aligned} S^{zz,\mathrm{ad}}_{A0B0}(t) &= -i\langle M_0|S(\infty,t)c_{A0}(t)S(t,0)c_{B0}(0)S(0,-\infty)|M_0\rangle \\ &= -ie^{itE_0}\langle M_F|c_{A0}e^{-it(H_0+V_z)}c_{B0}|M_F\rangle \end{aligned} \tag{3.54}$$

such that the Lehmann representation is

$$S^{zz,\mathrm{ad}}_{A0B0}(\omega) = -2\pi i \sum_{\tilde{\lambda}} \langle M_F|c_{A0}|\tilde{\lambda}\rangle\langle\tilde{\lambda}|c_{B0}|M_F\rangle \delta[\omega - (E^F_{\tilde{\lambda}} - E_0)]. \tag{3.55}$$

The only difference with the exact Eq. (3.17) is that the ground state $|M_0\rangle$ has been replaced by $|M_F\rangle$ such that different flux sectors are not mixed. Due to the Dirac spectrum, the low energy Eigenstates with and without two extra fluxes coincide in the gapless phase as $\omega \to 0$ (Chalker, 2013, private communication). Therefore, the adiabatic approximation gives the correct behavior in the low energy limit.

References

A.A. Abrikosov, L.P. Gorkov, I.E. Dzyaloshinski, *Methods of Quantum Field Theory in Statistical Physics* (Courier Dover Publications, New York, 2012)

P.W. Anderson, Infrared catastrophe in fermi gases with local scattering potentials. Phys. Rev. Lett. **18**(24), 1049–1051 (1967)

G. Baskaran, S. Mandal, R. Shankar, Exact results for spin dynamics and fractionalization in the Kitaev model. Phys. Rev. Lett. **98**(24), 247201 (2007)

H. Bethe, Zur theorie der metalle (German). Z. Phys. **71**(3–4), 205–226 (1931)

A. Castro Neto, F. Guinea, N. Peres, K. Novoselov, A. Geim, The electronic properties of graphene. Rev. Mod. Phys. **81**(1), 109–162 (2009)

J.-S. Caux, Correlation functions of integrable models: a description of the ABACUS algorithm. J. Math. Phys. **50**(9), 095214 (2009)

A.O. Gogolin, A.A. Nersesjan, A.M. Tsvelik, *Bosonization and Strongly Correlated Systems* (Cambridge University Press, Cambridge, 1998)

V. Grebennikov, Y. Babanov, O. Sokolov, Extra-atomic relaxation and X-ray-spectra of narrow-band metals. 2. Results. Phys. Status Solidi B Basic Res. **80**(1), 73–82 (1977)

D.B. Gutman, Y. Gefen, A.D. Mirlin, Non-equilibrium 1D many-body problems and asymptotic properties of Toeplitz determinants. J. Phys. A Math. Theor. **44**(16), 165003 (2011)

T.-H. Han, J.S. Helton, S. Chu, D.G. Nocera, J.A. Rodriguez-Rivera, C. Broholm, Y.S. Lee, Fractionalized excitations in the spin-liquid state of a kagome-lattice antiferromagnet. Nature **492**(7429), 406–410 (2012)

M. Hentschel, F. Guinea, Orthogonality catastrophe and Kondo effect in graphene. Phys. Rev. B **76**(11), 115407 (2007)

A. Kitaev, Anyons in an exactly solved model and beyond. Ann. Phys. **321**(1), 2–111 (2006)

S. Lovesey, *Theory of Neutron Scattering from Condensed Matter*. International Series of Monographs on Physics, vol. 2 (Clarendon Press, Oxford, 1984)

G.D. Mahan, Excitons in metals: infinite hole mass. Phys. Rev. **163**(3), 612–617 (1967)

M. Mourigal, M. Enderle, A. Kloepperpieper, J.-S. Caux, A. Stunault, H.M. Ronnow, Fractional spinon excitations in the quantum Heisenberg antiferromagnetic chain. Nat. Phys. **9**(7), 435–441 (2013)

N.I. Muskhelishvili, *Singular Integral Equations* (P. Noordhoff, Groningh, 1953), 468 pp.

P. Nozieres, C. DeDominicis, Singularities in the X-ray absorption and emission of metals. III. One-body theory exact solution. Phys. Rev. **178**(3), 1097–1107 (1969)

K. Ohtaka, Y. Tanabe, Theory of the soft-X-ray edge problem in simple metals: historical survey and recent developments. Rev. Mod. Phys. **62**(4), 929–991 (1990)

W.H. Press, S.A. Teukolsky, W.T. Vetterling, B.P. Flannery, *Numerical Recipes: The Art of Scientific Computing*, 3rd edn. (Cambridge University Press, New York, NY, 2007)

G. Röder, G. Tkachov, M. Hentschel, Photoabsorption spectra and the X-ray edge problem in graphene. Europhys. Lett. **94**(6), 67002 (2011)
K. Tikhonov, M. Feigelman, Quantum spin metal state on a decorated honeycomb lattice. Phys. Rev. Lett. **105**(6), 067207 (2010)
K. Tikhonov, M. Feigelman, A. Kitaev, Power-law spin correlations in a perturbed spin model on a honeycomb lattice. Phys. Rev. Lett. **106**(6), 067203 (2011)
J. von Delft, H. Schoeller, Bosonization for beginners: refermionization for experts. Ann. Phys. **7**(4), 225–305 (1998)
S.-R.E. Yang, H.C. Lee, X-ray edge problem of graphene. Phys. Rev. B **76**(24), 245411 (2007)
J. Zinn-Justin, *Quantum Field Theory and Critical Phenomena*. The International Series of Monographs on Physics Series (Clarendon Press, Oxford, 2002)

Chapter 4
Results for the Structure Factor

So far I have explained how to calculate the exact spin correlation function $S_{ij}^{ab}(t)$ to obtain the Fourier transform in space and time, the dynamical structure factor $S(\mathbf{q}, \omega)$, Eq. (3.1). The latter is proportional to the cross section as measured in INS and at $\mathbf{q} = 0$ in ESR. So far, I have introduced the theoretical background and details of the exact solution. In this chapter, I present the results of my analysis. I concentrate on three representative points A, B, C in Fig. 4.1b in gapless and gapped QSL phases.

The calculation of the correlation function can be mapped to a local quantum quench, in which two adjacent Z_2 fluxes, shown in blue in Fig. 4.1a, are inserted, see Sect. 3.1. Here, I show that there are direct signatures—qualitative and quantitative—in the spin structure factor of the Majorana fermions and gauge fluxes emerging in the Kitaev model. These include counterintuitive manifestations of quantum number fractionalization, such as a neutron scattering response with a gap even in the presence of gapless excitations, and a sharp component despite the fractionalization of electron spin, e.g. for the component $S^{zz}(\mathbf{q}, \omega)$ in the red region of the dynamical phase diagram Fig. 4.1b.

My analysis of Sect. 3.1 has uncovered an entirely new structure in the phase diagram of the Kitaev model, Fig. 4.1. In particular, by studying the Lehmann representation, Eq. (3.17), I find that the relative matter fermion parity of the ground states in the zero and two flux sector has important consequences, because two distinctively different alternatives exist: Either (I) the ground states $|M_0\rangle$ (flux free) and $|M_F\rangle$ (two extra fluxes) have the same parity, in which case the excited states $|\lambda\rangle$, which are involved in the calculation of the structure factor, must contain an odd number of excitations; or (II) the ground states have opposite parity and $|\lambda\rangle$ contains an even number of excitations. In case (II), the sector with zero excitations is an important special case with a contribution to $S(\mathbf{q}, \omega)$ sharp in frequency ω.

The reason why the two ground states may have opposite parity is most transparent deep in the gapped phase, e.g. $J_x, J_y \ll J_z$. There, each z-bond can be occupied or empty with a single complex fermion, and the ground state of the system

J. Knolle, *Dynamics of a Quantum Spin Liquid*, Springer Theses,
DOI 10.1007/978-3-319-23953-8_4

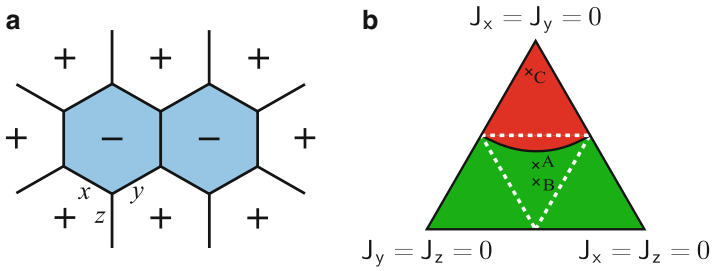

Fig. 4.1 The calculation of the dynamical response can be mapped to a local quantum quench, in which two adjoining Z_2 fluxes, shown in *blue* in *left panel* (**a**), are inserted. In panel (**b**), the ground state and the dynamical phase diagram of the Kitaev model is shown ($J_x + J_y + J_z = 1$). Only the *central triangle* hosts a gapless QSL. The dynamical response $S^{zz}(\mathbf{q}, \omega)$ includes a contribution sharp in ω in the *red region*, but not in the *green region*. I present results for the three different points A, B, C in Figs. 4.3, 4.5, and 4.6

without a flux has an even number of those. The addition of the flux pair amounts to flipping the sign of J_z, hence inverting the energy of that fermion. The ground state with flux thence has opposite parity, as its energy is lowered by occupying the previously empty state. It is remarkable that this sharp δ-function contribution persists from the strong bond limit $J_x, J_y \ll J_z$ all the way into the gapless phase, compare to the red region in Fig. 4.1b.

4.1 Gapless Quantum Spin Liquid Phase

In the gapless phase case (I) no sharp δ-function is expected. In Fig. 4.2 the behavior of the spin correlation function in real time is shown for the isotropic point A ($J_x = J_y = J_z$). The on-site and N.N. correlators $S^{zz}_{A0,A0/B0}(t)$ ($\mathbf{r} = 0$) decay exponentially at short times and have an overall oscillation at the flux gap frequency. In the following, I concentrate on the Fourier transform in space and time which gives the structure factor, see Appendix B.3.2 for a more detailed discussion of the real time behavior.

In Fig. 4.3 (left panel), I show the total dynamical structure factor $S(\mathbf{q}, \omega)$, Eq. (3.1), on a logarithmic color scale as a function of frequency ω along the cut $M\Gamma KM$ through the Brillouin zone (inset). In the right panel, the $\mathbf{q} = 0$ response of the structure factor is presented. The latter contains already all the characteristic features.

First, the response vanishes below the two-flux gap $\Delta = E_0^F - E_0 \simeq 0.26 J_z$, the difference between the ground state energies in a system with and without the flux pair. It is remarkable that in an INS experiment the response of a gapless QSL will show an excitation gap which is directly related to the emergent gauge field.

Second, above the gap Δ, the response thus reflects the physics of the matter sector and can be related to characteristic features of the fermionic density of states shown in the inset of the right panel. Response is substantial over the entire

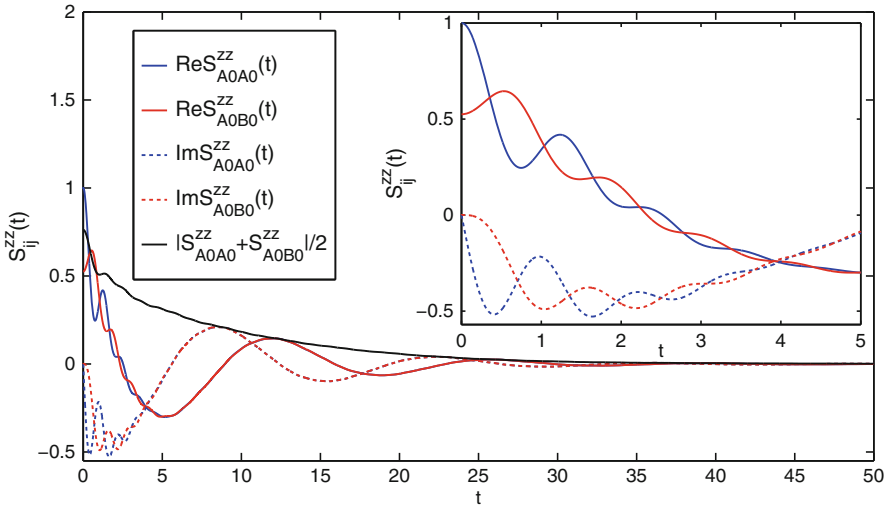

Fig. 4.2 The dynamical spin correlation function in real time is shown for the symmetric point A (J_x=J_y=J_z) in the thermodynamic limit $N \to \infty$. The site diagonal $S^{zz}_{A0A0}(t)$ (*blue*) and the N.N. $S^{zz}_{A0B0}(t)$ (*red*) have an overall exponential decay and a small out of phase oscillation, see the inset for short time behavior. The large overall oscillation comes from the flux gap

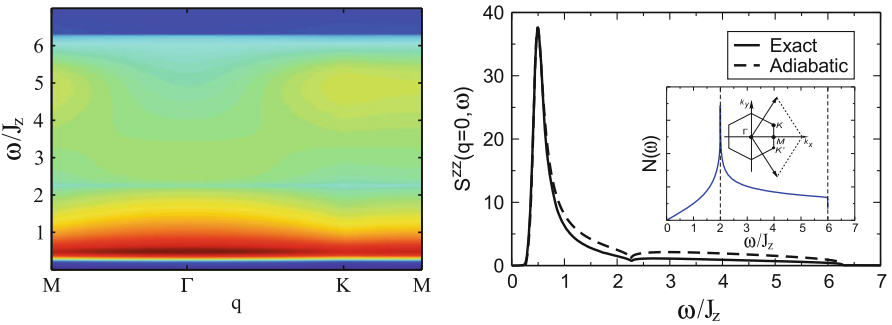

Fig. 4.3 The total dynamical structure factor is shown for the symmetric point (J_x=J_y=J_z): On the *left* the full $S(\mathbf{q}, \omega)$ on a logarithmic color scale as a function of ω along the cut MΓKM through the Brillouin zone as would be measured in inelastic neutron scattering; On the *right*, the dynamical susceptibility $S^{aa}(0, \omega)$ as measured in electron spin resonance (all components $a = z, x, y$ are identical at the isotropic point). The response vanishes below the two-flux gap $\Delta = E_0^F - E_0 \simeq 0.26 J_z$. A comparison with the adiabatic response, as explained in the main text, is given by the *black dashed line*. The *inset* shows the density of states of the matter fermions with the characteristic van Hove singularity and bandwidth which is reflected in the response

single-particle bandwidth (up to $6J_z$ and shifted in energy by Δ), with a linear onset above the gap. However, as a qualitative signature of the effect of gauge fluxes on matter fermion dynamics, the response is far from being simply proportional to the density of states. Instead, the peak due to the van Hove singularity at $2J_z$

yields *a dip* in the response. Quite surprisingly, the overall shape including the dip can be well approximated by replacing the instantaneous insertion of fluxes by an adiabatically slow switching on, see Sect. 3.4.3 especially Eq. (3.53). The adiabatic approximation is shown as a black dashed line in Fig. 4.3 right panel.

Third, as expected for a QSL and similar to the experimental results of the candidate material Herbertsmithite (Han et al. 2012), the full $S(\mathbf{q}, \omega)$ (left panel) exhibits only broad features. The main structure discussed for the $\mathbf{q} = 0$ contribution is simply modulated by a nearest neighbor form factor of the honeycomb lattice due to the ultra short ranged nature of the spin correlations.

Starting from the Lehmann representation of the structure factor, Eq. (3.17), I have shown in Sect. 3.2 how to calculate the different number of particle contributions, see Eq. (3.18). At the isotropic point, single particle excitations dominate the total response, such that its amplitude is appreciable only within the matter fermion bandwidth up to $6J_z$. Indeed, a direct comparison of the single particle component, Eq. (3.25), with the full response yields that only about 2.5 % of the signal at the symmetric point arises from higher multi-particle contributions in stark contrast to the case of the Heisenberg chain (Mourigal et al. 2013), where the corresponding number is almost 30 %. To investigate the role of higher particle excitations I compare the cumulants

$$\mu^n(\omega) = \int_0^\omega d\Omega S(\mathbf{q} = 0, \Omega)\Omega^n \tag{4.1}$$

of the full response (black) and the single particle contributions (color) in Fig. 4.4. Note that beyond $\omega = 6J_z + \Delta$ the cumulant μ^n is a constant for the pure single particle results. In contrast, μ^n keeps growing for the full response due to higher particle processes.

Moving away from the isotropic point A, I show in Fig. 4.5 the structure factor for the anisotropic gapless point B ($J_x = J_y = 0.7J_z$). Away from the symmetric point the saddle points of the single-particle dispersion become inequivalent and two van Hove singularities appear in the density of states (see inset). In addition, different spin components along z and x, y bonds are distinct showing one or two minima in the corresponding dynamical susceptibility (right panel).

In general, the energy of the flux gap, the van Hove singularities, and the bandwidth all scale differently with J_x, J_y, J_z, which could be used as a smoking gun signature to diagnose a QSL in a tentative tunable experiment in the future.

4.2 Gapped Quantum Spin Liquid Phase

Next, I present the result for the gapped QSL phase corresponding to the outer triangles in Fig. 4.1 left panel. For point C ($J_x = J_y = 0.15J_z$) the structure factor in the BZ and for $\mathbf{q} = 0$ are shown in Fig. 4.6. The components S^{zz} and $S^{xx/yy}$ are strongly anisotropic with the former dominated by zero and two-particle

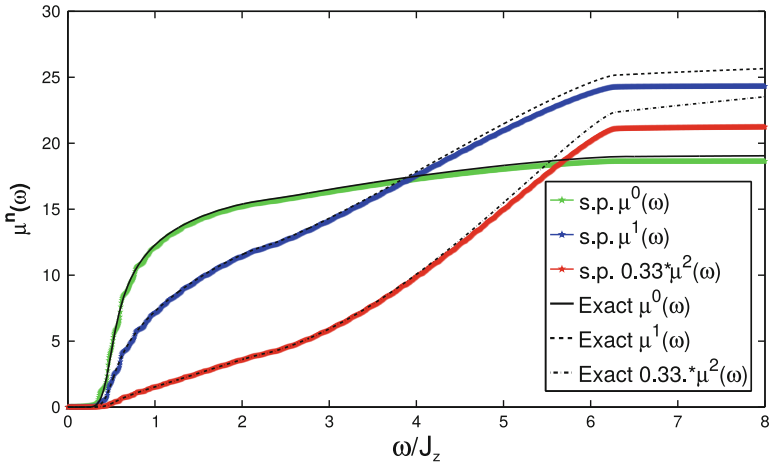

Fig. 4.4 For the isotropic point the cumulants μ^n ($n = 0, 1, 2$) given by Eq. (4.1) are plotted for the full dynamical response (*black*) and the single particle approximation (*green*, *blue*, *red*). Note that at $\omega = 6J_z + \Delta$ already about 98 % of the response are captured by single particle excitations. The single particle results are calculated on a finite size system with 8450 sites (65×65 unit cells). At low energies it shows weak wiggles from finite size effects but the overall weight at higher energies is well converged

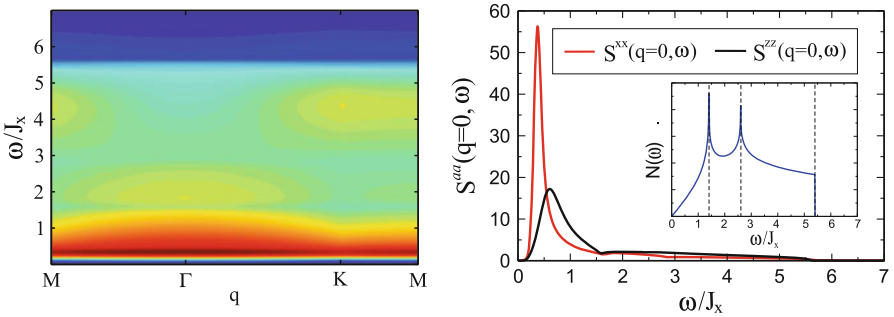

Fig. 4.5 The total dynamical structure factor is shown for the anisotropic point B ($0.7J_x{=}0.7J_y{=}J_z$): On the *left*, the full $S(\mathbf{q}, \omega)$ on a logarithmic *color scale* along the cut MΓKM through the BZ; and on the *right*, the dynamical susceptibility $S^{aa}(0, \omega)$ for inequivalent components $a = z, x$. The *inset* shows the density of states of the matter fermions with two characteristic van Hove singularities and a reduced bandwidth which is reflected in the response

and the latter by single particle excitations, case (II) and (I), respectively. In striking opposition to the gapless isotropic case, the response includes a finite-weight δ-function component in ω at the difference Δ in the ground state energies. It is a remarkable and unexpected finding that—despite fractionalization—the INS response has a component sharp in energy. Again note that the location in the phase

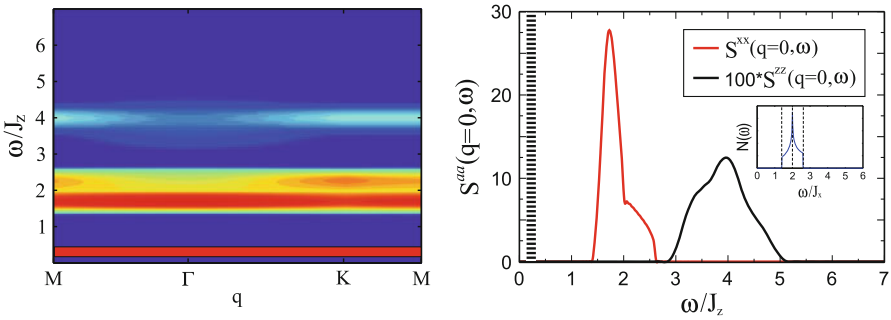

Fig. 4.6 The total dynamical structure factor is shown for the gapped phase point C (J_x=J_y=0.15J_z): On the *left*, the full $S(\mathbf{q},\omega)$ on a logarithmic color scale along the cut MΓKM through the BZ; and on the *right*, the dynamical susceptibility $S^{aa}(0,\omega)$ for inequivalent components $a = z, x$. The *inset* shows the density of states of the matter fermions with a gap in the fermionic spectrum and a strongly reduced bandwidth. The zz-correlator has a δ-function contribution from zero particle excitations at the flux gap Δ from the nonzero ground state overlap $|\langle M_0|M_F^{x,y}\rangle|$, Eq. (3.23). In addition the much weaker response outside of the single particle bandwidth around $4J_z$ is due to two-particle processes. The weak bond correlators xx/yy are mainly captured by single particle excitations

diagram of the dynamical transition at which this sharp response appears is distinct from the ground state phase boundary: It lies entirely within the gapless phase, see Fig. 4.1 red region in the right panel.

Most of the weight of the zz-correlator (black) is carried by the δ-function. The next two-particle contribution around $4J_z$ is two orders of magnitude smaller. The two-particle contribution at higher energies reflects the two-particle density of states of the matter fermions. In fact, the full response apart from the sharp feature at low energies, is entirely captured by the two particle approximation, Eq. (3.27), such that both curves are indistinguishable.

In strong contrast, the weak bond xx/yy-correlators are almost entirely from single particle excitations such that the full response and the approximate calculation, Eq. (3.25), are indistinguishable on the scale of the figure. Moreover, the presence of the single particle gap prevents the creation of low energy particle-hole pairs, hence, the adiabatic approximation is very good as well. It lies right on top of the full response for the weak bond correlators. Each of these features carries over to the structure factor $S(\mathbf{q},\omega)$ in the full BZ with an overall broad modulation (left panel).

In order to check some of the above findings, I have diagonalized the original spin model for eight spins or four dimers, see Appendix C for details. In the strong dimer limit, $J_x, J_y \ll J_z$, in the gapped QSL phase, I observe small amplitude oscillations with a frequency $\omega_z = 4J_z + \Delta$ for the zz-correlator. The weak bond xx- or yy-correlators oscillate with large amplitudes around the frequency $\omega_\perp = 2J_z$. In the gapped phase, the presence of a finite lengthscale set by the inverse fermion gap allows the development of a heuristic based on an even smaller cluster of spins which can be adduced to account for some of the main features. I find that, even by only considering the properties of a single plaquette of four spins with alternating

interactions J_z, J_x and $j = J_x/J_z \ll 1$, I can account for the main oscillation frequencies and for the amplitude scaling with j. The main oscillation with tiny amplitude $O(j^2)$ of the strong bond is at a frequency $4J_z$, which is outside of the single particle bandwidth in the thermodynamic limit corresponding to an almost flat band around $2J_z$. In this toy model sizable contributions with a larger amplitude $O(1)$ to the structure factor are from the weak bonds $S^{xx/yy}$. They are centered around the frequency $2J_z$. All these features are in agreement with the characteristic behavior in the thermodynamic limit $N \to \infty$ as shown in Fig. 4.6.

Overall, the qualitative and quantitative features described above are characteristic of the QSL phase of the Kitaev model. While a potential cold atom realization will likely harbor few perturbations to the Kitaev Hamiltonian, Eq. (2.1), magnetic materials usually include other terms, as extensively discussed for Kitaev–Heisenberg models following (Jackeli and Khaliullin 2009). Both the flux gap and the fermion parity underpinning these results are robust to such perturbations. Just as in the analogous case of the Heisenberg chain (Mourigal et al. 2013), where integrability is imperfect in reality but all qualitative features are well-observed experimentally, I similarly expect quantitative changes such as a small degree of smearing out of the δ-function response or a more gradual onset of the signal around Δ. Crucially, the central features I have discovered will be visible as fingerprints betraying the presence of fractionalized Majorana fermions and emergent gauge fluxes in INS and ESR experiments.

References

T.-H. Han, J.S. Helton, S. Chu, D.G. Nocera, J.A. Rodriguez-Rivera, C. Broholm, Y.S. Lee, Fractionalized excitations in the spin-liquid state of a kagome-lattice antiferromagnet. Nature **492**(7429), 406–410 (2012)

G. Jackeli, G. Khaliullin, Mott insulators in the strong spin-orbit coupling limit: from Heisenberg to a quantum compass and Kitaev models. Phys. Rev. Lett. **102**(1), 017205 (2009)

M. Mourigal, M. Enderle, A. Kloepperpieper, J.-S. Caux, A. Stunault, H.M. Ronnow, Fractional spinon excitations in the quantum Heisenberg antiferromagnetic chain. Nat. Phys. **9**(7), 435–441 (2013)

Chapter 5
Non-Abelian Phase and the Effect of Disorder

5.1 Extended Kitaev Model and Its Exact Solution

Already Kitaev's original paper (Kitaev 2006) introducing the honeycomb lattice model is mainly concerned with an extended version of the Hamiltonian, Eq. (2.1), which gives rise to excitations with non-Abelian statistics. These quasiparticles play a central role in topological quantum computation due to their inherent stability against local perturbations that could lead to decoherence, for a review see Nayak et al. (2008). In this thesis I am mainly interested in the spin liquid properties. Thus, the objective of this chapter is to calculate the spin excitations in such an exactly solvable non-Abelian spin liquid and to search for salient signatures of the phase in the structure factor.

Adding an external magnetic field to the pure Kitaev model leads in third order perturbation theory to an additional three spin interaction which generates a non-Abelian phase (Kitaev 2006). In the following, I add the three spin interaction ad hoc as a term to the Hamiltonian which breaks time reversal symmetry. In the formerly gapless phase the Dirac spectrum of the matter fermions becomes gapped and the bands acquire a nonzero Chern number, which serves as a topological number characterizing gapped non-interacting fermions in 2D (Kitaev 2006).

Recall that there are three inequivalent bond directions on the honeycomb lattice. The additional interaction is such that three spins of each pair of bonds $\langle i,j\rangle_\alpha, \langle j,k\rangle_\beta$ that share a common site j interact via $\hat{\sigma}_i^\alpha \hat{\sigma}_j^\gamma \hat{\sigma}_k^\beta$. The component γ of the middle Pauli matrix is 'perpendicular' to the two other ones α, β.

$$H = -J_x \sum_{\langle ij\rangle_x} \hat{\sigma}_i^x \hat{\sigma}_j^x - J_y \sum_{\langle ij\rangle_y} \hat{\sigma}_i^y \hat{\sigma}_j^y - J_z \sum_{\langle ij\rangle_z} \hat{\sigma}_i^z \hat{\sigma}_j^z - K \underbrace{\sum_{\langle i,j\rangle_\alpha, \langle j,k\rangle_\beta}}_{\gamma \perp \alpha,\beta} \hat{\sigma}_i^\alpha \hat{\sigma}_j^\gamma \hat{\sigma}_k^\beta \quad (5.1)$$

J. Knolle, *Dynamics of a Quantum Spin Liquid*, Springer Theses,
DOI 10.1007/978-3-319-23953-8_5

With the help of the commutation relations $[\hat{\sigma}_a, \hat{\sigma}_b] = 2i\sum_c \epsilon_{abc}\hat{\sigma}_c$ it is possible to express the Hamiltonian in terms of our standard Majorana fermions $c_{A\mathbf{r}}/c_{B\mathbf{r}}$, Eqs. (2.4), (2.5), and bond variables u_{ij} defining the gauge configuration, Eq. (2.6). The extended Hamiltonian, Eq. (5.1), is still exactly solvable. As before, it can be block diagonalized in each flux sector. The key difference is the appearance of N.N.N. hopping terms after fermionization

$$\begin{aligned}\hat{H} = &\sum_{\mathbf{r}} \sum_{\mathbf{n_i}\in\{\mathbf{n_0},\mathbf{n_1},\mathbf{n_2}\}} \frac{iJ_{\alpha(\mathbf{n}_i)}}{2}\hat{u}_{A\mathbf{r}B\mathbf{r}+\mathbf{n_i}}\left[c_{A\mathbf{r}}c_{B\mathbf{r}+\mathbf{n_i}} - c_{B\mathbf{r}+\mathbf{n_i}}c_{A\mathbf{r}}\right] \\ &-iK\sum_{\mathbf{r}} \sum_{\mathbf{d_i}\in\mathbf{d_1},\mathbf{d_3},\mathbf{d_5}} \hat{u}_{A\mathbf{r}B\mathbf{r}+\mathbf{n_j}}\hat{u}_{A\mathbf{r}+\mathbf{d_i}B\mathbf{r}+\mathbf{n_j}}\left[c_{A\mathbf{r}}c_{A\mathbf{r}+\mathbf{d_i}} - c_{A\mathbf{r}}c_{A\mathbf{r}-\mathbf{d_i}}\right] \\ &+iK\sum_{\mathbf{r}} \sum_{\mathbf{d_i}\in\mathbf{d_1},\mathbf{d_3},\mathbf{d_5}} \hat{u}_{A\mathbf{r}+\mathbf{n_k}B\mathbf{r}}\hat{u}_{A\mathbf{r}+\mathbf{n_k}B\mathbf{r}+\mathbf{d_i}}\left[c_{B\mathbf{r}}c_{B\mathbf{r}+\mathbf{d_i}} - c_{B\mathbf{r}}c_{B\mathbf{r}-\mathbf{d_i}}\right], \qquad (5.2)\end{aligned}$$

with a slightly changed notation for the bond operators $\hat{u}_{A\mathbf{r}B\mathbf{r}+\mathbf{n_i}} = ib_{A\mathbf{r}}^{\alpha(\mathbf{n_i})}b_{B\mathbf{r}+\mathbf{n_i}}^{\alpha(\mathbf{n_i})}$ and $\alpha(\mathbf{n_0}) = z, \alpha(\mathbf{n_1}) = x, \alpha(\mathbf{n_2}) = y$. The N.N. vectors are $\mathbf{n_0} = (0,0)$ and $\mathbf{n_1}, \mathbf{n_2}$ as defined before. Each site has six N.N.N. vectors $\mathbf{d_1} = \mathbf{n_1} - \mathbf{n_2}, \mathbf{d_2} = \mathbf{n_1}, \mathbf{d_3} = \mathbf{n_2}, \mathbf{d_4} = -\mathbf{d_1}, \mathbf{d_5} = -\mathbf{d_2}, \mathbf{d_6} = -\mathbf{d_3}$, see Fig. 5.1a. Note that the sign of the N.N.N. hopping is given by the product of the two bond variables linking the two sites. Therefore, in a fixed gauge, the hopping of the effective Majorana problem can be

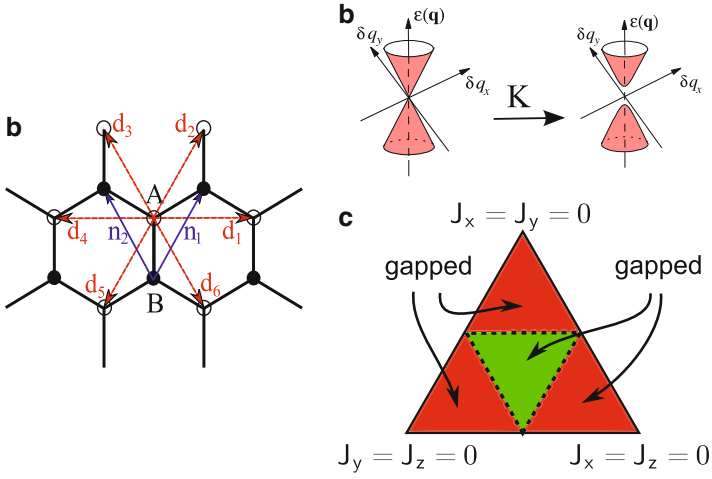

Fig. 5.1 The inclusion of a three spin interaction (with strength K) leads to N.N.N. hopping of the effective Majorana Hamiltonian in a given flux sector along the N.N.N. vectors $\mathbf{d}_1 - \mathbf{d}_6$ shown in panel (**a**). The Dirac cones of the formerly gapless phase are gapped out, panel (**b**). In the new phase diagram, panel (**c**), the formerly gapless central triangle (*green*) is replaced by a gapped QSL hosting quasi-particles with non-Abelian statistics. The outer triangles (*red*) are gapped Abelian QSL phases. The spectrum is gapless only at the transition lines (*dashed*)

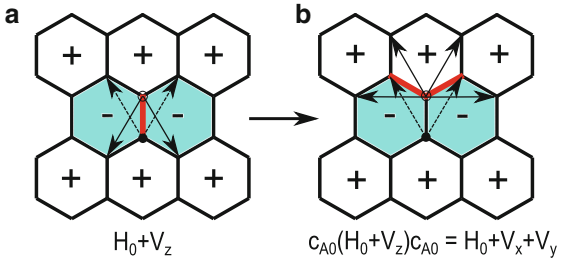

Fig. 5.2 A schematic picture of two Majorana hopping Hamiltonians is presented: On the *left*, $H+V_z$ with the single flipped link variable u_{A0B0} in *red*; on the *right*, $c_{A0}(H+V_z)c_{A0} = H+V_x+V_y$ with the two flipped link variables in *red*. Note that in the latter case, the N.N.N. hoppings indicated by the *arrows* are changed differently for the A (*solid arrows*) and B (*dashed arrows*) sublattices

different for A and B sublattices. This will turn out to be important when taking into account the effect of two extra fluxes, e.g. by either flipping a single or two bonds, as discussed below and depicted in Fig. 5.2.

5.1.1 Flux Free Sector

The ground state of the extended Kitaev model is again flux free (Kitaev 2006; Lieb 1994). I put all Eigenvalues of the bond operators $u_{ij} = +1$ and rewrite the Majorana Hamiltonian, Eq. (5.2), in terms of complex matter fermions, Eq. (2.10), in momentum representation $f_{\mathbf{r}} = \frac{1}{\sqrt{N}} \sum_{\mathbf{q}} e^{-i\mathbf{q}\mathbf{r}} f_{\mathbf{q}}$

$$H_0 = \sum_{\mathbf{q}} \left(f_{\mathbf{q}}^{\dagger} \; f_{-\mathbf{q}} \right) \begin{pmatrix} \xi_{\mathbf{q}} & -\Delta_{\mathbf{q}} \\ -\Delta_{\mathbf{q}}^{*} & -\xi_{\mathbf{q}} \end{pmatrix} \begin{pmatrix} f_{\mathbf{q}} \\ f_{-\mathbf{q}}^{\dagger}. \end{pmatrix} \tag{5.3}$$

Similarly to the pure Kitaev case the Hamiltonian looks just like a superconductor with a momentum dependent gap $\Delta_{\mathbf{q}} = -i\mathrm{Im}S(\mathbf{q}) - \kappa(\mathbf{q})$ and the *normal state* dispersion $\xi_{\mathbf{q}} = \mathrm{Re}S(\mathbf{q})$. However, in contrast to Eq. (2.28) the gap has real and imaginary components and is nonzero at the location of the former Dirac points with $S(\mathbf{q}) = \sum_{\mathbf{n_i}} J_{\alpha(\mathbf{n_i})} e^{i\mathbf{q}\mathbf{n_i}}$ and $\kappa_{\mathbf{q}} = -4K \sum_{\mathbf{d_i} \in \{\mathbf{d_1}, \mathbf{d_3}, \mathbf{d_5}\}} \sin(\mathbf{q}\mathbf{d_i})$.

Putting $\Delta_{\mathbf{q}} = |\Delta_{\mathbf{q}}| e^{i\phi_{\mathbf{q}}}$ the Hamiltonian is diagonalized by a more general Bogoliubov transformation

$$\begin{pmatrix} f_{\mathbf{q}} \\ f_{-\mathbf{q}}^{\dagger} \end{pmatrix} = \begin{pmatrix} \cos(\theta_{\mathbf{q}}) & e^{i\phi_{\mathbf{q}}} \sin(\theta_{\mathbf{q}}) \\ -e^{-i\phi_{\mathbf{q}}} \sin(\theta_{\mathbf{q}}) & \cos(\theta_{\mathbf{q}}) \end{pmatrix} \begin{pmatrix} a_{\mathbf{q}} \\ a_{-\mathbf{q}}^{\dagger} \end{pmatrix}. \tag{5.4}$$

The angles are fixed by the condition $\tan(2\theta_{\mathbf{q}}) = \frac{|\Delta_{\mathbf{q}}|}{\xi_{\mathbf{q}}}$. With the equation $E(\mathbf{q}) = \xi_{\mathbf{q}} \cos(2\theta_{\mathbf{q}}) + |\Delta_{\mathbf{q}}| \sin(2\theta_{\mathbf{q}})$ the final diagonalized Hamiltonian is

$$H_0 = \sum_{\mathbf{q}} E(\mathbf{q}) \left(2a_{\mathbf{q}}^{\dagger} a_{\mathbf{q}} - 1\right) \tag{5.5}$$

with the new dispersion $E(\mathbf{q}) = \sqrt{\xi_{\mathbf{q}}^2 + |\Delta_{\mathbf{q}}|^2}$. The Dirac cones of the formerly gapless part of the phase diagram are gapped out by the N.N.N. hopping, see Fig. 5.1b. The new phase diagram for any nonzero value of the three spin interaction K is shown in Fig. 5.1c. Only along the dashed lines the spectrum is gapless with a quadratic band touching at zero energy. The outer triangles are gapped Abelian spin liquids with trivial Chern numbers of the bands. Only the formerly gapless phase in the central triangle has Chern numbers $\nu = \pm 1$ hosting non-Abelian excitations.

5.2 Role of Fluxes and Transition from Abelian to Non-Abelian Phase

The extended Kitaev model stays exactly solvable. Hence, the calculation of the spin correlation function, Sect. 3.1, via an exact mapping to a quantum quench (Baskaran et al. 2007) carries over step by step. Similarly to the pure Kitaev model the calculation of spin correlations involves two extra fluxes neighboring the bond along which the correlations are measured, see Eq. (3.7).

5.2.1 Two Nearest Neighbor Fluxes

I choose to insert the two fluxes next to the z-bond at $\mathbf{r} = 0$ by flipping the sign of the bond variable u_{A0B0}. The sector with the two extra fluxes is described by the effective hopping problem $H_z = H + V_z$. Previously, for $K = 0$ the Majorana hopping problem was purely between N.N., hence, the *impurity* term V_z was a simple local on-site potential in terms of complex matter fermions $f_{\mathbf{r}}$, Eq. (3.38). Due to this particularly simple form of V_z the calculation of the spin correlation function could be mapped to a standard form of the X-ray edge problem, Sect. 3.4. This is no longer true with the present three spin interaction which introduces N.N.N. hoppings in the Majorana Hamiltonian, Eq. (5.2). Moreover, as the sign of the N.N.N. hopping in a fixed gauge is determined by the product of the two link variables connecting the N.N.N. sites, V_z can also break the sublattice symmetry, as shown in Fig. 5.2. Explicitly written out I obtain

$$\begin{aligned} V_z = & -2iJ_z c_{A0} c_{B0} \\ & +2iK \left[c_{A0} c_{A\mathbf{0}+\mathbf{d_5}} - c_{A\mathbf{0}+\mathbf{d_5}} c_{A0} - c_{A0} c_{A\mathbf{0}+\mathbf{d_6}} + c_{A\mathbf{0}+\mathbf{d_6}} c_{A0} \right] \\ & +2iK \left[c_{B0} c_{B\mathbf{0}+\mathbf{d_2}} - c_{B\mathbf{0}+\mathbf{d_2}} c_{B0} - c_{B0} c_{B\mathbf{0}+\mathbf{d_3}} + c_{B\mathbf{0}+\mathbf{d_3}} c_{B0} \right]. \end{aligned} \tag{5.6}$$

As discussed in detail in Sect. 3.2.1 depending on the ground state parity of $|M_0\rangle$ and $|M_F\rangle$, I need the gauge equivalent expression $c_{A0} H_z c_{A0} = H + V_x + V_y$. Here V_i means that the link variable $u_{A0B0+\mathbf{n_i}}$ changes from $+1$ to -1

$$\begin{aligned} V_x + V_y = & -2i \left[J_x c_{A0} c_{B0+\mathbf{n_1}} + J_y c_{A0} c_{B0+\mathbf{n_2}} \right] \\ & +2iK \left[c_{A0} c_{A\mathbf{0}+\mathbf{d_1}} - c_{A\mathbf{0}+\mathbf{d_1}} c_{A0} - c_{A0} c_{A\mathbf{0}+\mathbf{d_2}} + c_{A\mathbf{0}+\mathbf{d_2}} c_{A0} \right] \\ & +2iK \left[c_{A0} c_{A\mathbf{0}+\mathbf{d_3}} - c_{A\mathbf{0}+\mathbf{d_3}} c_{A0} - c_{A0} c_{A\mathbf{0}+\mathbf{d_4}} + c_{A\mathbf{0}+\mathbf{d_4}} c_{A0} \right] \\ & +2iK \left[c_{B0} c_{B\mathbf{0}+\mathbf{d_2}} - c_{B\mathbf{0}+\mathbf{d_2}} c_{B0} - c_{B0} c_{B\mathbf{0}+\mathbf{d_3}} + c_{B\mathbf{0}+\mathbf{d_3}} c_{B0} \right]. \end{aligned} \tag{5.7}$$

As advertised above, for nonzero K the impurity V_z is more complicated, and therefore, I cannot straightforwardly adapt the previous formalism in terms the X-ray edge approach (Sect. 3.4). However, the exact Pfaffian approach and the few-particle formalism introduced in Sects. 3.3 and 3.2 are still applicable. Before calculating the spin correlations I briefly discuss the special role of fluxes in the non-Abelian phase.

5.2.2 *Continuous Flux Transport in the Non-Abelian Phase*

In the non-Abelian phase each flux carries an unpaired Majorana mode (Kitaev 2006), similar to vortices in a $p_x + ip_y$ superconductor (Ivanov 2001). Fluxes can only be created in pairs and the two bound Majorana fermions correspond to one standard complex fermion at the lowest single particle energy, E_1^F, below the bulk single particle gap at $E_2^F \approx E_1^0$, see Fig. 5.3a. As before, the superscripts 0 and F refer to the matter sectors without and with a flux pair.

If two N.N. fluxes are separated by a distance d, for example by flipping the sign of link variables $u_{An\cdot d_1, Bn\cdot d_1}$ with integers $n \leq d$, the energy of the bound state quickly goes to zero such that the ground state is twofold degenerate, a nice discussion can be found in Lahtinen (2011). In Fig. 5.3b, I plot the energy of the bound state E_1^F as a function of *continuous* flux separation d. In principle the two fluxes can only have a discrete separation distance corresponding to the length of the string of flipped link variables in between the two fluxes. However, it is possible to *continuously* change the link variables u_{AB} from $+1$ to -1, and thus, simulate a continuous flux transport (Lahtinen 2011). Numerically I change u_{AB} in M equidistant steps from +1 to -1. As shown in Fig. 5.3b the energy goes to zero exponentially and has a characteristic oscillatory behavior (Cheng et al. 2009). The energy splitting can be well approximated at the isotropic point as

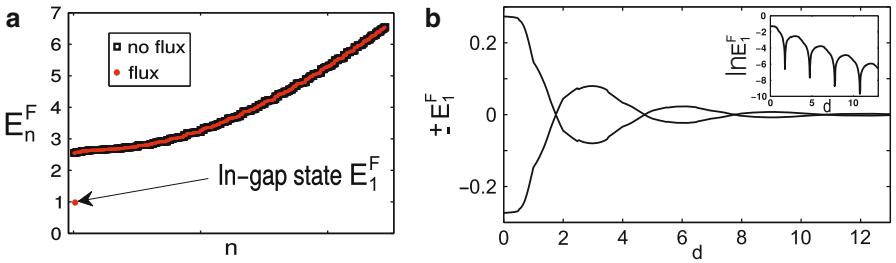

Fig. 5.3 For the isotropic point $J_x = J_y = J_z$, $K = 0.025 J_z$ the spectrum is shown in panel (**a**). Energies E_n^F (*red*) and E_n^0 (*black*) are with and without two N.N. fluxes (energy index n). The lowest energy E_1^F of the spectrum with fluxes, which corresponds to the energy of the localized bound state inside the single particle gap, is shown as a function of *continuous* flux separation d in panel (**b**)

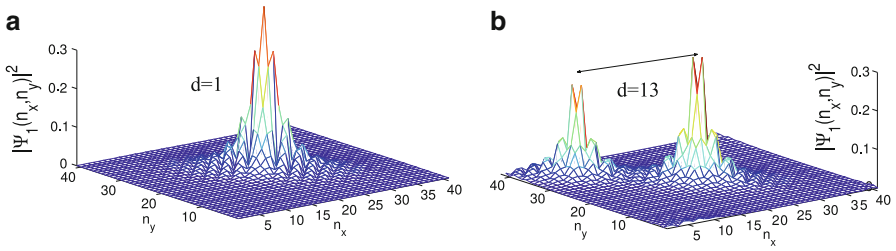

Fig. 5.4 The exponentially localized wave functions $\Psi_1^F(n_x, n_y)$ for flux separation $d = 1$ and $d = 13$ lattice sites are shown in panels (**a**) and (**b**)

$$\pm E_1^F = \Delta_0 \cos(\Omega d)\, e^{-\frac{d}{\xi}}, \tag{5.8}$$

with the energy gap of the non-Abelian phase $\Delta_0 = 6\sqrt{3}K$, $\Omega = k_F^+ - k_F^-$ the difference of the two Fermi momenta at the Dirac points for $K = 0$ and the coherence length $\xi = \frac{1.4}{\Delta_0}$ set by the inverse single particle gap (Lahtinen 2011).

In Fig. 5.4a, b, I show the wave functions of the lowest fermionic Eigenstate $\Psi_1^F(n_x, n_y)$ on the discrete lattice with sites $\mathbf{r} = (n_x, n_y)$ (41×41 unit cells) corresponding to the energy E_1^F for an N.N. flux pair ($d = 1$) and two separated fluxes with $d = 13$. In both cases the wave function of the single state is exponentially localized around the fluxes. It is this latter non-local state, protected by the single particle gap, which has been proposed as a robust memory to store and manipulate quantum information (Nayak et al. 2008).

Once the fluxes are brought into proximity, the degeneracy is lifted and the fermionic state is either occupied or empty depending on energetic details. In the degenerate limit for large flux separation, the occupation of the state is captured by fusion rules (Kitaev 2006; Ivanov 2001). Two fluxes σ can either fuse to the vacuum 1 or a fermion Ψ (Kitaev 2006) which is written as

$$\sigma \times \sigma = 1 + \Psi. \tag{5.9}$$

In fact, the parity of the ground state corresponds to the two different fusion outcomes of the two fluxes σ (Lahtinen 2011). In Fig. 5.4b at each distance at which the energy crosses zero the parity of the ground state matter sector in a fixed gauge changes. In the following $d_c(J_x, J_y, J_z, K)$ refers to the smallest distance at which the energy crosses zero. Note that for the isotropic point $d_c > 1$. Therefore, the parity of the ground state $|M_F\rangle$ and $|M_0\rangle$ is the same.

Note that the parameters J_x, J_y, J_z and K shift d_c. By studying the *continuous* flux transport I have found a simple intuitive explanation of the parity change: The hypersphere $d_c(J_x^c, J_y^c, J_z^c, K^c) = 1$ separates two regions in the phase diagram. This turns out to be important because previously for the pure Kitaev model ($K = 0$), the even and odd parity regions differed strongly, either with the presence or the absence of a δ-function peak in the structure factor as discussed in Sect. 3.2.1 and shown in Fig. 2.4.

Overall, the single fermionic state localized at two fluxes has a two dimensional Fock space corresponding to the two different fusion outcomes. Once the fluxes are separated, the degeneracy of the occupation is robust to local perturbations. A systems of $2l$ separated fluxes has a protected Hilbert space of size 2^l providing the basic ingredient for topological quantum computations (Kitaev 2006). In general, protected Majorana bound states localized at flux pairs are a hallmark of the non-Abelian phase. Hence, the main question in the calculation of the structure factor is how these in-gap states influence the response?

5.2.3 *Quantum Phase Transition in the Extended Kitaev Model*

Before continuing with the calculation of the structure factor, I digress briefly into possible transitions within the phase diagram of the extended Kitaev model.

In the Landau theory of second order phase transitions, thermal fluctuations can trigger a continuous transition between an ordered and a disordered phase which are distinguished by the presence or absence of a symmetry quantified by a local order parameter. Quantum phase transitions (QPT) happen at zero temperature. In this case the change of a parameter in the Hamiltonian leads to level crossings in the spectrum and pushes the system across a critical point. In contrast to Landau theory, QPT driven entirely by quantum fluctuations can occur between two disordered phases without any symmetry breaking (Wegner 1971; Sachdev 2001; Vojta 2003). Here, I briefly discuss such a QPT between Abelian and non-Abelian QSL phases in the extended Kitaev model (Feng et al. 2007; Shi et al. 2009).

I fix the parameter $K = 0.1J_z$ and study the system as a function of $j = J_x/J_z = J_y/J_z$. The transition between the Abelian and non-Abelian phase occurs at $j = 0.5$. In Fig. 5.5, I plot various spectral quantities as a function of j. In red I show the ground state overlap between the flux free and the two flux sector $|\langle M_0|M_F^{x,y}\rangle|$

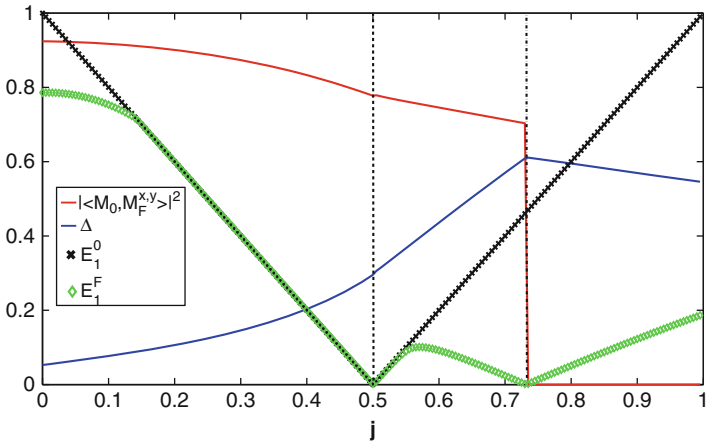

Fig. 5.5 For $K = 0.1J_z$ the evolution of spectral properties are plotted as a function of $j = J_x/J_z = J_y/J_z$ to look for signatures of the transition between the Abelian and non-Abelian phase at $j = 0.5$. The overlap $|\langle M_0|M_F^{x,y}\rangle|$ is shown in *red* and the behavior of the flux gap Δ in *blue*. Both quantities are continuous at the transition but their derivative is discontinuous, signaling the phase transition (Shi et al. 2009). In addition, I show the behavior of the lowest energy Eigenstate of the flux free (*black crosses*) and two flux system (*green diamond*). The single particle gap closes at the transition $j = 0.5$. Only in the non-Abelian phase with extra fluxes an in-gap energy level appears (*green diamond*). It disperses as a function of j and touches zero at the point when the parity of the matter sector changes

and in black the behavior of the flux gap Δ. Both quantities are continuous at $j = 0.5$ but their derivatives are discontinuous, signaling the phase transition. It was shown recently that the ground state energy E_0 of the flux free ground state is only discontinuous in the third derivative $\frac{\partial^3 E_0}{\partial j^3}$ (Shi et al. 2009). I find the same discontinuity for the flux gap, see also Fig. 5.8 inset.

In addition, I present the behavior of the lowest energy Eigenstate E_1^0 of the flux free (black open circles) and the two-flux system E_1^F (black dots) . The spectrum closes its gap when crossing the phase boundary at $j = 0.5$. Most interestingly, only in the non-Abelian phase an in-gap energy level appears such that E_1^F is separated from the single particle continuum beginning at the next level E_2^F. Similarly to Fig. 5.4 the in-gap state disperses as a function of j and touches zero at the point where the parity of the matter sector changes around $j \approx 0.73$.

5.3 Spin Structure Factor

Similarly to the case of pure Kitaev model in Chap. 3, the main objective is the calculation of the structure factor $S(\mathbf{q}, \omega)$. Since the three spin interaction conserves the exact solubility, the spin correlation function can be expressed in the ground

state flux sector as a quantum quench, Eq. (3.9). I put $\mathbf{r} = 0$ and calculate the same N.N. and site diagonal correlators S^{zz} as given in Eq. (3.9) with V_z replaced by the new expression Eq. (5.6).

Before presenting the results, I discuss the calculation of the leading few particle contributions and the exact Pfaffian approach.

5.3.1 Few-Particle Contributions

Again, I study the contributions of the different number of particle sectors to the Lehmann representation, Eq. (3.18). Depending on whether the ground state parity of the flux sectors $|M_0\rangle$ and $|M_F\rangle$ are the same (I), or different (II), only even or odd numbers contribute.

Following Sect. 3.2.1, in case (II) all states $|\lambda\rangle$ in the Lehmann representation Eq. (3.17) have the same parity as the ground state $|M_0\rangle$. Therefore, only even number of particle processes contribute. The first contribution arises from the ground state of the two flux sector. In addition, note that the operator $c_{A0}H_z c_{A0} = H_{x,y}$ is the gauge equivalent Majorana hopping Hamiltonian with the two link variables along the x and y bonds flipped instead of the z bond, see Eq. (5.7). I express all operators in terms of a-operators and the corresponding ground state, Eq. (2.26), to obtain

$$S^{zz}_{A0B0,(0)}(t) = \sqrt{\det\left(\mathcal{X}^\dagger\mathcal{X}\right)}e^{it(E_0-E_0^F)}\left\{1-2\sum_k |Y_{k0}|^2 - 2\sum_{j,k} Y^\dagger_{0k}\mathcal{F}^*_{kj}X^*_{j0}\right\} \tag{5.10}$$

$$S^{zz}_{A0A0,(0)}(t) = \sqrt{\det\left(\mathcal{X}^\dagger\mathcal{X}\right)}e^{it(E_0-E_0^F)} \tag{5.11}$$

$$S^{zz}_{A0A0,(0)}(t) = \sqrt{\det\left(\tilde{\mathcal{X}}^\dagger\tilde{\mathcal{X}}\right)}e^{it(E_0-\tilde{E}_0^F)} \tag{5.12}$$

$$S^{zz}_{B0A0,(0)}(t) = \sqrt{\det\left(\mathcal{X}^\dagger\mathcal{X}\right)}e^{it(E_0-E_0^F)}\left\{1-2\sum_k |Y_{k0}|^2 - 2\sum_{j,k}\left(Y^\dagger_{0k}\mathcal{F}^*_{kj}X^*_{j0}\right)^*\right\}. \tag{5.13}$$

In the third line, the tilde means that the Hamiltonian in the two flux sector has the lower x and y bonds flipped $c_{B0}H_z c_{B0} = \tilde{H}_{x,y}$ which does not change the spectrum and E_0^F. The only difference with respect to the pure Kitaev model, Eqs. (3.23) and (D.3), is the form of the Bogoliubov transformation which diagonalizes the flux free system. Here, I work directly in real space since the extra flux in the excited flux sector breaks translational invariance. The flux is local and simple in real space such that the Hamiltonian matrix is sparse, which leads to a better performance

in numerical computations as compared to a representation in momentum space. For the Fourier transformation of the structure factor at $\mathbf{q} = \mathbf{0}$ I obtain (summation over double indices):

$$S^{zz}_{(0)}(\mathbf{q}=\mathbf{0},\omega) = 8\pi\sqrt{\det\left(\mathcal{X}^\dagger\mathcal{X}\right)}\left\{1-\sum_k |Y_{k0}|^2 - \mathrm{Re}\left[Y^\dagger_{0k}\mathcal{F}^*_{kj}X^*_{j0}\right]\right\}\,\delta\left(\omega-\left[E_0-E_0^F\right]\right) \tag{5.14}$$

In case (I), the first contribution arises from single particle states, see Sect. 3.2.2. I insert the identity into the Lehmann representation of the correlator, Eq. (3.9), such that only states with opposite parity contribute. I restrict to single particle states $|\lambda\rangle = b^\dagger_\lambda|M_0^F\rangle$. With the help of the identity $\mathcal{X}_{\lambda j}-\mathcal{V}_{\lambda l}\mathcal{F}_{lj} = \left[\mathcal{X}^\dagger\right]^{-1}_{\lambda j}$ the final results are

$$S^{zz}_{A0B0,(1)}(t) = \sqrt{\det\left(\mathcal{X}^\dagger\mathcal{X}\right)}\sum_\lambda e^{it(E_0-E^F_\lambda)}\sum_{j,l}\left[X^\dagger_{0l}-Y^\dagger_{0l}\right]\mathcal{X}^{-1}_{l\lambda}\left[\mathcal{X}^{-1}\right]^\dagger_{\lambda j}\left[X_{j0}+Y_{j0}\right] \tag{5.15}$$

$$S^{zz}_{A0A0,(1)}(t) = \sqrt{\det\left(\mathcal{X}^\dagger\mathcal{X}\right)}\sum_\lambda e^{it(E_0-E^F_\lambda)}\sum_{j,l}\left[X^\dagger_{0l}+Y^\dagger_{0l}\right]\mathcal{X}^{-1}_{l\lambda}\left[\mathcal{X}^{-1}\right]^\dagger_{\lambda j}\left[X_{j0}+Y_{j0}\right] \tag{5.16}$$

$$S^{zz}_{B0B0,(1)}(t) = \sqrt{\det\left(\mathcal{X}^\dagger\mathcal{X}\right)}\sum_\lambda e^{it(E_0-E^F_\lambda)}\sum_{j,l}\left[X^\dagger_{0l}-Y^\dagger_{0l}\right]\mathcal{X}^{-1}_{l\lambda}\left[\mathcal{X}^{-1}\right]^\dagger_{\lambda j}\left[X_{j0}-Y_{j0}\right] \tag{5.17}$$

$$S^{zz}_{B0A0,(1)}(t) = \sqrt{\det\left(\mathcal{X}^\dagger\mathcal{X}\right)}\sum_\lambda e^{it(E_0-E^F_\lambda)}\sum_{j,l}\left[X^\dagger_{0l}+Y^\dagger_{0l}\right]\mathcal{X}^{-1}_{l\lambda}\left[\mathcal{X}^{-1}\right]^\dagger_{\lambda j}\left[X_{j0}-Y_{j0}\right]. \tag{5.18}$$

The Fourier transformation gives

$$S^{zz}_{(1)}(\mathbf{q}=\mathbf{0},\omega) = 8\pi\sqrt{\det\left(\mathcal{X}^\dagger\mathcal{X}\right)}\sum_\lambda \delta\left(\omega-\left[E_0-E^F_\lambda\right]\right)\sum_{j,l}X^\dagger_{0l}\mathcal{X}^{-1}_{l\lambda}\left[\mathcal{X}^{-1}\right]^\dagger_{\lambda j}X_{j0}. \tag{5.19}$$

For case (II), the first frequency dependent contribution beyond the δ-function from the ground state overlaps, Eq. (5.14), comes from two-particle contributions. The expression is the same as for the pure Kitaev model, see Eq. (3.27).

5.3.2 Exact Pfaffian Approach

Calculating spin correlations in the extended Kitaev model remains equivalent to a local quantum quench. However, because of the additional N.N.N. hoppings, the impurity like contribution V_z, Eq. (5.6), is not a pure on-site potential anymore. Hence, I cannot simply use the previous exact X-ray edge formalism of Chap. 3.4. Fortunately, the exact evaluation via Pfaffians, Sect. 3.3, is still possible. As before, I express all correlators, Eq. (3.9), in terms of the a-operators diagonalizing the flux free ground state to obtain

$$S^{zz}_{A0B0}(t) = e^{itE_0} \sum_{j,l} \left[X^\dagger_{0l} - Y^\dagger_{0l} \right] \mathbf{M}_{j,l} \left[X_{j0} + Y_{j0} \right] \tag{5.20}$$

$$S^{zz}_{A0A0}(t) = e^{itE_0} \sum_{j,l} \left[X^\dagger_{0l} + Y^\dagger_{0l} \right] \mathbf{M}_{j,l} \left[X_{j0} + Y_{j0} \right] \tag{5.21}$$

$$S^{zz}_{B0B0}(t) = e^{itE_0} \sum_{j,l} \left[X^\dagger_{0l} - Y^\dagger_{0l} \right] \mathbf{M}_{j,l} \left[X_{j0} - Y_{j0} \right] \tag{5.22}$$

$$S^{zz}_{B0A0}(t) = e^{itE_0} \sum_{j,l} \left[X^\dagger_{0l} + Y^\dagger_{0l} \right] \mathbf{M}_{j,l} \left[X_{j0} - Y_{j0} \right] \tag{5.23}$$

with the matrix element

$$\mathbf{M}_{j,l} = \langle M_0 | a_j e^{-it(H_0+V_z)} a^\dagger_l | M_0 \rangle, \tag{5.24}$$

which is calculated in terms of Pfaffians as outlined in detail in Appendix A, for the final expression see Eq. (3.35).

5.3.3 Results: Signatures of Localized Majorana Bound States

Majorana bound states localized at fluxes and protected by a gap are a hallmark of the non-Abelian phase. In the structure factor of the pure Kitaev model a sharp component in energy appeared only away from the isotropic point ($J_x = J_y = J_z$) in, or close to, the gapped QSL phases. In the following, I show that in the non-Abelian phase boundstates of Majorana fermions localized at the inserted flux pair lead to a δ-function response even at the isotropic point.

In this section, I only discuss results from the few-particle contributions, which allows me to go to much larger systems sizes than for the Pfaffian approach. For the pure Kitaev model, I have shown in Fig. 4.4 (Chap. 4) that single particle contributions capture already 98 % of the full response at the isotropic point. Thus, restricting the calculation of the structure factor to the few particle sectors should be a good approximation at least for small K. Fortunately, the presence of a single

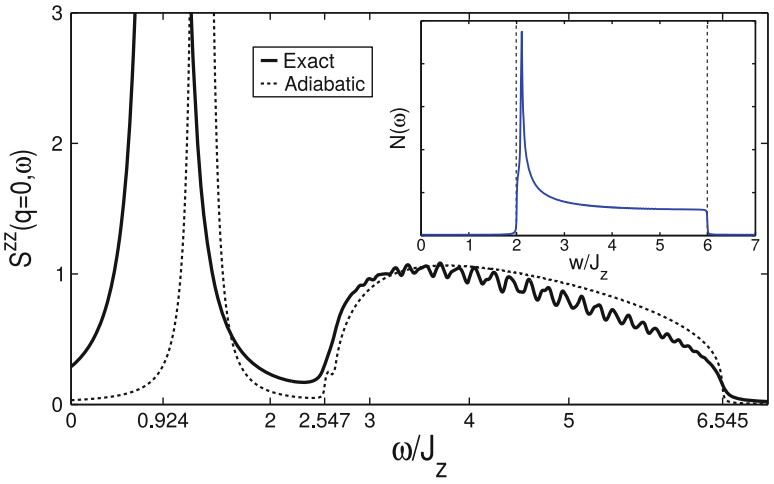

Fig. 5.6 The single particle contribution of the dynamical structure factor $S(\mathbf{q} = 0, \omega)$ (*solid black*) is plotted for the isotropic point in the non-Abelian phase ($J_x = J_y = J_z$ and $K = 0.1J_z$). Note the larger δ-function contribution from the localized state at the N.N. flux pair at an energy $\Delta + E_1^F = 0.924J_z$ below the single particle gap (broadening of the δ-function $\Gamma = 0.025J_z$ and 56×56 unit cells). The adiabatic approximation is shown by the *dashed line* and the single particle density of states $N(\omega)$ is given in the *inset*

particle gap set by the three spin interaction K avoids strong finite size effects observed in the gapless QSL phase of the pure model. In addition, I have checked that for small system sizes the results of the exact Pfaffian approach and the few-particle approximation almost coincide.

I begin with the formerly gapless phase which hosts non-Abelian quasiparticles. I concentrate on $J_x = J_y = J_z$ and put $K = 0.1J_z$. Both ground states $|M_0\rangle$ and $|M_F\rangle$ have the same parity, case (I), such that no sharp δ-function is expected from the ground state overlap. In Fig. 5.6, I show the total dynamical structure factor $S(\mathbf{q} = 0, \omega)$ (solid black), which contains all characteristic features of the full momentum dependent $S(\mathbf{q}, \omega)$. Its salient features can again be related to either the emergent matter fermions, or the flux sector.

First, the continuous frequency dependent response vanishes below the continuum gap $\tilde{\Delta} = \Delta + E_2^F$ which is set by the sum of the two-flux gap, $\Delta = E_0^F - E_0 \simeq 0.545J_z$, and the on-set of the single particle continuum at the second energy level $E_2^F = 2.002J_z$.

Second, a sharp δ-function contribution from the localized fermionic bound state is observed even at this isotropic point at an energy $\omega = \Delta + E_1^F = 0.924J_z$ below the on-set of the continuous response at $\tilde{\Delta}$. The sharp feature carries most of the weight of the total response. It is remarkable that in an INS experiment the response of a non-Abelian QSL will show a sharp component directly related to the composite flux-Majorana pair which is a hallmark of this topological phase.

Third, above the gap $\tilde{\Delta}$, the response reflects the physics of the matter sector and can be related to characteristic features of the fermionic density of states $N(\omega)$, see Fig. 5.6 inset. Response is substantial over the entire single particle bandwidth. As before, I compare the response to the adiabatic approximation (black dashed) which now contains the additional approximation that the potential is of the simple local form $V_z = -2iJ_z c_{A0} c_{B0}$ which neglects inverted N.N.N. hoppings in Eq. (5.6). Surprisingly, the overall shape including the δ-function can be well approximated by replacing the instantaneous insertion of fluxes by an adiabatically slow switching on, see Sect. 3.4.3, especially Eq. (3.53). However, due to the oversimplified potential V_z the energy of the bound state comes out wrong. In reality, the additional terms in V_z, Eq. (5.6), create an even deeper potential which pulls the true energy of the bound state to lower energies.

Next, I show in Fig. 5.7 the inequivalent components $a = z, x$ of the structure factor $S^{aa}(\mathbf{q} = 0, \omega)$ for the anisotropic point $J_x = J_y = 0.15J_z$ ($K = 0.1J_z$). This point corresponds to the formerly gapped QSL, and it hosts an Abelian QSL even for nonzero three spin interaction K. The components S^{zz} (black) and $S^{xx/yy}$ (red) are strongly anisotropic, with the former dominated by zero as well as two-particle and the latter by single particle excitations, case (II) and (I), respectively. The response includes a δ-function component for S^{zz} (black) at the energy of the flux gap $\Delta = 0.0905J_z$. The next contribution is at much higher energies from two particle excitations in the two particle bandwidth $[\Delta + 2E_1^F, \Delta + 2E_N^F]$. Note that

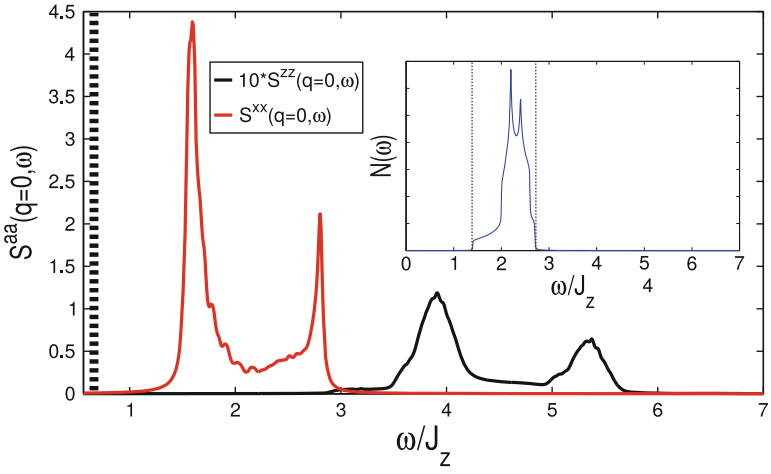

Fig. 5.7 The dynamical structure factor $S^{aa}(0, \omega)$ for inequivalent components $a = z, x$ is shown for the also formerly gapped phase (J_x=J_y=$0.15J_z$ and $K = 0.1J_z$, 56×56 unit cells and δ-function broadening $\Gamma = 0.025J_z$). The *inset* shows the density of states of the matter fermions with a strongly reduced bandwidth. The zz-correlator has a δ-function contribution from zero particle excitations at the flux gap Δ from the nonzero ground state overlap $|\langle M_0 | M_F^{x,y} \rangle|$. In addition, the much weaker response outside of the single particle bandwidth is due to two particle processes. The weak bond correlators xx/yy are from single particle excitations

the origin of the δ-function in the Abelian and non-Abelian phase is different. In the former, it is due to the ground state overlap of the two different flux sectors. In the latter, it is a signature of the localized fermionic state in the two flux sector. The latter is calculated from single particle contributions.

As discussed in Sect. 5.2.3, clear signatures of the QPT from the Abelian to the non-Abelian phase are observable in spectral properties. For example, higher derivatives of the ground state energy and the flux gap are discontinuous. An important question is whether there are clear signatures of the transition in the structure factor. In addition, are there traces of the transition between different parity sectors, from case (I) to case (II)? In contrast to the pure Kitaev model the structure factor with additional three spin interactions has a sharp contribution in both sectors. In Fig. 5.8, I show the weight of the δ-function of the structure factor $S(\mathbf{q} = 0, \omega_{\min})$ as a function of $j = J_x/J_z = J_y/J_z$ ($K = 0.1J_z$). The inset displays the corresponding energy $\omega_{\min}$. For $j < 0.73$, case (II), the sharp component stems from the finite ground state overlap, $\omega_{\min} = \Delta$ (blue crosses). The phase transition between the Abelian and non-Abelian phase at $j = 0.5$ is clearly seen as a kink in the weight of the δ-function and in derivatives of $\omega_{\min} = \Delta$. Therefore, the QPT between both QSL phases is clearly observable in the structure factor.

In case (I) $j > 0.73$, the lowest contribution at $\omega_{\min} = \Delta + E_1^F$ (red) arises from the localized bound state at energy E_1^F of the single particle spectrum. Surprisingly, the evolution of the weight and energy across the two different parity sectors is

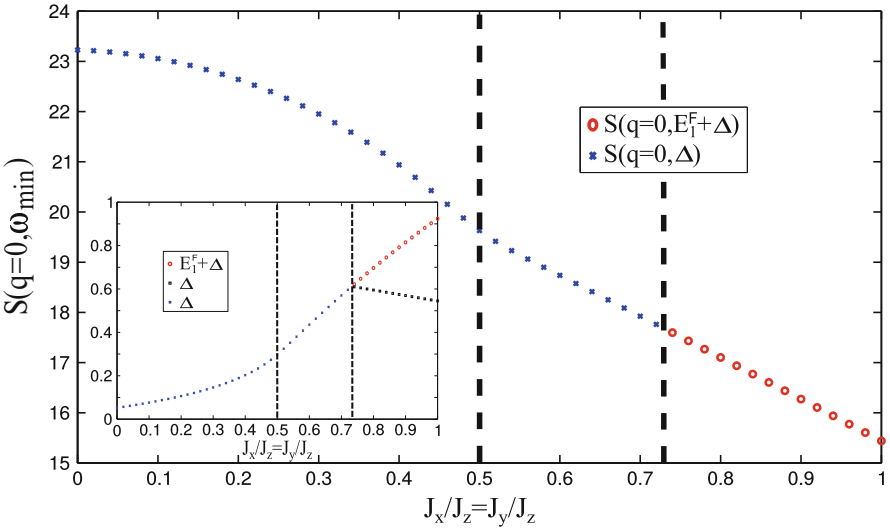

Fig. 5.8 The evolution of the weight of the δ-function $S(\mathbf{q} = 0, \omega_{\min})$ is shown as a function of $j = J_x/J_z = J_y/J_z$ ($K = 0.1J_z$). The *inset* displays the corresponding energy $\omega_{\min}$. For $j < 0.73$, case (II), $\omega_{\min} = \Delta$ (*blue crosses*) but for case (I), $j > 0.73$, the lowest contribution is at $\omega_{\min} = \Delta + E_1^F$ (*red*). The phase transition between the Abelian and non-Abelian phase at $j = 0.5$ is clearly seen as a kink in the weight and in derivatives of $\omega_{\min} = \Delta$. In contrast, the evolution across the two different parity sectors is smooth

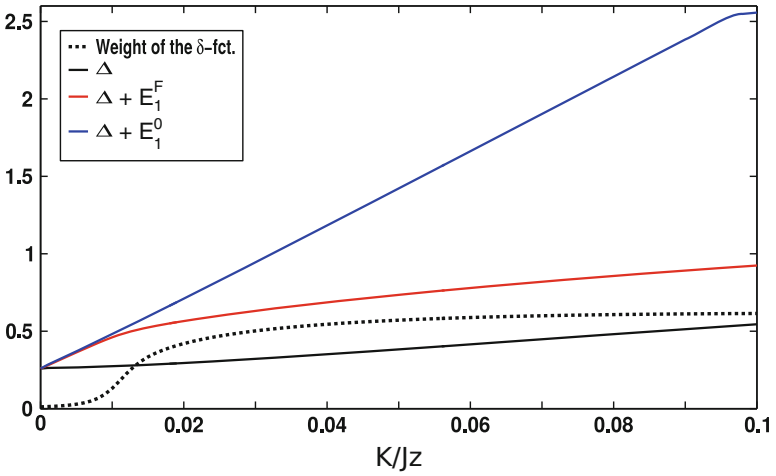

Fig. 5.9 It is shown how the weight of the δ-peak $S(\mathbf{q} = 0, \Delta + E_1^F)$ (*black dashed)* vanishes as the system goes gapless with $K \to 0$ (isotropic point). It vanishes as a high power in K. The single particle gap closes (*blue*) such that the in-gap state (*red*) drops to zero energy above the flux gap

totally smooth and no singularity can be found in the derivatives. Note that $E_1^F \to 0$ at the transition point, see Fig. 5.5. I checked that the full frequency dependence for $j < 0.73$ (zero+two-particle contributions) and for $j > 0.73$ (single particle contributions) smoothly interpolates between the sectors. Only in the on-set of the continuum $S(\mathbf{q} = 0, \omega > \omega_{\min})$ weak traces of the transition are visible.

Finally, Fig. 5.9 presents how the δ-peak $S(\mathbf{q} = 0, \omega_{\min})$ (black dashed) vanishes at the isotropic point as the system goes gapless with $K \to 0$. As the system approaches the Abelian phase the single particle gap (blue) closes such that the in-gap state merges with the continuum (red). The δ-function (black dashed) vanishes as a high power in K. Due to the gapless nature of the limiting phase ($K = 0$), I have not been able to determine the precise exponent from finite size scaling.

5.4 Effect of Disorder

A key question for the non-Abelian phase is the stability of its characteristic features with respect to various perturbations. Most importantly, how robust is the sharp δ-function contribution from the localized bound state at the flux pair, which distinguishes the non-Abelian phase from the Abelian one at the isotropic point? In this section, I concentrate on a particular perturbation and study the effect of exchange disorder on the structure factor in the non-Abelian phase.

Recently, several groups have studied disordered effective Majorana models. By calculating a topological invariant for systems without translational invariance (Loring and Hastings 2010), it is possible to study the stability of the non-Abelian

phase with respect to increasing disorder. On the one hand, it was shown for one particular model that the non-Abelian phase is stable with respect to a small density of sign disorder in the corresponding effective Majorana hopping problem (Laumann et al. 2012), but for strong sign disorder the non-Abelian character is lost. On the other hand, random exchange constants can also enlarge the region of the non-Abelian phase, which was found for a different exactly solvable QSL (Yao and Kivelson 2007) by studying energy level statistics (Chua and Fiete 2011). All studies agree that at very large disorder strength, a so-called *thermal metal phase* appears (Chalker et al. 2001; Laumann et al. 2012; Kraus and Stern 2011). This is a gapless state characterized by broken time reversal symmetry and by a logarithmically diverging density of states, which exhibits characteristic oscillations at low energies (Lahtinen et al. 2014).

In the context of the extended Kitaev model, the effect of disorder including the appearance of the thermal metal phase was recently verified in Lahtinen et al. (2014). I follow their work and model a randomly deformed lattice by a local flat random distribution of the exchange couplings J_{ij},

$$J_{ij} \to (1 + \delta_{ij}) \;\text{ with }\; \delta_{ij} \in [-\delta J, \delta J]\,. \tag{5.25}$$

The system is still exactly solvable but with disordered hopping amplitudes of the effective Majorana Hamiltonian in the ground state flux sector with $u_{ij} + 1$. I restrict myself to the isotropic point $J_x = J_y = J_z$ for $\delta J \to 0$ and set $K = 0.1 J_z$. Note for $\delta J > 1$ the sign of the couplings is negative which effectively introduces new fluxes or moves existing ones around.

In Fig. 5.10, I show several disorder averaged quantities as a function of disorder strength δJ. In the left panel, the averaged single particle gap in the flux free

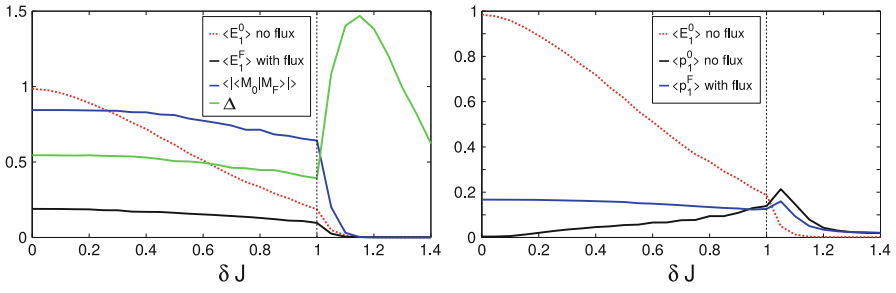

Fig. 5.10 Disorder averaged spectral properties are shown for the isotropic point $J_x = J_y = J_z$ and $K = 0.1 J_z$ as a function of disorder strength δJ (1000 disorder realizations, 23×23 unit cells). In the *left panel*, I show the disorder averaged single particle gap in the flux free system $\langle E_1^0 \rangle$ (*red dashed*), the average energy of the in-gap state of the two localized Majorana modes in the two flux sector $\langle E_1^F \rangle$ (*black*), the averaged overlap between the two ground states $\langle |\langle M_0 | M_F \rangle| \rangle$ (*blue*) and the average flux gap $\langle \Delta \rangle$ (*green*). In the *right panel*, I plot the disorder averaged participation ratio $\langle p_1^0 \rangle$ and $\langle p_1^F \rangle$ in the flux free (*black*) and the two flux (*blue*) sector for the lowest lying Eigenstate as a function of disorder strength δJ, see text for discussion

system $\langle E_1^0 \rangle$ (red dashed) drops and closes around $\delta J \approx 1.1$. The in-gap state of the two localized Majorana modes in the two flux sector, $\langle E_1^F \rangle$ (black), shows only weak dependence on δJ for small disorder strength; it only drops to zero once the single particle gap pushes it down. Similar to the flux gap $\langle \Delta \rangle$ (green), the overlap $\langle |\langle M_0 | M_F \rangle| \rangle$ (blue) is only effected when approaching the critical disorder strength $\delta J = 1$. Slightly above this value few isolated fluxes appear and additional fermionic states are localized. However, above $\delta J > 1$, the flux gap (green) quickly grows with a large standard deviation (not shown). Due to flux–flux interactions the insertion of an additional N.N. flux pair can cost a significant amount of energy if other fluxes are close. The maximum of the two flux gap at $\delta J_{\max} \approx 1.18$ corresponds to a flux density of 1/3 (Lahtinen et al. 2014). It can be understood in the following way: 1/3 is the largest flux density with the possibility of having only N.N.N. fluxes (no N.N. flux pairs). Then, the two extra N.N. fluxes from the quantum quench form a four flux cluster which is energetically costly. At higher flux densities the insertion of two extra N.N. fluxes mostly moves existing fluxes around.

Another important quantity to look at is the participation ratio

$$p_n = \int d^2 r |\Psi_n(r)|^4 \tag{5.26}$$

which quantifies how localized a wave function $\Psi_n(r)$ is. In Fig. 5.10 right panel, I plot the participation ratio $\langle p_1^0 \rangle$ and $\langle p_1^F \rangle$ in the flux free (black) and the two flux (blue) sector for the lowest energy Eigenstates $\Psi_1^0(r), \Psi_1^F(r)$. As expected for the localized mode, $\langle p_1^F \rangle$ is large for all values of $\delta J < 1$ and hardly changes as long as the single particle gap is appreciable. In the zero flux sector the participation ratio $\langle p_1^0 \rangle$ grows linearly until its maximum around $\delta J \approx 1.1$ is reached, where isolated fluxes locally bind fermionic modes. For larger disorder strength more and more fluxes are introduced, therefore localized Majorana modes hybridize forming a metallic state. This delocalization is clearly seen by a sharp drop in $\langle p_1^0 \rangle$ beyond $\delta J > 1.1$ and signals the appearance of the thermal metal phase (Lahtinen et al. 2014).

Next in Fig. 5.11, the disorder averaged single particle density of states of the two flux sector $N^F(\omega) = \sum_n \delta\left(\omega - E_n^F\right)$ is shown. I have used 12,000 disorder realizations and 23×23 unit cells. As a comparison, I show $N(\omega)$ without disorder for 51×51 unit cells (black) (broadening $\Gamma = 0.025 J_z$ of the δ-functions). Note that with increasing δJ the upper and lower band edges are smeared out and the gap is filled. In the inset, I show how the single peak from the localized in-gap state is broadened. Its disappearing around $\delta J \approx 0.7$ is expected to have a strong effect on the structure factor, because it is this bound state which leads to the dominant δ-function contribution below the single particle continuum.

Finally in Fig. 5.12, I present the disorder averaged single particle contribution of $\langle S(\mathbf{q} = 0, \omega) \rangle$. Similarly to the DOS, the edges of the continuum are quickly washed out but the sharp in-gap component is surprisingly stable. For increasing disorder strength, the δ-function contribution in the single particle gap is broadened (see inset). However, as long as the average single particle gap $\langle E_1^0 \rangle$ is larger than

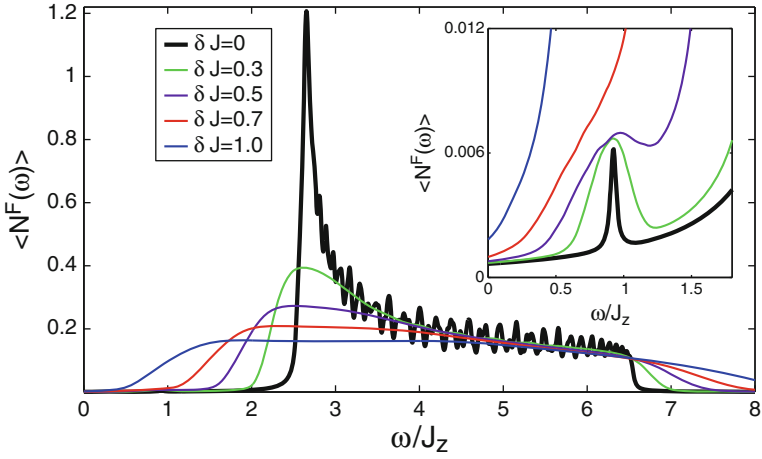

Fig. 5.11 The disorder averaged single particle density of states for the two flux sector $\langle N^F(\omega)\rangle$ is shown for the isotropic point ($J_x = J_y = J_z, K = 0.1J_z$). I have used 12,000 disorder realizations and 23×23 unit cells. As a comparison I show the result without disorder in *black* (51×51 unit cells and broadening $\Gamma = 0.025J_z$ for the δ-functions). The *inset* zooms in around the energy of the localized in-gap state

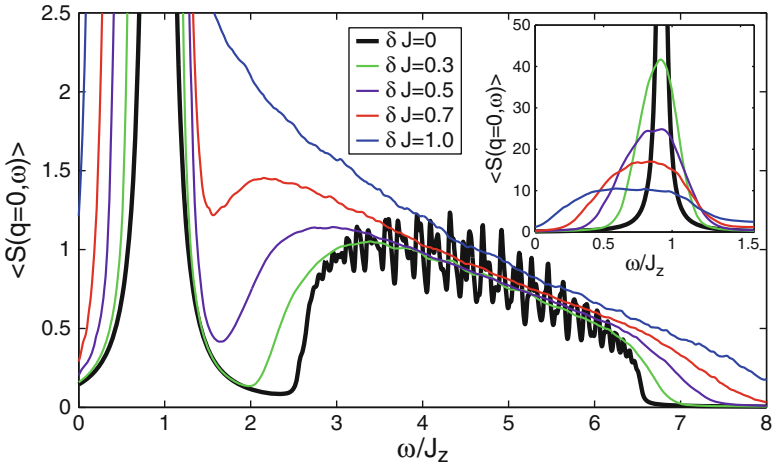

Fig. 5.12 The disorder averaged single particle contribution of $S(\mathbf{q} = 0, \omega)$ is shown for the isotropic point ($J_x = J_y = J_z$ and $K = 0.1J_z$) for several δJ (12,000 disorder realizations and 23×23 unit cells). As a comparison, I show $S(\mathbf{q} = 0, \omega)$ without disorder in *black* (51×51 unit cells and broadening $\Gamma = 0.025J_z$ of the δ-functions). For increasing disorder strength the δ-function contribution is broadened, but a well-separated peak is still resolved until $\delta J \approx 0.7$, see *inset* for a zoom in at low energies

the energy of the in-gap state $\langle E_1^F \rangle$, a well-separated peak is resolved. Overall, the main features of the response are robust up to quite strong disorder strength, at least up to $\delta J \approx 0.7$.

I have also calculated the structure factor in the thermal metal phase, e.g. $\delta J = 1.2$, but several problems appear: The parity of the two ground states with and without flipped fluxes changes randomly. Even if both have the same parity the overlap is very small $O(10^{-4})$. Moreover, on average the lowest lying state is not anymore localized at the bond at which the correlator is measured. Overall, the intensity of the single particle contributions drops abruptly for $\delta J > 1$ which signals the influence of higher particle contributions and the limitation of simple disorder averaging.

References

G. Baskaran, S. Mandal, R. Shankar, Exact results for spin dynamics and fractionalization in the Kitaev model. Phys. Rev. Lett. **98**(24), 247201 (2007)

J.T. Chalker, N. Read, V. Kagalovsky, B. Horovitz, Y. Avishai, A.W.W. Ludwig, Thermal metal in network models of a disordered two-dimensional superconductor. Phys. Rev. B **65**(1), 012506 (2001)

M. Cheng, R.M. Lutchyn, V. Galitski, S. Das Sarma, Splitting of Majorana-Fermion modes due to intervortex tunneling in a $p_x + ip_y$ superconductor. Phys. Rev. Lett. **103**(10), 107001 (2009)

V. Chua, G.A. Fiete, Exactly solvable topological chiral spin liquid with random exchange. Phys. Rev. B **84**(19), 195129 (2011)

X.-Y. Feng, G.-M. Zhang, T. Xiang, Topological characterization of quantum phase transitions in a spin-model. Phys. Rev. Lett. **98**(8), 087204 (2007)

D.A. Ivanov, Non-Abelian statistics of half-quantum vortices in p-wave superconductors. Phys. Rev. Lett. **86**(2), 268–271 (2001)

A. Kitaev, Anyons in an exactly solved model and beyond. Ann. Phys. **321**(1), 2–111 (2006)

Y.E. Kraus, A. Stern, Majorana fermions on a disordered triangular lattice. New J. Phys. **13**(10), 105006 (2011)

V. Lahtinen, Interacting non-Abelian anyons as Majorana fermions in the honeycomb lattice model. New J. Phys. **13**(7), 075009 (2011)

V. Lahtinen, A.W.W. Ludwig, S. Trebst, Perturbed vortex lattices and the stability of nucleated topological phases. Phys. Rev. B **89**(8), 085121 (2014)

C.R. Laumann, A.W.W. Ludwig, D.A. Huse, S. Trebst, Disorder-induced Majorana metal in interacting non-Abelian anyon systems. Phys. Rev. B **85**(16), 161301 (2012)

E.H. Lieb, Flux phase of the half-filled band. Phys. Rev. Lett. **73**(16), 2158–2161 (1994)

T.A. Loring, M.B. Hastings, Disordered topological insulators via C * -algebras. Europhys. Lett. **92**(6), 67004 (2010)

C. Nayak, S.H. Simon, A. Stern, M. Freedman, S. Das Sarma, Non-Abelian anyons and topological quantum computation. Rev. Mod. Phys. **80**(3), 1083–1159 (2008)

S. Sachdev, *Quantum Phase Transitions* (Cambridge University Press, Cambridge, 2001)

X.-F. Shi, Y. Yu, J.Q. You, F. Nori, Topological quantum phase transition in the extended Kitaev spin model. Phys. Rev. B **79**(13), 134431 (2009)

M. Vojta, Quantum phase transitions. Rep. Prog. Phys. **66**(12), 2069 (2003)

F.J. Wegner, Duality in generalized ising models and phase transitions without local order parameters. J. Math. Phys. **12**(10), 2259–2272 (1971)

H. Yao, S.A. Kivelson, Exact chiral spin liquid with non-Abelian anyons. Phys. Rev. Lett **99**(24), 247203 (2007)

Chapter 6
Raman Scattering

In recent years, inelastic Raman scattering has been proven to be a valuable tool for probing collective excitations in strongly correlated electron systems because its polarization dependence allows to probe different regions of the Brollouin zone, see Devereaux and Hackl (2007) for a review. Inelastic Raman scattering is a photon-in photon-out process. Light couples to electronic charges in solids and the transferred energy can excite different types of excitations. For example, optical phonons lead to sharp lines at well-known positions and orientations of the incoming and outgoing photon polarizations, whereas at higher energies a much broader signal can be attributed to two-magnon scattering occurring in materials with antiferromagnetic correlations (Devereaux and Hackl 2007). In Mott insulators, the Raman excitation process couples the induced electron–hole pair exactly to the two-magnon states which are relevant for magnetism (Shastry and Shraiman 1990). Thereby, Raman scattering has been successfully used for understanding the dynamics and interactions of magnons in various antiferromagnetically ordered 3d transition metal oxides, especially in the high-Tc superconductor parent compounds (Chubukov and Frenkel 1995a,b; Blumberg et al. 1996, 1997).

More recently, it has been theoretically proposed (Cépas et al. 2008; Ko et al. 2010) that inelastic Raman scattering is also a promising technique to unravel the features of magnetic excitations in QSLs, even though a simple spin wave picture of the low energy excitations is not applicable. A general signature should be an overall polarization independence or only weak dependence of the signal (Cépas et al. 2008). Indeed, recent Raman scattering experiments revealed spin-liquid like features in the Heisenberg spin one-half Kagome-lattice antiferromagnet, Herbertsmithite $ZnCu_3(OH)_6Cl_2$ (Wulferding et al. 2010).

Kitaev's honeycomb lattice model investigated in this thesis provides an exactly solvable example of a Z_2 quantum spin liquid which may be realized in A_2IrO_3 systems (Jackeli and Khaliullin 2009; Chaloupka et al. 2010; Singh et al. 2012), see Sect. 2.3. In these compounds, Ir^{4+} ions are in a low spin $5d^5$ configuration and form weakly coupled hexagonal layers. Due to strong spin-orbit coupling, the

J. Knolle, *Dynamics of a Quantum Spin Liquid*, Springer Theses,
DOI 10.1007/978-3-319-23953-8_6

atomic ground state of Ir^{4+} ion is a Kramers doublet of magnetic moments in which the spin and orbital angular momenta are strongly entangled. In general, the N.N. interactions between these magnetic moments can be described by the Kitaev–Heisenberg (KH) model containing both, a highly anisotropic ferromagnetic FM Kitaev interaction and an isotropic AF Heisenberg exchange interaction. The Hamiltonian $\hat{H} = \hat{H}_K + \hat{H}_H$ of the KH model reads

$$\hat{H} = -J_K \sum_{\langle ij \rangle_a} \hat{\sigma}_i^a \hat{\sigma}_j^a + J_H \sum_{\langle ij \rangle} \hat{\boldsymbol{\sigma}}_i \cdot \hat{\boldsymbol{\sigma}}_j. \tag{6.1}$$

The Kitaev QSL is stable in the KH model with respect to sufficiently small Heisenberg interactions, as shown by several studies (Chaloupka et al. 2010; Reuther et al. 2011; Schaffer et al. 2012). Thus, it might be realizable in A_2IrO_3 systems, although the first proposed material Na_2IrO_3 is magnetically ordered below 15K (Singh et al. 2012).

In this chapter, I perform a theoretical analysis of the inelastic Raman scattering response from the KH model in the limit of small Heisenberg interaction such that the Kitaev spin liquid is the ground state of the model. To evaluate the Raman operator, I use the semi-phenomenological Loudon–Fleury approach (Fleury and Loudon 1968; Shastry and Shraiman 1990) which assumes that the matrix elements of the interaction between photons and excitations in the system are frequency independent. I compute contributions to the Raman response $I(\omega)$ from both Kitaev and Heisenberg interactions. I show that the main contributions arise from pure Kitaev $I_K(\omega)$ and Heisenberg terms $I_H(\omega)$, while the mixed Kitaev–Heisenberg terms are either zero due to selection rules from the flux sector or they involve weaker and subleading higher order multi-particle processes.

6.1 Loudon–Fleury Raman Vertex

The Raman scattering operator is given by the photon-induced super-exchange operator which for the KH model contains two terms $\mathcal{R} = \mathcal{R}_K + \mathcal{R}_H$, the counterpart of the Loudon–Fleury vertex (Fleury and Loudon 1968; Shastry and Shraiman 1990) for the Heisenberg model:

$$\mathcal{R} = \sum_{\langle ij \rangle_a} (\hat{\boldsymbol{\epsilon}}_{\text{in}} \cdot \mathbf{n}_a)(\hat{\boldsymbol{\epsilon}}_{\text{out}} \cdot \mathbf{n}_a) \left(K_K \hat{\sigma}_i^a \hat{\sigma}_j^a + K_H \hat{\boldsymbol{\sigma}}_i \cdot \hat{\boldsymbol{\sigma}}_j \right), \tag{6.2}$$

$\mathbf{n}_a$ denotes the N.N. vectors, and $\hat{\boldsymbol{\epsilon}}_{\text{in,out}}$ indicates the polarizations of the incident and the outgoing photons. The constants $K_K \propto J_K$ and $K_H \propto J_H$ are proportional to the corresponding exchange constants in the KH Hamiltonian; hence, $\lambda = K_H/K_K \ll 1$ is small in the Kitaev spin liquid limit.

The Raman response of the KH model, Eq. (6.1), is directly related to the Fourier transformation

$$I(\omega) = \int_{-\infty}^{\infty} dt e^{i\omega t} iF(t) \tag{6.3}$$

of the Raman vertex correlation function

$$iF(t) = \langle \mathbb{T}\mathcal{R}(t)\mathcal{R}(0)\rangle, \tag{6.4}$$

here $\langle . \rangle$ is the average in the full ground state $|\Psi_0\rangle$ of the KH Hamiltonian, and $\mathbb{T}$ is the time ordering operator. Treating the Heisenberg term $\hat{H}_H$ as a perturbation, and switching to the interaction picture, the correlation function can be written as

$$iF(t) = \langle 0|S^{\dagger}(t,-\infty)\mathcal{R}(t)S(t,0)\mathcal{R}(0)S(0,-\infty)|0\rangle, \tag{6.5}$$

$$S(t,t') = \mathbb{T}\exp\left\{-i\int_{t'}^{t}\hat{H}_H(\tau)d\tau\right\}. \tag{6.6}$$

Note that the expectation value is now computed with respect to the Kitaev ground state $|0\rangle$. One can then perturbatively compute the Raman response by expanding to leading order in λ.

In the following, I derive the leading contributions of Eq. (6.5) by restricting my analysis to the Kitaev limit $K_H/K_K = J_H/J_K = \lambda \ll 1$. I explicitly take the small parameter λ out of the definition of the coupling constants such that $\hat{H} = \hat{H}_K + \lambda\hat{H}_H$ and $\mathcal{R} = \mathcal{R}_K + \lambda\mathcal{R}_H$. The Kitaev like contributions of the Heisenberg Hamiltonian and Raman vertex are absorbed into the Kitaev exchange constants such that $J_K \to J_K(1+\lambda)$, $K_K \to K_K(1+\lambda)$. Hence, all terms in H_H and $\mathcal{R}_H$ change the flux sector when acting on the ground state $|0\rangle$. Note that I remove the $\hat{\text{hat}}$ when working in terms of Majorana fermions. I obtain for the S matrix up to $O(\lambda^2)$

$$S(t,t') = \left\{1 + \lambda \underbrace{\mathbb{T}(-i)\int_{t'}^{t} d\tau H_H(\tau)}_{\equiv h_H^{(1)}(t,t')} + \lambda^2 \underbrace{\mathbb{T}\frac{(-i)^2}{2}\int_{t'}^{t} d\tau_1 \int_{t'}^{t} d\tau_2 H_H(\tau_2)H_H(\tau_2)}_{\equiv h_H^{(2)}(t,t')} + \cdots\right\}, \tag{6.7}$$

such that the leading order Raman response

$$\begin{aligned} iF(t) \simeq \Big\langle 0\Big| &\left[1 + \lambda h_H^{(1)}(t,-\infty) + \lambda^2 h_H^{(2)}(t,-\infty)\right]^{\dagger}\left[\mathcal{R}_K(t) + \lambda\mathcal{R}_H(t)\right] \\ &\times \left[1 + \lambda h_H^{(1)}(t,0) + \lambda^2 h_H^{(2)}(t,0)\right]\left[\mathcal{R}_K(0) + \lambda\mathcal{R}_H(0)\right] \\ &\times \left[1 + \lambda h_H^{(1)}(0,-\infty) + \lambda^2 h_H^{(2)}(0,-\infty)\right]\Big|0\Big\rangle \end{aligned} \tag{6.8}$$

can be approximated by

$$iF(t) \approx \langle 0|\mathcal{R}_K(t)\mathcal{R}_K(0)|0\rangle + \lambda^2\langle 0|\mathcal{R}_H(t)\mathcal{R}_H(0)|0\rangle. \tag{6.9}$$

All terms linear in λ vanish due to orthogonality of the flux sectors. The two terms in Eq. (6.9) are the main contributions F_K and F_H. Note that the contribution F_H is a sum of purely local terms, see discussion in the next section, especially Eq. (6.19).

The omitted λ^2 terms involve non-local contributions. For example, four fluxes which are inserted by the term $\mathcal{R}_H$ can be locally annihilated by a suitable term in H_H. The remaining matter degrees of freedom are non-local, e.g. of the schematic form $\langle M_0|c_i c_j c_{i'} c_{j'}|M_0\rangle \delta_{\langle i,j\rangle_{N.N.}} \delta_{\langle i',j'\rangle_{N.N.}}$ or higher orders in Majorana operators. Such multi-particle excitations are proportional to density–density fluctuations (Tikhonov et al. 2011) having higher orders of the matter fermion density of states and would contribute a small correction at low frequencies which is broad in energy (Tikhonov et al. 2011). This is because in a Dirac system with only Fermi points instead of a proper Fermi surface, particle-hole excitations are suppressed at low energies due to the linearly vanishing density of states (Kotov et al. 2012). This perturbation theory amounts to approximating the ground state of the KH model with the integrable one. However, the calculation of the response goes one step beyond integrability by including contributions to the Raman vertex arising from the integrability-breaking Heisenberg term.

In the remainder of this chapter, I restrict my calculation of the Raman response to the leading terms, which is equivalent to a *static flux approximation*

$$I(\omega) \approx I_K(\omega) + I_H(\omega). \tag{6.10}$$

6.1.1 Kitaev Contribution

First, I study the Kitaev contribution $I_K(\omega)$ and express the vertex in terms of Majorana fermions. I work in the ground state flux sector such that

$$\mathcal{R}_K = \sum_{\mathbf{r}} \sum_{\alpha=x,y,z} K_K \left(\hat{\boldsymbol{\epsilon}}_{\text{in}} \cdot \mathbf{n}_{\boldsymbol{\alpha}}\right)\left(\hat{\boldsymbol{\epsilon}}_{\text{out}} \cdot \mathbf{n}_{\boldsymbol{\alpha}}\right) \frac{i}{2} \left\{c_{A\mathbf{r}} c_{B\mathbf{r}+\mathbf{n}_\alpha} - c_{B\mathbf{r}+\mathbf{n}_\alpha} c_{A\mathbf{r}}\right\} \tag{6.11}$$

can be written in terms of complex matter fermions as

$$\mathcal{R}_K = \sum_{\mathbf{q}} \begin{pmatrix} f_{\mathbf{q}}^\dagger & f_{-\mathbf{q}} \end{pmatrix} \begin{pmatrix} \text{Re}h(\mathbf{q}) & i\text{Im}h(\mathbf{q}) \\ -i\text{Im}h(\mathbf{q}) & -\text{Re}h(\mathbf{q}) \end{pmatrix} \begin{pmatrix} f_{\mathbf{q}} \\ f_{-\mathbf{q}}^\dagger \end{pmatrix} \tag{6.12}$$

with

$$h(\mathbf{q}) = \sum_{\alpha} K_K \left(\hat{\boldsymbol{\epsilon}}_{\text{in}} \cdot \mathbf{n}_{\boldsymbol{\alpha}}\right) \left(\hat{\boldsymbol{\epsilon}}_{\text{out}} \cdot \mathbf{n}_{\boldsymbol{\alpha}}\right) e^{i\mathbf{q}\mathbf{n}_{\boldsymbol{\alpha}}}. \tag{6.13}$$

In order to calculate the Raman response function in the ground state of the zero flux sector, I perform a final Bogoliubov rotation to get an expression in terms of $a_{\mathbf{q}}$ operators that diagonalize the Kitaev Hamiltonian, Eq. (2.29),

$$\mathcal{R}_K(t) = \sum_{\mathbf{q}} \left\{ r(\mathbf{q}) a^{\dagger}_{\mathbf{q}}(t) a_{\mathbf{q}}(t) + g(\mathbf{q}) a^{\dagger}_{\mathbf{q}}(t) a^{\dagger}_{-\mathbf{q}}(t) + g^*(\mathbf{q}) a_{-\mathbf{q}}(t) a_{-\mathbf{q}}(t) - r(\mathbf{q}) a_{-\mathbf{q}}(t) a^{\dagger}_{-\mathbf{q}}(t) \right\}. \tag{6.14}$$

Using the simple time dependence of the Heisenberg picture, $a_{\mathbf{q}}(t) = a_{\mathbf{q}} e^{-it2|S(\mathbf{q})|}$, and defining the two functions

$$r(\mathbf{q}) = \text{Re}h(\mathbf{q}) \cos 2\theta_{\mathbf{q}} - \text{Im}h(\mathbf{q}) \sin 2\theta_{\mathbf{q}} \tag{6.15}$$

$$g(\mathbf{q}) = i\text{Re}h(\mathbf{q}) \sin 2\theta_{\mathbf{q}} + i\text{Im}h(\mathbf{q}) \cos 2\theta_{\mathbf{q}}, \tag{6.16}$$

I finally obtain the Raman Kitaev contribution for $\omega > 0$

$$I_K(\omega) = 4\pi \sum_{\mathbf{q}} \delta\left(\omega - 4|S(\mathbf{q})|\right) \left[\frac{\text{Im}\left[h(\mathbf{q}) S^*(\mathbf{q})\right]}{|S(\mathbf{q})|} \right]^2, \tag{6.17}$$

which is totally independent of polarization.

6.1.2 Heisenberg Contribution

The Heisenberg vertex $\mathcal{R}_H$ can be separated into three parts from the inequivalent bond directions

$$\begin{aligned} \mathcal{R}_H = & \sum_{\langle ij \rangle_z} K_H \left(\hat{\boldsymbol{\epsilon}}_{\text{in}} \cdot \mathbf{n}_{\mathbf{z}}\right) \left(\hat{\boldsymbol{\epsilon}}_{\text{out}} \cdot \mathbf{n}_{\mathbf{z}}\right) \left[\sigma_i^x \sigma_j^x + \sigma_i^y \sigma_j^y\right] \\ & + \sum_{\langle ij \rangle_x} K_H \left(\hat{\boldsymbol{\epsilon}}_{\text{in}} \cdot \mathbf{n}_{\mathbf{x}}\right) \left(\hat{\boldsymbol{\epsilon}}_{\text{out}} \cdot \mathbf{n}_{\mathbf{x}}\right) \left[\sigma_i^z \sigma_j^z + \sigma_i^y \sigma_j^y\right] \\ & + \sum_{\langle ij \rangle_y} K_H \left(\hat{\boldsymbol{\epsilon}}_{\text{in}} \cdot \mathbf{n}_{\mathbf{y}}\right) \left(\hat{\boldsymbol{\epsilon}}_{\text{out}} \cdot \mathbf{n}_{\mathbf{y}}\right) \left[\sigma_i^x \sigma_j^x + \sigma_i^z \sigma_j^z\right]. \end{aligned} \tag{6.18}$$

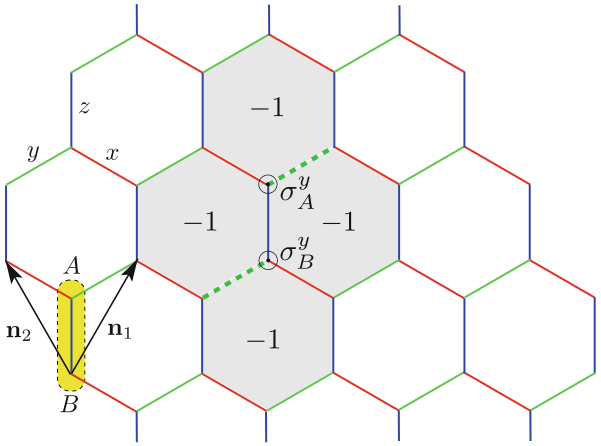

Fig. 6.1 The calculation of the Raman response due to the Heisenberg part can be mapped to a local quantum quench, in which four adjoining Z_2 fluxes, shown as *gray hexagons*, are inserted. For example, the contribution from nearest-neighbor $\sigma^y_{A\mathbf{r}}\sigma^y_{B\mathbf{r}}$ interactions along a z-bond which flips the sign of the link variables is shown by *green dashed bonds*

Each of the terms $\mathcal{R}_{H,\langle ij\rangle_\alpha}$ puts in four fluxes around the α-bond at site $\mathbf{r}$, see Fig. 6.1. The orthogonality of the flux sector greatly simplifies the calculation of the Raman intensity by making it bond diagonal

$$iF_H(t) = \sum_{\langle ij\rangle_\alpha}\sum_{\langle kl\rangle_\beta}\langle \mathcal{R}_{H,\langle ij\rangle_\alpha}(t)\mathcal{R}_{H,\langle kl\rangle_\beta}(0)\rangle = \sum_{\langle ij\rangle_\alpha}\langle \mathcal{R}_{H,\langle ij\rangle_\alpha}(t)\mathcal{R}_{H,\langle ij\rangle_\alpha}(0)\rangle. \tag{6.19}$$

As the system is translationally invariant, I concentrate on the Raman operator of a single z bond, e.g. $\mathcal{R}_{H,\langle A\mathbf{r}B\mathbf{r}\rangle_z} \propto \sigma^x_{A\mathbf{r}}\sigma^x_{B\mathbf{r}} + \sigma^y_{A\mathbf{r}}\sigma^y_{B\mathbf{r}}$. In case of an anisotropic system the other x/y-contributions can be obtained by cyclic permutation of the exchange constants J_x, J_y, J_z and a rotation of the in- and out-going scattering angles by multiples of $\frac{2\pi}{3}$. The Raman intensity from the z-bond is given by

$$\begin{aligned} iF_{H,z}(t) = \lambda^2 \left[K_K\,(\hat{\boldsymbol{\epsilon}}_{\text{in}}\cdot\mathbf{n}_\mathbf{z})\,(\hat{\boldsymbol{\epsilon}}_{\text{out}}\cdot\mathbf{n}_\mathbf{z})\right]^2 \langle\left[\sigma^x_{A\mathbf{r}}(t)\sigma^x_{B\mathbf{r}}(t) + \sigma^y_{A\mathbf{r}}(t)\sigma^y_{B\mathbf{r}}(t)\right] \\ \times\left[\sigma^x_{A\mathbf{r}}(0)\sigma^x_{B\mathbf{r}}(0) + \sigma^y_{A\mathbf{r}}(0)\sigma^y_{B\mathbf{r}}(0)\right]\rangle \end{aligned} \tag{6.20}$$

with two different types of matrix elements: First, spin component diagonal elements, e.g. $\langle\sigma^x\sigma^x\sigma^x\sigma^x\rangle$, and second, off-diagonal ones, e.g. $\langle\sigma^x\sigma^x\sigma^y\sigma^y\rangle$. The former operator can be calculated without projection onto the physical state (Baskaran et al. 2007) because it neither changes the flux sector nor the bond fermion number. The off-diagonal term not only conserves the flux sector but also changes the bond fermion number χ. Therefore, it is necessary to project the contribution from this term onto the physical state (Yao et al. 2009). However, while the correlation

function $\langle \sigma^x(t)\sigma^x(t)\sigma^y(0)\sigma^y(0)\rangle$ is non-zero, its contribution to the Raman response is exactly canceled by the $\langle \sigma^y(t)\sigma^y(t)\sigma^x(0)\sigma^x(0)\rangle$ term, see below.

The calculation of the diagonal term

$$\begin{aligned}&\langle \sigma^x_{A\mathbf{r}}(t)\sigma^x_{B\mathbf{r}}(t)\sigma^x_{A\mathbf{r}}(0)\sigma^x_{B\mathbf{r}}(0)\rangle \\ &= \Big\langle e^{itH_0} i c_{A\mathbf{r}} \left[\chi_{\langle A\mathbf{r},B\mathbf{r}+\mathbf{n_x}\rangle_x} + \chi^\dagger_{\langle A\mathbf{r},B\mathbf{r}+\mathbf{n_x}\rangle_x}\right] c_{B\mathbf{r}} \left[\chi_{\langle A\mathbf{r}-\mathbf{n_x},B\mathbf{r}\rangle_x} - \chi^\dagger_{\langle A\mathbf{r}-\mathbf{n_x},B\mathbf{r}\rangle_x}\right] \\ &\quad \times e^{-itH_0} i c_{A\mathbf{r}} \left[\chi_{\langle A\mathbf{r},B\mathbf{r}+\mathbf{n_x}\rangle_x} + \chi^\dagger_{\langle A\mathbf{r},B\mathbf{r}+\mathbf{n_x}\rangle_x}\right] c_{B\mathbf{r}} \left[\chi_{\langle A\mathbf{r}-\mathbf{n_x},B\mathbf{r}\rangle_x} - \chi^\dagger_{\langle A\mathbf{r}-\mathbf{n_x},B\mathbf{r}\rangle_x}\right]\Big\rangle\end{aligned} \tag{6.21}$$

precedes in a similar fashion as for the spin correlation function, see Sect. 3.1. I eliminate the bond fermions to work only in the ground state flux sector. Recall, the expectation value is taken over the ground state $|0\rangle = |F_0\rangle|M_0\rangle$. I use a gauge with $\chi^\dagger_i \chi_i |F_0\rangle = |F_0\rangle$ and commute all bond operators to the right

$$\chi^\dagger_{\langle A\mathbf{r},B\mathbf{r}+\mathbf{n_x}\rangle_x} \chi^\dagger_{\langle A\mathbf{r}-\mathbf{n_x},B\mathbf{r}\rangle_x} e^{-itH_0} = e^{-itH_K[\langle A\mathbf{r},B\mathbf{r}+\mathbf{n_x}\rangle_x,\langle A\mathbf{r}-\mathbf{n_x},B\mathbf{r}\rangle_x]} \chi^\dagger_{\langle A\mathbf{r},B\mathbf{r}+\mathbf{n_x}\rangle_x} \chi^\dagger_{\langle A\mathbf{r}-\mathbf{n_x},B\mathbf{r}\rangle_x} \tag{6.22}$$

where $H_K\left[\langle A\mathbf{r}, B\mathbf{r}+\mathbf{n_x}\rangle_x, \langle A\mathbf{r}-\mathbf{n_x}, B\mathbf{r}\rangle_x\right]$ is the Majorana hopping Hamiltonian with flipped link variables $u_{\langle A\mathbf{r},B\mathbf{r}+\mathbf{n_x}\rangle_x} = -1$ and $u_{\langle A\mathbf{r}-\mathbf{n_x},B\mathbf{r}\rangle_x} = -1$ which corresponds to four fluxes around the z-bond. Note that H_0 is the standard hopping Hamiltonian in the ground state flux sector. In the remainder, I use the shorthand notation $H_K\left[\langle A\mathbf{r}, B\mathbf{r}+\mathbf{n_x}\rangle_x, \langle A\mathbf{r}-\mathbf{n_x}, B\mathbf{r}\rangle_x\right] = H_K\left[+\mathbf{n_x}, -\mathbf{n_x}\right]$. The diagonal correlation function is expressed entirely in the ground state flux sector

$$\langle \sigma^x_{A\mathbf{r}}(t)\sigma^x_{B\mathbf{r}}(t)\sigma^x_{A\mathbf{r}}(0)\sigma^x_{B\mathbf{r}}(0)\rangle = \quad \langle M_0| e^{itH_0} c_{A\mathbf{r}} c_{B\mathbf{r}} e^{-itH_K[+\mathbf{n_x},-\mathbf{n_x}]} c_{B\mathbf{r}} c_{A\mathbf{r}} |M_0\rangle \ . \tag{6.23}$$

This expression can be further simplified with the gauge equivalent $c_{A\mathbf{r}} c_{B\mathbf{r}} e^{-itH_K[+\mathbf{n_x},-\mathbf{n_x}]} c_{B\mathbf{r}} c_{A\mathbf{r}} = e^{-itc_{A\mathbf{r}}c_{B\mathbf{r}}H_K[+\mathbf{n_x},-\mathbf{n_x}]c_{B\mathbf{r}}c_{A\mathbf{r}}} = e^{-itH_K\left[+\mathbf{n_y},-\mathbf{n_y}\right]}$ such that I obtain the final expression

$$\langle \sigma^x_{A\mathbf{r}}(t)\sigma^x_{B\mathbf{r}}(t)\sigma^x_{A\mathbf{r}}(0)\sigma^x_{B\mathbf{r}}(0)\rangle = \langle M_0| e^{itH_0} e^{-itH_K\left[+\mathbf{n_y},-\mathbf{n_y}\right]} |M_0\rangle. \tag{6.24}$$

It is a quantum quench in which the ground state $|M_0\rangle$ of H_0 is time evolved with the four flux Hamiltonian $H_K\left[+\mathbf{n_y}, -\mathbf{n_y}\right]$, compare to Sect. 3.1.

Next, I study the off-diagonal term $\langle \sigma^x\sigma^x\sigma^y\sigma^y\rangle$ for which it is necessary to include the projection operator $P|\Phi\rangle = \prod_j \frac{1+D_j}{2}|\Phi\rangle = |\Phi_{\text{phys}}\rangle$, see Eq. (2.8). Note that operators D_j commute with the Hamiltonian H_K and all spin operators σ^a_i. As discussed in Sect. 2.1, the projection can be factorized into $P = P' \frac{1+\prod_j D_j}{2}$, Eq. (2.13) where P' is the sum of all operators that change the bond fermion number in an inequivalent way. I work with even total fermion number and use the fact that

P commutes with all spin operators such that $\langle P\sigma^x_{A\mathbf{r}}(t)\sigma^x_{B\mathbf{r}}(t)\sigma^y_{A\mathbf{r}}(0)\sigma^y_{B\mathbf{r}}(0)P\rangle = \langle\sigma^x_{A\mathbf{r}}(t)\sigma^x_{B\mathbf{r}}(t)\sigma^y_{A\mathbf{r}}(0)\sigma^y_{B\mathbf{r}}(0)P'\rangle$ which can be simplified in a similar fashion as before to

$$\begin{aligned}\langle P\sigma^x_{A\mathbf{r}}(t)\sigma^x_{B\mathbf{r}}(t)\sigma^y_{A\mathbf{r}}(0)\sigma^y_{B\mathbf{r}}(0)P\rangle = -\langle e^{itH_0}e^{-itH_K\left[+\mathbf{n}_\mathbf{y},-\mathbf{n}_\mathbf{y}\right]} \\ \times \chi^\dagger_{\langle A\mathbf{r},B\mathbf{r}+\mathbf{n}_\mathbf{x}\rangle_x}\chi^\dagger_{\langle A\mathbf{r}-\mathbf{n}_\mathbf{x},B\mathbf{r}\rangle_x}\left[\chi_{\langle A\mathbf{r},B\mathbf{r}+\mathbf{n}_\mathbf{y}\rangle_y}+\chi^\dagger_{\langle A\mathbf{r},B\mathbf{r}+\mathbf{n}_\mathbf{y}\rangle_y}\right]\left[\chi_{\langle A\mathbf{r}-\mathbf{n}_\mathbf{y},B\mathbf{r}\rangle_y}-\chi^\dagger_{\langle A\mathbf{r}-\mathbf{n}_\mathbf{y},B\mathbf{r}\rangle_y}\right]P'\rangle.\end{aligned} \tag{6.25}$$

In this expression, only the part $D_{A\mathbf{r}}D_{B\mathbf{r}}$ of P' together with the product of χ operators does not change the bond fermion number. On the one hand, the operator $D_{A\mathbf{r}}D_{B\mathbf{r}}$ eliminates the additional bond fermions, but on the other hand, it introduces new matter fermions. Finally, I obtain for the off-diagonal component

$$\langle\sigma^x_{A\mathbf{r}}(t)\sigma^x_{B\mathbf{r}}(t)\sigma^y_{A\mathbf{r}}(0)\sigma^y_{B\mathbf{r}}(0)\rangle = \langle M_0|e^{itH_0}e^{-itH_K\left[+\mathbf{n}_\mathbf{y},-\mathbf{n}_\mathbf{y}\right]}c_{A\mathbf{r}}c_{B\mathbf{r}}|M_0\rangle \tag{6.26}$$

such that overall the full Heisenberg response of the z-bond is given by

$$\begin{aligned}iF_{H,z}(t) = \sum_\mathbf{r}\left\{\langle M_0|e^{itH_0}\,e^{-itH_K\left[\mathbf{r}+\mathbf{n}_\mathbf{y},\mathbf{r}-\mathbf{n}_\mathbf{y}\right]}|M_0\rangle + \langle M_0|e^{itH_0}\,e^{-itH_K[\mathbf{r}+\mathbf{n}_\mathbf{x},\mathbf{r}-\mathbf{n}_\mathbf{x}]}|M_0\rangle\right\} \\ + \sum_\mathbf{r}\left\{\langle M_0|e^{itH_0}\,e^{-itH_K\left[\mathbf{r}+\mathbf{n}_\mathbf{y},\mathbf{r}-\mathbf{n}_\mathbf{y}\right]}c_{A,\mathbf{r}}c_{B,\mathbf{r}}|M_0\rangle + \text{h.c.}\right\}.\end{aligned} \tag{6.27}$$

6.1.3 Few-Particle Response

Following Sect. 3.2, for the Lehmann representation I insert a complete set of states $\sum_\lambda|\lambda\rangle\langle\lambda|$ into Eq. (6.27) with Eigenstates $|\lambda\rangle$ of the four flux Hamiltonian $H_K\left[+\mathbf{n}_\mathbf{y},-\mathbf{n}_\mathbf{y}\right]$. After Fourier transformation to frequency domain I obtain for the Raman intensity of the Heisenberg part

$$I_{H,z}(\omega) = I^{xx}_{H,z}(\omega) + I^{yy}_{H,z}(\omega) + I^{xy}_{H,z}(\omega) + I^{yx}_{H,z}(\omega) \tag{6.28}$$

with the diagonal and off-diagonal components

$$\begin{aligned}I^{xx}_{H,z}(\omega) &= 2\pi\sum_\lambda\delta\left[\omega-(E_\lambda-E_0)\right]|\langle M_0|\lambda\rangle|^2, \\ I^{xy}_{H,z}(\omega) &= 2\pi\sum_\lambda\delta\left[\omega-(E_\lambda-E_0)\right]\langle M_0|\lambda\rangle\langle\lambda|c_{A,\mathbf{r}}c_{B,\mathbf{r}}|M_0\rangle.\end{aligned} \tag{6.29}$$

Note that $I^{xx}_{H,z}(\omega) = I^{yy}_{H,z}(\omega)$ at the isotropic point ($J^x_K = J^y_K = J^z_K$) and $I^{xy}_{H,z}(\omega) = \left[I^{yx}_{H,z}(\omega)\right]^*$. The ground state of the four flux sector $|M_F\rangle$ has the same parity as

the zero flux sector $|M_0\rangle$, therefore only even number of excitations $b_\lambda^\dagger$, which diagonalize the four flux sector $H_K\left[\mathbf{r}+\mathbf{n}_\mathbf{y}, \mathbf{r}-\mathbf{n}_\mathbf{y}\right]$, contribute. In the following, I derive the formulas of the leading few-particle contributions similar to Sect. 3.2. I numerically calculate the main contributions $I_H^{[0]}(\omega), I_H^{[2]}(\omega)$ from zero- $|\lambda\rangle = |M_F\rangle$ and two-particle $|\lambda\rangle = b_{\lambda'}^\dagger b_\lambda^\dagger |M_F\rangle$ processes.

The first contribution to the sum of the Lehmann representation, Eq. (6.29), comes from the ground state overlaps

$$I_{\mathrm{H},z}^{xx,[0]}(\omega) = 2\pi\delta\left(\omega-\Delta_F\right)\sqrt{\det\left(\mathcal{X}^\dagger\mathcal{X}\right)} \tag{6.30}$$

$$I_{\mathrm{H},z}^{xy,[0]}(\omega) = i2\pi\delta\left(\omega-\Delta_F\right)\sqrt{\det\left(\mathcal{X}^\dagger\mathcal{X}\right)}\left[1-2\sum_k|Y_{k0}|^2-2\sum_{j,k}Y_{0k}^\dagger\mathcal{F}_{kj}^*X_{j0}^*\right]. \tag{6.31}$$

It gives a sharp δ-function peak at the four flux gap Δ_F in the Raman response. The next signal from single particle contributions $b_\lambda^\dagger|M_F\rangle$ is zero because of their opposite parity to the zero flux ground state $|M_0\rangle$. Only even number of particles contribute. The first frequency dependence arises from two-particle contributions $b_\lambda^\dagger b_{\lambda'}^\dagger|M_F\rangle$ which leads to

$$\begin{aligned} I_{\mathrm{H},z}^{xx,[2]}(\omega) &= 2\pi\sum_{\lambda,\lambda'}\delta\left(\omega-[E_\lambda+E_{\lambda'}-E_0]\right)\left|\langle M_0|b_\lambda^\dagger b_{\lambda'}^\dagger|M_F\rangle\right|^2 \\ I_{\mathrm{H},z}^{xy,[2]}(\omega) &= 2\pi\sum_{\lambda,\lambda'}\delta\left(\omega-[E_\lambda+E_{\lambda'}-E_0]\right)\langle M_0|b_\lambda^\dagger b_{\lambda'}^\dagger|M_F\rangle\langle M_F|b_{\lambda'}b_\lambda c_{A0}c_{B0}|M_0\rangle. \end{aligned} \tag{6.32}$$

The matrix elements are given at the end of Appendix D. I have numerically studied systems up to 62×62 unit cells (7688 spins). It turns out that the off-diagonal contribution $I_{\mathrm{H},z}^{xy,[2]}(\omega)$, which involves the projection operator, is purely imaginary. Therefore, it is exactly canceled by the complex conjugate $I_{\mathrm{H},z}^{yx}(\omega)$ and does not contribute to the total Raman response. I truncate the λ sum at this two particle level since the intensity of higher order processes is significantly reduced.

6.2 Results

The Raman response, shown in Fig. 6.2, is markedly different from the known strongly polarization dependent behavior seen in the two-magnon response of antiferromagnetically ordered systems. In fact, the characteristic features of the weakly polarization-dependent response $I(\omega)$ can be related either to the flux, or the Majorana fermion sector: First, the polarization-independent Kitaev contribution

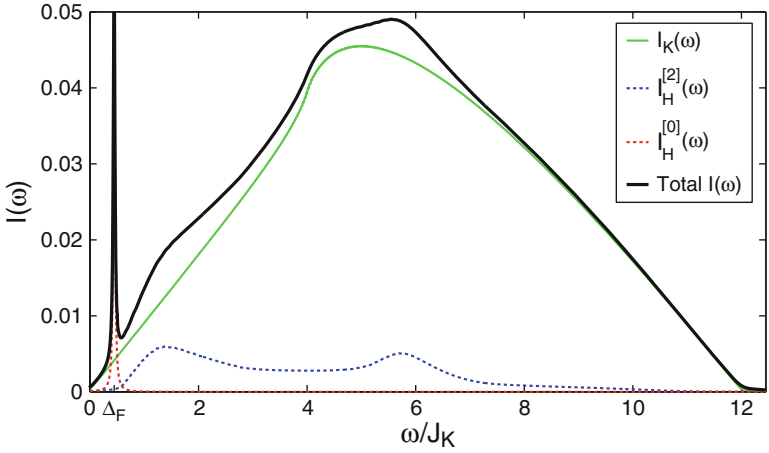

Fig. 6.2 The Raman response $I(\omega)$ (*black curve*) is shown together with its various contributions for $J_K = 10J_H$. The Kitaev contribution $I_K(\omega)$, shown in *green*, is independent of the photon polarization and shows characteristic features of the matter fermion density of states including the linear onset at low energies and the band-edge at $12J_K$, note the additional factor of 2 in Eq. (6.17). The van Hove singularity at $2J_K$ is seen as a small dip at $4J_K$ (a discontinuity of the derivative). The zero and two-particle responses, $I_H^{[0]}(\omega)$ and $I_H^{[2]}(\omega)$, of the Heisenberg Raman contribution are shown in *blue* and *red* (*dashed*) respectively. A δ-function peak occurs at the four flux gap $\Delta_F = 0.446J_K$, while the frequency dependence of the two-particle contribution reflects the local two-particle density of states in the presence of four fluxes

$I_K(\omega)$ reflects the Majorana matter fermion density of states in the ground state flux sector. It has a linear onset at low energies, a sharp band-edge at $12J_K$, and a dip at $4J_K$ due to the van Hove singularity. Second, the Heisenberg contribution, which has a weak polarization dependence with a simple overall intensity change, is related to flux excitations, e.g. $I_H(\omega) = 0$ for $\omega < \Delta_F$. A striking feature is a sharp peak at the energy of the four flux gap $\Delta_F = 0.446J_K$ originating from the zero-particle contribution (overlap between ground states), see Eq. (6.28). This is a clear signature of a pure flux excitation for the *isotropic* gapless QSL ($J_K^x = J_K^y = J_K^z$). Note that normally sharp lines in Raman scattering are attributed to optical phonons which appear at different energy scales (Devereaux and Hackl 2007). In addition, $I_H(\omega)$ has a broad response in energy reflecting the two-particle density of states of matter fermions propagating in the background of four inserted fluxes.

My analysis of the Raman response relies on the stability of the Kitaev QSL with respect to the addition of small Heisenberg exchanges. I expect that for small Heisenberg couplings, all the features which I find in the response are robust. They will only be somewhat renormalized by non-local fluctuations originating from the dynamics of the fluxes generated by the Heisenberg exchange or disorder which is present in real materials. Crucially, there is a window of parameters where the features that I obtain should be observable, thus, making Raman scattering an important experimental tool for diagnosing Kitaev QSLs.

In conclusion, I have shown that Raman scattering renders visible both flux and Majorana fermion excitations potentially relevant to Iridates. It thus presents a valuable alternative tool for diagnosing topological quantum states.

References

G. Baskaran, S. Mandal, R. Shankar, Exact results for spin dynamics and fractionalization in the Kitaev model. Phys. Rev. Lett. **98**(24), 247201 (2007)

G. Blumberg, P. Abbamonte, M.V. Klein, W.C. Lee, D.M. Ginsberg, L.L. Miller, A. Zibold, Resonant two-magnon Raman scattering in cuprate antiferromagnetic insulators. Phys. Rev. B **53**(18), R11930–R11933 (1996)

G. Blumberg, M. Kang, M.V. Klein, K. Kadowaki, C. Kendziora, Evolution of magnetic and superconducting fluctuations with doping of high-tc superconductors. Science **278**(5342), 1427–1432 (1997)

O. Cépas, J.O. Haerter, C. Lhuillier, Detection of weak emergent brokensymmetries of the kagome antiferromagnet by Raman spectroscopy. Phys. Rev. B **77**(17), 172406 (2008)

J. Chaloupka, G. Jackeli, G. Khaliullin, Kitaev-Heisenberg model on a honeycomb lattice: possible exotic phases in iridium oxides. Phys. Rev. Lett. **105**(2), 027204 (2010)

A.V. Chubukov, D.M. Frenkel, Resonant two-magnon Raman scattering in antiferromagnetic insulators. Phys. Rev. Lett. **74**(15), 3057–3060 (1995)

A.V. Chubukov, D.M. Frenkel, Resonant two-magnon Raman scattering in parent compounds of high-T_c superconductors. Phys. Rev. B **52**(13), 9760–9783 (1995)

T.P. Devereaux, R. Hackl, Inelastic light scattering from correlated electrons. Rev. Mod. Phys. **79**(1), 175–233 (2007)

P.A. Fleury, R. Loudon, Scattering of light by one- and two-magnon excitations. Phys. Rev. **166**(2), 514–530 (1968)

G. Jackeli, G. Khaliullin, Mott insulators in the strong spin-orbit coupling limit: from Heisenberg to a quantum compass and Kitaev models. Phys. Rev. Lett. **102**(1), 017205 (2009)

W.-H. Ko, Z.-X. Liu, T.-K. Ng, P.A. Lee, Raman signature of the U(1) Dirac spin-liquid state in the spin-$\frac{1}{2}$ kagome system. Phys. Rev. B **81**(2), 024414 (2010)

V.N. Kotov, B. Uchoa, V.M. Pereira, F. Guinea, A.H. Castro Neto, Electron-electron interactions in graphene: current status and perspectives. Rev. Mod. Phys. **84**(3), 1067–1125 (2012)

J. Reuther, R. Thomale, S. Trebst, Finite-temperature phase diagram of the Heisenberg-Kitaev model. Phys. Rev. B **84**(10), 100406 (2011)

R. Schaffer, S. Bhattacharjee, Y.B. Kim, Quantum phase transition in Heisenberg-Kitaev model. Phys. Rev. B **86**(22), 224417 (2012)

B.S. Shastry, B.I. Shraiman, Theory of Raman scattering in Mott-Hubbard systems. Phys. Rev. Lett. **65**(8), 1068–1071 (1990)

Y. Singh, S. Manni, J. Reuther, T. Berlijn, R. Thomale, W. Ku, S. Trebst, P. Gegenwart. Relevance of the Heisenberg-Kitaev model for the honeycomb lattice iridates. Phys. Rev. Lett. **108**(12), 127203 (2012)

K. Tikhonov, M. Feigelman, A. Kitaev, Power-law spin correlations in a perturbed spin model on a honeycomb lattice. Phys. Rev. Lett. **106**(6), 067203 (2011)

D. Wulferding, P. Lemmens, P. Scheib, J. Röder, P. Mendels, S. Chu, T. Han, Y. S. Lee, Interplay of thermal and quantum spin fluctuations in the kagome lattice compound herbertsmithite. Phys. Rev. B **82**(14), 144412 (2010)

H. Yao, S.-C. Zhang, S.A. Kivelson algebraic spin liquid in an exactly solvable spin model. Phys. Rev. Lett. **102**(21), 217202 (2009)

Chapter 7
Conclusion and Outlook

I have presented a study of exact dynamical correlation functions in different phases of a model QSL with the objective to look for discernible signatures of the emergent fractionalized quasiparticles in response functions directly accessible in standard experiments. The main result is the identification of salient features—qualitative and quantitative—of the Majorana fermions and gauge fluxes emerging in the Kitaev honeycomb lattice model. For the first time, my thesis provides such exact calculations of dynamical correlation functions of a 2D QSL. The resulting characteristic signatures of fractionalization, which is a hallmark of a topologically ordered phase, are visible as fingerprints betraying the presence of a QSL in future INS, ESR, and Raman scattering experiments.

7.1 Experimental Prospect and Materials

Materials with bond dependent anisotropic spin interactions can exhibit novel QSL phases. The original dream that the layered Iridium oxide Na_2IrO_3 captures the physics of the Kitaev model (Jackeli and Khaliullin 2009; Singh et al. 2012) turned out be too optimistic, because this material orders into a spiral AF state at low temperatures. Unfortunately, it seems that in these quasi-2D materials the influence of spin anisotropic interactions is miniscule and not even necessary for explaining the observed magnetism. A new boost to the field comes from theoretical proposals with 3D generalizations of the Kitaev model (Mandal and Surendran 2009; Lee et al. 2014; Hermanns and Trebst 2014; Kimchi et al. 2014), which conjectured that 3D analogues of the honeycomb lattice might be more promising for realizing QSLs. Indeed, the recently synthesized 3D *hyperhoneycomb* β-Li_2IrO_3 (Takayama et al. 2014) and the 3D *harmonic* honeycomb γ-Li_2IrO_3 (Biffin et al. 2014) seem to be much closer to the Kitaev regime than their layered cousins. Despite the fact that they are still magnetically ordered, it seems that a dominant Kitaev interaction is

J. Knolle, *Dynamics of a Quantum Spin Liquid*, Springer Theses,
DOI 10.1007/978-3-319-23953-8_7

crucially needed to describe the peculiar non-coplanar magnetic ordering. Hence, they might not be far from the QSL region, which could therefore conceivably be reachable by doping or pressure.

Many aspects of the 2D Kitaev model carry over to 3D generalizations including the exact solubility in terms of Majorana fermions and static fluxes. The low energy response of future INS experiments on the presently known ordered 3D Iridates will be dominated by spin wave excitations. However, it is tempting to speculate that some traces of the characteristic high energy features which I discover in the QSL regime could still be observable. Just as in the analogous case of one dimensional spin chains, which often eventually order because of residual inter-chain couplings, a broad spinon continuum can be well observed experimentally. In fact, integrability is always imperfect but qualitative high-energy features are likely to survive. Similarly, in any instantiation of Kiteav QSLs in real materials, I expect quantitative changes such as a small degree of smearing out of the distinct signatures which I have discovered in this thesis. Importantly, central aspects of fractionalization are expected to remain observable.

7.2 Signatures of Fractionalization

The calculated spin structure factor of the 2D Kitaev model is mostly broad in energy and momentum as expected for a fractionalized system. However, there are clear characteristic manifestations of the QSL nature of the ground state: First, in both gapped and gapless phases, the response vanishes below the two-flux gap. It is remarkable that in an INS experiment, the response of a gapless QSL shows an excitation gap which is directly related to the emergent gauge field. Second, above the gap, the response reflects the physics of the matter sector, e.g. the van Hove singularity of the matter fermions hopping on the honeycomb lattice appears as a dip in the structure factor. Third, a surprising and counterintuitive manifestation of quantum number fractionalization in the anisotropic model is a sharp component as a function of frequency in the response from a pure flux excitation.

A similar feature, even for an isotropic system, can be found in an extended Kitaev model. The inclusion of a three spin interaction, which captures perturbatively the effect of an external magnetic field, gaps out the Dirac spectrum of the formerly gapless regime. The resulting QSL phase hosts excitations with non-Abelian statistics. As a hallmark of this non-Abelian phase and in stark contrast to the Abelian phase of the original model, flux pairs lead to bound in-gap states of Majorana fermions. The latter are manifest in the dynamical structure factor as a sharp component at an energy below the single particle continuum. The clear distinction in the response between a δ-function in-gap component and a continuum at higher energies is surprisingly robust with respect to the inclusion of exchange disorder, which is always present in real materials.

Overall, an intuitive understanding of the INS response in Kitaev QSLs emerges in which spins fractionalize into a static Z_2 flux pair and additional itinerant Majorana fermions. Fluxes form a flat band which leads to the ultra short ranged

nature of the spin correlations. In addition, these infinitely heavy quasiparticles are responsible for the broad momentum independence and for the gap in the response even for a gapless QSL. On top of this, Majorana fermions propagate in the perturbed flux background and scatter of the additional flux pair, which can even lead to the formation of bound states. The resulting fermionic density of states determines the shape of the response above the flux gap.

Apart from the spin structure factor, I identify similar signatures of fractionalization in Raman scattering. This establishes this experimental method as an alternative tool for diagnosing QSLs in candidate materials, which is of particular interest given the difficulty of using neutrons to study materials hosting iridium ions, e.g. the compounds Na_2/Li_2IrO_3. The Raman signal of the integrable Kitaev model is polarization-independent and reflects the density of states of the emergent Majorana fermions in the ground state flux sector. The addition of an extra weak integrability-breaking Heisenberg exchange term generates a second contribution. The latter is connected to the abrupt insertion of four emergent Z_2 fluxes, which results in a weakly polarization dependent response, and which also contains a sharp peak but here at the energy of a pure localized four-flux excitation. Beyond this concrete example of Raman scattering, the calculation with the weakly perturbed Kitaev model suggests that while a QSL phase might be stable with respect to weak integrability breaking, the induced change in response functions can in some cases be considerable.

In conclusion, dynamical response functions have the advantage that they probe the full excitation spectrum, which allows a detailed comparison between experiments and theoretical calculations beyond the low energy properties dominating, e.g., thermodynamic measurements. The signatures of fractionalization, which I discover in low and high energy properties, establish INS, ESR, and Raman scattering as valuable tools for diagnosing QSLs in candidate materials.

7.3 Methodological Progress and Connection to Non-equilibrium Physics

Exact calculations of correlation functions are usually restricted to 1D systems because of the special methods available, e.g. the Bethe-Ansatz. Due to the absence of corresponding theoretical methods in 2D up to date, the study of QSLs can be roughly divided into two lines of research. On the one hand, slave-particle mean-field treatments offer an intuitive physical picture of QSL phases, but they are ultimately uncontrolled approximations. On the other hand, numerical methods such as ED, DMRG, or quantum Monte Carlo permit exact or at least well-controlled calculations, but they are limited to small system sizes, to systems with a robust excitation gap, or to models that avoid the sign problem. These obstacles often limit a full understanding. The exact results of this thesis establish a third line of research, which allows to calculate exact correlation functions in 2D in the thermodynamic limit, thereby providing a benchmark at an integrable point, as well as a possible starting point for perturbation theory.

Despite the fact that the Kitaev model has an exact solution, the full analysis of its correlation functions turns out to be a challenging task. By eliminating the emergent gauge degrees of freedom, the calculation of the dynamical spin correlation function can be mapped to a local quantum quench of Majorana fermions perturbed by the sudden insertion of a nearest neighbor Z_2 flux pair. I derive two complementary exact solutions for this non-equilibrium problem, which enable me to obtain results in the entire phase diagram and in the thermodynamic limit. These methods can be applied to other non-equilibrium problems in the future.

The analysis of the quench proceeds in three steps: First, the Lehmann representation allows an intuitive understanding of central features of the response. In addition, it permits an approximate treatment of arbitrary quantum quenches by studying the contributions of different number of particle sectors. Second, I derive an exact solution via many-body path integrals for a finite size system which leads to an expression in terms of Pfaffians—a generalized determinant for antisymmetric matrices. This approach can be easily generalized to arbitrary non-local quench types. Third, I deduce an alternative exact solution based on a formal similarity of the local quench with a classic X-ray edge problem which reduces it to a non-linear integral equation. I adapt a fine method from the theory of singular integral equations which allows obtaining exact results for arbitrarily large systems. This mathematical formalism provides a general recipe for numerically exact calculations of a whole class of local quantum quenches.

Besides offering a deeper understanding of QSLs, I hope my thesis will have an impact on two different methodological strands of research. On the one hand, the benchmark results for an interacting 2D quantum spin system should lead to an improved understanding of widely used approximations and of purely numerical methods. On the other hand, the formalism which I have developed can address open questions concerning quench dynamics of integrable models.

7.4 Open Questions and Outlook

Finally, I close the thesis by indicating open issues and by suggesting promising directions for future research. Arguably, the most interesting question is how general my findings are? The Kitaev model is a representative of a class of QSLs with Majorana fermions coupled to a Z_2 gauge field. Therefore, the qualitative features I discover in response functions should be characteristic of this broad class of topological states.

While a potential cold atom realization likely harbors few perturbations to the Kitaev Hamiltonian, magnetic materials usually include other terms, e.g. additional Heisenberg interactions. Both the flux gap and the fermion parity underpinning my results are robust to such perturbations. Just as in the analogous case of the Heisenberg chain, where integrability is imperfect in reality but all qualitative features are well-observed experimentally, so I similarly expect quantitative changes such as a small degree of smearing out of the δ-function response or a more gradual

onset of the signal around the flux gap. A suitable starting point for studying how breaking of integrability washes out these sharp features in the structure factor is given by slave-particle mean-field approaches because they exactly reproduce ground state properties of the integrable limit of the Kitaev–Heisenberg model (Burnell and Nayak 2011; Schaffer et al. 2012). Hence, after using my exact results as a benchmark at the integrable point, it is possible to take into account integrability breaking corrections. In addition, it would be of great interest to calculate the Raman scattering of the Kitaev–Heisenberg model via numerical methods, e.g. via ED or DMRG, to confirm the validity of our perturbative treatment in Sect. 6.1.

A different interesting question concerns the influence of finite temperatures (Nasu et al. 2014) on dynamical correlation functions in the Kitaev model. Due to the fact that fluxes can be thermally excited, I expect that with increasing temperature the sharp gap of the structure factor will be slowly filled in and again the sharp δ-function component is likely to be broadened.

In the non-Abelian phase of the extended Kitaev model, a pair of fluxes leads to a fermionic boundstate below the continuum, which in turn results in a δ-function component in the structure factor. This particular example points to a generic phenomenon. Hence, a more general study of the effect of boundstates on dynamical response functions presents a promising area for future investigations.

Another direction for new research is the application of the theoretical methods explained in detail in this thesis to generalizations of the Kitaev model to other classes of QSLs and, especially, to higher dimensions. For the latter, the calculation of the spin correlation function still takes the form of a local quantum quench because each spin operator acting on the ground state introduces fluxes. The response in the resulting quench will be mainly determined by the low energy spectrum of the matter fermions. Therefore, depending on the Fermi surface topology, singular behavior may appear.

From a different perspective, there are numerous open questions in the field of non-equilibrium physics which can be partly addressed by the methods developed in this thesis. One possibility is the study of defect production after different local and global quench types including the effect of disorder.

Overall, one of the gratifying features of this work has been the bringing together of questions on fractionalization at the cutting edge of modern condensed matter physics with problems in many-body physics—both from the old days and very current ones—from the X-ray edge to quantum quenches. For this reason alone, I expect the topics discussed here, along with the methods developed, to remain of considerable general interest for the foreseeable future.

References

A. Biffin, R. Johnson, I. Kimchi, R. Morris, A. Bombardi, J. Analytis, A. Vishwanath, R. Coldea, Non-coplanar and counter-rotating incommensurate magnetic order stabilized by Kitaev interactions in γ-Li_2IrO_3. arXiv:1407.3954. Unpublished (2014)

F.J. Burnell, C. Nayak, SU(2) slave fermion solution of the Kitaev honeycomb lattice model. Phys. Rev. B **84**(12), 125125 (2011)

M. Hermanns, S. Trebst, Quantum spin liquid with a Majorana Fermi surface on the three-dimensional hyperoctagon lattice. Phys. Rev. B **89**(23), 235102 (2014)

G. Jackeli, G. Khaliullin, Mott insulators in the strong spin-orbit coupling limit: from Heisenberg to a quantum compass and Kitaev models. Phys. Rev. Lett. **102**(1), 017205 (2009)

I. Kimchi, J.G. Analytis, A. Vishwanath, Three dimensional quantum spin liquid in 3D-honeycomb iridate models and phase diagram in an infinite-D approximation. arXiv:1309.1171. Unpublished (2014)

E.K.-H. Lee, R. Schaffer, S. Bhattacharjee, Y.B. Kim, Heisenberg-Kitaev model on the hyperhoneycomb lattice. Phys. Rev. B **89**(4), 045117 (2014)

S. Mandal, N. Surendran, Exactly solvable Kitaev model in three dimensions. Phys. Rev. B **79**(2), 024426 (2009)

J. Nasu, M. Udagawa, Y. Motome, Vaporization of quantum spin liquids. arXiv:1406.5415. Unpublished (2014)

R. Schaffer, S. Bhattacharjee, Y.B. Kim Quantum phase transition in Heisenberg-Kitaev model. Phys. Rev. B **86**(22), 224417 (2012)

Y. Singh, S. Manni, J. Reuther, T. Berlijn, R. Thomale, W. Ku, S. Trebst, P. Gegenwart, Relevance of the Heisenberg-Kitaev Model for the honeycomb lattice iridates. Phys. Rev. Lett. **108**(12), 127203 (2012)

T. Takayama, A. Kato, R. Dinnebier, J. Nuss, H. Takagi, Hyper-honeycomb iridate β-Li_2IrO_3 as a platform for Kitaev magnetism. arXiv:1403.3296. Unpublished (2014)

Appendix A
Pfaffians from Path Integrals

In this appendix, I present the calculation of the dynamical spin correlation function for a finite size systems via an expression in terms of Pfaffians. In particular, I concentrate on calculating the matrix element, Eq. (3.35),

$$M_{q,l} = \langle M_0 | a_q e^{-it\mathcal{H}} a_l^\dagger | M_0 \rangle \tag{A.1}$$

with anomalous terms in the Bogoliubov de Gennes Hamiltonian, see Eq. (2.16),

$$\mathcal{H} = \sum_{ij} \left[h_{ij} a_i^\dagger a_j + \frac{1}{2} \Delta_{ij}^\dagger a_i a_j + \frac{1}{2} \Delta_{ij} a_i^\dagger a_j^\dagger \right]. \tag{A.2}$$

For the calculation of the correlation function, $\mathcal{H}$ is the two flux Hamiltonian, $\mathcal{H} = H_0 + V_z$. However, the following derivation is completely general for an arbitrary Hamiltonian $\mathcal{H}$ with the state $|M_0\rangle$ not being its ground state or any Eigenstate. The only requirement is that it can be written in terms of operators a_i which annihilate $|M_0\rangle$ (the ground state of a_i).

A.1 Pfaffians: Definition and Properties

As shown below, the so-called *Pfaffians* appear in Gaussian Grassmann integration (Zinn-Justin 2002). Before embarking on the detailed calculation of the matrix element, I briefly define what a Pfaffian is. I list some of the properties further down. A Pfaffian is a generalization of the determinant for skew-symmetric (or anti-symmetric) matrices $-A = A^T$. It is always possible to write the determinant of a skew symmetric matrix as a square of a polynomial in the matrix entries (Zinn-Justin 2002)

J. Knolle, *Dynamics of a Quantum Spin Liquid*, Springer Theses,
DOI 10.1007/978-3-319-23953-8

$$\mathrm{Pf}^2(A) = \det(A). \tag{A.3}$$

The formal definition of a Pfaffian for a $2N \times 2N$ skew symmetric matrix A is

$$\mathrm{Pf}(A) = \frac{1}{2^N N!} \sum_{P \in i_1 \ldots i_{2N}} \mathrm{sgn}(P) a_{i_1,i_2} a_{i_3,i_4} \cdots a_{i_{2N-1},i_{2N}} \tag{A.4}$$

with matrix elements $a_{i,j}$ and sign $\mathrm{sgn}(P) = \pm$ of the permutation P. Hence, the Pfaffian is a unique choice of the sign for the square root $\mathrm{Pf}(A) = \pm\sqrt{\det(A)}$. Note that the Pfaffian of an odd dimensional matrix is zero. Several properties known from determinants carry over in a modified way to Pfaffians (Zinn-Justin 2002; Wimmer 2012):

- Multiplying a row and a column with a constant is the same as multiplying the entire Pfaffian with this constant.
- Interchanging two rows and the corresponding columns flips the sign of the Pfaffian.
- Adding multiples of a row and the corresponding column to another row and corresponding column leaves the Pfaffian invariant.

Another very useful property for numerical computations is the expansion formula for Pfaffians

$$\mathrm{Pf}(A) = \sum_{i=2}^{2N} (-1)^i a_{1i} \mathrm{Pf}(A_{1i}) \tag{A.5}$$

with the reduced matrix A_{1i} being the matrix with rows and columns 1 and i removed. In addition, I will use the relation

$$\mathrm{Pf}(BAB^T) = \det(B)\mathrm{Pf}(A) \tag{A.6}$$

for an arbitrary $2N \times 2N$ matrix B.

A.2 Path Integrals

In order to calculate the matrix element, Eq. (A.1), via path integrals, I rewrite it with the help of projectors as

$$\begin{aligned} M_{q,l} &= \sum_n \langle n | a_N^\dagger a_{N-1}^\dagger \ldots a_1^\dagger a_q e^{-it\mathcal{H}} a_l^\dagger a_1 \ldots a_N | n \rangle \\ &= \mathrm{Tr}\left\{ e^{-it\mathcal{H}} a_l^\dagger a_1 \ldots a_N a_N^\dagger a_{N-1}^\dagger \ldots a_1^\dagger a_q \right\}. \end{aligned} \tag{A.7}$$

Here, N is the total number of degrees of freedom. I commute $a_l^\dagger$ to the right and a_q to the left

$$M_{q,l} = (-1)^{q+l}\mathrm{Tr}\left\{a_N^\dagger \dots a_{l+1}^\dagger a_{l-1}^\dagger \dots a_1^\dagger e^{-it\mathcal{H}} a_1 \dots a_{q-1} a_{q+1} \dots a_N\right\} - \delta_{q,l}\mathrm{Tr}\left\{a_N^\dagger \dots a_1^\dagger e^{-it\mathcal{H}} a_1 \dots a_N\right\} \tag{A.8}$$

such that one creation and one annihilation operator is missing in the first term and all operators are present in the second term.

For the calculation of both matrix elements in Eq. (A.8) I continue with path integrals. In Sect. A.4 I propose an alternative way.

The standard strategy proceeds as follows (Negele and Orland 2008): I derive a generating functional $\mathbf{F}(J^*, J)$ such that the matrix elements, or higher order Greens functions, are obtained by differentiating with respect to the corresponding sources J_k^*, J_l. (This is equivalent to deriving Wick's theorem.)

$$\mathrm{Tr}\left\{a_N^\dagger \dots a_1^\dagger e^{-it\mathcal{H}} a_1 \dots a_N\right\} = \frac{\partial^{2N}}{\partial J_N \dots \partial J_1 \partial J_1^* \dots \partial J_N^*}\mathbf{F}[J_k^*, J_l] \tag{A.9}$$

The identity of anti-commuting Grassmann variables ϕ can be written as (Negele and Orland 2008)

$$\mathbf{1} = \int \prod_{i=1}^{N} d\phi_i^* d\phi_i e^{-\sum_i \phi_i^* \phi_i} |\phi\rangle\langle\phi|. \tag{A.10}$$

such that

$$\begin{aligned}\mathrm{Tr}\left\{e^{-it\mathcal{H}}\right\} &= \sum_n \langle n|e^{-it\mathcal{H}}|n\rangle \\ &= \int \prod_{i=1}^{N} d\phi_i^* d\phi_i e^{-\sum_i \phi_i^* \phi_i} \sum_n \langle n|\phi\rangle\langle\phi|e^{-it\mathcal{H}}|n\rangle \\ &= \int \prod_{i=1}^{N} d\phi_i^* d\phi_i e^{-\sum_i \phi_i^* \phi_i} \langle -\phi|e^{-it\mathcal{H}}|\phi\rangle.\end{aligned} \tag{A.11}$$

Now, I insert M-1 times the identity $\mathbf{1}$

$$\begin{aligned}&\mathrm{Tr}\left\{e^{-it\mathcal{H}}\right\} \\ &= \int \prod_{l=1}^{M} d\phi^{l*} d\phi^l e^{-\sum_l \phi^{l*}\phi^l} \int d\phi^* d\phi e^{-\phi^*\phi} \langle -\phi|e^{-i\Delta t\mathcal{H}}|\phi^{M-1}\rangle \\ &\quad \langle \phi^{M-1}|e^{-i\Delta t\mathcal{H}} \cdots \langle \phi^1|e^{-i\Delta t\mathcal{H}}|\phi\rangle\end{aligned} \tag{A.12}$$

with $\Delta t = \frac{t}{M}$. The label i for the degrees of freedom is not written explicitly. I relabel $-\phi^* = \phi^{M*}$, $\phi = \phi^0$ and normal order the exponential in each time step. All creation operators $a^\dagger$ act on the left time step and all destruction operators a on the right

$$\langle \phi^l | e^{-i\Delta t \mathcal{H}} | \phi^{l-1} \rangle = e^{-i\Delta t \left\{ h_{ij} \phi_i^{l*} \phi_j^{l-1} + \frac{1}{2} \Delta_{ij} \phi_i^{l*} \phi_j^{l*} + \frac{1}{2} \Delta_{ij}^\dagger \phi_i^{l-1} \phi_j^{l-1} \right\}} e^{\phi_i^{l*} \phi_i^{l-1}}. \quad \text{(A.13)}$$

Overall, I obtain (with all indices)

$$\begin{aligned} \mathrm{Tr}\left\{ e^{-i t \mathcal{H}} \right\} = & \underbrace{\int \prod_{l=1}^{M} \prod_{i=1}^{N} d\phi_i^{l*} d\phi_i^l}_{\int D[\phi]} \\ & \times \exp\left\{ - \sum_{i,j=1}^{N} \sum_{l=1}^{M} \left[\phi_i^{l*} \phi_i^l - \phi_i^{l*} \phi_i^{l-1} + i\Delta t \right.\right. \\ & \left.\left. \left(h_{i,j} \phi_i^{l*} \phi_j^{l-1} + \frac{1}{2} \Delta_{ij} \phi_i^{l*} \phi_j^{l*} + \frac{1}{2} \Delta_{ij}^* \phi_i^{l-1} \phi_j^{l-1} \right) \right] \right\}. \end{aligned} \quad \text{(A.14)}$$

Instead of going to the continuum limit as usually done, I Fourier transform to Matsubara space

$$\phi_i^l = \frac{1}{\sqrt{M}} \sum_{p=-\frac{M}{2}}^{p=\frac{M}{2}} \varphi_i^p e^{i\omega_p l} \text{ with } \omega_p = \frac{2\pi}{M} \left(p + \tfrac{1}{2} \right). \quad \text{(A.15)}$$

The sum over Matsubara frequencies can be split into positive and negative components (note $e^{-i\omega_{-p-1}} = e^{+i\omega_p}$). I put a common factor it into the definition of h and Δ,

$$\begin{aligned} \mathrm{Tr}\left\{ e^{-i t \mathcal{H}} \right\} = & \int D[\phi] \\ & \times \exp\left\{ - \sum_{i,j=1,p=0}^{N,\frac{M}{2}} \left[\varphi_i^{p*} \ \varphi_i^{-p-1} \right] \begin{bmatrix} \delta_{i,j} - e^{-i\omega_p} (\delta_{i,j} - \frac{1}{2} h_{i,j}) & \frac{1}{2} \Delta_{i,j} \\ \frac{1}{2} \Delta_{i,j}^\dagger & -\delta_{i,j} + e^{+i\omega_p} (\delta_{i,j} - \frac{1}{2} h_{i,j}^T) \end{bmatrix} \begin{bmatrix} \varphi_j^p \\ \varphi_j^{-p-1*} \end{bmatrix} \right\} \end{aligned} \quad \text{(A.16)}$$

which can be further simplified in the large $M \to \infty$ limit:

$$\mathrm{Tr}\left\{ e^{-i t \mathcal{H}} \right\} = \int D[\phi] \exp\left\{ - \sum_p \left[\varphi^{p*} \ \varphi^{-p-1} \right] \begin{bmatrix} i\omega_p + \frac{1}{2} h & \frac{1}{2} \Delta \\ \frac{1}{2} \Delta^\dagger & i\omega_p - \frac{1}{2} h^T \end{bmatrix} \begin{bmatrix} \varphi^p \\ \varphi^{-p-1*} \end{bmatrix} \right\}. \quad \text{(A.17)}$$

The large M limit actually introduces a phase ambiguity which needs to be handled with care, see further down.

To evaluate Eq. (A.17), I follow Sect. 2.1.1 and diagonalize the Hamiltonian

$$\mathcal{H} = \frac{1}{2}\begin{bmatrix} a_i^\dagger & a_i \end{bmatrix}\begin{bmatrix} h & \Delta \\ \Delta^\dagger & -h^T \end{bmatrix}\begin{bmatrix} a_j \\ a_j^\dagger \end{bmatrix} \equiv \hat{\alpha}^\dagger \hat{H} \hat{\alpha} \tag{A.18}$$

with the Bogoliubov transformation $\hat{T}$ (Blaizot and Ripka 1986)

$$\hat{\beta} = \hat{T}\hat{\alpha} \text{ and } \hat{T}\hat{H}\hat{T}^{-1} = \frac{1}{2}\begin{bmatrix} \Omega_n & 0 \\ 0 & -\Omega_n \end{bmatrix} \tag{A.19}$$

with Eigenvalues Ω_n on the diagonal and a positive sign on the upper $N \times N$ block and a negative sign for the lower $N \times N$ block. Note, in Eq. (2.19) the Eigenvalues are called E_n but here the Eigenvalues come with an additional factor it. To keep this in mind they are relabeled by Ω_n. The Hamiltonian becomes

$$\mathcal{H} = \sum_{n>0} \Omega_n b_n^\dagger b_n - \frac{1}{2}\sum_{n>0} \Omega_n \tag{A.20}$$

and by having redefined the energies, I do not need to carry around the additional factor of it. I also ignore the constant phase in the remainder and restore it in the final expression. As before the Eigenvector matrices are given by

$$\hat{T}^{-1} = \begin{bmatrix} \mathcal{X}^T & \mathcal{Y}^\dagger \\ \mathcal{Y}^T & \mathcal{X}^\dagger \end{bmatrix} \text{ and } \hat{T} = \begin{bmatrix} \mathcal{X}^* & \mathcal{Y}^* \\ \mathcal{Y} & \mathcal{X} \end{bmatrix} \tag{A.21}$$

with each entry being an $N \times N$ matrix. Recall, the present Bogoliubov transformation relates the flux free sector (a operators diagonalizing H_0) and the two flux sector (b operators diagonalizing $H_0 + V_z$), therefore, my curley notation follows the convention of Sect. 2.1.1.

A.2.1 Determinant

To evaluate Eq. (A.17) I introduce $\hat{\varphi}^{p\dagger} = \begin{bmatrix} \varphi^{p*} & \varphi^{-p-1} \end{bmatrix}$ and $\hat{\varphi}^{p\dagger}\hat{T}^{-1} = \hat{\psi}^{p\dagger} = \begin{bmatrix} \psi_1^{p*} & \psi_2^{p} \end{bmatrix}$ to obtain

$$\mathrm{Tr}\left\{e^{-it\mathcal{H}}\right\} = \int D[\psi] \exp\left\{ -\sum_{p>0} \hat{\psi}^{p\dagger} \begin{bmatrix} i\omega_p + \Omega_n & 0 \\ 0 & i\omega_p - \Omega_n \end{bmatrix} \hat{\psi}^p \right\}. \tag{A.22}$$

Written in components I evaluate the Gaussian integral

$$\begin{aligned}\mathrm{Tr}\left\{e^{-it\mathcal{H}}\right\} &= \int \prod_{p=0}^{\infty}\prod_{n=1}^{N} d\psi_{1n}^{p*} d\psi_{1n}^{p} d\psi_{2n}^{p*} d\psi_{2n}^{p} \\ &\times \exp\left\{-\sum_{p=0}^{\infty}\sum_{n}^{N}\left(\psi_{1n}^{p*}(i\omega_p+\Omega_n)\psi_{1n}^{p} + \underbrace{\psi_{2n}^{p}(i\omega_p-\Omega_n)\psi_{2n}^{p*}}_{\psi_{2n}^{p*}(-i\omega_p+\Omega_n)\psi_{2n}^{p}}\right)\right\} \\ &= \prod_{p=0}^{\infty}\prod_{n=1}^{N}(i\omega_p+\Omega_n)(-i\omega_p+\Omega_n) \\ &= \prod_{n=1}^{N}\exp\left\{\sum_{p=0}^{\infty}\log\left(i\omega_p+\Omega_n\right)+\log\left(-i\omega_p+\Omega_n\right)\right\} \\ \mathrm{Tr}\left\{e^{-it\mathcal{H}}\right\} &= \prod_{n=1}^{N}\exp\left\{\sum_{p=-\infty}^{\infty}\log\left(i\omega_p+\Omega_n\right)\right\} = \prod_{n=1}^{N}\left(1+e^{-itE_n^F}\right) \equiv \mathcal{D}_0.\end{aligned} \tag{A.23, A.24}$$

I used the formula $\sum_{p=-\infty}^{\infty}\log\left(i\omega_p+\Omega_n\right) = \log\left[1+\exp\left(-\Omega_n\right)\right]$, see, for example, the book Altland and Simons (2006). Note, in the last line I have taken out the factor it from the definition of Ω_n to recover the standard energies E_n^F.

A.2.2 Generating Functional

I construct the generating functional by adding source terms to the path integral

$$\begin{aligned}\mathbf{F}[J^*,J] &= \int D[\phi]\exp\left\{-\sum_{p>0}\hat{\varphi}^{p\dagger}\hat{T}^{-1}\hat{T}\begin{bmatrix} i\omega_p+\frac{1}{2}h & \frac{1}{2}\Delta \\ \frac{1}{2}\Delta^{\dagger} & i\omega_p-\frac{1}{2}h^{T}\end{bmatrix}\hat{T}^{-1}\hat{T}\hat{\varphi}^{p}\right\} \\ &\times\exp\left\{\sum_{p>0}\left(\varphi_i^{p*}J_i^{p}+\varphi_i^{-p-1*}J_i^{-p-1}+J_i^{p*}\varphi_i^{p}+J_i^{-p-1*}\varphi_i^{-p-1}\right)\right\}.\end{aligned} \tag{A.25}$$

I define $\hat{J}^{p\dagger} = \begin{bmatrix} J_i^{p*} & -J_i^{-p-1} \end{bmatrix}$ and rewrite the sources as $\sum_p \hat{\varphi}^{p\dagger}\hat{J}^p + \hat{J}^{p\dagger}\hat{\varphi}^p$. With the Bogoliubov transformation the Gaussian integrals are calculated as

$$\begin{aligned}\mathbf{F}[J^*, J] &= \int D[\psi] \exp\left\{ -\sum_{p>0} \hat{\psi}^{p\dagger} \begin{bmatrix} i\omega_p + \Omega_n & 0 \\ 0 & i\omega_p - \Omega_n \end{bmatrix} \hat{\psi}^p + \hat{\psi}^{p\dagger}\hat{T}\hat{J}^p + \hat{J}^{p\dagger}\hat{T}^{-1}\hat{\psi}^p \right\} \\ &= \mathcal{D}_0 \exp\left\{ +\sum_{p>0} \hat{J}^{p\dagger}\hat{T}^{-1} \begin{bmatrix} \frac{1}{i\omega_p + \Omega_n} & 0 \\ 0 & \frac{1}{i\omega_p - \Omega_n} \end{bmatrix} \hat{T}\hat{J}^p \right\}. \end{aligned} \tag{A.26}$$

The expression is in Matsubara frequency space. Since all operators $a_i^\dagger, a_j$ in $\mathrm{Tr}\left\{ \cdots a_i^\dagger \cdots e^{-it\mathcal{H}} \cdots a_j \cdots \right\}$ act on the same real time index M, I Fourier transform back

$$\begin{aligned} J_i^{p*} &= \frac{1}{\sqrt{M}} \sum_{m=1}^{M} e^{-i\omega_p m} \tilde{J}_i^{m*} \\ J_i^{-p-1*} &= \frac{1}{\sqrt{M}} \sum_{m=1}^{M} e^{+i\omega_p m} \tilde{J}_i^{m*} \end{aligned} \tag{A.27}$$

to get

$$\mathbf{F}[J^*, J] = \quad \mathcal{D}_0 \exp\left\{ +\sum_{p>0} \sum_{m,m'} \tilde{J}^{m\dagger}\hat{T}^{-1} \begin{bmatrix} \frac{e^{-i\omega_p(m-m')}}{i\omega_p + \Omega_n} & 0 \\ 0 & \frac{e^{+i\omega_p(m-m')}}{i\omega_p - \Omega_n} \end{bmatrix} \hat{T}\tilde{J}^{m'} \right\}. \tag{A.28}$$

I only need time index M for the functional derivatives, e.g. $\frac{\partial^2}{\partial J_i^M \partial J_j^{M*}} \mathbf{F}[J^*, J]$, thus I can put $m = m' = M$ and all the exponentials are 1. Then, the sum over Matsubara frequencies can be put into the matrix because the transformation $\hat{T}$ is independent of p. Because of the previous large M limit, the resulting sums are actually not convergent and need to be properly regularized. Therefore, there is a phase ambiguity in carrying out the sums. To proceed, I extend the sum from $-\infty$ to $+\infty$ and introduce the following preliminary definitions

$$\sum_{p=-\infty}^{\infty} \frac{1}{i\omega_p \pm \Omega_n} \equiv n^{\mp}(\Omega_n). \tag{A.29}$$

I take care of the regularization further down when comparing the path integral approach to an alternative calculation, see Sect. A.4. In fact, $n^{\mp}(\Omega_n) = \frac{1}{1+e^{\pm\Omega_n}}$ turns out to be the Fermi function.

With these definitions I obtain

$$\mathbf{F}[J^*, J] = \mathcal{D}_0 \exp\left\{ \frac{1}{2} \begin{bmatrix} J_i^* & -J_i \end{bmatrix} \hat{T}^{-1} \begin{bmatrix} n^-(\Omega_n) & 0 \\ 0 & n^+(\Omega_n) \end{bmatrix} \hat{T} \begin{bmatrix} J_j \\ -J_j^* \end{bmatrix} \right\} \quad \text{(A.30)}$$

and the factor of $\frac{1}{2}$ is due to the fact that the sums are extended to negative frequencies. I dropped the time index M. The matrix can now be simplified to

$$\begin{aligned} \hat{T}^{-1} \begin{bmatrix} n^-(\Omega_n) & 0 \\ 0 & n^+(\Omega_n) \end{bmatrix} \hat{T} &= \begin{bmatrix} \mathcal{A} & \mathcal{B} \\ \mathcal{C} & \mathcal{D} \end{bmatrix} \quad \text{with} \\ \mathcal{A} &= \mathcal{X}^T n^- \mathcal{X}^* + \mathcal{Y}^\dagger n^+ \mathcal{Y} \\ \mathcal{B} &= \mathcal{X}^T n^- \mathcal{Y}^* + \mathcal{Y}^\dagger n^+ \mathcal{X} \\ \mathcal{C} &= \mathcal{Y}^T n^- \mathcal{X}^* + \mathcal{X}^\dagger n^+ \mathcal{Y} \\ \mathcal{D} &= \mathcal{Y}^T n^- \mathcal{Y}^* + \mathcal{X}^\dagger n^+ \mathcal{X} \end{aligned} \quad \text{(A.31)}$$

such that overall the generating functional is

$$\mathbf{F}[J^*, J] = \mathcal{D}_0 \exp\left(\frac{1}{2} \left\{ J_i^* \mathcal{A}_{i,j} J_j - J_i^* \mathcal{B}_{i,j} J_j^* - J_i \mathcal{C}_{i,j} J_j + J_i \mathcal{D}_{i,j} J_j^* \right\} \right). \quad \text{(A.32)}$$

I can check its validity by looking at the situation without anomalous terms. In this case, I need $\mathcal{A}_{i,j} = -\mathcal{D}_{i,j}^T$ to recover the standard result (Negele and Orland 2008). At this point, the phase ambiguity from the regularization of the sums becomes obvious. It needs to be resolved in a different way, see Sect. A.4.

A.2.3 Matrix Elements

In principle, I could start with differentiating with respect to the sources to calculate both matrix elements, Eq. (A.8), but the procedure turns out to be difficult due to the appearance of the anomalous contributions. To make progress in deriving a version of the Wick theorem with anomalous terms, I proceed in a different way. I reorder the exponential into an antisymmetric matrix

$$\mathbf{F}[J^*, J] = \mathcal{D}_0 \exp\left\{ \frac{1}{2} \begin{bmatrix} J_i^* & J_i \end{bmatrix} \underbrace{\begin{bmatrix} -\mathcal{B}_{i,j} & \mathcal{A}_{i,j} \\ -\mathcal{A}_{i,j}^T & -\mathcal{C}_{i,j} \end{bmatrix}}_{\equiv \hat{S}_{i,j}^{-1}} \begin{bmatrix} J_j^* \\ J_j \end{bmatrix} \right\}, \quad \text{(A.33)}$$

which gives the final expression for the generating functional. The matrix $\hat{S}^{-1}_{i,j} = -\hat{S}^{-1}_{j,i}$ is antisymmetric by construction.

Next, I concentrate on the matrix elements, e.g.

$$\begin{aligned}\mathrm{Tr}\left\{a_N^\dagger \dots a_1^\dagger e^{-it\mathcal{H}} a_1 \dots a_N\right\} &= (-1)^N \int D[\phi] e^{-S[\phi,\phi*]} \phi_N^{M*} \dots \phi_1^{M*} \phi_1^0 \dots \phi_N^0 \\ &= \underbrace{(-1)^N \cdot (-1)^N}_{=1} \frac{\partial^{2N}}{\partial J_N \dots \partial J_1 \partial J_1^* \dots \partial J_N^*} \mathbf{F}[J^*, J] \\ &. \end{aligned} \tag{A.34}$$

On the left side, in the trace all creation and annihilation operators act on the same time $t = 0$. In constructing the path integral all $a^\dagger$ act on the left time step $\langle -\phi|$ which gives a factor $(-1)^N$ and all a act on the right time step with index 0. As usual I identify the time steps $M = 0$ such that Eq. (A.9) is recovered. I have dropped the time index.

For Grassman variables differentiation is the same as integration (Zinn-Justin 2002) such that $\int d\theta_i A = \frac{\partial}{\partial \theta_i} A$ or

$$\frac{\partial^{2N}}{\partial J_N \dots \partial J_1 \partial J_1^* \dots \partial J_N^*} \mathbf{F}[J^*, J] = \int dJ_N \dots dJ_1 dJ_1^* \dots dJ_N^* \mathbf{F}[J^*, J]. \tag{A.35}$$

I use this mathematical identity for deriving all the matrix elements because in the end integration is formally easier. First, I check the simple single-particle Greens function

$$\mathrm{Tr}\left\{a_j^\dagger e^{-it\mathcal{H}} a_i\right\} = \frac{\partial^2}{\partial J_j \partial J_i^*} \mathbf{F}[J^*, J] = \mathcal{D}_0 \int dJ_j dJ_i^* \frac{1}{2} \left(\sum_{k,l} J_k^* \mathcal{A}_{k,l} J_l - J_k \mathcal{A}^T_{k,l} J_l^* \right) \tag{A.36}$$

such that

$$\mathrm{Tr}\left\{a_j^\dagger e^{-it\mathcal{H}} a_i\right\} = \mathcal{D}_0 \mathcal{A}_{i,j}. \tag{A.37}$$

In a similar way, I obtain

$$\begin{aligned}\mathrm{Tr}\left\{a_j e^{-it\mathcal{H}} a_i\right\} &= \mathcal{D}_0 \mathcal{B}_{i,j} \\ \mathrm{Tr}\left\{a_j^\dagger e^{-it\mathcal{H}} a_i^\dagger\right\} &= \mathcal{D}_0 \mathcal{C}_{i,j}. \end{aligned} \tag{A.38}$$

A comparison with Eqs. (A.55)–(A.57) of Sect. A.4 fixes the phase ambiguity.

Second, I consider the higher Greens functions by relabeling $[J_1^* \dots J_N^* J_1 \dots J_N] \rightarrow [\theta_1 \dots \theta_{2N}]$. I start with the matrix element with creation and annihilation operators running over the entire degrees of freedom $1 \dots N$.

$$\mathrm{Tr}\left\{a_N^\dagger \dots a_1^\dagger e^{-it\mathcal{H}} a_1 \dots a_N\right\} = \mathcal{D}_0 \int d\theta_{2N} \dots d\theta_{N+1} \underbrace{d\theta_1 \dots d\theta_N}_{(-1)^{\frac{N(N-1)}{2}} d\theta_N \dots d\theta_1} e^{\frac{1}{2}\sum_{i,j=1}^{2N} \theta_i \hat{S}^{-1}_{i,j} \theta_j} \tag{A.39}$$

The Gaussian integration of antisymmetric matrices with Grassmann variables, see, e.g., the book Zinn-Justin (2002), gives a Pfaffian for

$$\mathrm{Tr}\left\{\underbrace{a_N^\dagger \dots a_1^\dagger}_{\text{all}} e^{-it\mathcal{H}} \underbrace{a_1 \dots a_N}_{\text{all}}\right\} = \mathcal{D}_0 (-1)^{\frac{N(N-1)}{2}} \mathrm{Pf}\left(\hat{S}^{-1}\right). \tag{A.40}$$

Third, in the matrix element $M_{q,l}$, see Eq. (A.8), there is a second contribution with one creation and one annihilation operator missing.

$$\begin{aligned}&\mathrm{Tr}\left\{a_N^\dagger \dots \cancel{a_k^\dagger} \dots a_1^\dagger e^{-it\mathcal{H}} a_1 \dots \cancel{a_l} \dots a_N\right\} \\ &= \mathcal{D}_0 (-1)^{\frac{(N-1)(N-2)}{2}} \int d\theta_{2N} \dots \cancel{d\theta_{2N-k}} \dots d\theta_{N+1} d\theta_N \dots \cancel{d\theta_l} \dots d\theta_1 e^{\frac{1}{2}\sum_{i,j=1}^{2N} \theta_i \hat{S}^{-1}_{i,j} \theta_j}\end{aligned} \tag{A.41}$$

How to evaluate this integral? Expanding the exponential only terms of the order $(2N-2)$ survives

$$\begin{aligned}&\int d\theta_{2N} \dots \cancel{d\theta_{2N-k}} \dots \cancel{d\theta_l} \dots d\theta_1 e^{\frac{1}{2}\sum_{i,j=1}^{2N} \theta_i \hat{S}^{-1}_{i,j} \theta_j} \\ &= \frac{1}{2^{N-1}(N-1)!} \int \underbrace{d\theta_{2N} \dots d\theta_1}_{2N-2 \text{ terms}} \underbrace{(\theta_i \hat{S}^{-1}_{i,j} \theta_j)^{N-1}}_{2N-2 \text{ terms}} \\ &= \frac{1}{2^{N-1}(N-1)!} \sum_{P \in i_1 \dots \cancel{i_k} \dots \cancel{i_{2N-k}} \dots i_{2N}} \mathrm{sgn}(P) S^{-1}_{i_1,i_2} S^{-1}_{i_3,i_4} \dots S^{-1}_{i_{2N-1},i_{2N}} = \mathrm{Pf}(\hat{S}^{-1}_{[2N-k,l]}).\end{aligned} \tag{A.42}$$

The matrix $\hat{S}^{-1}_{[2N-k,l]}$ is defined as the $(2N-2) \times (2N-2)$ matrix with lines $(2N-k)$ and l, as well as, columns $(2N-k)$ and l removed. I obtain

$$\mathrm{Tr}\left\{a_N^\dagger \dots \cancel{a_k^\dagger} \dots a_1^\dagger e^{-it\mathcal{H}} a_1 \dots \cancel{a_l} \dots a_N\right\} = \mathcal{D}_0 (-1)^{\frac{(N-1)(N-2)}{2}} \mathrm{Pf}\left(\hat{S}^{-1}_{[2N-k,l]}\right). \tag{A.43}$$

A.3 Final Result

Finally, I want to combine all contributions. In Eq. (A.43) I need to calculate the Pfaffian of a $(2N-2)\times(2N-2)$ matrix (two lines and columns in $\hat{S}^{-1}_{[2N-k,l]}$ removed). While programming the above expressions I realized that the determinant $\mathcal{D}_0$ is getting very large while the Pfaffians are very small which creates problems due to numerical errors. To overcome this issue, I take advantage of the property $\mathrm{Pf}(BAB^T) = \det(B)\mathrm{Pf}(A)$ Eq. (A.6). I construct a matrix $\hat{B}$ by observing that the determinant can be written as

$$\mathcal{D}_0 = \prod_n (1+e^{-itE_n^F}) = \det\begin{bmatrix} 1+e^{-itE_1^F} & & & & & \\ & \ddots & & & & \\ & & 1+e^{-itE_N^F} & & & \\ & & & 1 & & \\ & & & & \ddots & \\ & & & & & 1 \end{bmatrix} = \det(\hat{B}). \tag{A.44}$$

Then, I can easily calculate $\mathcal{D}_0\mathrm{Pf}\left(\hat{S}^{-1}\right) = \mathrm{Pf}\left(\hat{B}\hat{S}^{-1}\hat{B}^T\right)$, which cures the numerical errors. For the other Pfaffian, I use the expansion formula, Eq. (A.5), to derive the identity

$$\mathrm{Pf}\underbrace{\begin{bmatrix} & \not{1} & & \not{2N-k} & \\ \not{1} & + & - & + & - \\ & | & & | & \\ \not{2N-k} & + & - & + & - \\ & | & & | & \end{bmatrix}}_{\equiv \hat{S}^{-1}_{[2N-k,l]}} = (-1)^{l+k}\cdot(-1)^{N+1}\mathrm{Pf}\underbrace{\begin{bmatrix} & 0 & & 0 & \\ 0 & 0 & 0 & +1 & 0 \\ & 0 & & 0 & \\ 0 & -1 & 0 & 0 & 0 \\ & 0 & & 0 & \end{bmatrix}}_{\equiv \hat{S}^{-1}_{\{2N-k,l\}}} \tag{A.45}$$

in which the Pfaffian on the right is calculated from the $2N\times 2N$ matrix $\hat{S}^{-1}_{\{2N-k,l\}}$ with all 0's on rows and columns $(2N-k)$, l and the matrix elements $\hat{S}^{-1}_{l,2N-k} = -1$ and $\hat{S}^{-1}_{2N-k,l} = +1$. Combining prefactors $(-1)^{\frac{(N-1)(N-2)}{2}} = (-1)^{\frac{N(N-1)}{2}}\cdot(-1)^{N-1}$ gives

$$(-1)^{k+l}\mathrm{Tr}\left\{a_N^\dagger \ldots \not{a}_k^\dagger \ldots a_1^\dagger e^{-it\mathcal{H}} a_1 \ldots \not{a}_l \ldots a_N\right\} = \mathcal{D}_0(-1)^{\frac{N(N-1)}{2}}\mathrm{Pf}\left(\hat{S}^{-1}_{\{2N-k,l\}}\right) \tag{A.46}$$

with a Pfaffian over the desired $2N\times 2N$ matrix. Now, I can again combine $\det(\hat{B})$ and $\mathrm{Pf}(\hat{S}^{-1}_{\{2N-k,l\}})$ via Eq. (A.6).

Finally, putting together all contributions of the matrix element

$$\begin{aligned} M_{q,l} &= \langle 0|a_q e^{-it\mathcal{H}} a_l^\dagger|0\rangle \\ &= (-1)^{q+l}\mathrm{Tr}\left\{a_N^\dagger \dots a_{l+1}^\dagger a_{l-1}^\dagger \dots a_1^\dagger e^{-it\mathcal{H}} a_1 \dots a_{q-1} a_{q+1} \dots a_N\right\} \\ &\quad - \delta_{q,l}\cdot \mathrm{Tr}\left\{a_N^\dagger \dots a_1^\dagger e^{-it\mathcal{H}} a_1 \dots a_N\right\} \end{aligned} \tag{A.47}$$

I obtain

$$M_{q,l} = e^{-itE_0^F}(-1)^{\frac{N(N-1)}{2}}\left\{\mathrm{Pf}\left(\hat{B}\hat{S}^{-1}_{\{2N-k,l\}}\hat{B}^T\right) - \delta_{q,l}\cdot\mathrm{Pf}\left(\hat{B}\hat{S}^{-1}\hat{B}^T\right)\right\}. \tag{A.48}$$

All numbers are of the same order such that the numerical calculation is well behaved. I calculate the Pfaffians with the numerical algorithm developed in Wimmer (2012).

A.4 Pfaffians Without Path Integrals

In this section I outline an alternative way of calculating the matrix elements Eq. (A.1) with anomalous terms in the Hamiltonian $\mathcal{H}$. In doing so, I can fix the proper regularization for the sums in Eq. (A.29). I recover identical results as for the path integral formalism for the single particle Greens function.

Again, a Bogoliubov transformation diagonalizes the two flux Hamiltonian. The operators transform as in Eq. (2.21)

$$\begin{aligned} a_i &= \mathcal{X}_{ik}^T b_k + \mathcal{Y}_{ik}^\dagger b_k^\dagger \\ a_j^\dagger &= \mathcal{Y}_{jl}^T b_l + \mathcal{X}_{jl}^\dagger b_l^\dagger \end{aligned} \tag{A.49}$$

with a summation over double indices.

A.4.1 Single Particle Greens Function

First, I consider the single particle Greens function of the "diagonal" operators b

$$\langle e^{-\Omega_n b_n^\dagger b_n} b_k b_p^\dagger\rangle = \tag{A.50}$$

with a sum over n implied in the exponent. For the statistical average $\langle \ldots \rangle$ I choose all states with a definite number of b particles.

$$\begin{aligned}
&= \langle e^{-\Omega_n b_n^\dagger b_n}(\delta_{k,p} - b_p^\dagger b_k)\rangle = \langle e^{-\Omega_n \hat{n}_n}(1-\hat{n}_p)\rangle \delta_{k,p} \\
&= \langle e^{-\Omega_1 \hat{n}_1} e^{-\Omega_2 \hat{n}_2} \ldots e^{-\Omega_N \hat{n}_N}(1-\hat{n}_p) e^{-\Omega_p \hat{n}_p}\rangle \delta_{k,p} \\
&= \prod_{n\neq p}(1+e^{-\Omega_n}) \underbrace{\langle (1-\hat{n}_p) e^{-\Omega_p \hat{n}_p}\rangle}_{=1} \delta_{k,p} = \underbrace{\prod_{n>0}(1+e^{-\Omega_n})}_{\mathcal{D}_0} \underbrace{\frac{1}{1+e^{-\Omega_p}}}_{\equiv n^-(\Omega_p)} \delta_{k,p}
\end{aligned} \tag{A.51}$$

All together I get

$$\langle e^{-\Omega_n b_n^\dagger b_n} b_k b_p^\dagger \rangle = \mathcal{D}_0 n^-(\Omega_p)\delta_{k,p} \tag{A.52}$$

and similarly

$$\langle e^{-\Omega_n b_n^\dagger b_n} b_k^\dagger b_p \rangle = \mathcal{D}_0 n^+(\Omega_p)\delta_{k,p}. \tag{A.53}$$

Second, I consider the single particle Greens function of the original a operators in which I am mainly interested in

$$\begin{aligned}
\langle e^{-\mathcal{H}} a_i a_j^\dagger \rangle &= \left\langle e^{-\mathcal{H}} \left[\mathcal{X}_{ik}^T b_k + \mathcal{Y}_{ik}^\dagger b_k^\dagger \right] \left[\mathcal{Y}_{jp}^T b_p + \mathcal{X}_{jp}^\dagger b_p^\dagger \right] \right\rangle \\
&= \left\langle e^{-\mathcal{H}} \left[\mathcal{X}_{ik}^T \mathcal{X}_{jp}^\dagger b_k b_p^\dagger + \mathcal{Y}_{ik}^\dagger \mathcal{Y}_{jp}^T b_k^\dagger b_p \right] \right\rangle \\
&= \left\{ \mathcal{X}_{ik}^T \mathcal{X}_{jp}^\dagger \underbrace{\langle e^{-\mathcal{H}} b_k b_p^\dagger \rangle}_{\text{Eq. (A.52)}} + \mathcal{Y}_{ik}^\dagger \mathcal{Y}_{jp}^T \underbrace{\langle e^{-\mathcal{H}} b_k^\dagger b_p \rangle}_{\text{Eq. (A.53)}} \right\}.
\end{aligned} \tag{A.54}$$

I obtain the familiar result

$$\langle e^{-\mathcal{H}} a_i a_j^\dagger \rangle = \mathcal{D}_0 \underbrace{\left\{ \mathcal{X}_{ik}^T \mathcal{X}_{jk}^\dagger n^-(\Omega_k) + \mathcal{Y}_{ik}^\dagger \mathcal{Y}_{jk}^T n^+(\Omega_k) \right\}}_{\equiv \mathcal{A}_{i,j} \text{ see Eq. (A.37)}} \tag{A.55}$$

with the definition of the matrix $\mathcal{A}$ being equivalent to the one obtained via path integrals, compare to Eq. (A.37). Here, $n^-(\Omega_k)$ is indeed the Fermi function and the phase ambiguity is resolved. Similarly, I calculate the other possibilities.

$$\langle e^{-\mathcal{H}} a_i a_j \rangle = \mathcal{D}_0 \underbrace{\left\{ \mathcal{X}^T_{ik} \mathcal{Y}^\dagger_{jk} n^-(\Omega_k) + \mathcal{Y}^\dagger_{ik} \mathcal{X}^T_{jk} n^+(\Omega_k) \right\}}_{\equiv \mathcal{B}_{i,j} \text{ see Eq. (A.38)}} \tag{A.56}$$

$$\langle e^{-\mathcal{H}} a^\dagger_i a^\dagger_j \rangle = \mathcal{D}_0 \underbrace{\left\{ \mathcal{Y}^T_{ik} \mathcal{X}^\dagger_{jk} n^-(\Omega_k) + \mathcal{X}^\dagger_{ik} \mathcal{Y}^T_{jk} n^+(\Omega_k) \right\}}_{\equiv \mathcal{C}_{i,j} \text{ see Eq. (A.38)}} \tag{A.57}$$

A.4.2 Two Particle Greens Function

Third, I calculate the two particle Greens function for the a operators.

$$\begin{aligned}
\langle e^{-\mathcal{H}} a_i a_{i'} a^\dagger_j a^\dagger_{j'} \rangle &= \Big\langle e^{-\mathcal{H}} \Big[\mathcal{X}^T_{ik} b_k + \mathcal{Y}^\dagger_{ik} b^\dagger_k \Big] \Big[\mathcal{X}^T_{i'k'} b_{k'} + \mathcal{Y}^\dagger_{i'k'} b^\dagger_{k'} \Big] \\
&\quad \Big[\mathcal{Y}^T_{jp} b_p + \mathcal{X}^\dagger_{jp} b^\dagger_p \Big] \Big[\mathcal{Y}^T_{j'p'} b_{p'} + \mathcal{X}^\dagger_{j'p'} b^\dagger_{p'} \Big] \Big\rangle \\
&= \langle e^{-\mathcal{H}} \{ \mathcal{X}^T_{ik} \mathcal{X}^T_{i'k'} \mathcal{X}^\dagger_{jp} \mathcal{X}^\dagger_{j'p'} b_k b_{k'} b^\dagger_p b^\dagger_{p'} + \mathcal{Y}^\dagger_{ik} \mathcal{Y}^\dagger_{i'k'} \mathcal{Y}^T_{jp} \mathcal{Y}^T_{j'p'} b^\dagger_k b^\dagger_{k'} b_p b_{p'} \\
&\quad + \mathcal{X}^T_{ik} \mathcal{Y}^\dagger_{i'k'} \mathcal{Y}^T_{jp} \mathcal{X}^\dagger_{j'p'} b_k b^\dagger_{k'} b_p b^\dagger_{p'} \\
&\quad + \mathcal{X}^T_{ik} \mathcal{Y}^\dagger_{i'k'} \mathcal{X}^\dagger_{jp} \mathcal{Y}^T_{j'p'} b_k b^\dagger_{k'} b^\dagger_p b_{p'} \\
&\quad + \mathcal{Y}^\dagger_{ik} \mathcal{X}^T_{i'k'} \mathcal{Y}^T_{jp} \mathcal{X}^\dagger_{j'p'} b^\dagger_k b_{k'} b_p b^\dagger_{p'} + \mathcal{Y}^\dagger_{ik} \mathcal{X}^T_{i'k'} \mathcal{X}^\dagger_{jp} \mathcal{Y}^T_{j'p'} b^\dagger_k b_{k'} b^\dagger_p b_{p'} \} \rangle
\end{aligned} \tag{A.58}$$

I need to consider all six different combinations of b operators and evaluate the averages

$$\begin{aligned}
\langle e^{-\mathcal{H}} b_k b_{k'} b^\dagger_p b^\dagger_{p'} \rangle &= \langle e^{-\mathcal{H}} b_k b_{k'} b^\dagger_{k'} b^\dagger_k \rangle \delta_{k,p'} \delta_{k',p} + \langle e^{-\mathcal{H}} b_k b_{k'} b^\dagger_k b^\dagger_{k'} \rangle \delta_{k,p} \delta_{k',p'} \\
&= \langle e^{-\Omega_n b^\dagger_n b_n} b_k \underbrace{b_{k'} b^\dagger_{k'}}_{1-\hat{n}_{k'}} b^\dagger_k \rangle \delta_{k,p'} \delta_{k',p} + \langle e^{-\Omega_n b^\dagger_n b_n} b_k b_{k'} \underbrace{b^\dagger_k b^\dagger_{k'}}_{-b^\dagger_{k'} b^\dagger_k} \rangle \delta_{k,p} \delta_{k',p'} \\
&= \langle e^{-\Omega_n b^\dagger_n b_n} (1 - \hat{n}_{k'})(1 - \hat{n}_k) \rangle \left[\delta_{k,p'} \delta_{k',p} - \delta_{k,p} \delta_{k',p'} \right] \\
&= \underbrace{\prod_{n>0} (1 + e^{-\Omega_n})}_{\mathcal{D}_0} n^-(\Omega_k) n^-(\Omega_{k'}) \left[\delta_{k,p'} \delta_{k',p} - \delta_{k,p} \delta_{k',p'} \right].
\end{aligned} \tag{A.59}$$

Overall, I obtain:

- $$\langle e^{-\mathcal{H}} b_k b_{k'} b_p^\dagger b_{p'}^\dagger \rangle = \mathcal{D}_0 \cdot n^-(\Omega_k) n^-(\Omega_{k'}) \left[\delta_{k,p'} \delta_{k',p} - \delta_{k,p} \delta_{k',p'} \right] \quad \text{(A.60)}$$

- $$\langle e^{-\mathcal{H}} b_k^\dagger b_{k'}^\dagger b_p b_{p'} \rangle = \mathcal{D}_0 \cdot n^+(\Omega_k) n^+(\Omega_{k'}) \left[\delta_{k,p'} \delta_{k',p} - \delta_{k,p} \delta_{k',p'} \right] \quad \text{(A.61)}$$

- $$\langle e^{-\mathcal{H}} b_k b_{k'}^\dagger b_p b_{p'}^\dagger \rangle = \mathcal{D}_0 \cdot n^-(\Omega_k) n^+(\Omega_{k'}) \delta_{k,p'} \delta_{k',p} + \mathcal{D}_0 \cdot n^-(\Omega_k) n^-(\Omega_p) \delta_{k,k'} \delta_{p,p'} \quad \text{(A.62)}$$

- $$\langle e^{-\mathcal{H}} b_k b_{k'}^\dagger b_p^\dagger b_{p'} \rangle = -\mathcal{D}_0 \cdot n^-(\Omega_k) n^+(\Omega_{k'}) \delta_{k,p} \delta_{k',p'} + \mathcal{D}_0 \cdot n^-(\Omega_k) n^+(\Omega_p) \delta_{k,k'} \delta_{p,p'} \quad \text{(A.63)}$$

- $$\langle e^{-\mathcal{H}} b_k^\dagger b_{k'} b_p b_{p'}^\dagger \rangle = -\mathcal{D}_0 \cdot n^+(\Omega_k) n^-(\Omega_{k'}) \delta_{k,p} \delta_{k',p'} + \mathcal{D}_0 \cdot n^+(\Omega_k) n^-(\Omega_p) \delta_{k,k'} \delta_{p,p'} \quad \text{(A.64)}$$

- $$\langle e^{-\mathcal{H}} b_k^\dagger b_{k'} b_p^\dagger b_{p'} \rangle = \mathcal{D}_0 \cdot n^+(\Omega_k) n^-(\Omega_{k'}) \delta_{k',p} \delta_{k,p'} + \mathcal{D}_0 \cdot n^+(\Omega_k) n^+(\Omega_p) \delta_{k,k'} \delta_{p,p'}. \quad \text{(A.65)}$$

I collect all terms

$$\begin{aligned}
\langle e^{-\mathcal{H}} a_i a_{i'} a_j^\dagger a_{j'}^\dagger \rangle = {} & \mathcal{D}_0 \delta_{k,k'} \delta_{p,p'} \{ \mathcal{X}_{ik}^T \mathcal{Y}_{i'k'}^\dagger \mathcal{Y}_{jp}^T \mathcal{X}_{j'p'}^\dagger n^-(\Omega_k) n^-(\Omega_p) \\
& + \mathcal{X}_{ik}^T \mathcal{Y}_{i'k'}^\dagger \mathcal{X}_{jp}^\dagger \mathcal{Y}_{j'p'}^T n^-(\Omega_k) n^+(\Omega_p) + \mathcal{Y}_{ik}^\dagger \mathcal{X}_{i'k'}^T \mathcal{Y}_{jp}^T \mathcal{X}_{j'p'}^\dagger n^+(\Omega_k) n^-(\Omega_p) \\
& + \mathcal{Y}_{ik}^\dagger \mathcal{X}_{i'k'}^T \mathcal{X}_{jp}^\dagger \mathcal{Y}_{j'p'}^T n^+(\Omega_k) n^+(\Omega_p) \} + \\
& - \mathcal{D}_0 \delta_{k,p} \delta_{k',p'} \{ \mathcal{X}_{ik}^T \mathcal{X}_{i'k'}^T \mathcal{X}_{jp}^\dagger \mathcal{X}_{j'p'}^\dagger n^-(\Omega_k) n^-(\Omega_{k'}) \\
& + \mathcal{Y}_{ik}^\dagger \mathcal{Y}_{i'k'}^\dagger \mathcal{Y}_{jp}^T \mathcal{Y}_{j'p'}^T n^+(\Omega_k) n^+(\Omega_{k'}) \\
& + \mathcal{X}_{ik}^T \mathcal{Y}_{i'k'}^\dagger \mathcal{X}_{jp}^\dagger \mathcal{Y}_{j'p'}^T n^-(\Omega_k) n^+(\Omega_{k'}) + \mathcal{Y}_{ik}^\dagger \mathcal{X}_{i'k'}^T \mathcal{Y}_{jp}^T \mathcal{X}_{j'p'}^\dagger n^+(\Omega_k) n^-(\Omega_{k'}) \} \\
& + \mathcal{D}_0 \delta_{k,p'} \delta_{k',p} \{ \mathcal{X}_{ik}^T \mathcal{X}_{i'k'}^T \mathcal{X}_{jp}^\dagger \mathcal{X}_{j'p'}^\dagger n^-(\Omega_k) n^-(\Omega_{k'})
\end{aligned}$$

$$
\begin{aligned}
&+ \mathcal{Y}^{\dagger}_{ik}\mathcal{Y}^{\dagger}_{i'k'}\mathcal{Y}^{T}_{jp}\mathcal{Y}^{T}_{j'p'}n^{+}(\Omega_k)n^{+}(\Omega_{k'}) \\
&+ \mathcal{X}^{T}_{ik}\mathcal{Y}^{\dagger}_{i'k'}\mathcal{Y}^{T}_{jp}\mathcal{X}^{\dagger}_{j'p'}n^{-}(\Omega_k)n^{+}(\Omega_{k'}) \\
&+ \mathcal{Y}^{\dagger}_{ik}\mathcal{X}^{T}_{i'k'}\mathcal{X}^{\dagger}_{jp}\mathcal{Y}^{T}_{j'p'}n^{+}(\Omega_k)n^{-}(\Omega_{k'})\}
\end{aligned} \tag{A.66}
$$

and regroup them

$$
\begin{aligned}
&\langle e^{-\mathcal{H}}a_i a_{i'}a^{\dagger}_j a^{\dagger}_{j'}\rangle \\
&= \mathcal{D}_0 \underbrace{\left[\mathcal{Y}^{T}_{jp}\mathcal{X}^{\dagger}_{j'p}n^{-}(\Omega_p)+\mathcal{X}^{\dagger}_{jp}\mathcal{Y}^{T}_{j'p}n^{+}(\Omega_p)\right]}_{\equiv \mathcal{C}_{j,j'}}\underbrace{\left[\mathcal{X}^{T}_{ik}\mathcal{Y}^{\dagger}_{i'k}n^{-}(\Omega_k)+\mathcal{Y}^{\dagger}_{ik}\mathcal{X}^{T}_{i'k}n^{+}(\Omega_k)\right]}_{\equiv \mathcal{B}_{i,i'}}+ \\
&\quad - \mathcal{D}_0\underbrace{\left[\mathcal{X}^{T}_{i'k'}\mathcal{X}^{\dagger}_{j'k'}n^{-}(\Omega_{k'})+\mathcal{Y}^{\dagger}_{i'k'}\mathcal{Y}^{T}_{j'k'}n^{+}(\Omega_{k'})\right]}_{\equiv \mathcal{A}_{i',j'}}\underbrace{\left[\mathcal{X}^{T}_{ik}\mathcal{X}^{\dagger}_{jk}n^{-}(\Omega_k)+\mathcal{Y}^{\dagger}_{ik}\mathcal{Y}^{T}_{jk}n^{+}(\Omega_k)\right]}_{\equiv \mathcal{A}_{i,j}} \\
&\quad + \mathcal{D}_0\underbrace{\left[\mathcal{X}^{T}_{i'k'}\mathcal{X}^{\dagger}_{jk'}n^{-}(\Omega_{k'})+\mathcal{Y}^{\dagger}_{i'k'}\mathcal{Y}^{T}_{jk'}n^{+}(\Omega_{k'})\right]}_{\equiv \mathcal{A}_{i',j}}\underbrace{\left[\mathcal{X}^{T}_{ik}\mathcal{X}^{\dagger}_{j'k}n^{-}(\Omega_k)+\mathcal{Y}^{\dagger}_{ik}\mathcal{Y}^{T}_{j'k}n^{+}(\Omega_k)\right]}_{\equiv \mathcal{A}_{i,j'}}.
\end{aligned} \tag{A.67}
$$

I obtain

$$
\langle e^{-\mathcal{H}}a_i a_{i'}a^{\dagger}_j a^{\dagger}_{j'}\rangle = \mathcal{D}_0\left[\mathcal{C}_{j,j'}\mathcal{B}_{i,i'} - \mathcal{A}_{i',j'}\mathcal{A}_{i,j} + \mathcal{A}_{i',j}\mathcal{A}_{i,j'}\right] \tag{A.68}
$$

with the previous definition of the matrices $\mathcal{A}$,$\mathcal{B}$, and $\mathcal{C}$ in Eq. (A.31). Finally, the right-hand side can be written as a Pfaffian.

$$
\langle e^{-\mathcal{H}}a_i a_{i'}a^{\dagger}_j a^{\dagger}_{j'}\rangle = \mathcal{D}_0\mathrm{Pf}\begin{bmatrix} 0 & -\mathcal{B}_{i,i'} & \mathcal{A}_{i,j} & \mathcal{A}_{i,j'} \\ \mathcal{B}_{i,i'} & 0 & \mathcal{A}_{i',j} & \mathcal{A}_{i',j'} \\ -\mathcal{A}_{i,j} & -\mathcal{A}_{i',j} & 0 & -\mathcal{C}_{j,j'} \\ -\mathcal{A}_{i,j'} & -\mathcal{A}_{i',j'} & \mathcal{C}_{j,j'} & 0 \end{bmatrix} \tag{A.69}
$$

A.4.3 Arbitrary Greens Function

So far, I have managed to show two things: On the one hand, I fixed the proper regularization of Matsubara sums in Eq. (A.29), which gives indeed the appropriate Fermi functions. On the other hand, I can write higher order Greens functions in terms of a Pfaffian in agreement with the result derived from path integrals. However, I have only shown the latter for the two particle Greens function. To obtain the general result, it would be necessary to generalize the procedure to arbitrary orders. I expect the same result as from path integrals:

$$\langle e^{-\mathcal{H}} a_{i_1} \cdots a_{i_n} a_{j_1}^\dagger \cdots a_{j_n}^\dagger \rangle$$

$$= \mathcal{D}_0 \mathrm{Pf} \underbrace{\begin{bmatrix} 0 & -\mathcal{B}_{i_1,i_2} & \cdots & -\mathcal{B}_{i_1,i_n} & \mathcal{A}_{i_1,j_1} & \mathcal{A}_{i_1,j_2} & \cdots & \mathcal{A}_{i_1,j_n} \\ -\mathcal{B}_{i_2,i_1} & \ddots & & \vdots & \mathcal{A}_{i_2,j_1} & \ddots & & \vdots \\ \vdots & & & \vdots & \vdots & & & \vdots \\ -\mathcal{B}_{i_n,i_1} & \cdots & \cdots & 0 & \mathcal{A}_{i_n,j_1} & \cdots & \cdots & \mathcal{A}_{i_n,j_n} \\ & & & & 0 & -\mathcal{C}_{i_1,i_2} & \cdots & -\mathcal{C}_{i_1,i_n} \\ & \hat{\mathcal{A}}^T & & & -\mathcal{C}_{i_2,i_1} & \ddots & & \vdots \\ & & & & \vdots & & & \vdots \\ & & & & -\mathcal{C}_{i_n,i_1} & \cdots & \cdots & 0 \end{bmatrix}}_{\equiv \hat{S}^{-1} \text{ see Eq. (A.33)}} \tag{A.70}$$

Appendix B
X-Ray Edge and Singular Integral Equations

In this appendix, I show the explicit calculation of the dynamical spin correlation function in terms of matter fermions, $S^{zz}_{A0B0/A0}(t) = i\,[G(t,0) \pm G(0,t)]$, via the X-ray edge approach which enables me to obtain exact results in the thermodynamic limit $N \to \infty$.

B.1 Mapping Without Anomalous Terms

At first sight, it seems that the spin correlation function $S^{zz}_{A0B0}(t) = \langle [f_0(t) + f_0^\dagger(t)][f_0^\dagger(0) - f_0(0)] S(t,0)\rangle$, Eq. (3.36), has contributions both from normal and anomalous bare GF (Abrikosov 2012)

$$G_0(t,t') = -i\langle \mathbb{T} f_0(t) f_0^\dagger(t')\rangle = -i\Big[\Theta(t-t')\langle f_0(t) f_0^\dagger(t')\rangle - \Theta(t'-t)\langle f_0^\dagger(t') f_0(t)\rangle\Big] \tag{B.1}$$

$$F_0(t,t') = -i\langle \mathbb{T} f_0(t) f_0(t')\rangle = -i\Big[\Theta(t-t')\langle f_0(t) f_0(t')\rangle - \Theta(t'-t)\langle f_0(t') f_0(t)\rangle\Big]$$

and analogous for $F_0^* \propto \langle f_0^\dagger f_0^\dagger\rangle$. The averages can be calculated with the time dependence in the Heisenberg picture as $i\dot{a}_{\mathbf{q}} = \big[a_{\mathbf{q}}, H_0\big] = 2|S(\mathbf{q})|a_{\mathbf{q}}$, which leads to $a_{\mathbf{q}}(t) = a_{\mathbf{q}} e^{-it2|S(\mathbf{q})|}$ such that the normal averages are $\langle f_0(t) f_0^\dagger(t')\rangle = \frac{1}{N}\sum_{\mathbf{q}} \cos^2\theta_{\mathbf{q}} e^{-i2|S(\mathbf{q})|(t-t')}$ and $\langle f_0^\dagger(t') f_0(t)\rangle = \frac{1}{N}\sum_{\mathbf{q}} \sin^2\theta_{\mathbf{q}} e^{+i2|S(\mathbf{q})|(t-t')}$. In the following, I need the bare normal GF in frequency space

J. Knolle, *Dynamics of a Quantum Spin Liquid*, Springer Theses,
DOI 10.1007/978-3-319-23953-8

$$G_0(\omega) = \int_{-\infty}^{\infty} dt G_0(t) e^{i\omega t} \tag{B.2}$$

$$G_0(\omega) = \frac{1}{N} \sum_{\mathbf{k}} \left[\frac{\cos(\theta_{\mathbf{k}})^2}{\omega - 2|S(\mathbf{k})| + i\delta} + \frac{\sin(\theta_{\mathbf{k}})^2}{\omega + 2|S(\mathbf{k})| - i\delta} \right].$$

which gives the standard retarded and advanced GF, see, for example, Abrikosov (2012)

$$G_0^{\substack{R \\ A}}(\omega) = \frac{1}{N} \sum_{\mathbf{k}} \left[\frac{\cos(\theta_{\mathbf{k}})^2}{\omega - 2|S(\mathbf{k})| \pm i\delta} + \frac{\sin(\theta_{\mathbf{k}})^2}{\omega + 2|S(\mathbf{k})| \pm i\delta} \right]; \tag{B.3}$$

the former is analytic in the upper and the latter in the lower half plane. From this expression the bare GF can be calculated up to arbitrary precision by adapting the size N of the BZ momentum grid.

A major simplification and one of the reasons why it is possible to compute the correlation function exactly via an X-ray edge analogy is the fact that the anomalous average $\langle f_0(t) f_0(t') \rangle = \frac{-i}{N} \sum_{\mathbf{q}} \sin\theta_{\mathbf{q}} \cos\theta_{\mathbf{q}} e^{-i2|S(\mathbf{q})|(t-t')}$ is always zero. Recall that $\theta_{-\mathbf{q}} = -\theta_{\mathbf{q}}$ and the sum over $\mathbf{q}$ has positive and negative contributions. Then $\cos\theta_{-\mathbf{q}} = \cos\theta_{\mathbf{q}}$ is even, $|S(-\mathbf{q})| = |S(\mathbf{q})|$ is even, but $\sin\theta_{-\mathbf{q}} = -\sin\theta_{\mathbf{q}}$ is odd; thus, the anomalous average is zero.

Moreover, due to the fact that V_z is of the simple local form $f_0^\dagger f_0$ the full anomalous GF is also zero

$$\langle f_0(t) f_0(t') \rangle = 0 \rightarrow \langle f_0(t) f_0(0) \mathbb{T} e^{-i\int_0^t dt' V_z(t')} \rangle = 0 \tag{B.4}$$

which is easily shown by expanding the exponential and applying Wicks theorem (Abrikosov 2012). Therefore, the correlation function is reduced to $S^{zz}_{A0B0/A0}(t) = i[G(t,0) \pm G(0,t)]$, Eq. (3.39). It is mathematically equivalent to an X-ray edge problem but the physics turns out to be quite different because of the vanishing density of states and the fact that it is a quench of Majorana fermions.

B.2 Dyson Equation

I concentrate on calculating the full GFs, Eqs. (3.40), (3.41), exactly by mapping them to an integral equation (Nozieres and DeDominicis 1969). The full GF is split into a product of connected and disconnected contributions $G(t,0) = G_c(t,0)L(t,0)$, analogous for $G(0,t)$, and I expand the time ordered exponential for the connected part

$$G_c(t,t') = -i\left\langle \mathbb{T} f(t)\left[\sum_{n=0}^{\infty}\frac{(i)^n}{n!}(4J_z)^n\int_{t'}^{t}dt_1\ldots\int_{t'}^{t}dt_n f_0^\dagger(t_1)f_0(t_1)\ldots f_0^\dagger(t_n)f_0(t_n)\right]f_0^\dagger(t')\right\rangle_c . \tag{B.5}$$

The sublabel $\langle\ldots\rangle_c$ indicates that in the expansion at a given order n the pairing from Wick's theorem is such that all times $t, t_1, t_2, \ldots, t_n, t'$ are connected. For example, the most obvious is the pairing (t,t_1),(t_1,t_2),$\ldots$,(t_n,t'), but this is not the only one. In general, different pairings can be thought of as a relabeling of the time indices t_i in the expansion which can be done in $n!$ ways at order n. This factor cancels the $\frac{1}{n!}$ of the expansion such that

$$G_c(t,t') = G_0(t,t') + \sum_{n=1}^{\infty}(-4J_z)^n\int_{t'}^{t}dt_1\ldots\int_{t'}^{t}dt_n G_0(t,t_1)G_0(t_1,t_2)\ldots G_0(t_n,t') \tag{B.6}$$

which is an infinite series whose sum gives the Dyson equation

$$G_c(t,t') = G_0(t,t') - 4J_z\int_{t'}^{t}dt_1 G_0(t,t_1)G_c(t_1,t'). \tag{B.7}$$

The diagrammatic form of the Dyson equation is shown in Fig. B.1 panel (a).

The same procedure gives a Dyson equation for the negative time GF, Eq. (3.41),

$$G_c(t',t) = G_0(t',t) - 4J_z\int_{t'}^{t}dt_1 G_0(t_1,t)G_c(t',t_1). \tag{B.8}$$

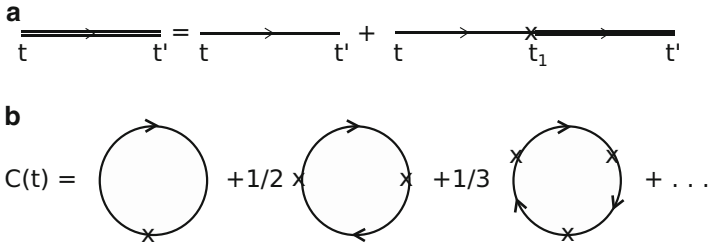

Fig. B.1 The diagrammatic form of the Dyson equation, Eq. (B.7), is shown in the upper panel (**a**). The closed loop contribution $C(t) = \sum_{n=1}^{\infty} C_n(t,0)$, Eq. (B.10), is presented in the lower panel (**b**). The bare GF G_0 is represented by a *single line* and the fully connected GF G_c by a *double line*. The impurity potential $4J_z$ and the intermediate time integral are denoted by a *cross*

B.2.1 Closed Loops

The second contribution to the full GF, see Eq. (3.45), comes from the disconnected parts

$$L(t,t') \equiv \langle \mathbb{T} e^{-i\int_{t'}^{t} dt_1 V(t_1)} \rangle = e^{\sum_{n=1}^{\infty} C_n(t,t')} \tag{B.9}$$

with C_n being the closed loop pairing of the nth order expansion of the exponential. The last equality is known as the Linked Cluster theorem (Abrikosov 2012). Closed loop pairing means that starting at time t_1, the paring goes all the way back to t_1, e.g., at order n the pairs (t_1,t_2),(t_2,t_3),$\ldots(t_n,t_1)$ appear. As before it is possible to account for the multiplicity of the equivalent diagrams by relabeling $(n-1)$ time arguments which gives a factor of $(n-1)!$. Together with the $\frac{1}{n!}$ of the exponential a nonuniversal factor $\frac{1}{n}$ appears in every order. This factor is a general feature of closed loop expansions and equivalently appears in the calculation of the thermodynamic potential (Abrikosov 2012)

$$\sum_{n=1}^{\infty} C_n(t,t') = \quad -\sum_{n=1}^{\infty} \frac{(-4J_z)^n}{n} \int_{t'}^{t} dt_1 \ldots \int_{t'}^{t} dt_n G_0(t_1,t_2) G_0(t_2,t_3) \ldots G_0(t_n,t_1). \tag{B.10}$$

Notice the extra minus sign from the closed loop. In Fig. B.1 panel (b) the diagrammatic form of the expansion is shown.

Of course, I would like to sum this series similar to the Dyson equation, Eq. (B.7), but what about the factor $\frac{1}{n}$? With the identity

$$\frac{(4J_z)^n}{n+1} = \int_0^1 d\lambda (\lambda 4J_z)^n \tag{B.11}$$

it is possible to overcome this problem (Nozieres and DeDominicis 1969) and I obtain for the closed loop contribution

$$L(t,t') = e^{\sum_{n=1}^{\infty} C_n(t,t')} = e^{4J_z \int_{t'}^{t} dt_1 \int_0^1 d\lambda G_c^{\lambda}(t_1,t_1+0^+;t',t)} \tag{B.12}$$

with a new Dyson equation for the λ-dependent connected GF $G_c^{\lambda}(t,t';\tau',\tau)$ which depends on the integration boundaries τ' and τ

$$G_c^{\lambda}(t,t';\tau',\tau) = G_0(t,t') - 4J_z\lambda \int_{\tau'}^{\tau} dt_1 G_0(t,t_1) G_{\text{con}}^{\lambda}(t_1,t';\tau',\tau). \tag{B.13}$$

B.2.2 Discretization in Real Time

The first and obvious way to solve the Dyson equations, Eqs. (B.7) and (B.13), is to treat them numerically in their discretized forms. For example, Eq. (B.7) can be written as

$$G_c(t_j, 0) = G_0(t_j, 0) + \sum_{n=1}^{M} \hat{K}_{t_j,t_n} G_c(t_n, 0) \tag{B.14}$$

with the time interval $[0, t]$ divided into M steps with size $\Delta_t = \frac{t}{M}$ and the matrix $\hat{K}_{t_j,t_n} \equiv -4J_z\Delta_t G_0(t_j, t_n)$. The closed loops are calculated as $\sum_{n=1}^{\infty} C_n(t, t') = -\mathrm{Tr}\sum_{n=1}^{\infty} \frac{1}{n}\left(\hat{K}\right)^n = \mathrm{Tr}\log\left(1-\hat{K}\right)$. Finally, I use the identity $\mathrm{Tr}\log = \log\det$ to obtain an expression which can be evaluated numerically instead of the additional λ-integral, Eq. (B.12),

$$L(t, t') \equiv \langle \mathbb{T} e^{-i\int_{t'}^{t} dt_1 V(t_1)} \rangle = \det\left(1-\hat{K}\right). \tag{B.15}$$

I tried to take advantage of the fact that $\hat{K} \propto \hat{G}_0 = G_0(t_j, t_i) = G_0(t_j - t_i)$ with t_j and t_i in the interval $[0, t]$ is a Toeplitz matrix, but a complication appears: For time arguments $(t_j - t_i)$ larger or smaller than 0 the bare GF $G_0(t_j - t_i)$ is smooth and depends only on the difference of the time arguments but at $t = 0$ a discontinuous step appears (because at $t = 0$ the Θ-functions in Eq. (B.1) switch). Thus the kernel of the integral equation is not smooth which spoils the convergence properties of a numerical treatment significantly (Press et al. 2007). The singularity also prevents the efficient use of asymptotic formulas of large Toeplitz matrix series (Gutman et al. 2011).

B.3 Dyson Equation in Frequency Representation-Muskhelishvili Method

A different way to solve the Dyson equation and to calculate the closed loop contributions is based on the idea to reduce a singular integral equation to a non-singular integral equation with the same solutions and with much better convergence properties (Muskhelishvili 1953). I elaborate a formalism which was first introduced in Grebennikov et al. (1977) for the X-ray edge problem. The authors investigated whether the exact result for the edge singularity (Nozieres and DeDominicis 1969), which crucially relies on the specific form $G_0(t) \propto \frac{i\rho_0}{t}$ of the long time asymptotic of the bare GF, is sufficient to describe the full X-ray photoelectron spectra. Their main conclusion is that for special fillings and for singularities in the density of states the behavior is not only governed by the low energy (or long time) asymptotic form of the bare GF.

I illustrate the treatment of the integral equation by looking at the Dyson equation for the positive time connected GF, Eq. (B.7), which I rewrite in a slightly modified form as

$$G_c(\tau, t) = G_0(\tau) - u \int_0^t d\tau_1 G_0(\tau - \tau_1) G_c(\tau_1, t) \tag{B.16}$$

with the interaction constant $u = 4J_z$ and the connected GF $G_c(\tau, t)$ which depends explicitly on the time argument τ and the upper integration boundary t. Instead of the λ-integral, Eq. (B.13), the closed loop contribution can also be calculated via

$$\sum_{n=1}^{\infty} C_n(t, 0) = u \int_0^t dt_1 G_c(\tau = 0^-, t_1). \tag{B.17}$$

Once the connected GF $G_c(\tau, t)$ is known, I am able to calculate the full GF, and thus, the full dynamical correlation function.

I Fourier transform the first time argument $G_c(\omega, t) = \int_{-\infty}^{\infty} d\tau e^{i\omega\tau} G_c(\tau, t)$ and the bare GF $G_0(\omega) = \int_{-\infty}^{\infty} d\tau e^{i\omega\tau} G_0(\tau)$ such that the Dyson equation, Eq. (B.16), is

$$G_c(\omega, t) = G_0(\omega) - u G_0(\omega) \int_{-\infty}^{\infty} \frac{d\omega_1}{2\pi i} \frac{e^{i(\omega-\omega_1)t} - 1}{\omega - \omega_1} G_c(\omega_1, t). \tag{B.18}$$

Next, I introduce the renormalized function

$$\tilde{G}_c(\omega, t) = \frac{G_c(\omega, t)}{G_0(\omega)} \tag{B.19}$$

and the Dyson equation becomes

$$\tilde{G}_c(\omega, t) = 1 - u \int_{-\infty}^{\infty} \frac{d\omega_1}{2\pi i} \frac{e^{i(\omega-\omega_1)t} - 1}{\omega - \omega_1} G_c(\omega_1, t). \tag{B.20}$$

By showing that the function defined by the closed loop integral around the upper half plane $\oint \frac{\tilde{G}_c(\omega, t)}{\omega - \omega'} = 0$, it is proven that $\tilde{G}_c(\omega, t)$ is analytic in the upper half plane. Similarly, $e^{-i\omega t}\tilde{G}_c(\omega, t)$ turns out to be analytic in the lower half plane. Then, I use analytic properties of the bare GF (Abrikosov 2012), which I separate into advanced and retarded components G_0^A and G_0^R, to split the integration into two parts. (Note that the chemical potential $\mu = 0$ in my case in contrast to Grebennikov et al. (1977).)

$$\begin{aligned} \tilde{G}_c(\omega, t) = 1 &- u \int_{-\infty}^{0} \frac{d\omega_1}{2\pi i} \frac{e^{i(\omega-\omega_1)t} - 1}{\omega - \omega_1} \tilde{G}_c(\omega_1, t) G_0^A(\omega_1) \\ &- u \int_{0}^{\infty} \frac{d\omega_1}{2\pi i} \frac{e^{i(\omega-\omega_1)t} - 1}{\omega - \omega_1} \tilde{G}_c(\omega_1, t) G_0^R(\omega_1) \end{aligned} \tag{B.21}$$

Finally, I use the standard relations $\mathrm{Re}G_0^A = \mathrm{Re}G_0^R$ and $\mathrm{Im}G_0^A = -\mathrm{Im}G_0^R$ to connect the retarded and advanced GF $G_0^R = G_0^A - 2i\mathrm{Im}G_0^A$ in order to obtain a singular integral equation (SIE) with a Cauchy type kernel

$$\begin{aligned}[1 + u\mathrm{Re}G_0(\omega)]\,\tilde{G}_c(\omega,t) + \frac{1}{i\pi}\int_{-\infty}^{\infty} d\omega_1 \frac{\tilde{G}_c(\omega_1,t)}{\omega_1-\omega} iu\mathrm{Im}G_0^A(\omega_1) \\ \times\left[e^{i(\omega-\omega_1)t} + \left(1-e^{i(\omega-\omega_1)t}\right)\Theta(-\omega_1)\right] = 1.\end{aligned} \tag{B.22}$$

In this equation only the first term of the sum under the integral is singular.

So far I succeeded in doing two things: First, the range of integration is finite since the density of state $\mathrm{Im}G_0^A$ has only finite support. Second, I have brought the present SIE into a form, such that I can remove the Cauchy type singularity via the technique of Muskhelishvili (1953).

In the most general form, a standard SIE for the function $\tilde{G}_c(\omega,t)$ can be written as

$$\begin{aligned} f &= \hat{K}_2\tilde{G}_c \\ f(\omega) &= A_2(\omega)\tilde{G}_c(\omega,t) + \frac{1}{i\pi}\int_L \frac{K_2(\omega,\omega_1)\tilde{G}_c(\omega_1,t)}{\omega_1-\omega}d\omega_1 \\ f(\omega) &= A_2(\omega)\tilde{G}_c(\omega,t) + \frac{B_2(\omega)}{i\pi}\int_L \frac{\tilde{G}_c(\omega_1,t)}{\omega_1-\omega}d\omega_1 + \frac{1}{i\pi}\int_L \frac{k(\omega,\omega_1)\tilde{G}_c(\omega_1,t)}{\omega_1-\omega}d\omega_1 \end{aligned} \tag{B.23}$$

with $B_2(\omega) = K_2(\omega,\omega)$ and $k(\omega,\omega_1) = K_2(\omega,\omega_1) - K_2(\omega,\omega)$. In the last line, I have separated out the singular term $\propto B_2(\omega)$.

Comparing my SIE, Eq. (B.22), with the general form, Eq. (B.23), I can read off

$$A_2(\omega) = [1 + u\mathrm{Re}G_0(\omega)] \tag{B.24}$$

$$K_2(\omega,\omega_1) = iu\mathrm{Im}G_0^A(\omega_1)\left[e^{i(\omega-\omega_1)t} + \left(1-e^{i(\omega-\omega_1)t}\right)\Theta(-\omega_1)\right] \tag{B.25}$$

$$B_2(\omega) = iu\mathrm{Im}G_0^A(\omega) \tag{B.26}$$

$$f(\omega) = 1. \tag{B.27}$$

Now, the central idea is to find a new integral operator $\hat{K}_1$ that reduces $\hat{K}_2$ such that the new integral equation

$$\hat{K}_1 f = \hat{K}_1\hat{K}_2\tilde{G}_c \tag{B.28}$$

is non-singular and has the same solutions as the SIE $f = \hat{K}_2\tilde{G}_c$. The key question is how to find such an operator $\hat{K}_1$?

With the help of the Poincare-Betrand formula for principal values (Nozieres and DeDominicis 1969)

$$\mathrm{P}\frac{1}{\omega_1-\omega}\mathrm{P}\frac{1}{\omega_1-\omega_2}=\mathrm{P}\frac{1}{\omega_2-\omega}\left[\mathrm{P}\frac{1}{\omega_1-\omega_2}-\mathrm{P}\frac{1}{\omega_1-\omega}\right]+\pi^2\delta(\omega_1-\omega)\delta(\omega_1-\omega_2) \tag{B.29}$$

I write the reduced integral equation, Eq. (B.28), as

$$\begin{aligned}\hat{K}_1\cdot 1 &= [A_1(\omega)A_2(\omega)+B_1(\omega)B_2(\omega)]\,\tilde{G}_c(\omega,t)+[A_1(\omega)B_2(\omega)+B_1(\omega)A_2(\omega)]\\ &\times\frac{1}{i\pi}\int_L\frac{\tilde{G}_c(\omega_1,t)}{\omega_1-\omega}d\omega_1+\frac{1}{i\pi}\int_L d\omega_1\frac{\tilde{G}_c(\omega_1,t)}{\omega_1-\omega}\\ &\times\{A_1(\omega)\,[K_2(\omega,\omega_1)-K_2(\omega,\omega)]+[A_2(\omega_1)K_1(\omega,\omega_1)-A_2(\omega)K_1(\omega,\omega)]\}\\ &+\frac{1}{\pi^2}\int_L d\omega_2\frac{\tilde{G}_c(\omega_2,t)}{\omega_2-\omega}\int_L d\omega_1 K_1(\omega,\omega_1)K_2(\omega_1,\omega_2)\left[\frac{1}{\omega_1-\omega_2}-\frac{1}{\omega_1-\omega}\right].\end{aligned} \tag{B.30}$$

To remove the singular part and to simplify the equation I impose the two conditions

$$\begin{aligned}1 &= A_1A_2+B_1B_2\\ 0 &= A_1B_2+B_1A_2\end{aligned} \tag{B.31}$$

which partly determine the reduction operator $\hat{K}_1$

$$B_1(\omega)=-ui\mathrm{Im}\tilde{G}^A(\omega) \tag{B.32}$$

$$A_1(\omega)=1-u\mathrm{Re}\tilde{G}^A(\omega) \tag{B.33}$$

$$\text{with}\ \ \tilde{G}^A(\omega)=\frac{G_0^A(\omega)}{1+uG_0^A(\omega)}. \tag{B.34}$$

However, I am still left with infinitely many choices for the kernel $K_1(\omega,\omega_1)$ but a good choice motivated by the physics turns out to be

$$K_1(\omega,\omega_1)=B_1(\omega_1)e^{i(\omega-\omega_1)t}=-ui\mathrm{Im}\tilde{G}^A(\omega_1)e^{i(\omega-\omega_1)t} \tag{B.35}$$

because it incorporates some of the long time behavior via the renormalized GF $\tilde{G}^A(\omega)=\frac{G_0^A(\omega)}{1+uG_0^A(\omega)}$, compare to Eq. (3.52). With the help of the Kramers–Kronig relation for the advanced GF which is analytic in the lower half plane

$$\mathrm{Re}\tilde{G}^A(\omega)=-\frac{1}{\pi}\int_{-\infty}^{\infty}d\omega_1\frac{\mathrm{Im}\tilde{G}^A(\omega_1)}{\omega_1-\omega} \tag{B.36}$$

and the identity $(1 - u\mathrm{Re}\tilde{G}^A) = \frac{\mathrm{Im}\tilde{G}^A(1+u\mathrm{Re}G_0^A)}{\mathrm{Im}G_0^A}$ I obtain after some algebra a non-singular integral equation. The final non-SIE is

$$\tilde{G}_c(\omega,t) = \mathbf{I}(\omega,t) + \frac{u}{\pi}\int_{-\infty}^{0} d\omega_1 \mathrm{Im}G_0^A(\omega_1)\mathbf{L}(\omega,\omega_1,t)\tilde{G}_c(\omega_1,t) \tag{B.37}$$

$$\text{with } \mathbf{I}(\omega,t) = 1 + \frac{u}{\pi}\int_{-\infty}^{\infty} d\omega_1 \mathrm{Im}\tilde{G}^A(\omega_1)\frac{e^{i(\omega-\omega_1)t}-1}{\omega-\omega_1} \tag{B.38}$$

$$\text{and } \mathbf{L}(\omega,\omega_1,t) = \frac{\mathbf{I}(\omega,t) - e^{i(\omega-\omega_1)t}\mathbf{I}(\omega_1,t)}{\omega-\omega_1}. \tag{B.39}$$

The equation is basically determined by $\hat{K}_1$ acting on $f = 1$ and acting on the non-singular term proportional to the Θ-function in $K_2(\omega,\omega_1)$, see Eq. (B.22). The rest cancels to zero.

This non-SIE, Eq. (B.37), can be solved numerically by discretizing the integration range. The integration interval is finite and the convergence is much better than in the real time formulation. The equation gives $\tilde{G}_c(\omega,t)$ which allows to calculate the desired full GF $G(t,0) = G_c(t,0)L(t,0)$ via

$$G_c(t,0) = G_c(t,t) = \frac{1}{i\pi}\int_0^{\infty} d\omega \mathrm{Im}G_0^A(\omega)\tilde{G}_c(\omega,t)e^{-i\omega t} \tag{B.40}$$

$$L(t,0) = e^{\sum_{i=1}^{\infty} C_i(t,0)} = e^{u\int_0^t dt_1 G_c(0^-,t_1)} = e^{-\frac{u}{i\pi}\int_0^t dt_1 \int_{-\infty}^0 d\omega \mathrm{Im}G_0^A(\omega)\tilde{G}_c(\omega,t_1)}.$$

B.3.1 Negative Time Greens Function

For negative times I carry out the same steps and rewrite the Dyson equation, Eq. (B.8), similar to Eq. (B.16) as

$$G_c^{\mathrm{neg}}(\tau,t) = G_0(-\tau) - u\int_0^t d\tau_1 G_0(-\tau+\tau_1)G_c^{\mathrm{neg}}(\tau_1,t). \tag{B.41}$$

I obtain

$$\tilde{G}_c^{\mathrm{neg}}(\omega,t) = \mathbf{I}^{\mathrm{neg}}(\omega,t) + \frac{u}{\pi}\int_0^{\infty} d\omega_1 \mathrm{Im}G_0^A(\omega_1)\mathbf{L}^{\mathrm{neg}}(\omega,\omega_1,t)\tilde{G}_c^{\mathrm{neg}}(\omega_1,t) \tag{B.42}$$

$$\text{with } \mathbf{I}^{\mathrm{neg}}(\omega,t) = 1 + \frac{u}{\pi}\int_{-\infty}^{\infty} d\omega_1 \mathrm{Im}\tilde{G}^A(\omega_1)\frac{e^{-i(\omega-\omega_1)t}-1}{\omega-\omega_1} \tag{B.43}$$

$$\text{and } \mathbf{L}^{\text{neg}}(\omega,\omega_1,t) = \frac{\mathbf{I}^{\text{neg}}(\omega,t) - e^{-i(\omega-\omega_1)t}\mathbf{I}^{\text{neg}}(\omega_1,t)}{\omega-\omega_1}. \tag{B.44}$$

Finally, I calculate the full GF $G(0,t) = G_c(0,t)L(t,0)$ via

$$G_c(0,t) = G_c^{\text{neg}}(t,t) = -\frac{1}{i\pi}\int_{-\infty}^{0} d\omega \text{Im}G_0^A(\omega)\tilde{G}_c^{\text{neg}}(\omega,t)e^{i\omega t} \tag{B.45}$$

with the same loops $L(t,0)$ as for positive times.

B.3.2 Real Time Results, Decaying GF and Finite Loops

In Fig. B.2, I show the real time behavior of the positive and negative time connected GF $G_c(t,0), G_c(0,t)$ and the loop contribution $L(t,0)$ as calculated by the X-ray edge method outlined above at the isotropic point ($J_x = J_y = J_z = 1$). The GFs decay exponentially at short times, see logarithmic inset, but surprisingly the loop contribution also seems to decay in contradiction to the absence of the Anderson orthogonality catastrophe. However, this decay is a numerical artifact of Eq. (B.17). It numerically calculates the sum of all linked clusters $C(t,0)$ and the finite frequency grid necessarily introduces a cut-off which is quickly amplified in

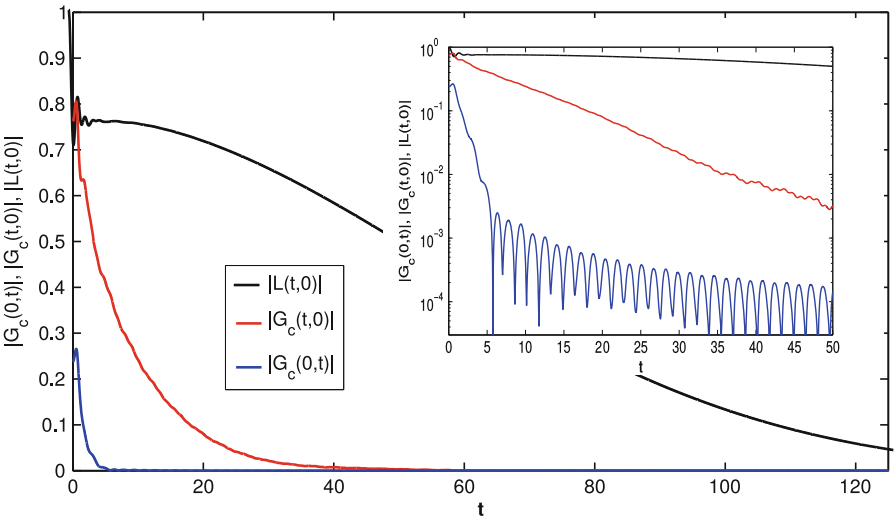

Fig. B.2 For the isotropic point the real time decay of the full positive time GF $G_c(t,0)$ and negative time GF $G_c(0,t)$ are shown together with the time dependent overlap (or closed loop contribution) $L(t,0)$ as calculated by the Muskhelishvili method (*inset*: logarithmic scale). Note the decay of the loop contribution is a numerical artifact, see text for discussion

the exponent $L(t,0) = e^{C(t,0)}$. This disadvantage of Eq. (B.17) was already noted in the original paper of Nozieres and DeDominicis (1969) see footnote 17 on page 1104. It is better to use Eq. (B.12) with the λ-integral.

Instead of doing this, I take advantage of the complimentary Pfaffian calculation and combine the two exact methods. In the Pfaffian approach the second contribution to the matrix element in Eq. (3.35) is precisely the loop contribution. For calculating $|L(t,0)|$, the overall sign does not matter and I can calculate the determinant instead of the Pfaffian such that much larger system sizes up to 5000 sites can be easily obtained.

In Fig. B.3, I show the loop contribution $|L(t,0)|$ as calculated from the X-ray edge approach (red) and from various system sizes of the Pfaffian approach together with the exact $N \to \infty$ value of the overlap, $|\langle M_0|M_F\rangle| = 0.7693$, as obtained from finite size scaling. For the full dynamical correlation functions, I calculate the loops via Pfaffians until they are converged with the $t \to \infty$ value of the overlap. Note that for small times both approaches agree as expected.

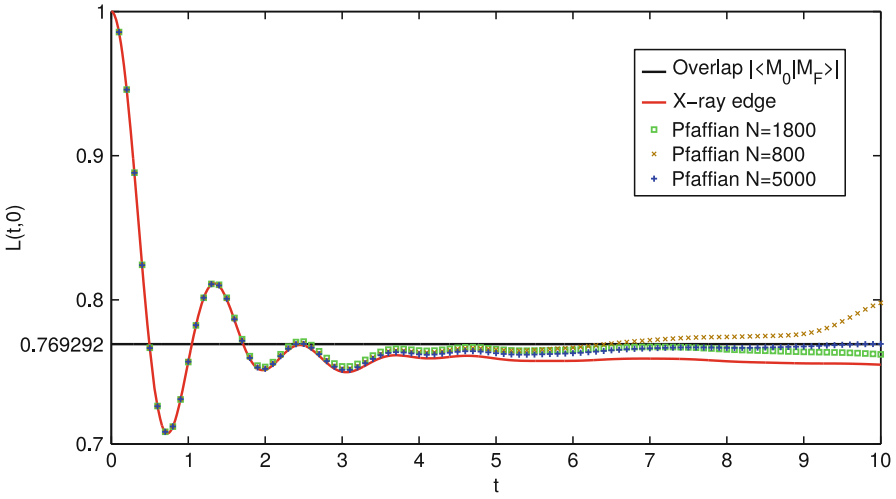

Fig. B.3 The time dependent overlap or closed loop contribution $L(t,0) = \langle e^{iH_0 t} e^{-it(H_0+V_z)}\rangle = \langle \mathbb{T} e^{-i\int_0^t dt' V_z(t')}\rangle$ is shown as calculated from the Muskhelishvili method (*red*), Eq. (B.40), and from the Pfaffian approach for various finite size systems. For $N = 5000$ unit cells the Pfaffian calculation of the time dependent overlap is well converged to the $N \to \infty$ value of the ground state overlap $|\langle M_0|M_F\rangle|$, which I have calculated from finite size scaling. For large times revivals due to the periodic boundary conditions appear for small system sizes

Appendix C
Exact Diagonalization of Four Dimers

To test some of my findings, I diagonalize the original spin model for eight spins or four dimers, see Fig. C.1. As expected, only N.N. spin correlations are nonzero. The bond direction dictates which of the correlation function is nonzero and I obtain $\langle S_z^z(0)S_8^z(0)\rangle = 0.57735$ for the equal time N.N. spin correlator at the isotropic point $J_x = J_y = J_z = 1$, which is close to the exact value 0.52487 of the infinite size system.

From exact diagonalization in the strong dimer limit, e.g. $J_x, J_y \ll J_z$, (gapped QSL phase) I always observe small amplitude oscillations with a frequency $\omega = 4J_z + \Delta$ for the zz-correlator. The weak bond xx- or yy-correlators oscillate with large amplitudes around the frequency $\omega = 2J_z$. These results are in agreement with the strong dimer limits of the other calculations via Pfaffians or the X-ray edge, compare to Fig. 4.6 in the results Chap. 4. As a concrete example, for $J_z = 1, j = J_x = J_y = 0.15$ I show in Fig. C.2 the real time behavior of the strong bond correlator $S_{18}^{zz}(t)$ (black) and the weak bond correlator $S_{12}^{xx}(t)$ (red) in the left panel. The main frequencies can be read of from the Fourier transform in the right panel. $S_{18}^{zz}(\omega)$ (blue) has a large amplitude at the flux gap energy $\Delta = 0.045$ and a tiny oscillation at $\omega = 4J_z + \Delta$ (see arrow). The weak $S_{12}^{xx}(\omega)$ (red) shows oscillations around $\omega = 2J_z$ all in agreement with Fig. 4.6.

In the gapped phase, the presence of a finite length-scale set by the inverse fermion gap allows the development of a heuristic based on an even smaller cluster of spins which can be adduced to account for some of the main features. I find that even considering the properties of a single plaquette of 4 spins with alternating interactions J_z, J_x (and $j = J_x/J_z \ll 1$), I can account for the main oscillation frequencies and for the amplitude scaling with j found in the $N \to \infty$ strong dimer limit. Up to order j^2 the strong bond correlator is $S_{A0B0}^{zz}(t) = e^{-itj^2} - \frac{j^2}{4}e^{-it(4J_z+j^2}$, while the weak one behaves as $S_{A0A1}^{xx}(t) = \frac{1}{4}\sin(2tJ_z)\sin(2tJ_zj) + \frac{j}{4}\cos(2tJ_z)\cos(2tJ_zj)$. Observe that the main oscillation with tiny amplitude $O(j^2)$ of the strong bond is at a frequency $4J_z$ outside of the single particle bandwidth which is an almost flat band around $2J_z$ (after fermionization in the thermodynamic limit). In agreement with this

J. Knolle, *Dynamics of a Quantum Spin Liquid*, Springer Theses,
DOI 10.1007/978-3-319-23953-8

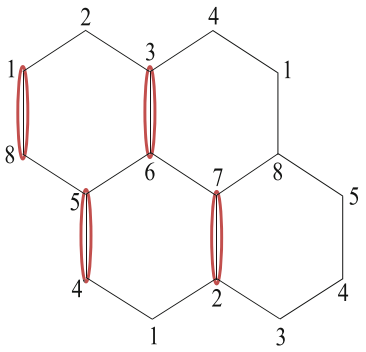

Fig. C.1 The four dimer or 8 spin problem with periodic boundary conditions. I checked our main findings on this small cluster by doing exact diagonalization of the original spin system

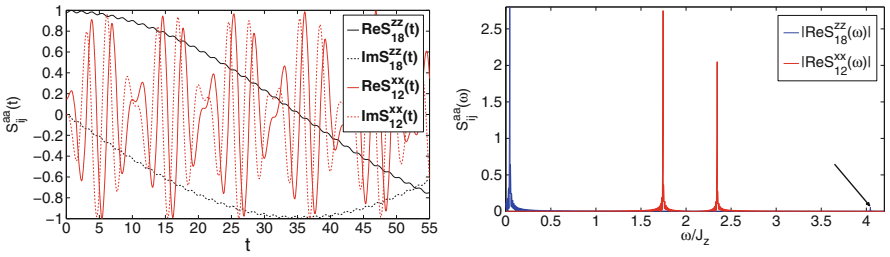

Fig. C.2 Exact diagonalization results are presented for four dimers and $J_z = 1, j = J_x = J_y = 0.15$. The real time behavior of the strong bond correlator $S^{zz}_{18}(t)$ (*black*) and the weak bond correlator $S^{xx}_{12}(t)$ (*red*) is shown in the *left panel*. The main frequencies can be read of from the Fourier transformation in the *right panel*. The strong bond correlator $S^{zz}_{18}(\omega)$ (*blue*) has a large amplitude at the flux gap energy $\Delta = 0.045$ and a tiny oscillation at $\omega = 4J_z + \Delta$ (see *arrow*). The weak $S^{xx}_{12}(\omega)$ (*red*) has oscillations around $\omega = 2J_z$. Compare to the exact structure factor in the $N \to \infty$ limit Fig. 4.6

toy model, sizable contribution to the structure factor comes from the weak bonds $S^{xx/yy}$ around the frequency $2J_z$, whereas the $4J_z$ oscillations due to multi-particle processes of the strong S^{zz} bond are orders of magnitude smaller.

Appendix D
Calculation of Matrix Elements

In this Appendix, I show details of the calculation for the matrix elements encountered in Sect. 3.2.

First, I concentrate on $\langle M_F^{x,y}|c_{A0}c_{B0}|M_0\rangle$ encountered in the zero particle response Eq. (3.22). In terms of matter fermions, Eq. (2.10), and with the ground state relation Eq. (2.26) I obtain

$$\langle M_F^{x,y}|c_{A0}c_{B0}|M_0\rangle = -i\det\left(\mathcal{X}^\dagger\mathcal{X}\right)^{\frac{1}{4}}\langle M_0|e^{\frac{1}{2}\mathcal{F}_{ji}^* a_j a_i}\left(2f_0^\dagger f_0 - 1\right)|M_0\rangle. \tag{D.1}$$

I express the matter fermions in terms of the Bogoliubov operators which diagonalize the flux free system $f_0 = \sum_{\mathbf{q}}\left[\cos\theta_{\mathbf{q}}a_{\mathbf{q}} + i\sin\theta_{\mathbf{q}}a_{-\mathbf{q}}^\dagger\right]$ and expand the exponential. With $\langle M_0|a_j a_i a_k^\dagger a_{-q}^\dagger|M_0\rangle = \delta_{j,-q}\delta_{i,k} - \delta_{i,-q}\delta_{j,k}$ and the property $\mathcal{F}_{ji} = -\mathcal{F}_{ij}$ (Blaizot and Ripka 1986) I obtain

$$\langle M_F^{x,y}|c_{A0}c_{B0}|M_0\rangle = i\det\left(\mathcal{X}^\dagger\mathcal{X}\right)^{\frac{1}{4}}\left[1 - \frac{2}{N}\sum_{\mathbf{k}}\sin^2\theta_{\mathbf{k}} + \frac{2i}{N}\sum_{\mathbf{q},\mathbf{k}}\cos\theta_{\mathbf{k}}\mathcal{F}_{\mathbf{k},\mathbf{q}}^*\sin\theta_{\mathbf{q}}\right] \tag{D.2}$$

which gives the real space and real time spin correlation functions

$$S_{A0B0,(0)}^{zz}(t) = \det\left(\mathcal{X}^\dagger\mathcal{X}\right)^{\frac{1}{2}}e^{it(E_0-E_0^F)}\left[1 - \frac{2}{N}\sum_{\mathbf{k}}\sin^2\theta_{\mathbf{k}} + \frac{2i}{N}\sum_{\mathbf{q},\mathbf{k}}\cos\theta_{\mathbf{k}}\mathcal{F}_{\mathbf{k},\mathbf{q}}^*\sin\theta_{\mathbf{q}}\right] \tag{D.3}$$

$$S_{A0A0,(0)}^{zz}(t) = \det\left(\mathcal{X}^\dagger\mathcal{X}\right)^{\frac{1}{2}}e^{it(E_0-E_0^F)} \tag{D.4}$$

$$S_{B0B0,(0)}^{zz}(t) = \det\left(\mathcal{X}^\dagger\mathcal{X}\right)^{\frac{1}{2}}e^{it(E_0-E_0^F)} \tag{D.5}$$

J. Knolle, *Dynamics of a Quantum Spin Liquid*, Springer Theses,
DOI 10.1007/978-3-319-23953-8

$$S^{zz}_{B0A0,(0)}(t) = \det\left(\mathcal{X}^\dagger\mathcal{X}\right)^{\frac{1}{2}} e^{it\left(E_0-E_0^F\right)}\left[1-\frac{2}{N}\sum_{\mathbf{k}}\sin^2\theta_{\mathbf{k}} - \frac{2i}{N}\sum_{\mathbf{q},\mathbf{k}}\cos\theta_{\mathbf{k}}\mathcal{F}_{\mathbf{k},\mathbf{q}}\sin\theta_{\mathbf{q}}\right]. \tag{D.6}$$

Next, I concentrate on the matrix element

$$\langle M_0|c_{A0}|\lambda\rangle = \langle M_0|c_{A0}b^\dagger_\lambda|M_F\rangle \tag{D.7}$$

which can be written in terms of a_i operators diagonalizing the flux free system, Eq. (2.24), as

$$\langle M_F|c_{A0}|\lambda\rangle = \frac{1}{\sqrt{N}}\det\left(\mathcal{X}^\dagger\mathcal{X}\right)^{\frac{1}{4}}\sum_{\mathbf{q}} e^{i\theta_{\mathbf{q}}}\left\langle M_0|a_{\mathbf{q}}\left[\mathcal{Y}_{\lambda,l}a_l + \mathcal{X}_{\lambda,l}a^\dagger_l\right]\left[1-\frac{1}{2}\mathcal{F}_{ij}a^\dagger_i a^\dagger_j\right]|M_0\right\rangle \tag{D.8}$$

(summation of double indices). After letting the operators a_i act on their ground state $|M_0\rangle$ I obtain

$$\langle M_F|c_{A0}|\lambda\rangle = \frac{1}{\sqrt{N}}\det\left(\mathcal{X}^\dagger\mathcal{X}\right)^{\frac{1}{4}}\sum_{\mathbf{q}} e^{i\theta_q}\left[\mathcal{X}_{\lambda,q} - \mathcal{Y}_{\lambda,l}\mathcal{F}_{l,q}\right] \tag{D.9}$$

which can be further simplified with the relation (Blaizot and Ripka 1986)

$$\mathcal{X}_{\lambda,q} - \mathcal{Y}_{\lambda,l}\mathcal{F}_{l,q} = \left[\mathcal{X}^\dagger\right]^{-1}_{\lambda q} \tag{D.10}$$

to

$$\langle M_F|c_{A0}|\lambda\rangle = \frac{1}{\sqrt{N}}\det\left(\mathcal{X}^\dagger\mathcal{X}\right)^{\frac{1}{4}}\sum_{\mathbf{q}} e^{i\theta_q}\left[\mathcal{X}^\dagger\right]^{-1}_{\lambda q}. \tag{D.11}$$

Similarly, I obtain

$$\langle M_F|c_{B0}|\lambda\rangle = -\frac{i}{\sqrt{N}}\det\left(\mathcal{X}^\dagger\mathcal{X}\right)^{\frac{1}{4}}\sum_{\mathbf{q}} e^{-i\theta_q}\left[\mathcal{X}^\dagger\right]^{-1}_{\lambda q}. \tag{D.12}$$

Overall, I calculate for the single-particle contribution to the real space and real time correlation functions

$$S^{zz}_{A0B0,(1)}(t) = \det\left(\mathcal{X}^\dagger\mathcal{X}\right)^{\frac{1}{2}}\sum_{\lambda} e^{it\left(E_0-E^F_\lambda\right)}\frac{1}{N}\sum_{k,q} e^{i(\theta_q+\theta_k)}\left[\mathcal{X}^\dagger\right]^{-1}_{\lambda,q}\left[\mathcal{X}\right]^{-1}_{k,\lambda} \tag{D.13}$$

$$S^{zz}_{A0A0,(1)}(t) = \det\left(\mathcal{X}^\dagger\mathcal{X}\right)^{\frac{1}{2}} \sum_\lambda e^{it\left(E_0 - E^F_\lambda\right)} \frac{1}{N} \sum_{k,q} e^{i(\theta_q - \theta_k)} \left[\mathcal{X}^\dagger\right]^{-1}_{\lambda,q} [\mathcal{X}]^{-1}_{k,\lambda} \tag{D.14}$$

$$S^{zz}_{B0B0,(1)}(t) = \det\left(\mathcal{X}^\dagger\mathcal{X}\right)^{\frac{1}{2}} \sum_\lambda e^{it\left(E_0 - E^F_\lambda\right)} \frac{1}{N} \sum_{k,q} e^{-i(\theta_q - \theta_k)} \left[\mathcal{X}^\dagger\right]^{-1}_{\lambda,q} [\mathcal{X}]^{-1}_{k,\lambda} \tag{D.15}$$

$$S^{zz}_{B0A0,(1)}(t) = \det\left(\mathcal{X}^\dagger\mathcal{X}\right)^{\frac{1}{2}} \sum_\lambda e^{it\left(E_0 - E^F_\lambda\right)} \frac{1}{N} \sum_{k,q} e^{-i(\theta_q + \theta_k)} \left[\mathcal{X}^\dagger\right]^{-1}_{\lambda,q} [\mathcal{X}]^{-1}_{k,\lambda}\,. \tag{D.16}$$

Note that $M = \left[\mathcal{X}^\dagger\right]^{-1}\mathcal{X}^{-1}$ has only positive real entries and is symmetric $M = M^T = M^\dagger$.

All matrix elements for the non-Abelian phase, see Chap. 5, are calculated in a similar way. The only difference is that I work in real space such that $f_0 = X^T_{0j}a_j + Y^\dagger_{0j}a^\dagger_j$ instead of the expression in momentum space.

The matrix elements for the two particle contributions, Eq. (6.32), are calculated in a similar fashion as

$$G^{[2]}_{\lambda\lambda'} = \langle M_0|b^\dagger_\lambda b^\dagger_{\lambda'}|M_F\rangle = \det\left(\mathcal{X}^\dagger\mathcal{X}\right)^{\frac{1}{4}} \left\{\mathcal{Y}_{\lambda l}\mathcal{X}^T_{l\lambda'} + \mathcal{Y}_{\lambda l}\mathcal{F}_{lk}\mathcal{Y}^T_{k\lambda'}\right\} \tag{D.17}$$

and

$$\begin{aligned}
G^{[4]}_{\lambda\lambda'} &= \langle M_0|c_{B0}c_{A0}b^\dagger_\lambda b^\dagger_{\lambda'}|M_F\rangle = -iG^{[2]}_{\lambda\lambda'} + g^{[4]}_{\lambda\lambda'} + \tilde{g}^{[4]}_{\lambda\lambda'} \quad \text{with} \qquad (D.18)\\
g^{[4]}_{\lambda\lambda'} &= 2i\det\left(\mathcal{X}^\dagger\mathcal{X}\right)^{\frac{1}{4}} \left\{\mathcal{X}_{\lambda i}X_{i0}\mathcal{X}_{\lambda' j}Y_{j0} - \mathcal{X}_{\lambda i}Y_{i0}\mathcal{X}_{\lambda' j}X_{j0} + Y^*_{i0}Y_{0i}\mathcal{Y}_{\lambda l}\mathcal{X}^T_{l\lambda'}\right\}\\
\tilde{g}^{[4]}_{\lambda\lambda'} &= 2i\det\left(\mathcal{X}^\dagger\mathcal{X}\right)^{\frac{1}{4}} \{\mathcal{Y}_{\lambda l}\mathcal{X}^T_{l\lambda'}X^T_{0j}\mathcal{F}_{ji}Y_{i0} + \mathcal{Y}_{\lambda l}\mathcal{F}_{li}X^T_{0i}\mathcal{X}_{\lambda' j}Y_{j0} + \mathcal{Y}_{\lambda l}\mathcal{F}^T_{li}Y_{i0}\mathcal{X}_{\lambda' j}X_{j0}\\
&\quad + \mathcal{X}_{\lambda i}X_{i0}\mathcal{Y}_{\lambda' l}\mathcal{F}_{lj}Y_{j0} - \mathcal{X}_{\lambda i}Y_{i0}\mathcal{Y}_{\lambda' l}\mathcal{F}_{lj}X_{j0} - \mathcal{Y}_{\lambda l}\mathcal{F}_{lk}\mathcal{Y}^T_{k\lambda'}Y^T_{0j}Y^*_{j0}\}.
\end{aligned}$$

References

A.A. Abrikosov, L.P. Gorkov, I.E. Dzyaloshinski, *Methods of Quantum Field Theory in Statistical Physics* (Courier Dover Publications, New York, 2012)

A. Altland, B. Simons, *Condensed Matter Field Theory* (Cambridge University Press, Cambridge, 2006)

J.-P. Blaizot, G. Ripka, *Quantum Theory of Finite Systems* (Cambridge, MA: MIT Press, 1986)

V. Grebennikov, Y. Babanov, O. Sokolov, Extra-atomic relaxation and X-Ray-Spectra of narrow-band metals. 2. Results. Physica Status Solidi Basic Res. **80**(1), 73–82 (1977)

D.B. Gutman, Y. Gefen, A.D. Mirlin, Non-equilibrium 1D many-body problems and asymptotic properties of Toeplitz determinants. J. Phys. A: Math. Theor. **44**(16), 165003 (2011)

N.I. Muskhelishvili, *Singular Integral Equations* (P. Noordhoff, Groningen, 1953), p. 468

J. Negele, H. Orland, *Quantum Many-Particle Systems*. Advanced Books Classics (Westview Press, Boulder, 2008)

P. Nozieres, C. DeDominicis, Singularities in the X-ray absorption and emission of metals. III. One-body theory exact solution. Phys. Rev. **178**(3), 1097–1107 (1969)

W.H. Press, S.A. Teukolsky, W.T. Vetterling, B.P. Flannery, *Numerical Recipes: The Art of Scientific Computing*, 3rd edn. (Cambridge University Press, New York, 2007)

M. Wimmer, Algorithm 923: efficient numerical computation of the Pfaffian for dense and banded skew-symmetric matrices. ACM Trans. Math. Softw. **38**(4), 30:1–30:17 (2012)

J. Zinn-Justin, *Quantum Field Theory and Critical Phenomena*. The International Series of Monographs on Physics Series (Clarendon Press, Oxford, 2002)